



With the support of the
Erasmus+ Programme
of the European Union



University of Évora
ARCHMAT (ERASMUS MUNDUS MASTER IN ARCHaeological
MATERials Science)

Mestrado em Arqueologia e Ambiente (Erasmus Mundus–ARCHMAT)

**Multi-analytical characterization of ceramics from Dhofar (Southern Oman):
provenance and trade.**

Daniele Zampierin., m43275

Assistant Prof. Patrícia S. M. Moita
(Supervisor – University of Évora)



Dr. Marike E. J. J. van Aerde
(Supervisor – Leiden University)



PhD Candidate Silvia Lischi
(Supervisor – University of Pisa)



UNIVERSITÀ DI PISA

Évora, Portugal, December 2020





With the support of the
Erasmus+ Programme
of the European Union



University of Évora
ARCHMAT (ERASMUS MUNDUS MASTER IN ARCHaeological
MATERials Science)

Mestrado em Arqueologia e Ambiente (Erasmus Mundus–ARCHMAT)

**Multi-analytical characterization of ceramics from Dhofar (Southern Oman):
provenance and trade.**

Daniele Zampierin., m43275

Assistant Prof. Patrícia Sofia Martins Moita
(Supervisor – University of Évora)



Dr. Marike E.J.J. van Aerde
(Supervisor – Leiden University)



PhD Candidate Silvia Lischi
(Supervisor – University of Pisa)



UNIVERSITÀ DI PISA

Évora, Portugal, December 2020



Jury members:

Presidente: Nicola Schiavon Investigador Principal Convidado – Universidade de Évora

Arguente: José António Paulo Mirão Professor Associado c/ Agregação – Universidade de Évora

Orientador: Patrícia Moita Professora Auxiliar – Universidade de Évora

Vogal: Donatella Magri Professora Associada – Università di Roma La Sapienza

Caracterização multi-analítica de cerâmicas de Dhofar (do Sul Oman): proveniência e comércio.

Os sítios arqueológicos de Sumhuram (séculos III a II aC - início V dC) e Inqitat (primeiro milénio aC - séculos I a II dC) estão envolvidos num dos exemplos mais importantes de rede de comércio a grande escala na antiguidade: a rede de comércio marítimo no Oceano Índico. Ambos, localizados na Província de Dhofar (Omã), ao longo do Wadi Darbat, estiveram diretamente envolvidos neste intercâmbio, sendo um exemplo extraordinário da sua complexidade.

A atenção deste trabalho está focada na caracterização do material cerâmico Local e Indiano, de ambos os locais, abrangendo idades desde o final do primeiro milénio aC até ao século IV dC. Realizou-se uma abordagem multi-analítica complementar com o objetivo de caracterização das cerâmicas e validação das proveniências resultantes da abordagem tipológica. As técnicas utilizadas na análise foram Difração de raio-X (XRD), Análise Petrográfica, Espectrometria de massa por plasma acoplado indutivamente (ICP-MS), perda ao rubro (LOI) e Microscopia eletrónica de varrimento acoplado a espectroscopia de energia dispersiva de raios-X (SEM-EDS). Os resultados obtidos identificam 8 grupos distintos com base na composição-*fabric* (desengordurante rico em conchas (ST), desengordurante rico em argilito (SF), *fabric* rico em talco (TF), *fabric* rico em basalto (BF), desengordurante rico em arroz (RT), material fino (FF), desengordurante médio-grosseiro em *fabric* fino (MLF) e desengordurante rico em conchas e areia (SSF)) traduzindo assinaturas geológicas muito distintas e destacando assim a enorme variabilidade na origem das matérias-primas. A maioria dos grupos tipológicos definidos como Indianos são aqui confirmados como provenientes do subcontinente indiano, mas a classificação tipológica existente não reflete o agrupamento *fabric*-composicional. Dentro dos grupos Locais (ST, SF e TF), a presença do grupo de cerâmica rica em talco (TF) e proveniente do Iémen levanta a discussão sobre o significado de “Local”.

Embora não seja possível associar diferentes matérias-primas com rotas comerciais estabelecidas, a variabilidade dos grupos indianos identificados implica a participação de várias áreas do subcontinente indiano na rede de comércio do Oceano Índico: Gujarat e a região centro-oeste, sul da Índia, Sri Lanka e a planície aluvial do norte da Índia. Os resultados destacam a grande extensão geográfica da rede de comércio, mas mais importante, sublinham o papel fundamental da abordagem multi-analítica no apoio à identificação de proveniências, representando o ponto de partida para uma nova abordagem de base científica para o fenómeno da globalização do Oceano Índico.

Palavras chave: Cerâmicas, Omã, Comércio Oceano Índico, Arqueometria

Multi-analytical characterization of ceramics from Dhofar (Southern Oman): provenance and trade.

The archaeological sites of Sumhuram (3rd-2nd century BC until the early 5th century AD) and Inqitat (1st millennium BC until the 1st-2nd century AD), are involved in one of the most important examples of large-scale trade network in the antiquity: the maritime trade network connecting the coasts of the Indian Ocean. Both sites, located in the Governorate of Dhofar in Oman, along the Wadi Darbat, were directly involved in the network being an extraordinary example of its complexity.

The attention of this work is focused on the material characterization of both local and Indian pottery from both sites spanning from the late 1st millennium BC until the 4th century AD. A multi-analytical complementary approach was carried out in order to characterize the ceramics and validate the provenance identification resulting from the typological approach. The techniques used in the analysis are X-Ray Diffraction (XRD), petrographic analysis, Inductively Coupled Plasma Mass Spectrometry (ICP-MS), Loss on Ignition (LOI) and Scanning Electron Microscope coupled to Energy Dispersive X-ray Spectroscopy (SEM-EDS).

The results obtained identify 8 different fabric-compositional groups (Shell-Temper (ST), Shale-rich Fabric (SF), Talc-rich Fabric (TF), Basalt-rich Fabric (BF), Rice Temper (RT), Fine Fabric (FF), Medium-Large temper grains in fine Fabric (MLF) and the Shell and Sand rich Fabric (SSF)) with very distinct geological signatures highlighting the enormous variability in the origin of raw materials. Most of the typological groups defined as Indian are here confirmed as actually from India, but the specific typological classification does not reflect the fabric grouping. Within local groups (ST, SF and TF) the presence of a pottery group (TF) coming from Yemen raises the discussion about the meaning of “local”.

Although it is not possible to associate different raw materials with specific known commercial routes, the variability of the Indian fabric-compositional groups indicates the participation of several areas of the Indian subcontinent in the Indian Ocean trade network: Gujarat and the central-west region, south of India, Sri Lanka and the alluvial plane of the north of India. The results highlight the large geographical extension of the trade network, but, more importantly, they underline the fundamental role of multi-analytical approach in support to the provenance identification representing the starting point for a new scientific-based approach to the Indian Ocean globalisation phenomenon.

Key words: Ceramics, Oman, Indian Ocean Trade, Archaeometry.

Acknowledgements

This M.A. thesis would not have been possible without the constant support of the supervisors, colleagues, friends and family.

Among the many I have to thank for the support, I would like to thank my supervisors for giving me never ending-support and trust in the analysis process as well as in the elaboration and writing of the thesis. In particular, Prof. Patrícia Sofia Martins Moita for the constant support and guidance in the different steps of the analysis in HERCULES Laboratory. Dr. Marike Van Aerde for the constant support, the indications in the writing process and the suggestions regarding the definition of the general archaeological context in which to set the research. PhD candidate Silvia Lischì for providing the archaeological material here analysed and providing information regarding the archaeological context of the two sites taken in considerations. I would like to thank all the researchers and colleagues working at the HERCULES Laboratory for the support and the availability for discussion and confrontation over the understanding of the data. In particular, I would like to thank Dr. Massimo Beltrame and Dr. Pedro Miguel Cambeiro Barrulas for guiding me in the LOI and ICP-MS analysis and for providing important indications on the management of the data. Special thank also to Prof. José Antonio Paulo Mirão for his valuable advice and support during this study, and mainly for intriguing and motivating me in every step of the process.

Thank also to ARCHMAT EMMC International Selection Committee for accepting me in this master program and all the professors and lecturers that contribute to acquire the knowledge and to develop the skills required for archaeometric research.

Various people deserve special thanks: the staff of HERCULES Laboratory, the fellow ARCHMAT students, all the flatmates that shared the very heavy and long period of lockdown with me and all the friends that helped me through the 2 years of MA and through the particularly long thesis period, especially the participants to the “video-group-studying” sections.

Last, but not least, I am also deeply grateful to my family for their logistic and moral support, encouragement and understanding.

Table of Contents:

| | |
|---|-----------|
| List of Illustration: | X |
| List of Tables | XVI |
| 1. Introduction | 1 |
| 1.1 Research Topic | 1 |
| 1.2 Research Approach and Questions | 1 |
| 1.3 Outline of the Chapters..... | 2 |
| 2. Background | 3 |
| 2.1 Theoretical background | 3 |
| 2.2 “Globalization” and “Network” | 4 |
| 2.3 Historical Background | 6 |
| 2.4 Archaeology | 9 |
| 2.4.1 <i>Inqitat</i> | 9 |
| 2.4.2 <i>Sumhuram</i> | 11 |
| 2.5 Historical sources | 14 |
| 2.6 Pottery..... | 15 |
| 3. Materials | 18 |
| 4. Methodology..... | 25 |
| 4.1 Photographic recording..... | 26 |
| 4.2 3D recording..... | 26 |
| 4.3 General Sample Preparation | 27 |

| | |
|--|-----------|
| 4.4 Optical Microscopy | 29 |
| 4.5 Loss on Ignition (LOI)..... | 29 |
| 4.6 X-ray Diffraction (XRD) | 30 |
| 4.7 Inductively Coupled Plasma Mass Spectrometry (ICP-MS) | 30 |
| 4.8 Scanning Electron Microscope coupled with Energy Dispersive X-ray Spectroscopy (SEM-EDS) | 32 |
| 5. Results..... | 33 |
| 5.1 Polarized Optical Microscopy observations | 33 |
| 5.1.1 <i>Shell Tempered (ST)</i> | 34 |
| 5.1.2 <i>Shale-rich Fabric (SF)</i> | 34 |
| 5.1.3 <i>Talc-rich Fabric (TF)</i> | 34 |
| 5.1.4 <i>Basalt-rich Fabric (BF)</i> | 35 |
| 5.1.5 <i>Rice Tempered (RT)</i> | 35 |
| 5.1.6 <i>Fine Fabric (FF)</i> | 36 |
| 5.1.7 <i>Medium-Large inclusions in fine Fabric (MLF)</i> | 36 |
| 5.1.8 <i>Shells and Sand rich Fabric (SSF)</i> | 37 |
| 5.2 X-ray Diffraction | 41 |
| 5.2.1 <i>Shell Tempered (ST)</i> | 41 |
| 5.2.2 <i>Shale-rich Fabric (SF)</i> | 42 |
| 5.2.3 <i>Talc-rich Fabric (TF)</i> | 43 |
| 5.2.4 <i>Basalt-rich Fabric (BF)</i> | 44 |
| 5.2.5 <i>Rice Tempered (RT)</i> | 45 |
| 5.2.6 <i>Fine Fabric (FF)</i> | 46 |

| | | |
|-----------|--|-----------|
| 5.2.7 | <i>Medium-Large inclusions in fine Fabric (MLF)</i> | 46 |
| 5.2.8 | <i>Shell and Sand rich Fabric (SSF)</i> | 47 |
| 5.3 | Loss on Ignition (LOI) | 49 |
| 5.3 | Inductively coupled plasma mass spectrometry (ICP-MS) | 50 |
| 5.3.1 | <i>Comparison of Major Element Oxides</i> | 51 |
| 5.3.2 | <i>Normalised Rare Earth Elements (REE)</i> | 58 |
| 5.3.3 | <i>General comparison Local vs Indian</i> | 62 |
| 5.4 | Scanning Electron Microscopy – Energy Dispersive X-rays Spectroscopy (SEM-EDS) | 63 |
| 5.4.1 | <i>Shell Tempered (ST)</i> | 64 |
| 5.4.2 | <i>Shale-rich Fabric (SF)</i> | 65 |
| 5.4.3 | <i>Talc-rich Fabric (TF)</i> | 67 |
| 5.4.4 | <i>Basalt-rich Fabric (BF)</i> | 69 |
| 5.4.5 | <i>Rice-rich Fabric (RT)</i> | 71 |
| 5.4.6 | <i>Fine Fabric (FF)</i> | 73 |
| 5.4.7 | <i>Medium-Large inclusions in fine Fabric (MLF)</i> | 75 |
| 5.4.8 | <i>Shell and Sand rich (SSF)</i> | 77 |
| 5.4.9 | <i>Paste comparison</i> | 78 |
| 5.5 | Geological data | 80 |
| 5.5.1 | <i>Arabia</i> | 80 |
| 5.5.2 | <i>Indian Subcontinent</i> | 83 |
| 6. | Discussion | 85 |
| 6.1 | Local vs. Indian pottery | 85 |

| | |
|---|------------|
| 6.2 Provenance | 89 |
| 6.2.1 <i>ST provenance</i> | 90 |
| 6.2.2 <i>SF group</i> | 91 |
| 6.2.3 <i>TF group</i> | 91 |
| 6.2.4 <i>BF group</i> | 93 |
| 6.2.5 <i>RT group</i> | 94 |
| 6.2.6 <i>FF group</i> | 95 |
| 6.2.7 <i>MLF group</i> | 96 |
| 6.2.8 <i>SSF group</i> | 99 |
| 6.2.9 <i>General distribution</i> | 100 |
| 6.2.10 <i>Technological characteristics</i> | 101 |
| 6.3: Implication from a general point of view | 102 |
| 6.3.1 <i>Sumhuram vs. Inqitat</i> | 102 |
| 6.3.2 <i>Trade network</i> | 104 |
| 7. Summary and Conclusion | 109 |
| 7.2 Summary | 109 |
| 7.2 Conclusion | 112 |
| 8. References..... | 113 |
| 9. Appendixes..... | 121 |
| 9.1 sample recording..... | 121 |
| 9.2 Polarized optical microscopy observations..... | 126 |
| 9.3 X-ray Diffraction | 129 |

| | |
|--|-----|
| 9.4 ICP-MS results and graphic representations | 135 |
| 9.5 SEM-EDS data | 139 |

List of Illustration:

| | |
|--|----|
| Figure 1.1: View of Sumhuram with Inqitat in background (IMTO project)..... | 1 |
| Figure 2.1: Map of Arabian Sea including some of the most important archaeological sites connected to the Arabian Sea trade (after Lischi et al. 2020). | 5 |
| Figure 2.2: Wadi Darbat and location of Sumhuram and Inqitat (after www.earth.google.com). 9 | |
| Figure 2.3: Aerial image of the Inqitat plateau with the HAS1 structures highlighted in white, HAS2 structures highlighted in yellow and the middens highlighted in red (DHOMIAP project). | 10 |
| Figure 2.4: Aerial view of the site of Sumhuram (IMTO project). | 12 |
| Figure 2.5: A) Headless statuette from Sumhuram (after Avanzini 2011). B) Bronze plaques from South Arabia representing the Indian motif "linga" (after Pavan 2016). C) "Hombrechtikon plaque" from South Arabia with the Indian goddess Yaksi on the right (after Pavan 2016). D) Bronze head tentatively identified as Shiva from Sumhuram (after Pavan 2016). E-F) Ivory Statuette from Pompeii (after Maiuri 1939). | 13 |
| Figure 3.1: Sample IQM18A.US80.3..... | 19 |
| Figure 3.2: Sample SUM11A.US174.232. | 19 |
| Figure 3.3: Sample SUM11A.US54.85. | 19 |
| Figure 3.4: Sample SUM09A.US297.2. | 19 |
| Figure 3.5: Sample IQM16B.US23.13..... | 20 |
| Figure 3.6: Sample SUM10C.US162.119..... | 20 |
| Figure 3.7: Sample IQM16B.US35.8..... | 20 |
| Figure 3.8: Sample SUMW03A.US1.1..... | 20 |
| Figure 3.9: Sample SUM10A.US412.1..... | 20 |

| | |
|---|----|
| Figure 4.1: A) Image of the 3D reconstruction of sample SUM03B.US93.42 done by the author. B) Image of the 3D reconstruction of sample IQM18B.US119.5 done by the author..... | 27 |
| Figure 5.1: Typical diffractogram of ST ceramics. | 42 |
| Figure 5.2: Typical diffractogram of SF ceramics. | 42 |
| Figure 5.3: Typical diffractogram of TF-1 ceramics..... | 43 |
| Figure 5.4: Typical diffractogram of TF-2 ceramics..... | 44 |
| Figure 5.5: Typical diffractogram of BF ceramics. | 45 |
| Figure 5.6: Typical diffractogram of RT ceramics. | 45 |
| Figure 5.7: Typical diffractogram of FF ceramics. | 46 |
| Figure 5.8: Typical diffractogram of MLF ceramics..... | 47 |
| Figure 5.9: Typical diffractogram of SSF ceramics. | 47 |
| Figure 5.10: Major Element (wt.%) comparison of one representative sample per group. | 51 |
| Figure 5.11: Major Elements (wt.%) divided in groups: A) ST; B) SF; C) TF. | 53 |
| Figure 5.12: Major Element (wt. %) divided in groups: A) BF; B) RT; C) FF; D) MLF; E) SSF. | 54 |
| Figure 5.13: REE data normalized to chondrite (McDonough and Sun, 1995). A) REE normalised per group (logarithmic scale); B) Normalised REE ratios per group (logarithmic scale). 58 | |
| Figure 5.14: REE data normalized to chondrite (McDonough and Sun, 1995). A) ST REE Normalized and in logarithmic scale B) ST REE ratios in logarithmic scale..... | 59 |
| Figure 5.15: REE data normalized to chondrite (McDonough and Sun, 1995). A) SF REE Normalized and in logarithmic scale B) SF REE ratios in logarithmic scale..... | 60 |
| Figure 5.16: REE data normalized to chondrite (McDonough and Sun, 1995). A) TF REE Normalized and in logarithmic scale B) TF REE ratios in logarithmic scale. | 60 |

| | |
|---|----|
| Figure 5.17: REE data normalized to chondrite (McDonough and Sun, 1995). A) BF REE Normalized and in logarithmic scale B) BF REE compared in logarithmic scale..... | 60 |
| Figure 5.18: REE data normalized to chondrite (McDonough and Sun, 1995). A) RT REE Normalized and in logarithmic scale B) RT REE ratios in logarithmic scale. | 61 |
| Figure 5.19: REE data normalized to chondrite (McDonough and Sun, 1995). A) FF REE Normalized and in logarithmic scale B) FF REE ratios in logarithmic scale. | 61 |
| Figure 5.20: REE data normalized to chondrite (McDonough and Sun, 1995). A) MLF REE Normalized and in logarithmic scale B) MLF REE ratios in logarithmic scale. | 61 |
| Figure 5.21: REE data normalized to chondrite (McDonough and Sun, 1995). A) SSF REE Normalized and in logarithmic scale B) SSF REE ratios in logarithmic scale..... | 62 |
| Figure 5.22: Binary plot comparing Al_2O_3/SiO_2 and MgO/SiO_2 with local samples in blue circle and Indian samples in red circle stylistically identified. | 63 |
| Figure 5.23: Ternary diagram of major oxides in correspondence of Al_2O_3 , SiO_2 and $CaO+MgO$ with local in blue circle and Indian in red circle stylistically identified (after Heimann and Maggetti 2019). | 63 |
| Figure 5.24: BSE image of ST on the left and the elemental distribution mapping with distribution of Si (yellow) and Ca (blue) on the right. | 65 |
| Figure 5.25: BSE images of SF group: On the left a shell fragment and on the right a bone fragment within SF with point of elemental composition analysis. | 66 |
| Figure 5.26: Point analysis of bone fragment. | 66 |
| Figure 5.27: BSE image of SF on the top left and the elemental distribution mapping with in the centre the distribution of Fe (green) and Ti (red) and on the top right the distribution of Na (red) and Mg (green). | 66 |
| Figure 5.28: BSE image of shale grain in SF on the left and the elemental distribution mapping with in the centre the distribution of Mg (green) and on the right the distribution of Al (pink) and Si (yellow). | 67 |
| Figure 5.29: Point analysis of talc inclusion. | 68 |

| | |
|--|----|
| Figure 5.30: BSE image of TF on the top left and the elemental distribution mapping with in the centre the distribution of Mg (green-talc) and Al (pink-paste) and on the top right the distribution of Fe (red-oxide). | 68 |
| Figure 5.31: On the left the elemental composition and on the right BSE image of the clast. | 68 |
| Figure 5.32: BSE images of BF group: On the left a rice husk and on the right an example of volcanic glass grain. | 69 |
| Figure 5.33: BSE image of BF on the left and on the right the elemental distribution mapping with the distribution of Mg (green-pyroxene) and Ca (blue plagioclase and pyroxene). | 70 |
| Figure 5.34: BSE image of basalt grain in BF on the top left and the elemental distribution mapping with in the centre the distribution of Ca (blue-pyroxene) and Al (orange-plagioclase and paste) and on the top right the distribution of Mg (green-pyroxene) and Ti (pink-oxide). | 70 |
| Figure 5.35: BSE image of volcanic glass grain in BF on the top left and the elemental distribution mapping with in the centre the distribution of Mg (green-pyroxene) and Na (red-plagioclase) and on the top right the distribution of Fe (green-pyroxene) and Al (pink-plagioclase and paste). | 71 |
| Figure 5.36: BSE images of RT group: On the left a general view and on the right a zoom-in on a rice husk. | 72 |
| Figure 5.37: Ternary diagram of pyroxenes from BF samples and RT sample. The comparison is also among pyroxene located within basalt grains (crossed empty symbol) and single pyroxene grains (full coloured symbols), both within BF samples (after Heimann and Maggetti 2019). | 72 |
| Figure 5.38: BSE image of RT on the top left and the elemental distribution mapping with in the centre the distribution of Mg (green-paste) and Na (red-plagioclase) and on the top right the distribution of Si (yellow-quartz). | 73 |
| Figure 5.39: BSE images of FF group: On the left a bone fragment and on the right a general view of the US80.3 sample composition. | 74 |
| Figure 5.40: Point analysis of bone fragment. | 74 |

| | |
|--|----|
| Figure 5.41: BSE image of FF on the top left and the elemental distribution mapping with in the centre the distribution of Ca (blue-pores, bone fragments and plagioclase) and Fe (orange-micas) and on the top right the distribution of Na (red-lithoclast), K (purple), Ca (blue) and Si (yellow-quartz). | 74 |
| Figure 5.42: BSE image of FF on the top left and the elemental distribution mapping with in the centre the distribution of Ca (blue) and Si (yellow) and on the top right the distribution of Fe (red)..... | 75 |
| Figure 5.43: BSE images of MLF group: On the left a view of US35.9 and on the right a view of US253.5..... | 76 |
| Figure 5.44: BSE image of MLF on the top left and the elemental distribution mapping with in the centre the distribution of Na (red-feldspar), Mg (green-micas), Ca (blue) and Si (yellow-quartz) and on the top right the distribution of Fe (green-micas). | 76 |
| Figure 5.45: BSE image of MLF on the left and the elemental distribution mapping with in the centre the distribution of Na (red- feldspar), Ca (blue-amphiboles) and Si (yellow-quartz) and on the right the distribution of Mg (green-amphiboles) and K (yellow-k-feldspar)..... | 77 |
| Figure 5.46: BSE image of SFF on the top left and the elemental distribution mapping with in the centre the distribution of K (purple-paste) and Ca (blue-calcitic shell) and on the top right the distribution of Fe (red-oxides) and Si (yellow- quartz)..... | 78 |
| Figure 5.47: Ternary plot representing the comparison of the binders according to CaO+MgO, SiO ₂ and Al ₂ O ₃ (wt.%). | 80 |
| Figure 5.48: Generic view of the geology of Yemen, Oman and south Saudi Arabia (after www.usgs.gov)..... | 81 |
| Figure 5.49: Geological close up of the Salalah region with including the sites of Sumhuram and Inqitat indicated by the red star (after M. I. Khaifa, 1988). | 82 |
| Figure 5.50: Generic geological map of South Asia (after www.usgs.gov). | 83 |
| Figure 6.1: Binary plot comparing Al ₂ O ₃ /SiO ₂ and MgO/SiO ₂ with local identified in blue circle, non-local in red circle and TF-2 in black. | 88 |
| Figure 6.2: Binary plot comparing Al ₂ O ₃ /SiO ₂ and MgO/SiO ₂ for all samples excluding TF-2. | 88 |

| | |
|--|-----|
| Figure 6.3: <i>ST possible provenance (after www.usgs.gov)</i> | 90 |
| Figure 6.4: <i>TF and SF possible provenance (after www.usgs.gov)</i> | 91 |
| Figure 6.5: <i>Comparison between TF samples (blue and green) and stoneware samples from UAE in yellow (Magee et al. 2005)</i> | 92 |
| Figure 6.6: <i>Possible provenance BF group (after www.usgs.gov)</i> | 93 |
| Figure 6.7: <i>Possible provenance RT group (after www.usgs.gov)</i> | 94 |
| Figure 6.8: <i>Possible provenance FF group (after www.usgs.gov)</i> | 95 |
| Figure 6.9: <i>Possible provenance MLF group (after www.usgs.gov)</i> | 96 |
| Figure 6.10: <i>Graphic comparison of the samples from MLF (blue) with different dataset: A) sedimentary composition in Sri Lanka (Hettiarachchi, Motha, and Pitawala 2010); B) sample oxide composition from Vellore (Naseerutheen et al. 2014); C) sample trace element composition from Arikamedu, Chandraketugarh and Tamluk (Das et al. 2017)</i> | 98 |
| Figure 6.11: <i>General map of South Arabian and Indian geology (after www.usgs.gov) with provenance of the different groups highlighted by means of circles of different colours: ST (yellow), SF and TF (black), BF (red), RT (grey), FF (green), MLF (blue)</i> | 101 |

List of Tables

| | |
|--|----|
| Table 2.1: <i>Most important political entities and their period of existence in the region touched by the Arabian Sea, the Mediterranean, the Red Sea and the Persian Gulf.</i> | 8 |
| Table 3.1: <i>Fabric types represented by the samples analysed in this thesis (Pavan 2017).</i> | 19 |
| Table 3.2: <i>List of samples from Sumhuram.</i> | 21 |
| Table 3.3: <i>List of samples from Inqitat (Fabric Type defined by the author of the thesis)</i> | 22 |
| Table 3.4: <i>Table presenting a summary of the macroscopic description samples from Sumhuram</i> | 23 |
| Table 3.5: <i>Table presenting a summary of the macroscopic description samples from Inqitat.</i> .. | 24 |
| Table 5.1: <i>Schematized presentation of the groups identified with petrographic analysis, of their main characteristics and of the colour code adopted throughout the thesis.</i> | 38 |
| Table 5.2: <i>XPL images presenting the composition of each sample from Sumhuram and Inqitat colour coded in relation to the group. The pictures have a 0,2 mm scale.</i> | 39 |
| Table 5.3: <i>XRD results for each sample colour coded: ST (yellow), SF (purple), TF-1 (dark green), TF-2 (dark blue), BF (red), RT (grey), FF (light green), MLF (light blue) and SSF (brown). The phases connected to the firing temperature of the ceramic are highlighted in yellow.</i> | 48 |
| Table 5.4: <i>LOI values (wt. %) for each sample, samples divided according to defined groups.</i> | 49 |
| Table 5.5: <i>Major elemental composition (wt. %) per sample. SiO₂ is highlighted in yellow because of its indirectly measured values.</i> | 55 |
| Table 5.6: <i>Trace elements composition per sample (ppm).</i> | 56 |
| Table 5.7: <i>Trace elements composition per sample (ppm). (cont.)</i> | 57 |
| Table 5.8: <i>Summary of the major oxides' composition done by EDS of the pastes (wt. %). The colour of the samples identifies the group of membership: ST (yellow), SF (purple), TF (dark blue), BF (red), RT (grey), FF (green), MLF (light blue) and SSF (brown).</i> | 79 |

Table 6.1: *Table of provenance and fabric type identification prior to the archaeometric analysis. The colouring reflects the grouping resulting from the petrographic analysis: ST (yellow), SF (violet), TF-1 (dark green), TF-2 (blue), MLF (light blue), BF (red), FF (light green), RT (grey), SSF (brown).....* 86

Table 6.2: *Summary of most important characteristics of ceramics by macro areas.* 89

Table 6.3: *Division of calcareous and non-calcareous ceramics according to table 5.9 and presence of specific minerals in relation to cooking temperature (El Ouahabi et al. 2015).* 102

1. Introduction

1.1 Research Topic

In Dhofar, in the southern region of Oman, more than 2000 years ago, the Ancient South Arabians decided to build a new city-port, Sumhuram. These people came from the Kingdom of Hadramawt with the probable aim of building an outpost to simplify the collection of frankincense from this area (Buffa 2019). The area where they decided to build Sumhuram (at the mouth of Wadi Darbat) was intensively inhabited since, at least, the first part of the first millennium BC. In fact, a few kilometers away, towards the coast (Fig. 1.1), a settlement was present since the 4th century BC and inhabited during the foundation of Sumhuram, the settlement named HAS1 (Lischi 2019a). HAS1 is located on the promontory of Inqitat and controlled the area close to the sea-shore. The two settlements are now within the same archaeological area known as Khor Rori. The material assemblages from both sites underline that they had the chance to be in contact with cultures and goods from territories as far away as India, Mesopotamia, Egypt and the Roman Empire. The co-presence of the two settlements lasting for some centuries and the presence of foreign material in both of them provides the unique opportunity to compare two different cultures involved in the same trading system from the same geographic location.

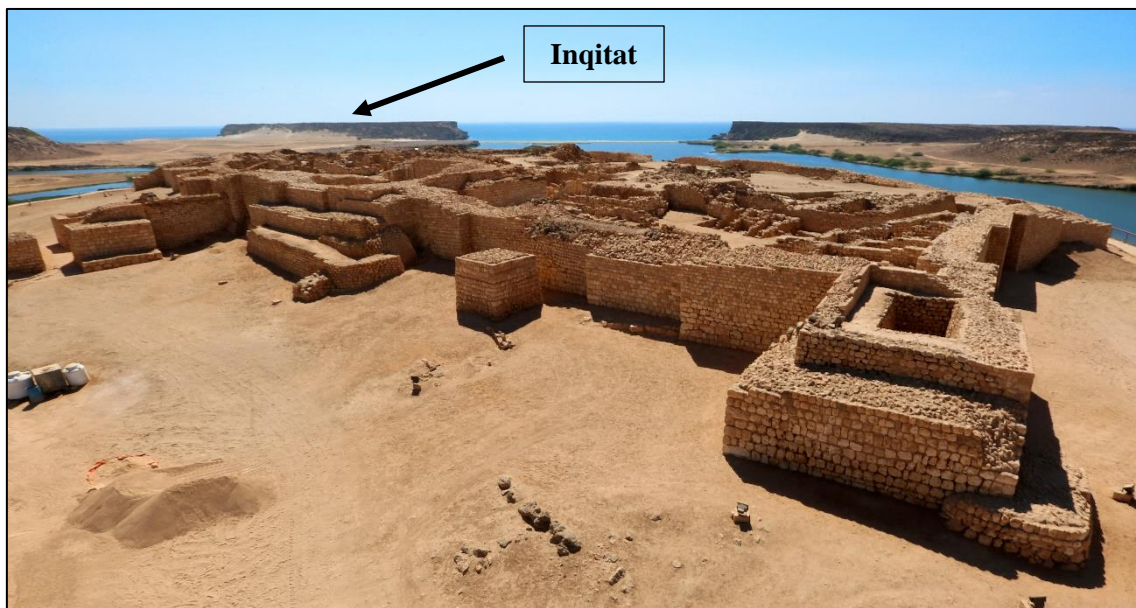


Figure 1.1: View of Sumhuram with Inqitat in background (IMTO project).

1.2 Research Approach and Questions

In the following work, the focus is on the general topic of international trade that developed within the coasts of the Arabian Sea. To tackle such a topic, the author adopts a bottom-up approach starting from the analysis of ceramic artefacts retrieved from HAS1 (from now on identified also

by the name “Inqitat” for better understanding) and Sumhuram. More precisely, both sites present a combination of foreign and local ceramics and, in this specific case study, the attention is centred on local ceramics and on ceramics that, from a typological point of view, are identified as Indian.

The leading research questions guiding the work are:

- *“Are the Indian pottery sherds manifesting a different archaeometric composition from the local pottery sherds?”*
- *“Can we suggest the provenance of the ceramic samples we are analysing?”*

To the previously presented main research questions, three sub-questions are added:

- *“Is it possible to identify specific archaeometric signatures differentiating Indian and local pottery sherds?”*
- *“What is the relation between the archaeometric classification and the stylistic typology?”*
- *“Is it possible to develop a better understanding of the technology used for the production of the artefacts?”*

To answer the presented research questions, the bottom-up approach proposes to start from the objective analysis and definition of the different mineralogical, chemical and textural characteristics of each ceramic. The definition of the mineralogical, chemical and technological characteristics of the 35 samples analysed in this study is then used to group them and to find general characteristics typical of the local ceramics, different from those of the Indian ceramics.

1.3 Outline of the Chapters

The discussion presented in this thesis is divided into 7 Chapters. Chapter 2 presents the historical and archaeological background as well as the up-to-date theoretical framework of “globalization” and of “network”. The subsequent chapters (chapters 3, 4 and 5) are respectively concerned with the presentation of the material analysed, the methods adopted and the data resulting from the analysis. Chapter 6 will present the discussion of the data in relation to the research questions. The last chapter (chapter 7) is the conclusion, where the results of the discussion are framed within the general theoretical framework, and proposals for further researches are presented.

2. Background

In this chapter, the author presents to the reader a general overview of the theoretical framework, the historical context and the archaeological background. The aim is to give the reader a better understanding of where to locate this thesis within both a theoretical and a cultural context.

2.1 Theoretical background

Traditional archaeological understanding of the past was very much site-focused, because the first archaeological experiences were bound to a limited number of sites and, of those, only a limited area was being excavated. Through time and with archaeological research and excavations involving multiple sites, the approach of archaeologists moved from site-focused, to region-focused, to interregional and then to an international approach. The presented steps followed by the archaeological world in understanding the past, result not only from the initial limited data, but also the bases of the “bottom-up logical approach” to the development of a comprehensive understanding of the past. In fact, the same approach from “micro” to “macro” is supposed to be the development of any interpretation of the data retrieved. Moreover, from an ideological point of view, the “bottom-up” approach should be free from any pre-assumed suitable frame within which to adapt the interpretation of the data retrieved (Hodos 2016).

The topic of international relations and connections is of particular complexity and importance when considering the area of the Indian Ocean and of central Asia. In fact, in those regions, it was clear since the first archaeological and historical analysis that long-distance trade connections were of extreme importance (Casson 1914, Wheeler 1971). Since the 2nd half of the 20th century, excavations spread around South Arabia, the Persian Gulf, West Africa, India, modern day Pakistan and Sri Lanka brought up artefacts proving that the local cultural clusters were much more interconnected than had been believed until then. Arikamedu in India (Wheeler 1946), and the excavation of Berenike (Sidebotham 1994-2009) in Egypt are great examples of sites providing new perspective regarding the international trade taking place in the Indian Ocean. Notwithstanding the lack of comprehension of the extension, mechanism and type of interactions taking place in the region, it is now evident that the Arabian Sea was the host of a great movement of people and goods even from the 3rd century BC (Pavan and Schenk 2012).

However, the theoretical bottom-up approach presented above, in the case of understanding the Arabian Sea trade system, has commonly been a victim of pre-established theories to which the data were adapted. That is probably the consequence of the fact that the field of Indian Ocean trade archaeology started to develop when international-focused interpretations were emerging in other fields of archaeology. The result of the “late-blooming” of Indian Ocean trade archaeology, is the tendency to borrow general interpretations and theoretical frames from other

archaeological fields and adapt the limited available data to such pre-formed frames. A very good example of the adaptation of data to a prepared frame is the first interpretative theory proposed for the explanation of the Arabian Sea trade system. The theory was proposed at the end of the 20th century and consisted of the idea that the Roman Empire had been the entity majorly responsible for, and most interested in, the maintenance of the trade system in the Indian Ocean (Wheeler 1971). The reason for such a single character approach towards trade is defined by the lack of information coming from historical sources other than from Classical ones, and because of the strong colonial background that authors, like M. Wheeler, had when approaching the interpretations of the archaeological evidence (De Romanis 1997). Only subsequently, with the development of excavations in sites like Arikamedu, Berenike, Myos Hormos, and Sumhuram, were archaeologists able to collect enough data to start to develop a more complex picture of the network involving the Indian Ocean (van Aerde and Zampierin 2020). The new picture, resulting from a more independently developed theory and free from pre-formed interpretations, is that of many different cultural entities taking part in the international trade network independently (Seland 2014). They were departing from different locations with different destinations and trading a wide variety of goods (Seland 2008). It is within this new wave of independently formed bottom-up theories that this thesis is set. In particular, Sumhuram and Inqitat, with their geographically centred location (Fig. 2.1) and with their extremely large dataset, cover a very important role in contributing to the general understanding of the different mechanisms affecting the trade system connecting people from Central Asia, South Asia, the Red Sea, Africa, Arabia and the Persian Gulf (Avanzini 2007).

2.2 “Globalization” and “Network”

Modern archaeology’s most fashionable theoretical approach is that of “globalization”, where the “global” does not necessarily stand for “globe”, but for very large populations and a plurality of cultures. The definition of “globalization”, even if quite fluid, involves a very broad series of factors that go beyond the identification of provenance and direction of objects, hence beyond the focus of this thesis. In fact, when considering factors to be identified in order to define a period or a culture as globalized, 8 factors are crucial: time-space compression, deterritorialization, standardization, unevenness, homogenization, cultural heterogeneity, re-embedding of local culture and vulnerability (Hodos 2016). The idea schematized here is that of a society where it is possible to identify signs of the acceleration of long-distance connections, signs of lacking connections with the geographically-defined local context and signs of the spreading of common practices among different cultures. The globalization concept also includes evidence of cultural homogenization contemporaneous with the strengthening and radicalization of local cultures, with the definition of cultural differences being demarcated, the development of power inequality

among the participants, and with signs of vulnerability of the single culture to events not directly affecting it (Hodos 2016).

Another commonly used term in modern archaeology, especially when talking about trade, is “network”. A group of people, entities and/or cultures that are closely connected to each other. Are identified by the term “network”. The characteristic of defining connections among people and cultures makes the concept of “network” strongly integrated within the definition of “globalization”. However, in contrast to globalization, a network is a dynamic structure that can change in time and space, but can also be directly studied through data such as the direction, the intensity and dimensions of the connection and the changes over time that affected such connections (Hodos 2016). The possibilities of building the definition of the case-specific network from raw data, and of comparing specific characteristic of the network to actual data, allows the archaeologists to compare different networks and to have a very case-specific constructed network that cannot be taken as pre-formed, but that has to be built out of the raw data. Due to the fact that the thesis presented here is a technical thesis and, considering the localized nature of the data recorded and presented (limited to only one geographical area), the definition of the Arabian Sea network (Fig. 2.1) and its characteristics is not part of this thesis. However, the purpose of presenting the definition of a network and, previously, of globalisation is to clarify the meaning intended to be given to the words “network” and “globalization” in this thesis. It is, in fact, important to understand that identifying a network does not mean identifying a globalization phenomenon, but in having a globalization phenomenon, it is necessary to identify network structure (Hodos 2016).



Figure 2.1: Map of Arabian Sea including some of the most important archaeological sites connected to the Arabian Sea trade (after Lischi et al. 2020).

2.3 Historical Background

Sumhuran was a colony founded by the South Arabian kingdom of Hadramawt in the Dhofar region. It is the easternmost culturally South Arabian site known. It was founded in the late 3rd century/ early 2nd century BC and it lasted until approximately the 5th century AD (Buffa 2019). The interaction between the Dhofar region and the South Arabian Kingdoms, before the foundation of the city of Sumhuran, is not well understood. What is known, is that the Dhofar region was inhabited by different ethnic groups, with the area taken in consideration in this thesis being mainly occupied by semi-nomadic people. The type of interactions between these populations and the South Arabian Kingdoms is still to be defined. The understanding of the local population is still limited to the studies of the settlement HAS1 in the Inqitat promontory. The later foundation of Sumhuran did not put an end to HAS1 in Inqitat, which was founded in the first half of the 1st millennium BC and abandoned only after a big fire around the end of the 1st - beginning of the 2nd century AD (Lischi 2019). The type of interactions between the two sites is still not completely understood. We still, do not know if the foundation of Sumhuran in that location was inspired by the presence of HAS1, if the two sites were interconnected or independent from each other. Notwithstanding the unclear relationship between the sites, the situation created by Sumhuran and Inqitat (HAS1) being so close, probably of two different cultures and, yet, probably sharing many aspects of their history, makes the understanding of both sites very unique.

Unfortunately, the precise history of Inqitat (HAS1) before the foundation of Sumhuran is not yet clear. The limited information that has been retrieved until the time of this thesis being written indicates that the dwelling consisted of semi-nomadic people, probably fishermen and shepherds, with an organized society lacking evidence of hierarchy. The archaeological material suggests that the dwelling dates from the Iron Age until the beginning of the 2nd century AD (Lischi 2016). The end of the occupation is related to a destruction phenomenon evident in most, if not all, circular structures (Lischi 2016). The *in situ* presence of imported ceramics within the circular structures covered by the destruction layer suggests that the village participated in international trade, but it is not clear if the participation was direct or was the result of the proximity with Sumhuran (Lischi 2016).

South Arabia, which indicates modern day Yemen, southwest Saudi Arabia, and the Dhofar region, was referred to by Roman authors as “*Arabia Felix*” and it is known to the Greek culture as early as Herodotus, who mentions it vaguely (Potts 2010). The ancient international knowledge of the existence of the South Arabian Kingdoms is related to their important role within the international trade system, and to the export of luxurious and religion-related goods

such as frankincense and myrrh. The South Arabian Kingdoms were involved in trade by land, with caravans crossing the Arabian desert, and by sea, with contacts developed on the Red Sea and across the Indian Ocean (Potts 2010). More specifically, the importance of the South Arabian Kingdoms is the consequence of their production of unique goods such as frankincense, which was used in the Mediterranean for both religious and non-religious purposes.

The first examples of kingdoms in South Arabia are believed to have formed around the beginning of the 1st millennium BC. Their history, spreading from the beginning of the 1st millennium to the 600 AD, can be divided into 4 macro-periods, according to D. T. Potts (Potts 2010). The first period, lasting roughly from the 1st millennium BC to the 6th century BC, can be considered as the kingdoms' formative period. It is in this period that the kingdom of Saba unified the territories on the west of modern day Yemen, probably with the help of the Hadramawt and the Qataban kingdoms. The second period, spanning from the end of the 6th/beginning of the 5th century BC to the 1st century BC is characterized by the shifting of power towards the kingdom of Qataban. It is considered to be the period in which South Arabia becomes famous for its caravan-based trading system. It is in this period that the "mercantile code of Qataban" was written. Towards the second half of this period, however, sea-based trading also developed and grew in importance, as attested to by the foundation of Sumhuram. After the 1st century BC, the equilibrium in the region changes. The period from 1st century BC to the 3rd century AD, which is considered as the 3rd macro-period, sees the kingdom of Hadramawt defeat Qataban and spread its territories with the kingdom of Saba and Himyar. The end of the Hadramawt leadership over the region, in favour of the Himyar kingdom is the turning point for the beginning of the 4th macro-period. In this period, spanning from the 4th century to the 6th century AD, the kingdom of Himyar is responsible for the unification of the whole of South Arabia. The 4th macro-period is also the last period of local leadership over the region. In fact, from the 6th century AD, date of conquest of South Arabia by Aksumite kingdom, onwards, the region is subjected to foreign conquests (Potts 2010).

The bases of the South Arabian kingdoms' economies were the agricultural products resulting from the very clever and methodological use of dams and irrigation techniques. However, the most important source of wealth and power was the geographical location, which gave them the opportunity, not only to produce frankincense, but also to be in the perfect spot to act as middleman among the Mediterranean, Mesopotamian and Indian Ocean markets. Evidence of the importance that trade had for the economy of the kingdom is provided by the many Arabian written sources underlining the direct interest of the kings in controlling, managing and expanding their rule over the trade routes and frankincense production territories (Potts 2010).

Within the context depicted above, Sumhuram had experienced quite a constant and regular political situation, which allowed for the stable involvement of the port in international trade. It had always been under the more or less strong rule of the Hadramawt Kingdom, from the foundation until the collapse of the dominating kingdom. After the collapse of the Hadramawt kingdom, Sumhuram passed under the influence of the Himyar kingdom until its abandonment which took place around the 5th century AD (Avanzini 2011).

To conclude the presentation of the historical background, which is necessary to better understand and interpret the data resulting from this study, it is important to have a general understanding of the political entities that are more or less involved in the trade. Presenting the complete overview of the political scenario, however, is obviously complicated and extremely extensive. Paraphrasing Romila Thapar's words, the most complicated aspect of the trade is that, in order to be understood as a whole, it requires an extensive study of different historical and archaeological contexts (De Romanis and Thapar 1997). In order to try to have a general image of the situation developing in the timespan lasting from the 3th century BC until the 5th century AD, a brief overview of the most important political entities active in the regions touched by the international trade and their period of existence is presented in the following table (Tab. 2.1):

Table 2.1: Most important political entities and their period of existence in the region touched by the Arabian Sea, the Mediterranean, the Red Sea and the Persian Gulf.

| Political Entity: | Location: | ... | 5 th | 4 th | 3 rd | 2 nd | 1 st | 1 st | 2 nd | 3 rd | 4 th | 5 th | ... |
|---------------------|-------------|-----|-----------------|-----------------|-----------------|-----------------|-----------------|-----------------|-----------------|-----------------|-----------------|-----------------|-----|
| | | BC | | | | | | AD | | | | | |
| Greeks | Greece | | | | | | | | | | | | |
| Tamil Kingdoms | S. India | | | | | | | | | | | | |
| Rome | Medit. | | | | | | | | | | | | |
| Maurya Emp. | N. India | | | | | | | | | | | | |
| Seleucid Emp. | Middle East | | | | | | | | | | | | |
| Ptolemaic Egypt | Egypt | | | | | | | | | | | | |
| Axum | Eritrea | | | | | | | | | | | | |
| Shunga Emp. | N-E India | | | | | | | | | | | | |
| Parthian Emp. | Middle East | | | | | | | | | | | | |
| Satavahanas Dynasty | C. India | | | | | | | | | | | | |
| Kushan Emp. | Pakistan | | | | | | | | | | | | |
| Sassanid Emp. | Middle East | | | | | | | | | | | | |
| Gupta Emp. | N-C India | | | | | | | | | | | | |
| Inqitat | Dhofar | | | | | | | | | | | | |
| Sumhuram | Dhofar | | | | | | | | | | | | |

2.4 Archaeology

The material under discussion, as already mentioned, comes from both Sumhuram and Inqitat (Fig. 2.2). In order to make the discussion, and the understanding of the work clearer, it is useful to present a brief overview of the archaeology of the sites. The importance of the overview of the archaeological sites lies in the visualization of the context from which the artefacts were retrieved, and to provide better understand of the meaning of the analysis results that will be presented later in this thesis.

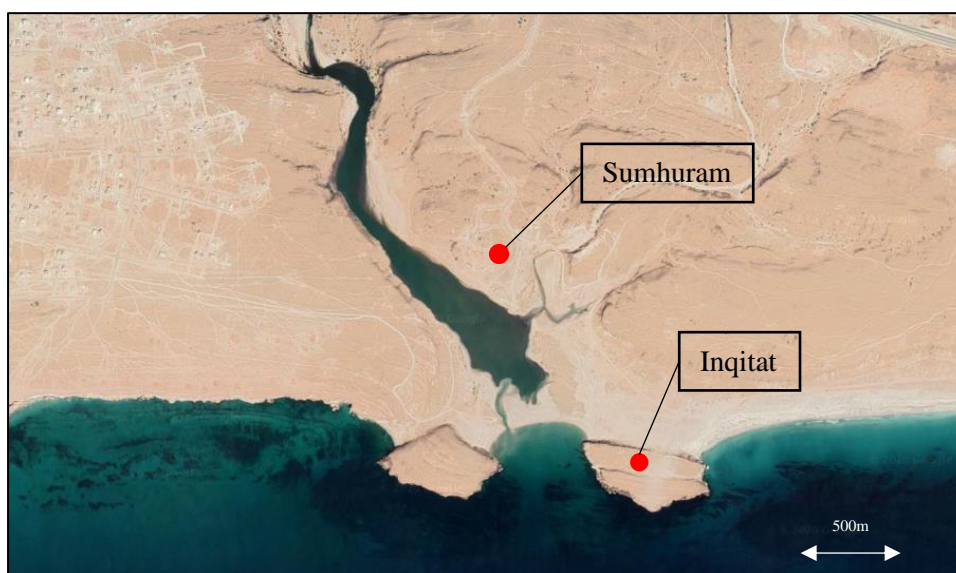


Figure 2.2: Wadi Darbat and location of Sumhuram and Inqitat (after www.earth.google.com).

2.4.1 Inqitat

The site is located on a promontory projecting into the sea. The promontory is 30m high and it roughly points South. A valley cuts the promontory into two plateaus: the northern plateau, where the highest concentration of archaeological remains is located, and the southern plateau that projects towards the coast and the mouth of Wadi Darbat (Fig. 2.3). The distances from the plateau to Sumhuram is around 2km, and it presents two settlements distinguishable not only spatially, but also from a cultural point of view, with Inqitat being occupied by the local semi-nomadic people and Sumhuram being a city founded by the South Arabian kingdom of Hadramawt. In particular, the plateau of Inqitat hosts site HAS1 and site HAS2 with the former being dated from the early 1st millennium BC until 1st/2nd century AD while the latter is from the early Islamic period (X-XI century AD) (Lischi 2019a and Rougeulle 2007). All the Inqitat samples taken into consideration in this thesis are from site HAS1, so the archaeological description is limited to the same site. HAS2 presents no superposition over HAS1, making the designation between the artefacts and the sites much easier. Subject to surveys while the site of Sumhuram was excavated, the plateau of Inqitat was first excavated in the early 2000s, but the excavation was only focused on three buildings of the Islamic settlement HAS2. In 2016, new surveys and excavations started

under the IMTO (Italian Mission to Oman) and successively continued under the DHOMIAP research project. HAS1, roughly 2 hectares in size, is located along the northern margin of the plateau where a wall running from side to side of the promontory can be found. Within the site, approximately 70 visible structures can be found, mostly circular or sub-circular in shape, with some being connected to others. The structures were built with megalithic stones, with the floor made either of simple bedrock or flattened with flat slabs. Unfortunately, we have no preserved roof, but from the remains found within the building, it is possible to infer that the roof was made of a wooden frame covered with straw and other organic material. Along the walls inside the house, runs a bench on which signs of food-processing activities have been identified (Lischi 2019a). On the southern side of HAS1 we can find a series of middens that partially end inside the valley. The middens present mainly food remains, but the youngest layers also show fire-related activities taking place on the top of the middens (Lischi 2019a). Among the artefacts retrieved within Inqitat (HAS1), the most common are ceramics, bones, shells, metals and glass. Ceramic material will be discussed more specifically in the next paragraph. Here it is worth mentioning that, within Inqitat, locally-produced ceramics can be found together with ceramic from foreign origins (Lischi, Pavan, and Fusaro 2020). As mentioned above, the abandonment of HAS1 took place roughly between the end of the 1st century and the 2nd century AD. On the North-eastern side of the site a rectangular structure, built on top of the destruction layer that generally covers the traditional circular structures of the HAS1 settlement, has been excavated by DHOMIAP (Lischi 2018). The structure is believed to be the only example of a structure built

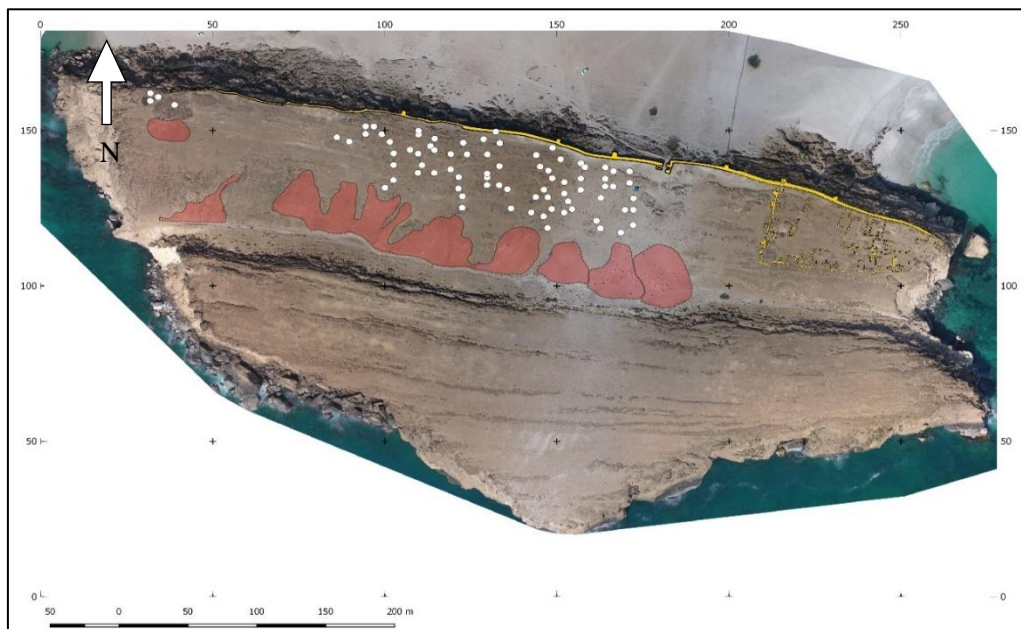


Figure 2.3: Aerial image of the Inqitat plateau with the HAS1 structures highlighted in white, HAS2 structures highlighted in yellow and the middens highlighted in red (DHOMIAP project).

after immediately the abandonment of HAS1 and its similarity to the structures from Sumhuram would suggest its relationship with the city (Lischi 2018).

2.4.2 Sumhuram

As mentioned above, the site of Sumhuram is the easternmost located city of the Hadramawt kingdom. The foundation is dated between the end of the 3rd century and the beginning of the 2nd century BC and it was occupied until the beginning of the 5th century AD (Buffa 2019). The earliest layers of occupation of the city present, along together with local material, also Indian artefacts *in situ* (Buffa 2019). The foundation of Sumhuram in the Dhofar can be related to two important aspects: the Dhofar is famous for the production of frankincense and the location along the Wadi Darbat, which was protected by two rocky plateaus at its mouth, was ideal for a port. The origin of the knowledge of this specific location within the Dhofar region, however, is yet unknown, but it proved to be a fruitful choice, especially when Sumhuram not only developed as a city, but also was included in the international network of trade connections. The settlement of Sumhuram (Fig. 2.4) was first excavated in the 1950s by an American mission, while later in the 1990s the IMTO started working on it until 2019 (Buffa 2019).

The colony was built on top of a limestone hill that dominates over Wadi Darbat. The dimensions of the site follow the dimension of the hilltop and there is evidences of some territorial control outside the city walls, such as the farm villages, the building in Inqitat and the extra-mural temple, (Buffa 2019). The city is surrounded by a monumental perimeter of walls with defensive towers and elaborate gates to control access to the city. Inside the walls, the city shows a well-structured urban organisation with one main road going from the main temple to the building defending the well of the city. On the south-eastern side of the city the archaeologists have excavated what were identified as warehouses built around a central square, which was identified as the market place (Avanzini 2011). On the opposite side of the site, the residential area was identified. The houses were probably at least two storeys tall with the ground floor being built with stone blocks and the first floor being constructed with mudbricks. The city seems to lack a specific location for a production area, while small kilns and simple furnaces can be found quite well-spread around the city (Avanzini 2011). Within the site of Sumhuram, two temples were identified. One, as already mentioned, is located outside the walls, towards the wadi. The other temple is located within the walls. It is dedicated to the moon goddess Sin and it was located at one end of the main road. Within the city there was also a shrine which was well decorated and it presents the motif of a snake. Such a symbol was not common within the South Arabian culture, but it was very much common in the Gulf coast of modern day Oman. The presence of the snake symbol probably represents some degree of integration of the local culture within the South Arabian culture of

Sumhuram (Avanzini 2011). The water supplies of the city were guaranteed by a well within the city, which was surrounded by a building that was probably protecting it. The building shows numerous different phases of construction and, from it, a very complex water system expanded throughout the city's walking surface and/or underground (Avanzini 2011). Sumhuram, according to the artefacts retrieved, was not only an outpost for trade and frankincense redistribution, but was also a local production centre for metal objects. Even if there are no signs of primary metal working, evidence of secondary metal production is attested to in Sumhuram with the additional possibility of minting activities at the site (Avanzini 2011). Further particular findings that need to be mentioned, are an headless Indian bronze statuette found by the American Mission in 1953, and the head of another bronze statuette excavated by the IMTO (Fig. 2.5) (Avanzini 2011; Pavan 2016). The headless statuette is identified as Salabhanjika which is interpreted either as a goddess or as a young woman. Such a character is gifted with the ability of making tree bud with the touch of her foot (Autiero 2018). On the other hand, the bronze head was excavated close to the entrance of the storage area dating 3rd AD. The identification of the head, representing Shiva, is complicated by the poor preservation conditions (Pavan 2016). However, more than the meaning of the statuettes themselves, the highlight here is on the nature of the statuettes. Similar Indian objects, in contrast to material from pottery or traditionally traded goods, are very rarely found in any of the regions involved in the maritime trade connections (Avanzini 2011). In the case of South Arabia, only two bronze plaques are identified in addition to the two bronze statuettes (Fig. 2.5). The first plaque, the "Hombrechtikon plaque", combines typically South Arabian motifs with typically Indian ones, while the second plaque, now located in Wien, is composed of a central panel, representative of the phallic symbol of Shiva, the "*linga*", while the other two panels are believed to be later copies attached to it (Pavan 2016). Examples of similar artistic value coming from the Indian subcontinent are rare, and an example of a similar object of Indian provenance is the Indian Lakshmi ivory statuette (Fig. 2.5) found in Pompeii and now exposed in the Archaeological Museum of Naples (D'Ancona 1950).



Figure 2.4: Aerial view of the site of Sumhuram (IMTO project).

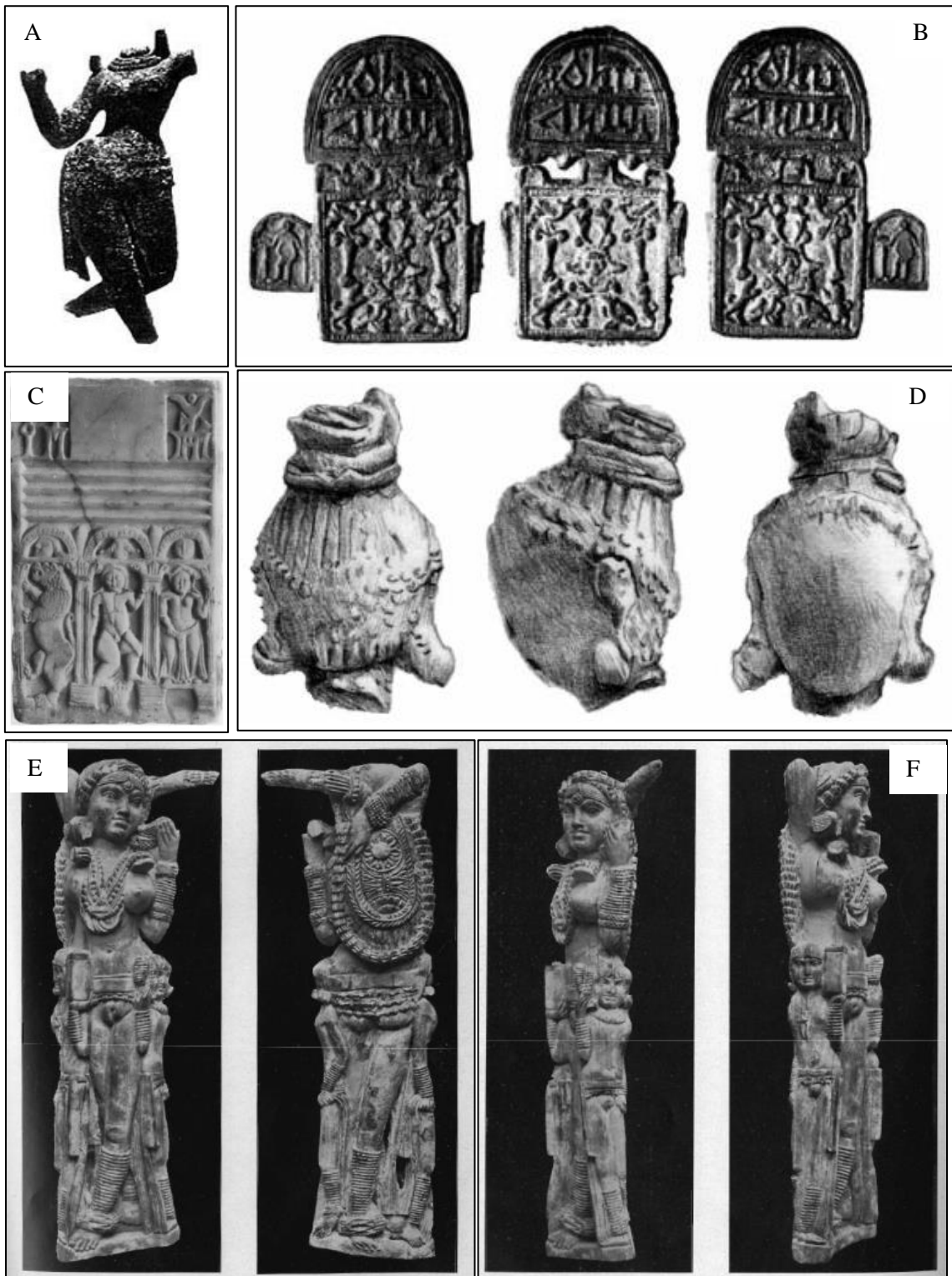


Figure 2.5: A) Headless statuette from Sumhuram (after Avanzini 2011). B) Bronze plaques from South Arabia representing the Indian motif "linga" (after Pavan 2016). C) "Hombrechtikon plaque" from South Arabia with the Indian goddess Yaksi on the right (after Pavan 2016). D) Bronze head tentatively identified as Shiva from Sumhuram (after Pavan 2016). E-F) Ivory Statuette from Pompeii (after Maiuri 1939).

2.5 Historical sources

Historical sources describing the trade taking place within the Indian Ocean are mainly limited to a handful of Indian sources and those of Greek and Roman writers. More specifically, the Greek and Latin written sources are “Geography” from Strabo, “Geography” by Ptolemy, “Naturalis Historia” by Pliny the Elder and the most famous one: “Periplus Maris Erythraei”, the author of which is still unknown. Of those, only the Periplus Maris Erythraei mentions the site of *Moscha limes* which has been identified as the site of Sumhuram in the 19th century (Avanzini 2011).

Sources regarding the trade from other cultural perspectives are limited to some written works from the Indian subcontinent where they mention Westerners, “Yavanas”, arriving in India or being present in the subcontinent (Hart 1999). Probably the most important piece of information regarding the arrival of merchants in India from the west can be found in the Akananuru where the harbour of Muziris is described as: “[...] the rich Muziris where the ships, perfect and amazing creation of the Yavanas, come with gold and leave with pepper [...]” (Akananuru 149, 7-16). Another passage worth mentioning can be found in the Puranànu, where it is possible to read about the Westerners who “[...] with ships they bring golden gifts brought to the shore with small boats” (Puranànu 343, 1-10).

Coming back to the *Periplus Maris Erythraei* (from now on referred as “PME”), it is believed to be a technical book for merchants with their economic interest set in Egypt. It describes the best routes to follow in order to go and come back from India, together with the route to follow to sail along the Eastern African coast (Seland 2008). It also mentions the most profitable goods to sell and buy in the different ports found along those routes (Avanzini 2011). It is with this practical objective that the unknown author of the PME in paragraph 32, talking about Sumhuram, says:

“Immediately after Syagros is a bay indenting deeply into the coast, Omana, [...] and, after these, a designed harbour for loading the Sachalite frankincense, called Moscha Limen. Some vessels are customarily sent to it from Kane; in addition, those sailing by from Limyrike or Barygaza that passed the winter [sc. At Moscha] because of the season being late, by arrangement with the royal agents take on, in exchange for cotton cloth and grain and oil, a return cargo of frankincense [...]. For, neither covertly nor overtly can frankincense be loaded aboard a ship without royal permission; if even a grain is lifted aboard, the ship cannot sail, since it is against the god’s will” (PME 32, 26-7).

By carefully analysing this part of the PME, De Romanis notices that the site of Sumhuram is not classified as an “emporium”, which would define a harbour for trade, but is identified with the classification of “limen”, an outpost for the redistribution of frankincense, a product, which is

mentioned as the main production of the Dhofar region and very famous (Avanzini 2011). In the same chapter within “Along the aroma and spice routes” (Avanzini 2011), De Romanis also analyses the type of trade connections in which the site of Sumhuram is the centre and he underlines the existence of 2 types of movements described by the passage of the PME presented before. The first route involving Sumhuram was bringing ships from Kane (one of the main trading harbours of the Hadramawt kingdom, towards the Red Sea) to Sumhuram to collect frankincense to bring back to Kane. Once in Kane, the frankincense was sold to Roman-Egyptian traders coming from the Red Sea, the whole mechanism was under the king’s management. The second direction of movement involving the site of Sumhuram was that of the long-distance traders coming back from Limyrike and Barygaza, who were stopping at the port to exchange oil, grain and cotton for frankincense. In the PME it is mentioned that those arriving in Sumhuram from India too late in the winter and probably not early enough to have favourable winds to reach Egypt, were stopping for the early months of the year at the Arabic port. These in particular, pushed De Romanis to distinguish two groups within the long-distance traders: those departing from India in the early winter monsoon season, stopping to load some autumn frankincense and leaving for Egypt, and those not able to safely reach Egypt. The latter were then stopping in *Moscha*, spending the winter there and then, as De Romanis suggests, they were loading the lower quality frankincense produced in spring and going back to India to sell it and to start the cycle all over again (Avanzini 2011).

However, De Romanis is using only the PME as source of interpretation, and he is mainly focusing on the Roman side of the trade. On the contrary, Seland (Seland 2008) observes the same trade network, but from the Indian point of view. In addition, he also uses literature from the later Medieval and Colonial period to better understand the mechanism of the monsoons in the Arabian Sea. In doing so, Seland noticed that the ships wintering in *Moscha* were not only Roman ships, but they were mainly Indian ships that were completing the trading voyage and waited in Sumhuram for the next suitable period to sail back to India. Indian ships that were traveling back across the Arabian Sea had specific periods in which to sail, because the Summer monsoons (the one blowing from west to east) were responsible for heavy storms, causing the closing of the main harbours on the Indian coast. The result is that it is much easier for Indian ships to decide to stop in Sumhuram and wait for safe weather conditions to sail towards India (Seland 2008).

2.6 Pottery

Pottery is probably one of the most important and common classes of artefacts for archaeologists and archaeological interpretations. Characterized by very strong resistance to weathering, pottery is commonly present in all settlements of sedentary populations, while it is not commonly used

by nomadic people. In many cases, due to its brittle nature, pottery is retrieved fragmented and incomplete. Despite the fragmentary nature of the artefacts, pottery has been at the centre of archaeological analysis for most of the history of archaeology, and it is still very much one of the cores of archaeological research. One of the most important aspects of ceramics is that, by being constantly present in every site, and by being subject to manifestations of cultural variations, it has been the bases of relative dating and cultural identification in archaeology. Seriation was, until the discovery of radiocarbon dating, the main dating method, in the absence of historical sources. Nowadays, even if relative dating is still important in the absence of possibilities for absolute dating, typology and typological identification of pottery is the main subject of analysis related to ceramic finds. More precisely, the wide range of aspects that can be studied for the identification of pots, is allowing pottery to continuously be fundamental for archaeological identification (Velde and Druc 1999).

In this thesis, the research question focuses on the provenance of the ceramic artefacts taken into consideration. The provenance analysis done on the samples, until now, was focused on a stylistic approach and, to some extent, on the petrographic analysis. In this thesis, on the other hand, the approach is focused on the use of archaeometric techniques (such as ICP-MS, SEM-EDS, XRD and petrography) to study the samples, with the aim of reaching a much deeper understanding of each and every single sample in order to, then, be able to divide different samples by means of different raw materials. The identification of the ceramic origins is possible thanks to the fact that the composition of the clay and temper collected in one place is defined by the nature of the geology of the region from which it weathered off, as explained in the next paragraph. The analysis of raw materials provides more certainty in the definition of different proveniences than stylistic analysis, because it looks at the geological origins of the clay and temper, which are rarely collected from very far away from the production area. On the other hand, ideas regarding pottery shapes can travel very far. An example of the combination of foreign culture and local raw material is represented by some amphorae retrieved in Sumhuram. Amphorae are generally identified as of Roman production, but in Sumhuram some amphorae made with a raw material very rich in talc inclusions were found, and talc inclusions are a characteristic of the ceramic production from the area South Arabia, modern day Yemen (Pavan and Pallecchi 2009).

In Sumhuram and Inqitat, local pottery is accompanied by foreign pottery. The definition of local pottery, by itself, is complicated. The main problem is represented by the scarcity of local material within the general amount of ceramic retrieved. In addition to that, the definition of material as “culturally local”, meaning that it is part of the culture, does not exclude the possibility that it has been produced far away making the distinction of local and non-local even more challenging.

On the other hand, within the corpus of ceramic artefacts retrieved within the context of Sumharam and Inqitat, it is possible to find ceramics coming from the Persian Gulf area, the Mediterranean region, the Red Sea and from as far as India (Pavan 2017). The presence of such a large variety of materials and origins is one of the reasons why analysing ceramic material from Sumharam and Inqitat is of extreme importance for a better general understanding. In addition to that, it is important to underline that Indian pottery is found in Sumharam as early as the beginning of the 2nd century BC, the time of its foundation, and Indian vessels are also found *in situ* within some of the residential structures in Inqitat under the destruction layer.

3. Materials





The analyses presented here were conducted on 35 samples spanning from the end of the 1st millennium BC to the end of the 4th century AD; 18 samples from the site of Inqitat (HAS1) and 17 samples from Sumhuram. The selection of the samples was done by Silvia Lischi and it faithfully translate the variety of Indian and local samples.

The definition of provenance was based on a stylistic analysis of the samples. However, the distinction was limited to macro areas such as the Indian subcontinent or the Arabian Peninsula. In fact, when we talk about “local” samples, we indicate materials with Arabic origins, but, among them, the actual local samples made in the Dhofar region and the ones from other areas of Arabia are not always distinguishable. The same problem is identifiable among the Indian samples. In fact, the definition of the region within India from which the samples are coming is not always possible. That is due to a combination of lack of understanding of ceramic distribution in India and because of a lack of study on the raw materials themselves.

The main purpose of the analysis, as explained in the introduction, is to develop a general understanding of the differences between Indian and Arabic samples, but, also, to explore the possibility of separating different groups of samples according to the combination of raw material characteristics and technological differences, with the intention of defining the provenance of them. It was with this main objective that the sample selection aimed to include a large variety of different samples including different fabric types and vessel types. In Tables 3.2 and 3.3, the 35 samples are presented with the definitions of which type of fabric group they are part of, according to the classification described in “A Cosmopolitan City on the Arabian Coast: The imported and local pottery from Khor Rori. Khor Rori Report 3” (Pavan 2017) and reported in Table 3.1. The identification is conducted by the author following the description of the groups presented in Pavan’s report (Pavan 2017). Samples from Inqitat are compared with the fabric types presented in Pavan’s report (Pavan 2017).

Tables 3.4 and 3.5 present the macroscopic description of each sample here considered for the analysis.

Table 3.1: Fabric types represented by the samples analysed in this thesis (Pavan 2017).

| Fabric Typology | General description comments | Examples of Fabric |
|---|--|---|
| <p>Black Slipped Ware (BSW)</p> | <ul style="list-style-type: none"> This ware type is characterized by black/dark grey core and black slip burnished or polished. Similar material can be identified in the so called Northern Black Polish Ware group as described by Odelli et al. (2020). |  <p>Figure 3.1: Sample IQM18A.US80.3.</p> |
| <p>Coarse Red Ware (CRW):</p> | <ul style="list-style-type: none"> Pottery rich in inclusions with un-levigated clay. Most of the samples are related to utilitarian vessels, but the definition of the group is quite large and it includes two subgroups CRW1 and CRW2. CRW1 is characterized by inclusions smaller than 1mm with a dark core and walls shifting from red to brown with some example of burnishing. CRW2 presents larger inclusions and a generally coarser feel. The type of ware (named differently in different archaeological sites) is largely associated with South Asian origins, even if the specific geographic origin is not well defined, yet. |  <p>Figure 3.2: Sample SUM11A.US174.232.</p> |
| <p>Fine Red Slipped Ware (FRSW):</p> | <ul style="list-style-type: none"> Very fine ware, with a well levigated clay constituting the red homogeneous body covered by an orange slip usually burnished or polished. No inclusion is visible within the fabric. FRSW is associated with material from South Asia, with a higher concentration located within the Gujarat area. |  <p>Figure 3.3: Sample SUM11A.US54.85.</p> |
| <p>Grit Temper Ware (GTW):</p> | <ul style="list-style-type: none"> Not common to find within Sumhuram. Characterized by very large inclusions and a general high friability of the fabric. The samples related to this group present no surface treatment. |  <p>Figure 3.4: Sample SUM09A.US297.2.</p> |






| | | | |
|--|--|---|---|
| <p>Paddle Impressed Ware (PDW):</p> | <ul style="list-style-type: none"> • the main characteristic is the presence of the impressions made with a grooved paddle on the surface. • Mainly connected to South-Eastern India and Sri Lanka in context datable from 1st century BC to 3rd/4th century AD. • Examples of PDW samples are found in Arikamedu in different fabrics, ranging from fine to coarse, with some not being made with local raw material. • Other examples are found in Egypt, where PDW is represented by two fabrics: one being red brown with grey core and silty matrix, the second being orange to orange brown with lighter surfaces |  | <p>Figure 3.5: Sample IQM16B.US23.13.</p> |
| <p>Red Slipped Ware (RSW):</p> | <ul style="list-style-type: none"> • Characterized by a hard and compact fabric, with some sand grains and some dark inclusions. • The finishing is characterized by a slip ranging from light red to red to red brown. • The core is usually reddish with some example of pinkish or brownish fabrics. |  | <p>Figure 3.6: Sample SUM10C.US162.119.</p> |
| <p>Shell Temper Ware (SHTW):</p> | <ul style="list-style-type: none"> • Shell tempered ceramics generally with reddish/buff colour of the fabric. • SHTW1 coarser version of the group • SHTW2 higher quality ceramics • SHTW has still direct comparison in the modern days indigenous ceramic production in the region of Dhofar, in the Sultanate of Oman |  | <p>Figure 3.7: Sample IQM16B.US35.8.</p> |
| <p>Steatite Temper Ware (STW):</p> | <ul style="list-style-type: none"> • Characterized by the very high concentration in soft-stone inclusions. • The composition is defined by the presence of soft-stone temper, greasy to the touch, and by a matrix that can vary from dark grey to pale brown with clear soot traces on the surfaces. • STW is quite characteristic of the ancient Yemen tradition being well documented in Hadramawt from 1st millennium BC till the 1st century. |  | <p>Figure 3.8: Sample SUMW03A.US1.1.</p> |
| <p>Vegetable Temper Ware (VTW):</p> | <ul style="list-style-type: none"> • Characterized by the presence of rice husks as main temper of the ceramic itself. • Regarding the fabric, most of the sample present a very dark colouring with few examples of lighter shades of red/brown. • The presence of such a large amount of rice husk within the matrix allows the pot to feel remarkably lighter than other wares of comparable dimensions. |  | <p>Figure 3.9: Sample SUM10A.US412.1.</p> |

Table 3.2: List of samples from Sumhuram.

| <i>Sample code:</i> | <i>Site</i> | <i>Excavation Year</i> | <i>Layer</i> | <i>Vessel Type</i> | <i>Fabric Type</i> | <i>Provenance</i> | <i>Comments</i> |
|--------------------------|-------------|------------------------|--------------|----------------------------|--------------------|-------------------|--|
| SUMW03A.US1.1 | SUM | 2003 | 1 | Bowl | STW | Local | Commonly present in early occupation layers. It slowly disappears by the 1 st century BC. |
| SUM08B.US162.104 | SUM | 2008 | 162 | Bowl | STW | Local | Commonly present in early occupation layers. It slowly disappears by the 1 st century BC. |
| SUM11A.US174.232 | SUM | 2011 | 174 | Lid-cum-Bowl | CRW | Indian | Commonly distributed in the sites related to the Indian Ocean trade. Dating from 1 st century BC to Medieval time. |
| SUM09A.US297.2 | SUM | 2009 | 292 | Carinated or globular pot | GTW | Indian | Part of the “Handi” Indian ware generally concentrated in South India, but commonly spread in the sites related to the Indian Ocean trade. Comparable to Wheeler’s Type 24. |
| SUM10C.US162.119* | SUM | 2010 | 162 | Bowl | RSW | Indian | Similar material in other sites like Kamrej and Nevasa dates to 2 nd /1 st century BC. Comparable with Wheeler’s type 2. |
| SUM11A.US54.85* | SUM | 2011 | 54 | ? | FRSW | Indian | The Vessel type, according to the author, needs to be revisited. The author of this thesis identifies it as FRSW. |
| SUM08A.US253.5 | SUM | 2008 | 253 | Carinated or globular pot. | CRW1 | Indian | Part of the “Handi” Indian ware generally concentrated in South India, but commonly spread in the sites related to the Indian Ocean trade. Comparable to Wheeler’s Type 24. |
| SUM10C.US174.79 | SUM | 2010 | 174 | Bowl | CRW1 | Indian | Similar material in other sites like Kamrej and Nevasa dates to 2 nd /1 st century BC. Comparable with Wheeler’s type 2. |
| SUM03A.US133.9* | SUM | 2003 | 133 | Carinated or globular pot | CRW1 | Indian | Similar material in other sites like Kamrej and Nevasa dates to 2 nd /1 st century BC. Comparable with Wheeler’s type 2. |
| SUM10A.US405.3 | SUM | 2010 | 405 | Carinated or globular pot | CRW1 | Indian | Similar material in other sites like Kamrej and Nevasa dates to 2 nd /1 st century BC. Comparable with Wheeler’s type 2. |
| SUM10C.US174.104 | SUM | 2010 | 174 | Shallow Bowl | VTW | Indian | - |
| SUM10A.US412.1 | SUM | 2010 | 412 | Carinated or globular pot | VTW | Indian | Similar material in other sites like Kamrej and Nevasa dates to 2 nd /1 st century BC. Comparable with Wheeler’s type 2. |
| SUM10C. US174.83 | SUM | 2010 | 174 | Lids-cum-Bowls | CRW | Indian | Commonly distributed in the sites related to the Indian Ocean trade. Dating from 1 st century BC to Medieval time. |
| SUM03B.US93.23 | SUM | 2003 | 93 | Table Jar | CRW | Indian | The dating of this type is to be roughly placed between the 2 nd century BC and the 3 rd century AD. |
| SUM09B. US309.4 | SUM | 2009 | 309 | Lamp/lid | CRW | Indian | Similar material, but not directly comparable, can be found in Sri Lanka, South Indian, Somalia and Arabia. It dates between the 1 st century AD and Medieval time. |
| SUM03B.US93.42 | SUM | 2003 | 93 | ? | CRW | Indian | The classification of the vessel type, according to the author of this thesis, needs to be revisited. |
| SUM08B.US975.4 | SUM | 2008 | 975 | - | - | Indian | Unclassified Indian cooking pot. |

(SUM) = Sumhuram, (*) = sample destroyed in the analysis process, (?) = Classification to be reconsidered according to the author of the thesis, (-) = data not available

Table 3.3: List of samples from Inqitat (Fabric Type defined by the author of the thesis)

| <i>Sample code:</i> | <i>Site</i> | <i>Excavation Year</i> | <i>Layer</i> | <i>Vessel Type</i> | <i>Fabric Type</i> | <i>Provenance</i> | <i>Comments</i> |
|-----------------------|-------------|------------------------|--------------|--------------------|--------------------|-------------------|--|
| IQM16B.US35.8 | IQM | 2016 | 35 | Pot | SHTW2 | Local | Wall of a pot with a tenon (pierced lug). Coarse fabric with many grey and white temper. Slightly smoothed surfaces. On the surface of the lug and on the wall, there are an incised decoration. |
| IQM18B.US119.5 | IQM | 2018 | 119 | Table/storage use | SHTW2 | Local | Fragment of wall with dot and circle motif decoration. |
| IQM17A.US58.5 | IQM | 2017 | 58 | Jar | SHTW2 | Local | Fragment of rim and neck of jar with short and vertical neck and flat rim. Small white inclusions, probably shell temper. Handmade. The colour of the fabric and the surfaces is blackish. |
| IQM17A.US58.8 | IQM | 2017 | 58 | Jar | STW? | Local | Fragment of rim and wall of jar with out-turned pointed rim. Pinkish fabric with big red inclusions and mica tempered. Handmade. |
| IQM16B.US35.34 | IQM | 2016 | 35 | Jar | STW? | Local (?) | Fragment of wall of a storage jar in mica ware (?) |
| IQM16B.US35.35 | IQM | 2016 | 35 | ? | STW? | Local | Fragment of wall of a mica ware |
| IQM16B.US35.33 | IQM | 2016 | 35 | ? | STW | Local | Fragment of wall of mica ware |
| IQM16B.US35.32 | IQM | 2016 | 35 | ? | STW | Local | Fragment of wall of mica ware |
| IQM16B.US30.6 | IQM | 2016 | 30 | Jar | CRW? | Indian | Fragment of a part of neck and shoulder of a big globular jars. There are two incised parallel line on the shoulder. The external surface is burnished. |
| IQM16B.US30.3 | IQM | 2016 | 30 | Jar | CRW | Indian | Fragment of out-turned rim of a storage jar with internal groove in the upper part of the wall. Internal and external surface are slipped and burnished. |
| IQM17A.US35.16 | IQM | 2017 | 35 | Jar | CRW | Indian | Fragment of rim of an Indian jar with out-turned rounded lip and almost triangular section, deep groove on the interior. Reddish medium coarse fabric with red and white inclusions. External and internal surfaces are burnished. |
| IQM16B.US35.31 | IQM | 2016 | 35 | Red Ware | CRW | Local | Fragment of wall of red ware |
| IQM17A.US35.18 | IQM | 2017 | 35 | Pot | CRW | Indian | Fragment of rim of pot with out-turned rim. Reddish fabric with red and white inclusions. The surfaces are slip and burnished. Very bad preserved. |
| IQM16B.US30.10 | IQM | 2016 | 30 | Jar (?) | CRW? | Indian | Fragment of wall of a storage container |
| IQM18A.US80.3 | IQM | 2018 | 80 | Jar | BSW | Indian | Table jar with flaring neck and enlarged everted rim. Slip or burnished on both sides. Secondary burning. |
| IQM16B.US35.9 | IQM | 2016 | 35 | Jar | CRW1 | Indian | Jar with short neck and simple everted rim, burnished surfaces. Light grey fabric with white, black and red temper. |
| IQM17B.US73.1 | IQM | 2017 | 73 | Storage use (?) | RSW? | Indian | Fragment of wall of a storage (?) container with orange slip on the external surface and in the upper part of the shoulder. |
| IQM16B.US23.13 | IQM | 2016 | 23 | Paddle Ware | PDW | Indian | Two fragments of wall of paddle ware |

(IQM) = Inqitat, (*) = sample destroyed in the analysis process, (?) = Unsure classification, (-) = data not available

Table 3.4: Table presenting a summary of the macroscopic description samples from Sumhuram

| Samples | | Description |
|-------------------|--|--|
| SUMW03A.US1.1 | <ul style="list-style-type: none"> • Thick walled • Inner wall and core brownish yellow | <ul style="list-style-type: none"> • Outer wall of a light grey |
| SUM08B.US162.104 | <ul style="list-style-type: none"> • Thin walled • Dark grey outer wall | <ul style="list-style-type: none"> • Inner wall of bright red • black and red separation is abrupt |
| SUM11A.US174.232 | <ul style="list-style-type: none"> • Thick walled • Reddish brown core and inner wall | <ul style="list-style-type: none"> • Blackening of the outer surface |
| SUM09A.US297.2 | <ul style="list-style-type: none"> • Thick walled • Light red core | <ul style="list-style-type: none"> • Light red surfaces • Out turned rim |
| SUM08B.US975.4 | <ul style="list-style-type: none"> • Thin walled • Reddish grey core • Red interna and external surface | <ul style="list-style-type: none"> • Soot marks • Out turned rim |
| SUM11A.US54.85* | <ul style="list-style-type: none"> • Very thin walled • Homogeneous orange-red core and surfaces | <ul style="list-style-type: none"> • Out turned simple rim |
| SUM08A.US253.5 | <ul style="list-style-type: none"> • Very thin walled • Very dark grey core | <ul style="list-style-type: none"> • Red internal and external surface • Presence of a slip |
| SUM10C.US174.79 | <ul style="list-style-type: none"> • Thin walled • Very dark grey core | <ul style="list-style-type: none"> • Red internal and external walls • Presence of a slip |
| SUM03A.US133.9* | <ul style="list-style-type: none"> • Thin walled • Grey to dark grey core | <ul style="list-style-type: none"> • Red internal and external walls |
| SUM10A.US405.3 | <ul style="list-style-type: none"> • Medium thick wall • Red core and walls | <ul style="list-style-type: none"> • Darkening of the rim |
| SUM10C.US174.104 | <ul style="list-style-type: none"> • Thick walled • Porous body | <ul style="list-style-type: none"> • Black core • Dark grey-brown walls |
| SUM10A.US412.1 | <ul style="list-style-type: none"> • Thick walled • Black core and inner wall | <ul style="list-style-type: none"> • Dark grey-brown outer wall • Porous body |
| SUM10C. US174.83 | <ul style="list-style-type: none"> • Thick walled • Light reddish grey core | <ul style="list-style-type: none"> • Light red walls |
| SUM03B.US93.23 | <ul style="list-style-type: none"> • Thin walled, thick rim • Reddish brown core | <ul style="list-style-type: none"> • Light brown internal wall and upper rim • Dark brown outer wall with soot marks |
| SUM09B. US309.4 | <ul style="list-style-type: none"> • Thick walled • Yellowish grey core | <ul style="list-style-type: none"> • Greyish light red walls |
| SUM03B.US93.42 | <ul style="list-style-type: none"> • Thick walled • Grey core | <ul style="list-style-type: none"> • Red walls • Possible weathered slip |
| SUM10C.US162.119* | <ul style="list-style-type: none"> • Very thin walled • Brownish red core | <ul style="list-style-type: none"> • Red surfaces • Red slip |

Table 3.5: Table presenting a summary of the macroscopic description samples from Inqitat

| Samples | | Description |
|----------------|---|--|
| IQM16B.US35.33 | <ul style="list-style-type: none"> • Brown core | <ul style="list-style-type: none"> • Dark brown surface |
| IQM16B.US35.32 | <ul style="list-style-type: none"> • Brown core | <ul style="list-style-type: none"> • Dark brown surface |
| IQM16B.US35.31 | <ul style="list-style-type: none"> • Thin walls • Dark grey core | <ul style="list-style-type: none"> • Red surface • Presence of a slip on the external wall |
| QM16B.US30.6 | <ul style="list-style-type: none"> • Thick walled • Light grey core | <ul style="list-style-type: none"> • Dark grey internal wall • Reddish-brown external wall with soot marks |
| IQM16B.US30.3 | <ul style="list-style-type: none"> • Thick walled • Light grey core | <ul style="list-style-type: none"> • Light red towards the surfaces • Out turned rim |
| IQM17A.US35.16 | <ul style="list-style-type: none"> • Thick walled • Light grey core | <ul style="list-style-type: none"> • Light brown external surface • Out turned rim |
| IQM17A.US35.18 | <ul style="list-style-type: none"> • Thick walled • Light grey core | <ul style="list-style-type: none"> • Bright light red surfaces • Out turned rim |
| IQM16B.US23.13 | <ul style="list-style-type: none"> • Thin walled • Yellowish core and inner wall | <ul style="list-style-type: none"> • Grey – dark grey outer wall • Paddle impressions |
| IQM16B.US35.9 | <ul style="list-style-type: none"> • Medium thick walled • Light grey core | <ul style="list-style-type: none"> • Red surface • Out turned rim |
| IQM17B.US73.1 | <ul style="list-style-type: none"> • Thin walled • Light grey core and inner wall | <ul style="list-style-type: none"> • Red slip covering the outer wall and the inner side of the missing rim |
| IQM16B.US30.10 | <ul style="list-style-type: none"> • Thick walled • Light grey core and inner wall | <ul style="list-style-type: none"> • Reddish brown outer surface with soot marks |
| IQM18A.US80.3 | <ul style="list-style-type: none"> • Thin walled • Grey core | <ul style="list-style-type: none"> • Black slip covering the surface • Out turned rim |
| IQM18B.US119.5 | <ul style="list-style-type: none"> • Thin walled • Light grey core and internal wall | <ul style="list-style-type: none"> • Light red external surface • Stripe and dot impressed decorations |
| IQM16B.US35.8 | <ul style="list-style-type: none"> • Thin walled • Dark grey core • Greyish yellow surfaces | <ul style="list-style-type: none"> • Small handle • Surface of handle and outer wall decorated with linear incisions |
| IQM17A.US58.5 | <ul style="list-style-type: none"> • Thin walled • Dark grey-brown core and surface | <ul style="list-style-type: none"> • Rich in white inclusions • Roughly out turned rim |
| IQM17A.US58.8 | <ul style="list-style-type: none"> • Thin walled • Dark grey-brown core and internal surface | <ul style="list-style-type: none"> • Light grey-brown outer surface • Out turned rim |
| IQM16B.US35.35 | <ul style="list-style-type: none"> • Thin walled • Greyish light brown core and external wall with soot marks | <ul style="list-style-type: none"> • Darker internal wall |
| IQM16B.US35.34 | <ul style="list-style-type: none"> • Thick walled • Light reddish-brown core and internal wall | <ul style="list-style-type: none"> • Grey outer wall |

4. Methodology

As previously mentioned, the aim of this project is to identify the main differences between locally and non-locally produced ceramic material excavated at the site of Sumhuram and the nearby site of Inqitat in Oman. In order to do so, the project combined a series of analytical methods aimed to define the specific characteristics of each artefact from as many different points of view as possible. More precisely, the aspects that were considered for the characterisation of local and non-local materials are the elemental composition, including major and trace elements, the identification of the minerals constituting the sherds and the definition of specific technological aspects, such as temper composition, inclusions selection and distribution, firing process and decoration.

With the aim of collecting all the data and information presented above, the author used the following analytical methods: Inductively Coupled Plasma Mass Spectrometry (ICP-MS), X-ray Diffraction (XRD), Polarized Petrographic Microscopy and Scanning Electron Microscopy coupled with Energy Dispersive X-ray Spectroscopy (SEM-EDS). The combination of such a diversified analytic methodology and data set allows us to define specific characteristics of the ceramic composition at different levels of material characterization. All the effort presented here for the identification of technological and raw material identification is based on two assumptions:

1. Ceramic material is made with raw material that is found close to the production site.
2. Different technological characteristics can be considered as a signature of the production centre itself, or of the culture of which they are the product. In case of similar technologies with different raw materials, we need to consider the possibility of ideas being transferred from one to other cultures.

In this chapter, the steps followed for the sample preparation and analysis are presented, divided by type of analysis. However, before the specific description of each analytical process, the presentation starts with the preparatory steps done which are common for all the analytical methods. All the sample preparation and analysis, except for the resin impregnation and thin section preparation, were conducted at the HERCULES Laboratory, University of Évora, in Évora (Portugal). The thin sections were prepared separately at the Geosciences Department of the University of Évora.

4.1 Photographic recording

The first and most important step done regarding the recording and preservation of heritage is taking pictures of the samples still untouched. The importance of this step lies in the fact that not all the samples were recorded before starting the analysis. Photographic recording of archaeological objects is the basic step to do before any modification of the sample. In this case, photographic recording was even more important, because of the destructive techniques included in this project (Mirulla 2018). Photographic recording of the samples aims to record the actual shape of the material in a way that allows future researchers to also have a good understanding of the general shape and characteristics of the artefact. In the case of the photographic recording for this project, the indications presented by Mirulla F. (Mirulla 2018) were followed, and the pictures were taken with a Sony x100 with 300mm and 50-70mm objective. The pictures were taken using a white background and a generic ruler as reference for the dimensions of the object, with the sample tag located near the object in order to be able to always identify the sample. The artefacts were recorded in at least 3 different orientations, recording the front, the back and at least one of the fractured sides. If needed, in case of more complex shapes and in the presence of specific characteristics that needed better recording, the number of pictures could exceed the 3 basic ones.

4.2 3D recording

As supplement to the photographic recording, in the case of complex shapes, 3D models were reconstructed by means of photogrammetry, with the support of the software 3DF Zephyr Free. With 3D reconstruction, the decorations and the complex shapes are better understandable, and significantly more evident than with photography, allowing a better perception of the specific distribution and organisation of the sample, in particular for samples which were going to be partially or completely destroyed for the analysis. The recording of shapes and decoration is of extreme importance in terms of the role that such shapes and decorations had in defining a culture, and defining the practical use of the vessels themselves. The 3D photogrammetry reconstruction, in this specific case, was applied only to samples IQM16B.US23.13, IQM16B.US35.8, IQM17B.US73.1, IQM18B.US119.5 (Fig. 4.1), SUM03B.US93.42 (Fig. 4.1), SUM09B.US309.4, SUM10C.US174.83 and SUM11A.US174.232. The selection of the samples for 3D reconstruction was based on the fact that the nature of those samples was more articulated and complex, making it difficult to produce good images by photography. 3D is, therefore, necessary for better visualisation and understanding of the decorations and of the articulated shapes for future researchers.

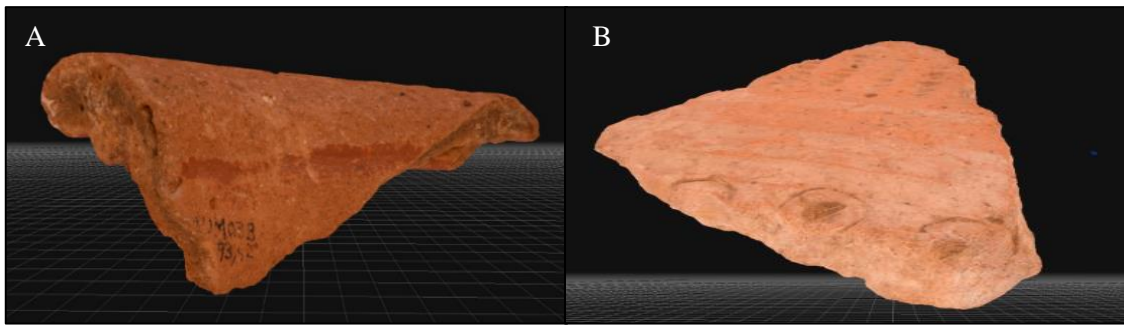


Figure 4.1: A) Image of the 3D reconstruction of sample SUM03B.US93.42 done by the author. B) Image of the 3D reconstruction of sample IQM18B.US119.5 done by the author

4.3 General Sample Preparation

In the following section, the general preparation preceding the analysis of the samples is presented. In order to conduct the different analyses mentioned in the introductory section, the samples needed to be powdered, digested and sectioned to a thickness of 0.03mm.

To properly prepare the samples, cutting off two pieces from each of the artefacts, powdering and impregnating those pieces was needed. The cutting was done by using a circular Discoplan saw and the aim was to collect two pieces of the sample without causing unnecessary damage. The first piece was of roughly 10 g and it was destined for powdering, the second was smaller and was destined for resin impregnation. The selection of the part to cut off was based on three principles:

1. Least invasive as possible.
2. Include the largest variability present within the sample structure.
3. Avoid contamination.

The reason for making an effort to be the least invasive as possible, is explained by the desire and the responsibility of modern researchers to preserve the value of the artefact, and to allow future generation to still be able to study the same artefact. In the process of preparing the samples, unfortunately, some samples were completely destroyed due to their already small dimensions. It is in eventualities like this, that taking pictures of the samples is fundamental. On the other hand, the purpose of including the largest variability possible within the resin-destined pieces, is related to the fact that once the thin section is ready, the analysis conducted on it will be considered to be representative of the whole sample. Such an assumption implies the necessity for the thin section to be the best representation of the sample's variability. Last, but not least, avoiding contamination imposes the need to be careful in the selection of the best way of cutting the samples. Particularly

important for elemental analysis, the inclusion of glues and or codes written in permanent marker directly on the sample, could be responsible for an alteration of the results of the analysis.

After cutting, the 10g samples were left to dry at 40°C for one day and then powdered. The powdering was initialised by hand on an agate mortar and completed using the automatic mill Retsch PM100. The powder of each sample was then stored in test tubes and, before every use, the open test tubes were stored in the oven at 40 °C in order to avoid the presence of humidity with the sample.

Contrary to the bigger pieces, the small cuts were destined to be impregnated in resin. The aim of the impregnation process is to produce 0.03m thick thin-sections for optical microscopy purposes. In order to prepare such a thin section of a fragile material like ceramic, resin impregnation is needed because it consolidates the macrostructure of the object. In the case here presented, the samples were impregnated with coloured resin. Colouring the resin was done with the purpose of make voids easier to identify, and to allow for possible future quantification of the voids, by means of image analysis. The impregnation was done using EpoResine mixed with EpoDye and, after 24h of mixing the resin and the colorant, EpoFix was added and heated up in order to allow the hardener to mix well with the solution. The heating is also important to make the solution more liquid increasing its impregnation capacity. The proportions used were 500 ml of EpoResine mixed with 2.5 g of EpoDye and 60 ml of EpoFix. To impregnate the samples, they were inserted in flexible plastic containers which were filled up with the resin solution, and left to rest for a weekend, allowing the resin to penetrate deep into the sample and, then, solidify. Unfortunately, all the process was done in a normal environment, due to the lack of a vacuum chamber in which to conduct the impregnation process. The consequence of doing the process in normal pressure is that not all the voids are filled up with resin, because of the permanence of bubbles of air within the voids. After the impregnation was completed, the desired side of the sample was glued to the glass support, after grinding off the resin covering it. In order to glue the samples to the glass, Bühler resin was used, also coloured with EpoDye with the following proportions: 5.45 g of Bühler resin, 0.05 g of EpoDye and 2.45g of EpoFix. The selection of the resin was dictated by its lower viscosity, and the smaller dimension of the internal structured formed, after solidifying. The colouring of the glue was needed in order to have a homogenous colouring of the resin within the thin section. The last step needed, after cutting a thin section of the sample with GTS1 Thin Section Cut-Off and Trim Saw, was the grinding and polishing of the samples, in order to reach 0.03mm of thickness. The larger part of the work was done mechanically with a Logitech PM5 using a mixture of 157.5 g of fine silicon powder grit size 600 in 1.5 l of water as a grinding agent. When the samples are close to the optimal thickness, a short polishing process was done by using

sandpaper grit size 1000 in order to reach the desired thickness with a nicely polished surface, which makes the understanding the components easier at the microscope.

4.4 Optical Microscopy

Petrographic analysis of the samples aimed to provide a direct observation of the sample composition, structure and technological characteristics. The functionality of Optical Microscopy applied to ceramics is bound to the ability of light to pass through the sample. It is for this reason that thin sections are prepared. The importance of having light passing through the sample is dictated by the fact that, in conditions of polarized light, the different behaviours of the light passing through the sample are the discriminants used to identify different components.

After the thin section preparation was completed, the samples were analysed by means of a polarized microscope Leica DM 2500P on which the camera Leica MC170 HD was mounted, in order to communicate with the software Leica Application Suite V 4.4, used to visualise and save the images. The identification of the components was done by observations of the different behaviours of the light passing through the sample and the comparison of the observation with reference materials. The general structure, general distribution of the inclusions and the description and identification of the inclusions, are the type of data collected with this method, as explained by P.S. Quinn in “*Interpreting Silent Archaeology: Petrographic Approaches to Archaeological Ceramics*” (P.S. Quinn, 2009).

4.5 Loss on Ignition (LOI)

Loss on Ignition (LOI) is the determination of volatile material that is lost at 1050°C from the samples. Such evaluation is needed both for a better understanding of the material analysed, and also to collect preliminary data for subsequent techniques. In fact, LOI indicates how much of the total weight of the sample is lost during 2h of heating the sample at 1050°C. This information is useful both to better understand the composition of the ceramic, but also to know how much of the sample is lost in the preparation of XRF pellets, if XRF analysis takes place. Unfortunately, even if initially planned for this research, XRF analysis could not be done on account of the machine being fixed.

The preparation of the samples for LOI analysis was done by adding 0.5-1 g of sample powder in a crucible that was then put inside a Nabertherm 30-3000 °C oven at 1050°C for 2h. The percentage of weight lost in the heating process was then calculated by comparing the weight of the sample before and after the heating process. Unfortunately, after the heating process, the

powder used for the analysis was thrown away. The necessity of throwing away the powder is dictated by the fact that the sample undergoes important compositional and structural alteration during the heating process, making it inappropriate for further analysis.

4.6 X-ray Diffraction (XRD)

XRD analysis were conducted on the powdered samples with the purpose of studying the different mineral comprising of both the matrix and the inclusions present in the ceramic samples. In order to have a better general picture of the composition, powdering is necessary, but in this case the analysis does not modify the composition of the powdered sample, allowing the reutilisation of the same sample. The powder preparation is that presented above. The analysis was conducted using a Bruker AXS D8 Discovery XRD with the Da Vinci design, with a Cu K α source operating at 40 kV and 40 mA, and a Lynxeye 1-dimensional detector. The scans were run from 3 to 75 ° 2 θ , with 0.05 2 θ step. The identification of the phases was done by the researcher with the support of the software Diffrac.Suite™ provided by Bruker. The process of the identification of peaks was based on the combination of possible matches presented by the software, and on the selection of the right matches by the author.

The subsequent step was characterized by the rough quantification of the phases identified as components of the powdered sample. The process is not an exact quantification, because it is based on the dimensions of the peaks, but it can be used and considered as guideline for a general understanding of the composition of the sample. The result of the quantification analysis is the presentation of the composition per percentages.

4.7 Inductively Coupled Plasma Mass Spectrometry (ICP-MS)

The ICP-MS analysis were conducted following the methods used by Eggins et al. (1997), Ottley et al. (2003), Finlay et al. (2012) and Beltrame et al (2019). The method consisted of the digestion of approximately 100 mg of powdered sample in PFA Savillex® beakers. The digestions were done in 3 different cycles in order to attack the different components of the ceramic material.

The first cycle of digestion was focused on the digestion of silicates by means of a solution composed of 2 mL 47% HF (OPTIMA grade) and 0.5 mL of 65% HNO₃ (Suprapur grade), for 48 h on a hotplate at 100 °C. Following the 48h, the samples were dried by means of evaporation. However, the evaporation was not complete in order to avoid the precipitation of the recently digested components, and the formation new stable compounds. Following the evaporation, the samples were subjected to the second cycle of digestion with 2mL of freshly-made Acqua Regia

solution composed of 3 parts of HCL and 1 part of HNO₃. The mix was left on the hot plate at 100°C for 24h. The last cycle of digestion was conducted the following day, after the nearly complete drying of the samples, with the addition of 2mL of pure NHO₃ (65%) to the samples to digest the remaining organic material at 100° for 24h.

After drying the samples following the 3rd and last cycle of digestion, the final solution for the trace elements was prepared by adding 1.6mL of NHO₃ (65%) and then filled with milliQ water up to a final complete volume of 50mL. The aim was to reach a solution concentration of NHO₃ \cong 2%. For the analysis of the major elements, namely Na, Mg, Al, P, K, Ca, Ti, Mn, and Fe, the solutions presented above were diluted by mixing 100 μ l of sample solution with 9.900 μ l of HNO₂ 2% concentrated. The reason for the dilution of the sample solution for the analysis of the major elements is that the concentration of the major elements is very high, high enough to possibly cause problems in the counting itself. The final analysis was conducted on an Agilent 8800 ICP Triple Quad (ICP-QQQ). Prior to the analysis, the equipment is always calibrated with the internal tuning solution provided by producer company Agilent. Moreover, before starting the analysis on the actual sample material, a Calibration Curve of the series of analysis was prepared by the analysis of 10 differently concentrated solutions of NHO₃ (2%) and Standard A and Standard B. The concentrations reached of Standard A and Standard B are: 0ppb, 5ppb, 10ppb, 20ppb, 50ppb, 100ppb, 200ppb, 400ppb, 800ppb, 1600ppb. The different concentrations of the known standards were needed to check the behaviour of the machine while counting the different elements during the analytical process. The elements taken into consideration for the analysis were the following: Na, Mg, Al, P, K, Ca, Ti, Mn, Fe, Sc, V, Cr, Co, Ni, Cu, Zn, Ga, Ge, Rb, Sr, Y, Zr, Nb, Cd, Sn, Sb, Cs, Ba, La, Ce, Pr, Nd, Sm, Eu, Gd, Tb, Dy, Ho, Er, Tm, Yb, Lu, Hf, Pb, Bi, Th, U. Unfortunately, it was not possible to analyse Si.

The validity of the elemental quantification was verified by the preparation of triplicates of each sample and the comparison of the counts amongst them. In the case of anomalies caused by contamination of one of the triplites during the sample preparation, the contamination would then be visible in the different counts of the elements. On the other hand, the accuracy of the general process of sample preparation and analysis was observed by running certified reference materials and the comparison of the results with the certified results. In the case of the results presented here, the certified reference materials were AGV-2 and W-2a. Experimental detection limits were performed by first measuring a 0ppb solution and then a solution water, and then a solution of 100ppb of Standard A and Standard B in 11 replicates each. The quantification limits were determined from 10 times the detection limits resulting from the analysis. The quantification limits as well as the detection limits are presented in ppb (part per billion).

The quantification for each of the major elements resulting from the analysis presented above was then transformed into oxides by stoichiometry, and their concentration normalised to 100%. On the other hand, for better interpretation of the rare earth elements (REE) data resulting from the ICP-MS analysis, the results were normalized to chondrite (Sun and McDonough, 1989).

4.8 Scanning Electron Microscope coupled with Energy Dispersive X-ray Spectroscopy (SEM-EDS)

The analysis and imaging at a micro scale are a powerful analytical method (Froh, 2004; Tite et al., 1982; Tite, 1991). In this case, the analysis was conducted using a variable pressure Hitachi S3700N Sem coupled with a Quantax EDS microanalysis system. More specifically, the Quantax system is equipped with a Bruker Axs 5010 XFlash Silicon Drift Detector (129 eV spectral resolution at FWHM/ $MnK\alpha$). The quantification of the elemental analysis was done using the software ESPIRIT by Bruker.

The analysis with SEM-EDS were done on the same thin sections prepared for the polarised microscope, the reason being that the data from the SEM-EDS analysis can be directly compared to the identifications done by optical microscopy and vice versa. The operating conditions were the following: backscattering mode (BSEM), 20 kV accelerating voltage, 10 mm working distance, 100 μ A emission current and 40 Pa pressure in the chamber

The aim of the analysis was to characterize the ceramic composition, more precisely, the elemental composition of the binder, of the single inclusions and of the possible surface treatments. The average process of analysis of the samples included the analysis of the elemental composition and quantification of the binder, the general map view of the sample with the elemental distribution and then a series of elemental analyses on the different inclusions or formations visible. The analysis of the inclusions, and of the bodies, included the mapping as well as the quantification of the composition of a point or of areas of the analysed subject. When the data was analysed, the elements were transformed into oxides by stoichiometry and normalized to 100%.

5. Results

In this chapter the data, resulting from previously described analyses, are presented. The exposition of results follows the order here presented: Polarized Optical Microscopy, XRD, L.O.I., ICP-MS and SEM-EDS. The exposition of the most meaningful results is followed by their discussion in the next chapter. The first step, i.e. the Polarized Optical Microscopy, determined the subdivision of the samples into groups according to fabric similarities. The presentation of the results and the subsequent discussions have the different fabrics, as subjects, and not the individual samples, except for specific cases. As a final section of the chapter, a presentation of the collected data related to the geological structure of modern day Yemen, Oman and India are provided. The collected data are not from first-hand analysis, but result from bibliographic research. It must not be forgotten that all the collected data regarding composition of the ceramics, aims to develop an understanding of the raw material constituting the samples that then allows comparisons to be drawn between samples and specific geological formations.

5.1 Polarized Optical Microscopy observations

Petrographic observations are useful for the researcher to have a general understanding of the material analysed, both from a material composition, and a structural point of view. In fact, while petrographic analysis allows for the study of general fabric structure and the identification of the nature of inclusions, it also helps to describe the surface treatments, to quantify the porosity and to identify particularities such as organic materials, temper orientation and the degree of homogeneity of the inclusions. In this specific case study, petrographic analysis was the starting point for separating the samples into different groups. The separation into groups was based on the identification of specific characteristics, mainly related to the raw material, that differentiate the samples from a production and compositional point of view. The observations made were responsible for the distinction of 8 different fabric groups (Tab. 5.1) defined as follows: Shell Tempered (ST), Shale-rich Fabric (SF), Talc-rich Fabric (TF), Basalt-rich Fabric (BF), Rice Tempered (RT), Fine Fabric (FF), Medium-Large inclusions in fine Fabric (MLF), Shell and Sand-rich Fabric (SSF). Each group is described here with the most representative characteristics and with the most interesting peculiarities in relation to the general topic of discussion of this thesis. The presentation of a more precise data list with the description of each sample resulting from the petrographic analysis is available in in the appendix 9.2.

5.1.1 Shell Tempered (ST)

As the name suggests, the Shell Tempered (ST) group is characterized by the remarkable concentration of shells fragments as temper (Tab. 5.1). The samples of this group are IQM16B.US35.8, IQM17A.US58.5 and IQM18B.US119.5 (Tab. 5.2). From a general compositional point of view, 30% to 50% of the samples is composed of the grog, with pores representing 10% to 20%, and the remaining 40-50% is represented by the temper. Most of the temper is composed of shells fragments, being nearly the only types of inclusions present with very angular shapes and no evidence of sorting according to dimensions. In addition to the crushed shell material, the ST samples also display some quartz grains and some carbonate crystals. It needs to be noted that sample IQM17A.US58.5 behaves differently to the other two samples presented. It is characterized by a much lower concentration of shell fragments and a higher presence of other inclusions such as quartz and rounded limestone grains.

5.1.2 Shale-rich Fabric (SF)

In contrast to the ST group, the SF group is characterized by the common presence of sedimentary grains identified as shales (Tab. 5.1). The samples comprising the group are: IQM17A.US58.8, IQM16B.US35.34 and IQM16B.US35.35 (Tab. 5.2). Shale is a sedimentary rock characterized by its very fine texture (silty and/or clayish). Shale is present in the samples in large quantities in the form of medium and large rounded grains, but it is not the only inclusion comprising the fabric. Within the same fabric it was possible to find shell fragments, calcite crystals, micas, quartz, feldspars and, in two out of three samples, amphiboles. The general composition of the fabric is characterized by inclusions representing 30% to 50% of the general composition, while the porosity is limited to 20% of the sample with the remaining 30% represented by the grog. A limited control over the composition of the raw material used for the preparation of the ceramic is evident in all the samples comprising the group. In fact, there is no evident selectivity of the nature or dimensions of the inclusions, with very large grains (visible to the naked eye) as well as very small ones. A particular characteristic that needs to be highlighted is the compresence of amphiboles (minerals usually constituting metamorphic and or igneous rocks), shell fragments and shale grains.

5.1.3 Talc-rich Fabric (TF)

The characteristic of the fabric from this group is the presence of talc (Tab. 5.1). Notwithstanding the presence of talc in both of them, two subgroups were identified within the TF group, namely TF-1 and TF-2.

TF-1 is composed of samples IQM16B.US35.33 and IQM16B.US35.32 (Tab. 5.2). Both of the samples present some talc, but it is not the only inclusion present. Together with talc, the samples also present calcite crystals, quartz, opaques and large sedimentary grains identified as shale. The constitution of the inclusions, varying from very small to large grains, shows no selection and no homogeneity, with the shale grains being rounded and the rest of the inclusions more angular. The general composition indicates poor preparation of the clay before the production of the ceramics with the inclusions representing 30 to 50 % of the fabric, 20% represented by the pores and 30 to 40% by the grog.

TF-2 is composed of sample SUMW03A.US1.1 and sample SUM08B.US162.104 (Tab. 5.2). As with TF-1, TF-2 also presents samples with talc, but, in this case, the mineral represents approximately 30% to 40% of the sample, with the other inclusions representing around 10% of the matrix, the pores 25-30% and the grog 25-30%. In addition to talc, the fabric TF-2 also includes some opaques, some quartz and some small chemogenic sedimentary grains. The talc temper grains are generally poorly-sorted, varying from very small to large grains, and the majority of the temper is angular. On the other hand, the few small sedimentary grains are rounded and have more homogeneous dimensions. The general composition shows some raw material preparation and the clear addition of the talc as a temper, characteristics that clearly separate TF-2 from TF-1.

5.1.4 Basalt-rich Fabric (BF)

Basalt-rich Fabric represents the largest group of samples within the 35 samples analysed. This group is characterized by the presences of basalt grains within the matrix (Tab. 5.1) and it includes 9 samples: IQM16B.US35.31, IQM16B.US30.6, IQM17A.US35.16, IQM16B.US30.3, IQM17A.US35.18, SUM11A.US174.232, SUM09A.US297.2, SUM08B.US975.4, SUM11A.US54.85 (Tab. 5.2). The concentration of basalt grains varies within the group as well as the presence of other inclusions. BF is generally characterized by pores varying from 10% to 40% of the fabric and grog varying between 30% and 40%. The rest is composed of generally poorly-sorted temper which includes basalt grains (of various dimensions, but generally rounded), quartz, feldspars, opaques, pyroxene, some crystalline calcite and, in some samples, also olivine and rice husks.

5.1.5 Rice Tempered (RT)

As the name suggests, Rice Tempered ceramic is characterized by the high concentration of rice husks used as temper (Tab. 5.1). The presence of rice husks remains is not always guaranteed due

to the firing process, but the original presence of it is demarcated by the characteristic imprint left on the clay body. Constituting the RF group are samples SUM10A.US412.1, SUM10C.US174.104 and SUM10C.US174.83 (Tab. 5.2). The fabric, in addition to the presence of rice husks and the relatively high porosity (30%), is also composed of grog for around 30%, and the other 40% is composed of grains of quartz, crystalline calcite, opaques, and small basalt grains. The inclusions show a high degree of sorting with the grains tending to be of small dimensions and rounded or poorly-rounded. Despite the presence of the basalt grains, the separation of RT from BF is required due to the characteristics very high concentration of rice husks. However, it is safe to assume that the two groups are from very similar and closely related geographical areas, and that the RT group can be considered as a particular subgroup of the BF group.

5.1.6 Fine Fabric (FF)

Samples IQM16B.US30.10, SUM10C.US162.119 and IQM18A.US80.3 (Tab. 5.2) are grouped within the “Fine Fabric” group (Tab. 5.1). The main characteristic that distinguishes those three samples from the others, is the high quality of the ceramic raw material. In fact, except for a few recognisable grains of quartz and crystalline calcite, the three sample are composed of such fine material that it is not possible to identify the nature of most of the inclusions. In the specific case of sample IQM18A.US80.3 the matrix and the inclusions are the thinnest of the three members of the group, except for very few medium-sized inclusions. The general composition of the fabric is characterized by pores (20% to 40%), 40% to 70% grog and 20% to 40% by inclusions.

5.1.7 Medium-Large inclusions in fine Fabric (MLF)

Representing the second largest grouping among the samples presented in this thesis, MLF is composed of 7 samples: SUM10A.US405.3, IQM16B.US35.9, IQM17B.US73.1, IQM16B.US23.13, SUM08A.US253.5, SUM10C.US174.79, SUM03A.US133.9 (Tab. 5.2). The group is characterized by the presence of homogeneously large temper grains within a fine matrix (Tab. 5.1). The homogenous character of the grains, even if medium-large (shifting from 100 μm to 500 μm), highlights a certain degree of temper selection and preparation. The temper grains are mainly quartz, but there is also the presence of feldspars, crystalline calcite, opaques, micas, pyroxenes and of debritic sedimentary rocks. The fabric is generally composed of 20% to 50% grog, 10% to 20% pores and the remaining 30% to 50% by the temper.

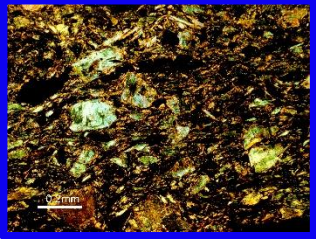
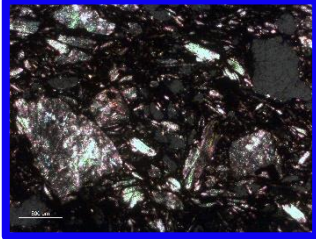
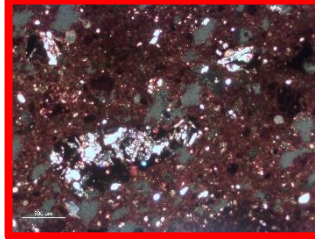
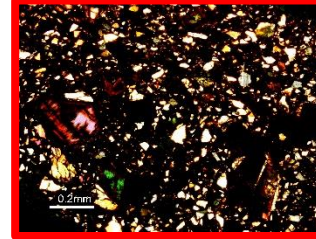
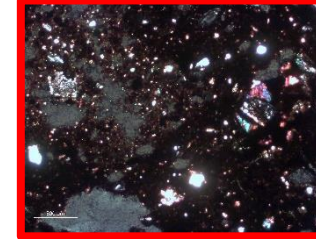
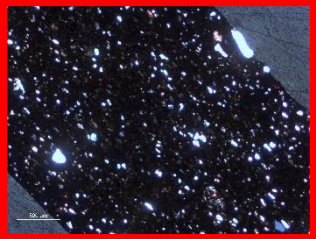
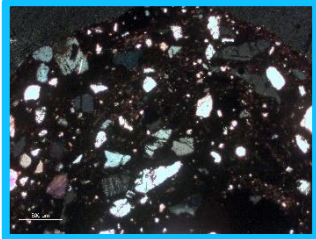
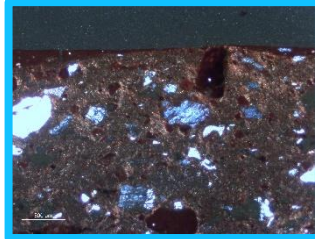
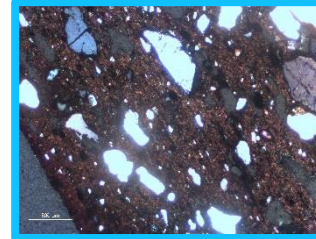
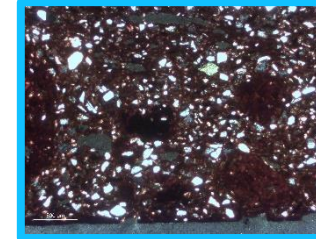
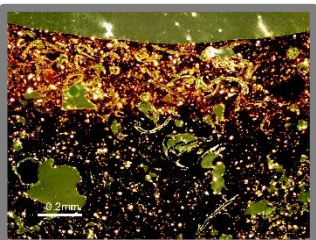
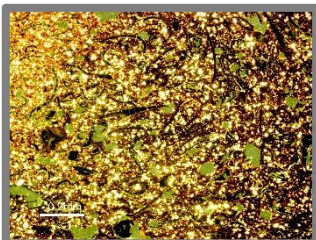
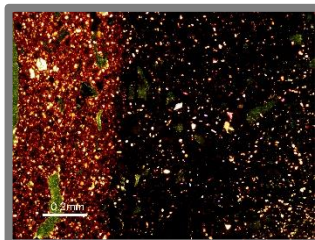
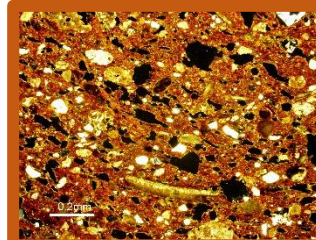
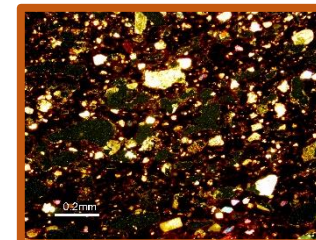
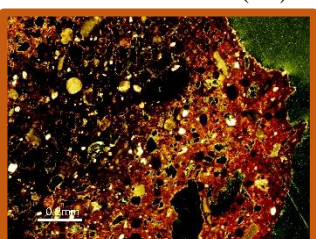
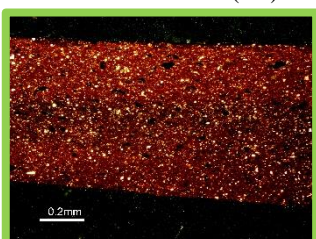
5.1.8 Shells and Sand rich Fabric (SSF)

Lastly, three of the samples here analysed constitute the Shells and Sand rich Fabric group. The presence of well-rounded shell fragments and of recrystallized limestone grains in a sand rich matrix characterizes this fabric (Tab. 5.1). The samples constituting the group are SUM03B.US93.23, SUM09B.US309.4 and SUM03B.US93.42 (Tab. 5.2). The fabric, in addition to the presence of the well-rounded shell fragments, also includes nicely-rounded chemogenic sedimentary grains and grains of quartz and opaques. The general composition of the fabric is of 30% to 40% grog as well as of 30% to 40% pores and similarly of inclusions.

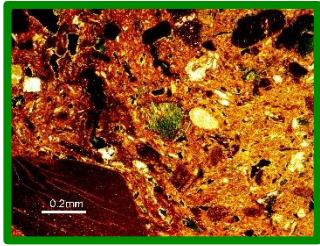
Table 5.1: Schematized presentation of the groups identified with petrographic analysis, of their main characteristics and of the colour code adopted throughout the thesis.

| Group | Samples | Main characteristic | Colour assigned | |
|---|---|--|--|----------------|
| Shell Tempered | <ul style="list-style-type: none"> IQM16B.US35.8 IQM17A.US58.5 | <ul style="list-style-type: none"> IQM18B.US119.5 | <ul style="list-style-type: none"> Shell angular fragments Temper nearly limited to only shell fragments | Yellow |
| Shale-rich Fabric | <ul style="list-style-type: none"> IQM17A.US58.8 IQM16B.US35.34 | <ul style="list-style-type: none"> IQM16B.US35.35 | <ul style="list-style-type: none"> Rich in large and rounded shale grains Large variety in temper composition Unprepared clay | Magenta |
| Talc-rich Fabric | <ul style="list-style-type: none"> IQM16B.US35.33 (TF-1) IQM16B.US35.32 (TF-1) | <ul style="list-style-type: none"> SUMW03A.US1.1 (TF-2) SUM08B.US162.104 (TF-2) | <ul style="list-style-type: none"> Talc Temper TF-2 nearly composed by only unsorted Talc grains TF-1 including rounded shale grains Large variety in temper composition (TF-1) | Green and Blue |
| Basalt-rich Fabric | <ul style="list-style-type: none"> IQM16B.US30.6 IQM117A.US35.16 IQM16B.US30.3 IQM17A.US35.18 IQM16B.US35.31 | <ul style="list-style-type: none"> SUM11A.US174.232 SUM09A.US297.2 SUM08B.US975.4 SUM11A.US54.85 | <ul style="list-style-type: none"> Presence of Basalt grains Possible presence of rice husks Temper grains including Olivine and Pyroxenes Variety in clay preparation level among the samples | Red |
| Rice Tempered | <ul style="list-style-type: none"> SUM10C.US174.83 SUM10A.US412.1 | <ul style="list-style-type: none"> SUM10C.US174.104 | <ul style="list-style-type: none"> Rice husks representing the main temper representing intentional addition Presence of small rounded basalt grains Small to extremely small temper grains Porous | Grey |
| Fine Fabric | <ul style="list-style-type: none"> SUM10C.US162.119 IQM16B.US30.10 | <ul style="list-style-type: none"> IQM18A.US80.3 | <ul style="list-style-type: none"> Very fine matrix composition with limited inclusions Inclusions of various type, but of very small dimensions Rare presence of shell fragments and or of rice husks | Light Green |
| Medium-Large inclusions in fine Fabric | <ul style="list-style-type: none"> SUM10A.US405.3 SUM03A.US133.9 IQM16B.US35.9 IQM17B.US73.1 | <ul style="list-style-type: none"> IQM16B.US23.13 SUM08A.US253.2 SUM10C.US174.79 | <ul style="list-style-type: none"> Medium-Large temper grains (between 100µm and 500µm) Homogeneous dimensions of temper grains within sample Majority of Temper composed by Quartz and Feldspars The grog is generally fine and homogeneous | Light Blue |
| Shell and Sand rich Fabric | <ul style="list-style-type: none"> SUM03B.US93.23 SUM03B.US93.42 | <ul style="list-style-type: none"> SUM09B.US309.4 | <ul style="list-style-type: none"> Rich in well-rounded and well sorted shell fragments Rich in recrystallized limestone and small rounded temper grains of various nature (mainly quartz) | Orange |

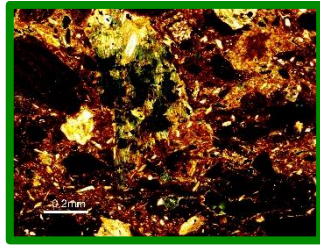
Table 5.2: XPL images presenting the composition of each sample from Sumhuram and Inqitat colour coded in relation to the group. The pictures have a 0,2 mm scale.

| | | | | |
|---|---|---|--|--|
|  |  |  |  |  |
| SUMW03A.US1.1(TF-2) | SUM08B.US162.104(TF-2) * | SUM11A.US174.232 (BF)* | SUM09A.US297.2 (BF)* | SUM08B.US975.4(BF)* |
|  |  |  |  |  |
| SUM11A.US54.85(BF)* | SUM08A.US253.5 (MLF)* | SUM10C.US174.79(MLF)* | SUM03A.US133.9(MLF)* | SUM10A.US405.3(MLF)* |
|  |  |  |  |  |
| SUM10C.US174.104(RT) | SUM10A.US412.1(RT) | SUM10C.US174.83(RT) | SUM03B.US93.23(SSF) | SUM09B.US309.4(SSF) |
|  |  | | | |
| SUM03B.US93.42(SSF) | SUM10C.US162.119(FF) | | | |

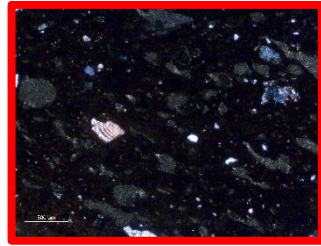
(*) pictures with scale 500 μm
 The difference in colouring between the 0,2 mm images and the 500 μm images is consequence of the different microscope and source of light used.
 ST: Shell Tempered; SF: Shale-rich Fabric; TF: Talc-rich Fabric; BF: Basalt-rich Fabric; RT: Rice Tempered; FF: Fine Fabric; MLF: Medium-Large inclusions in fine Fabric; SSF: Shell and Sand rich Fabric.



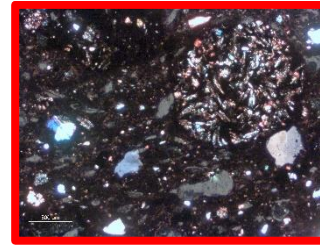
IQM16B.US35.33(TF-1)



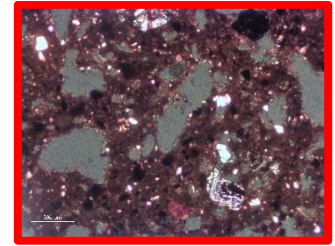
IQM16B.US35.32(TF-1)



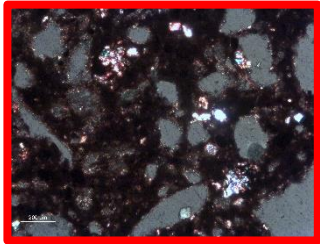
IQM16B.US35.31 (BF)*



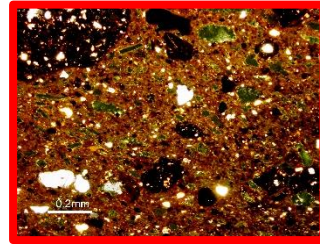
IQM16B.US30.6 (BF)*



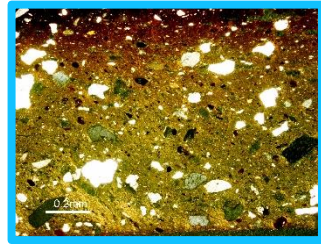
IQM16B.US30.3(BF)*



IQM17A.US35.16(BF)*



IQM17A.US35.18(BF)



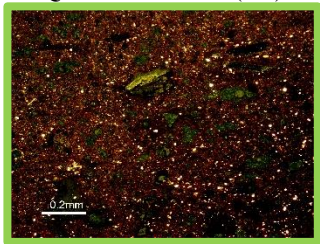
IQM16B.US23.13(MLF)



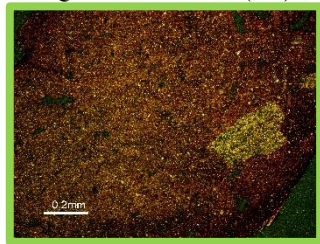
IQM16B.US35.9(MLF)



IQM17B.US73.1(MLF)



IQM16B.US30.10(FF)



IQM18A.US80.3(FF)*



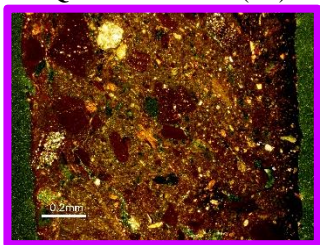
IQM18B.US119.5(ST)



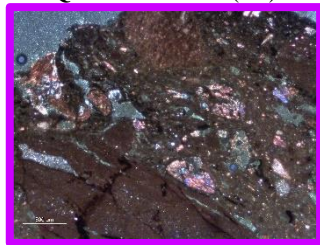
IQM16B.US35.8(ST)



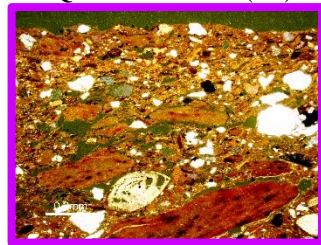
IQM17A.US58.5(ST)



IQM17A.US58.8(SF)



IQM16B.US35.35(SF)*



IQM16B.US35.34(SF)

(* pictures with scale 500 µm

The difference in colouring between the 0,2 mm images and the 500 µm images is consequence of the different microscope and source of light used.
ST: Shell Tempered; SF: Shale-rich Fabric; TF: Talc-rich Fabric; BF: Basalt-rich Fabric; RT: Rice Tempered; FF: Fine Fabric; MLF: Medium-Large inclusions in fine Fabric; SSF: Shell and Sand rich Fabric.

5.2 X-ray Diffraction

Even though petrographic analysis is a powerful technique, it has some weak points, one of which is the limited possibility of identifying minerals below certain dimensions. Another weak point, as mentioned previously, is the fact that the analysis is focused on a thin section that is assumed to be representative of the whole sample. With XRD, on the other hand, it is possible to also identify extremely small minerals constituting the paste and, in this case study, the analysis was a bulk analysis that can more easily be considered representative of the whole sample.

The result of the XRD analysis are presented here according to the groups defined previously, and summarised in table 5.3. It is possible to visualize the diffractograms of every single sample in the appendix 9.3. The concentration mentioned in the descriptions below result from the quantitative analysis provided by the software Diffrac.Suite™. The quantitative analyses of XRD data are not to be considered of extreme accuracy, done using the Reference Intensity Ration (RIR) method (Snyder, 1992), but can be used as a survey of the composition of the sample. The XRD analyses, then result in the completion of observations and the data collected by means of petrographic analysis. Particular attention was given to minerals that were considered representative for the understanding of the temperature used in the firing of the ceramics: pyroxenes (in particular neo-formed diopside), wollastonite, gehlenite, spinel, mullite and cristobalite among others (Tab. 5.3). An important aspect to be considered is the fact that such minerals, such as pyroxenes for example, can be naturally present, so their inclusion in the composition of the ceramic can be, but is not only indicative of, the firing temperature (El Ouahabi et al. 2015). In the case of diopside, if it was part of the raw material together with other pyroxenes, it would be recognisable in petrography (except for very fine raw material), but its presence in XRD analysis and absence in petrographic analysis can be considered as indications of its formation during the firing process of the ceramic.

5.2.1 Shell Tempered (ST)

The analysis conducted on XRD for the samples constituting ST displayed quite homogenous behaviour. All the three samples were characterized by calcite (Fig. 5.1), representative of the many shell fragments identified in petrography, being predominant (with samples IQM16B.US35.8 and IQM17A.US58.5 showing a concentration above 70%) and quartz representing the only other major phase composing the diffractograms (Tab. 5.3)). Such a high concentration of quartz was not visible in the microscope, suggesting that quartz was of primary importance for the matrix composition. In contrast to petrography, XRD analysis also highlighted the presence of micas and of diopside (pyroxene).

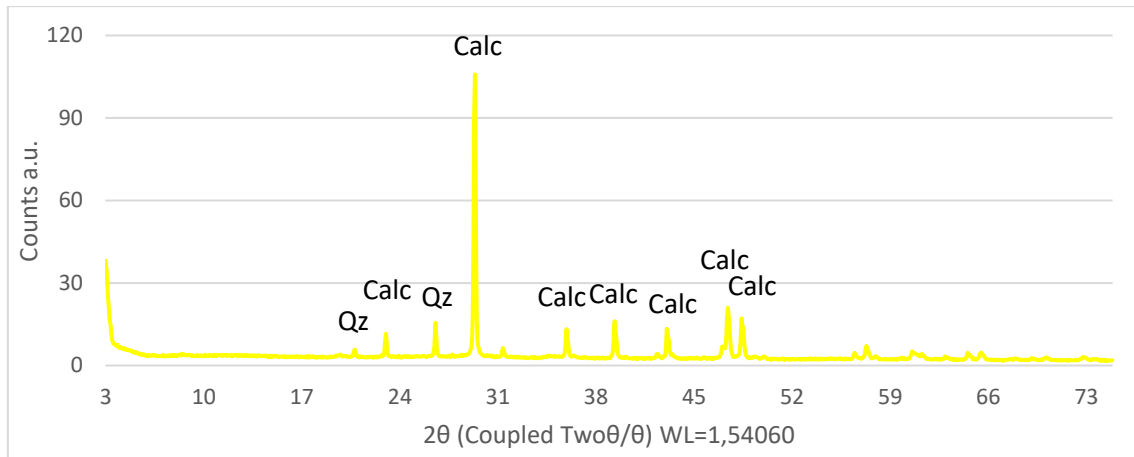


Figure 5.1: Typical diffractogram of ST ceramics.

5.2.2 Shale-rich Fabric (SF)

The XRD analysis on the sample from SF group presented a great variability of phases (Fig. 5.2) constituting the samples, with some composition differences identifiable among themselves. All the samples presented quartz being a major component and calcite being a minor component (except for sample IQM117A.US58.8 in which was above 10%). Also major component among the samples were Ca-plagioclases, while amphiboles represented the predominant phase within the diffractogram (Tab. 5.3) Among the other phases identified, even if not present in all the samples, it is worth mentioning micas that, when present, were representing a minor component, while only traces of diopside were identifiable. Diopside is not present in sample IQM17A.US58.8, which presented mullite and cristobalite instead. Sample IQM16B.US35.35, on the other hand, was characterized by the presence of hematite and gehlenite. The variability in the nature of the inclusions has already been highlighted in the petrographic description of the samples, but with XRD it was possible to observe how the variability was not only related to the nature of the inclusions, but also related to the concentrations of the same inclusions and the presence of new phases possibly related to firing (e.g. mullite and gehlenite).

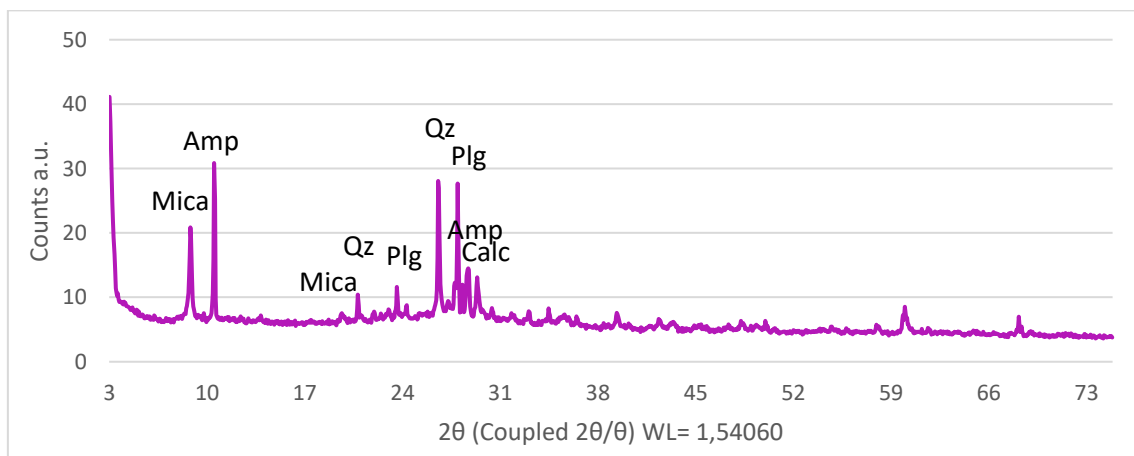


Figure 5.2: Typical diffractogram of SF ceramics.

5.2.3 Talc-rich Fabric (TF)

As mentioned previously, within the TF group the author has identified 2 subgroups: TF-1 and TF-2.

TF-1 is the group represented by a less carefully prepared clay and no temper sorting (Fig. 5.3). The lack of sorting of the temper could also be identified in XRD where it was possible to identify a large variety of phases. According to XRD data (Tab. 5.3), the samples were composed predominantly of talc, but with minor presence also of quartz, chlorite, calcite, plagioclase and major presence of amphiboles. The group was also characterized by the presence of diopside (pyroxene), while zeolite, chlorite and kaolinite are particularities of the single sample. The importance of talc in the composition of the sample is at the base of the definition of the group as TF, but the high concentration of amphiboles, unclear in petrography was clarified in XRD.

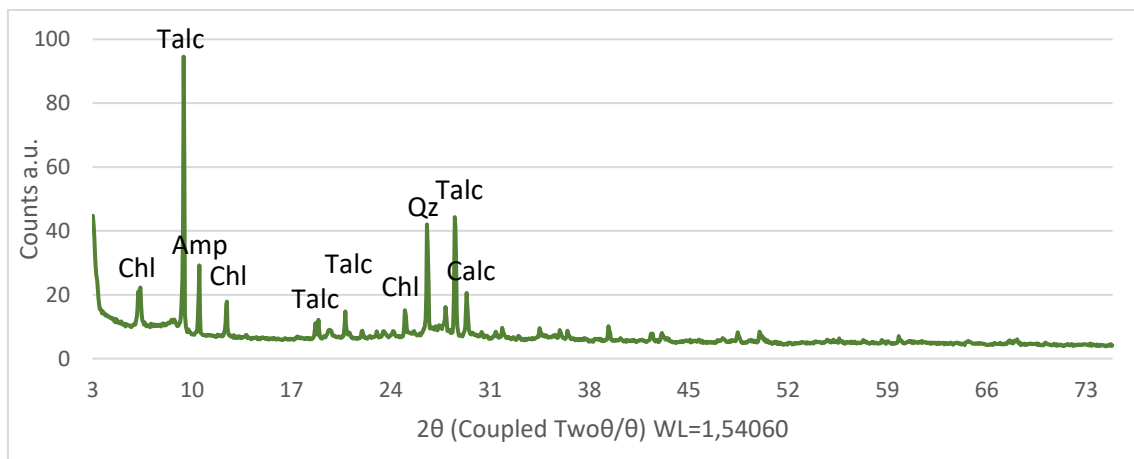


Figure 5.3: Typical diffractogram of TF-1 ceramics.

TF-2, according to petrographic analysis, was characterized by the predominance of talc as temper and by the evidence of some clay preparation. In fact, the variability of phases within the group was strongly limited (Fig. 5.4), when compared to the TF-1 samples. In TF-2 talc represents 70% to 100% of the phase identified with XRD (Tab. 5.3). Among the other phases highlighted by XRD analysis, it was possible to identify the presence of quartz, calcite, micas, zeolites and chlorite, all with a very limited concentration. Sample SUM08B.US162.104 was characterized by the presence of hematite and gypsum.

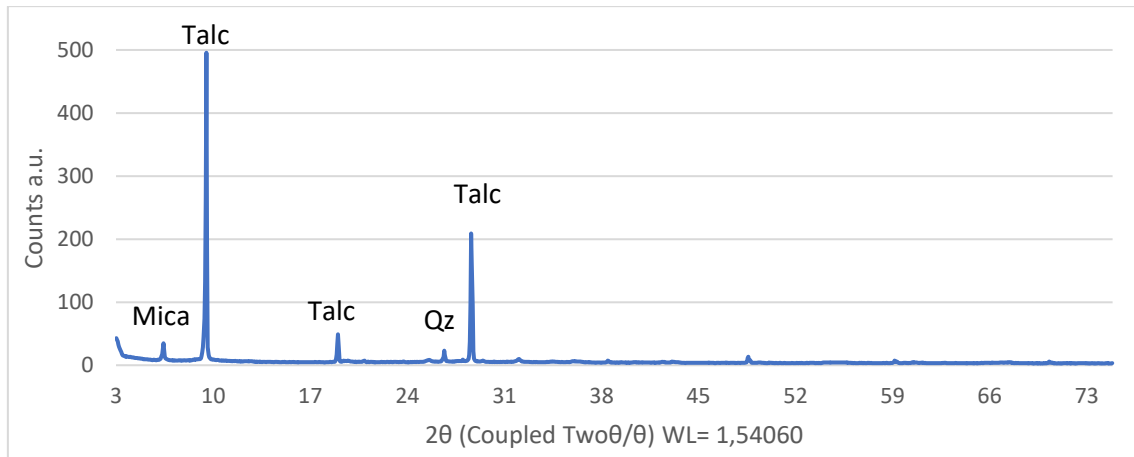


Figure 5.4: Typical diffractogram of TF-2 ceramics.

5.2.4 Basalt-rich Fabric (BF)

The large composition of the group guaranteed the presence of a good variability of phases identified by XRD among the different samples (Fig. 5.5). Despite the variability, some important common characteristics could be identified, such as the major presence of plagioclases and quartz in nearly every BF sample (Tab. 5.3). Other phases commonly present in in all or nearly all the samples were hematite and calcite, which was sometimes missing in favour of dolomite. Anatase is also worth being mentioned as commonly present within the samples of BF group, even if missing in sample sSUM09A.US297.2, SUM08B.US975.4 and SUM11A.US54.85. Among such a large group it was not surprising to find some variability in the composition of the samples. Mineral phases only present in some of the samples were micas being of major importance in samples SUM08B.US975.4, SUM11A.US174.232 and IQM16B.US30.3, olivine, pyroxene, amphiboles, alkali feldspars and gypsum. Regarding the phases that could be considered for possible firing temperature analysis, most of the samples present diopside, except for sample SUM09A.US297.2 and sample IQM17A.US35.18. Cristobalite, mullite, gehlenite and spinel were also singularly identified in some samples. The wealth of mineralogical variability could be related to the large number of samples constituting the group and it could also be connected with the observations presented in the petrographic analysis.

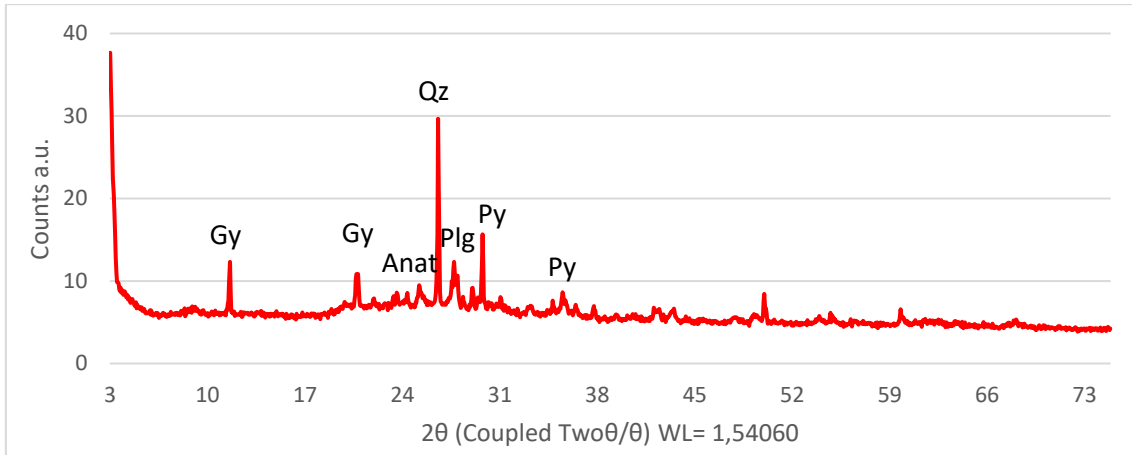


Figure 5.5: Typical diffractogram of BF ceramics.

5.2.5 Rice Tempered (RT)

The composition of RT was characterized by the presence of rice husks, but they were not identifiable in XRD. On the other hand, with XRD, it was possible to investigate the composition of the matrix and the nature of the inclusions that are not rice (Fig. 5.6). Among the phases commonly present within the group, quartz represented the predominant component of the sample, while plagioclases were another major component of the sample composition (Tab. 5.3). Other phases commonly present minorly present were alkali feldspars, micas and pyroxenes (SUM10C.US174.104 presented a major composition of alkali feldspars and micas). Among the samples, only SUM10C.US174.83 has diopside and mullite. From a petrographic analysis point of view, such variability in the nature of inclusions was not evident, due to the very small dimensions of the inclusive grains.

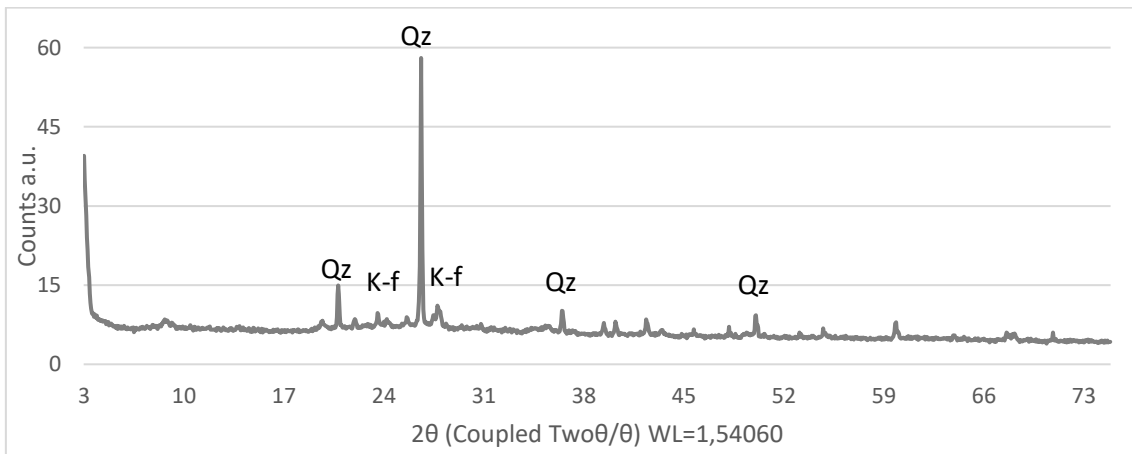


Figure 5.6: Typical diffractogram of RT ceramics.

5.2.6 Fine Fabric (FF)

The importance of XRD was particularly highlighted by the analysis of the FF group. In this case, petrographic analyses were not able to identify the composition, except for the few larger inclusions present in the fabric. However, with XRD (Fig. 5.7) it was possible to highlight the fact that quartz is the prevalent component of the sample, with plagioclases and micas representing the other major phases of the composition of the samples (Tab. 5.3). In addition to those, another phase identified by XRD and commonly present in all the samples is calcite. Samples SUM10C.US162.119 and IQM18A.US80.3 were found to also be composed of by alkali feldspars, while sample IQM16B.US30.10 was the only one presenting gypsum in its composition. Among the minerals useful for firing temperature analysis, all the sample presented diopside (pyroxene) and mullite with sample IQM16B.US30.10 and SUM10C.US162.119 also presenting gehlenite. SUM10C.US162.119 also showed the presence of some cristobalite, a unique example within the FF group.

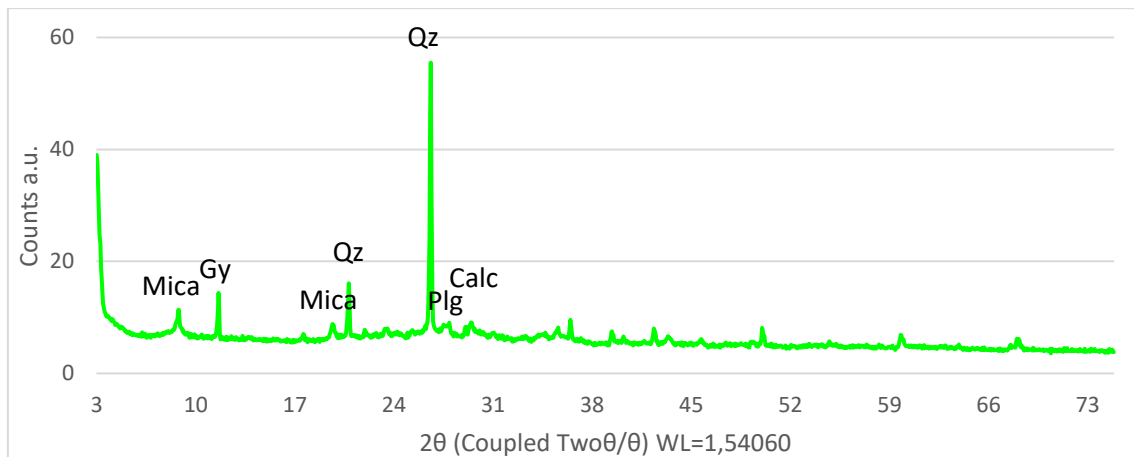


Figure 5.7: Typical diffractogram of FF ceramics.

5.2.7 Medium-Large inclusions in fine Fabric (MLF)

The samples included in this group, even if part of the same group, presented quite some variability when considering the mineralogical composition. According to the petrographic description, the majority of the medium-large inclusions were quartz grains and feldspars. That observation was confirmed by the XRD analysis (Fig. 5.8), which highlighted the predominant role of quartz in the sample composition, while alkali feldspars represent the second major phase in some of the samples (Tab 5.3). Regarding plagioclases, SUM03A.US133.9 was the only sample lacking them, while in all the other samples plagioclases represented a minor component. Micas were present in the majority of the samples, excluding samples IQM17B.US73.1 and IQM16B.US23.13. Among the less common minerals identified, calcite (possible soil contamination) was only present in 3 samples, while anatase, amphiboles and pyroxenes in only two samples (not the same two samples). Regarding the phases possibly connected to the firing

process, sample IQM16B.US35.9 presented diopside (pyroxene), wollastonite, goethite and sillimanite. Diopside (pyroxene) was also present in sample IQM16B.US23.13, while the diffractogram of IQM17B.US73.1 manifested the presence of mullite and goethite.

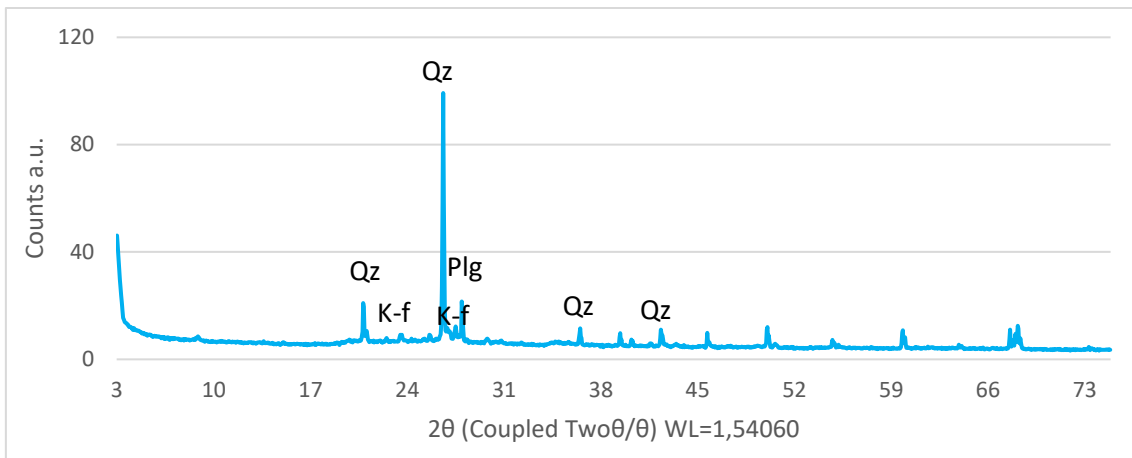


Figure 5.8: Typical diffractogram of MLF ceramics.

5.2.8 Shell and Sand rich Fabric (SSF)

The composition of the samples from SSF was characterized by the presence of shell fragments, as the name suggests and as underlined by the petrographic analysis, but they were not the only inclusions present. XRD analyses (Fig. 5.9) identified a large variety of phases constituting the samples. All the shell fragments present in the samples were responsible for the calcite being the predominant component of the samples, but it was not the only very highly concentrated component, with quartz also representing a major component (Tab. 5.3). The other minor components present in all the samples constituting SSF were plagioclases, alkali feldspars and micas (up to 10%) while pyroxene, gypsum and hematite were only present in sample SUM09B.US309.4. Lastly, considering the minerals relevant for firing temperature studies, all the samples presented mullite and gehlenite, while diopside was present in samples SUM09B.US309.4 and SUM03B.US93.42 and wollastonite in sample SUM03B.US93.23.

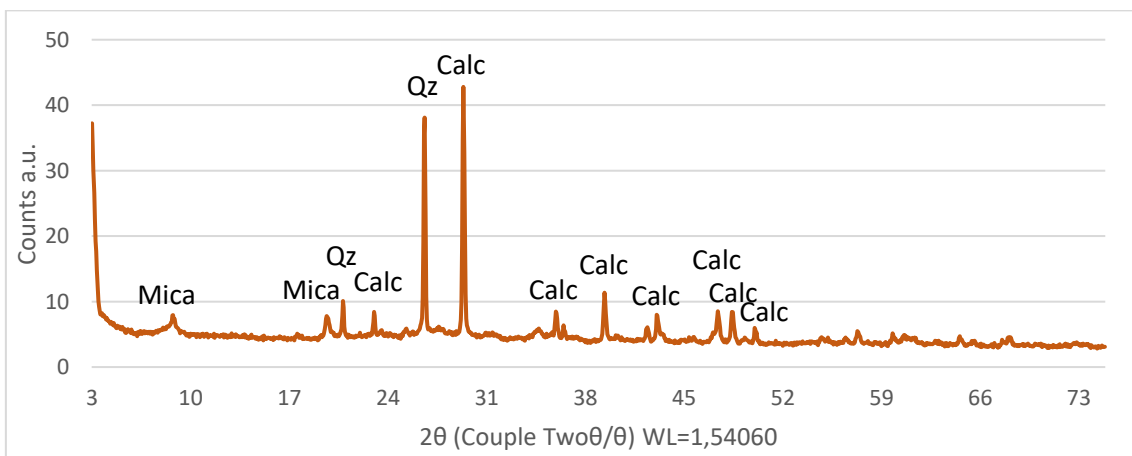


Figure 5.9: Typical diffractogram of SSF ceramics.

Table 5.3: XRD results for each sample colour coded: ST (yellow), SF (purple), TF-1 (dark green), TF-2 (dark blue), BF (red), RT (grey), FF (light green), MLF (light blue) and SSF (brown). The phases connected to the firing temperature of the ceramic are highlighted in yellow.

| Sample Name | Q | C | Do | Pl | K-F | H | M | Ol | Py | Am | An | Ta | Gy | Ze | Ch | Sp | Cr | Mu | Ge | Wo | Ka | Go | Si | Rh |
|--------------------|------|------|----|-----|-----|---|----|----|----|-----|----|------|----|----|----|----|----|----|----|----|----|----|----|----|
| IQM16B.US35.8 | x | xxxx | - | - | - | - | xx | - | x | - | - | - | - | - | - | - | - | - | - | - | - | - | - | - |
| IQM17A.US58.5 | xx | xxxx | - | - | - | - | x | - | x | - | - | - | - | - | - | - | - | - | - | - | - | - | - | - |
| IQM18B.US119.5 | xxx | xxx | - | - | - | - | x | - | x | - | - | - | - | - | - | - | - | + | - | - | - | - | - | - |
| IQM17A.US58.8 | xx | xxx | - | x | - | - | x | - | - | xx | - | - | - | - | xx | - | + | x | - | - | - | - | - | - |
| IQM16B.US35.34 | xx | x | - | xx | - | - | xx | - | x | xx | - | - | - | - | - | - | - | - | - | - | - | - | - | - |
| IQM16B.US35.35 | xx | x | - | xx | - | x | - | - | x | xxx | - | - | - | - | - | - | - | - | x | - | - | - | - | - |
| IQM16B.US35.33 | xx | x | - | x | - | - | - | - | x | xx | - | xxx | - | - | xx | - | - | - | - | - | - | - | - | - |
| IQM16B.US35.32 | x | x | - | x | - | - | - | - | + | xx | - | xxx | - | x | - | - | - | - | - | - | x | - | - | - |
| SUMW03A.US1.1 | x | + | - | - | - | - | x | - | - | - | - | xxxx | - | + | x | - | - | - | - | - | - | - | - | - |
| SUM08B.US162.104 | + | + | - | - | - | + | + | - | - | - | - | xxxx | + | - | + | - | - | - | - | - | - | - | - | - |
| IQM16B.US35.31 | xx | x | x | xxx | - | + | x | - | x | - | x | - | - | - | - | - | - | - | - | - | - | - | - | - |
| IQM16B.US30.6 | xx | - | x | xx | - | x | - | - | x | x | x | - | x | - | - | - | - | - | - | - | - | - | - | - |
| IQM17A.US35.16 | xxx | x | - | xx | - | x | - | - | x | - | x | - | - | - | - | - | - | x | - | - | - | - | - | - |
| IQM16B.US30.3 | xx | - | x | xx | - | x | xx | - | x | - | x | - | xx | - | - | - | - | - | - | - | - | - | - | - |
| IQM17A.US35.18 | xx | x | - | xxx | - | x | - | - | xx | - | x | - | - | - | - | - | - | - | - | - | - | - | - | - |
| SUM11A.US174.232 | xxx | x | - | xx | - | x | xx | - | x | - | + | - | - | - | - | - | - | - | - | - | - | - | - | - |
| SUM09A.US297.2 (*) | xx | x | - | xxx | - | x | x | - | - | - | - | - | + | - | - | - | + | - | - | - | - | - | - | x |
| SUM08B.US975.4 | xx | + | - | xx | x | x | xx | x | x | - | - | - | - | - | - | x | - | - | + | - | - | - | - | - |
| SUM11A.US54.85 | xxx | x | - | xx | - | x | x | - | x | - | - | - | - | - | - | - | + | - | - | - | - | - | - | - |
| SUM10A.US412.1 | xxx | + | - | xx | - | - | x | - | x | - | - | - | - | - | - | - | - | - | - | x | - | - | - | - |
| SUM10C.US174.104 | xxx | + | - | xx | xx | - | xx | x | x | - | - | - | - | - | - | - | - | - | - | - | - | - | - | - |
| SUM10C.US174.83 | xxx | + | - | xx | x | x | x | - | x | - | - | - | - | - | - | - | - | x | - | - | - | - | - | - |
| IQM16B.US30.10 | xxx | x | - | xx | - | + | xx | - | x | - | - | - | xx | - | - | - | - | x | + | - | - | - | - | - |
| SUM10C.US162.119 | xxx | x | - | xx | xx | + | xx | - | x | - | - | - | - | - | - | - | + | x | x | - | - | - | - | - |
| IQM18A.US80.3 | xxx | x | - | x | x | + | xx | - | x | - | - | - | - | - | - | - | - | x | - | - | - | - | - | - |
| SUM10A.US405.3 | xx | - | - | xx | xx | - | x | - | - | xx | - | - | - | - | - | - | - | - | - | - | - | - | - | - |
| IQM16B.US35.9 | xxx | - | x | x | xx | - | xx | - | x | - | + | - | - | - | - | - | - | - | - | x | - | x | x | - |
| IQM17B.US73.1 | xxxx | + | - | x | xx | - | - | - | - | - | x | - | - | - | - | - | - | x | - | - | - | x | - | - |
| IQM16B.US23.13 | xxx | + | - | xx | xx | - | - | - | x | - | - | - | - | - | - | - | - | - | - | - | - | - | - | - |
| SUM08A.US253.5 | xx | + | - | xx | xx | - | x | - | - | x | - | - | - | - | - | - | - | - | - | - | - | - | - | - |
| SUM10C.US174.79 | xxx | - | - | x | xx | - | xx | - | x | - | - | - | - | - | - | - | - | x | - | - | - | - | - | - |
| SUM03A.US133.9 | xxx | - | - | - | xx | + | x | - | - | - | - | - | - | - | - | - | - | x | - | - | - | - | - | - |
| SUM03B.US93.23 | xxx | xx | - | x | x | - | xx | - | - | - | - | - | - | - | - | - | - | x | + | x | - | - | - | - |
| SUM09B.US309.4 | xx | xxx | - | x | x | + | x | - | x | - | - | - | + | - | - | - | - | x | x | - | - | - | - | - |
| SUM03B.US93.42 | xx | xx | - | x | x | - | xx | - | x | - | - | - | - | - | - | - | - | x | x | - | - | - | - | - |

xxxx = between 70% and 100%; xxx = between 40% and 70%; xx = between 10% and 40%; x = less than 10%; + = present; - = absent; (*) = rhodonite present

Q= Quartz; C= Calcite; Do= Dolomite; Pl= Plagioclase; K-F= K-feldspars; H= Hematite; M= Micas; Ol= Olivine; Py= Pyroxene; Am= Amphiboles; Ta= Talc; Gy= Gypsum; Ze= Zeolite; Ch= Chlorite; Sp= Spinel; Cr= Cristobalite; Mu= Mullite; Ge= Gehlenite; Wo= Wollastonite; Ka= Kaolinite; Go= Goethite; Si= Sillimanite; Rh= Rhodonite

5.3 Loss on Ignition (LOI)

Loss on Ignition (LOI), as has already been mentioned in the previous chapter, is both a preparative analysis for XRF analysis, but also a source of information of certain importance on its own. LOI provides indirect information regarding the composition of the ceramic and the technology used for the production, because in the process of heating at 1050°, the samples may lose H₂O and CO₂, both as result of structural changes or as content loss. In fact, collecting information related to the weight loss at a fixed temperature gives insight related to the firing process and the composition of the samples. This is possible because, especially in the case of structural changes caused by high temperature, such changes would not happen in the case of the same temperature already being reached in the firing process. Moreover, the quantification of volatiles lost in the process can give insight to the composition of the sample itself, in relation to decomposition of calcite, of organic material and other components vulnerable to temperature.

Table 5.4 presents a comparison of the % of weight loss within the groups and among the groups. It is clear that the samples from ST were the ones characterized by the highest weight loss due to the wealth in shell fragments. At 1050° C they lost 20% to 30 % of their weight, while the rest of the groups behaves similarly to each other, but within the individual groups, important variability is observable. Because of its high concentration in shells, SSF was the group with the second highest percentage of weight lost, but similar behaviour to this was manifested by sample SUM03A.US133.9 of the MLF group, and by sample IQM17A.US58.8 of the SF group. The average weight lost by the BF group was of roughly 5 % with samples SUM09A.US297.2 and SUM11A.US54.85 having hardly any weight loss, as can be expected from igneous raw material. Samples from SF, except for sample IQM17A.US58.8, had an average mass loss of between 7 and 14 % after the heating process. Both the subgroups of the TF, as well as the samples from FF group, had a weight loss of between 5 and 10 %. The relatively high LOI value for TF is connected to the hydrated nature of talc. The MLF group had remarkable variability within the group, agreeing with the petrographic description, with the majority of the samples losing between 5 and 10 % of their mass, but with sample IQM17B.US73.1 losing less than 5 % and sample SUM03A.US133.9 around 16%. Lastly, group RT had sample SUM10C.US174.83 losing 3% while the other two samples behaved similarly, with a loss between 7 and 10 %.

Table 5.4: LOI values (wt. %) for each sample, samples divided according to defined groups ST: Shell Tempered; SF: Shale-rich Fabric; TF: Talc-rich Fabric; BF: Basalt-rich Fabric; RT: Rice Tempered; FF: Fine Fabric; MLF: Medium-Large inclusions in fine Fabric; SSF: Shell and Sand rich Fabric.

| GROUP | SAMPLES | LOI | GROUP | SAMPLES | LOI |
|-------|------------------|---------|-------|------------------|--------|
| ST | • IQM16B.US35.8 | • 24,81 | BF | • IQM16B.US30.6 | • 4,93 |
| | • IQM17A.US58.5 | • 33,12 | | • IQM17B.US35.16 | • 6,33 |
| | • IQM18B.US119.5 | • 27,94 | | • IQM16B.US30.3 | • 6,62 |

| | | | | | |
|-------------|---|---|------------|--|--|
| SF | <ul style="list-style-type: none"> • IQM17A.US58.8 • IQM16B.US35.34 • IQM16B.US35.35 | <ul style="list-style-type: none"> • 13,29 • 7,25 • 7,78 | | <ul style="list-style-type: none"> • IQM17A.US35.18 • IQM16B.US35.31 • SUM11A.US174.232 • SUM09A.US297.2 • SUM08B.US975.4 • SUM11A.US54.85 | <ul style="list-style-type: none"> • 7,01 • 5,31 • 7,33 • 1,65 • 5,31 • 2,50 |
| TF-1 | <ul style="list-style-type: none"> • IQM16B.US35.33 • IQM16B.US35.32 | <ul style="list-style-type: none"> • 9,05 • 7,44 | | | |
| TF-2 | <ul style="list-style-type: none"> • SUMW03A.US1.1 • SUM08B.US162.104 | <ul style="list-style-type: none"> • 8,30 • 5,95 | RT | <ul style="list-style-type: none"> • SUM10C.US174.83 • SUM10A.US412.1 • SUM10C.US174.104 | <ul style="list-style-type: none"> • 3,06 • 7,39 • 9,01 |
| MLF | <ul style="list-style-type: none"> • SUM10A.US405.3 • SUM03A.US133.9 • IQM16B.US35.9 • IQM17B.US73.1 • IQM16B.US23.13 • SUM08A.US253.5 • SUM10C.US174.79 | <ul style="list-style-type: none"> • 6,25 • 16,36 • 9,44 • 2,33 • 9,17 • 4,50 • 8,94 | FF | <ul style="list-style-type: none"> • SUM10C.US162.119 • IQM18A.US80.3 • IQM16B.US30.10 | <ul style="list-style-type: none"> • 5,93 • 10,19 • 8,20 |
| | | | SSF | <ul style="list-style-type: none"> • SUM03B.US93.23 • SUM09B.US309.4 • SUM03B.US93.42 | <ul style="list-style-type: none"> • 15,90 • 13,26 • 17,43 |

5.3 Inductively coupled plasma mass spectrometry (ICP-MS)

Within this methodology, the focus of attention changes significantly from the one before. With ICP-MS, the attention is focused on the elemental composition of the ceramic artefacts. The importance of the chemical analysis is bound to the possibility of looking at the general signal that the different samples have in elemental composition. The general concentration of the different elements, as well as that of specific groups of elements, is strongly bound to the chemical composition of the raw materials used in the composition of the ceramic. The dependence of the elemental signal on the raw material composition and the production technology used, helps in defining groups of samples according to similarity. The similarity can be analysed in terms of the major elements (i.e. elements representing more than 0,1 wt.%), but also in terms of the trace elements, those representing less than 0.1 wt.%. The presentation of the data in this thesis is mainly based on graphic comparison of the groups previously presented. The aim of this approach was to investigate the differences and similarities present within and among the groups. All the data presented (Tab. 5.5, 5.6 and 5.7) and analysed in this work are direct measurements, all except for SiO₂. In order to conduct bulk elemental analysis in ICP-MS, the digestion of the samples was needed and, during the digestion by NH₄NO₃, Si was lost. Considering the importance of the data related to SiO₂, an idea of the quantification of SiO₂ is presented here. The data related to the SiO₂ was based on a calculation whereby the quantification of the major element oxides was compared to the LOI weight data by means of the difference between LOI results and the total % that the major oxides represent of the sample.

5.3.1 Comparison of Major Element Oxides

The principle at the base of the comparison between samples and their composition is the following: samples with a similar composition have similar behaviour when represented on a linear graph. When following the presented principle while observing Fig. 5.10, it is possible to notice strong differences among the samples. On Fig. 5.10 the most representative samples of each group are projected, in order to emphasise the clear differences in behaviour, especially when looking at the variations the in concentrations of MgO, Al₂O₃ and CaO. In Fig. 5.10 SiO₂ is omitted in order to highlight the differences in concentration of the other major oxides.

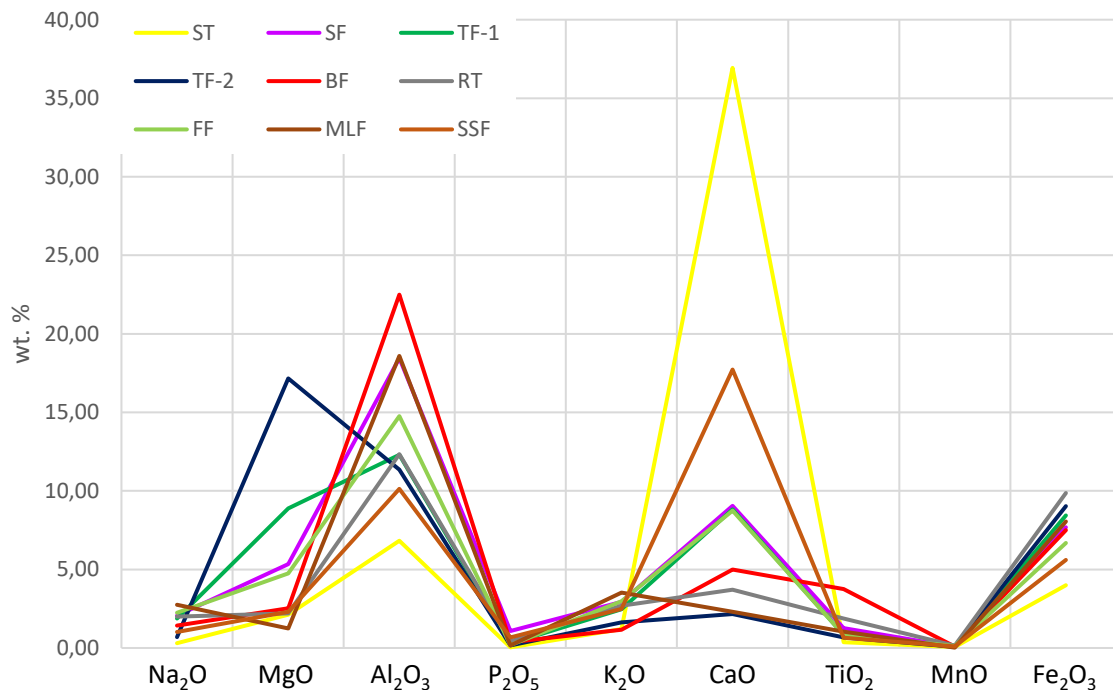


Figure 5.10: Major Element (wt.%) comparison of one representative sample per group. ST: Shell Tempered; SF: Shale-rich Fabric; TF: Talc-rich Fabric; BF: Basalt-rich Fabric; RT: Rice Tempered; FF: Fine Fabric; MLF: Medium-Large inclusions in fine Fabric; SSF: Shell and Sand rich Fabric.

With the possibility of differentiating the groups verified, the subsequent step, being the focus of the presentation below, was to shift attention to the comparison of the signals of the members of each group. The intent was to display the data, group by group, with the simultaneous aim of showing the effectiveness of the grouping and the individual behaviour of all the samples. In all representations, SiO₂ is omitted for two different reasons: firstly, it is not directly measured data, but rather calculated, and secondly, omitting the very high concentration of SiO₂ allows for a closer look at the smaller concentrations of the other oxides (all the graphs are set to a maximum of 50% in order to have comparable graphs all along the section). The representation (Fig. 5.11) of the results of the analysis conducted on the elemental composition of the samples forming the ST group clearly manifest their similar behaviour. The particularity of ST is the presence of shells,

and it is underlined also by the elemental analysis. In fact, the concentration of CaO is the highest peak of the graph and it was the highest among all the samples.

On the other hand, the characteristic of the samples from the SF group was the presence of shale grains and the concomitant wealth of different inclusions. As is noticeable from Fig. 5.11, the samples from SF had very similar behaviour in most cases, except for the concentration of CaO. The higher concentration in CaO, has already been highlighted by XRD variability in calcite concentration among the samples of the SF group.

As mentioned in the presentation of the groups, within the TF group, two subgroups were identified: TF-1 and TF-2. In Fig. 5.11, samples from TF-1 are in green and those from TF-2 are in blue. The key characteristic of the TF group was the presence of talc, a mineral extremely rich in MgO. The same characteristic is highlighted by the presence of the highest concentration of MgO in the TF group, compared to the other groups (Fig 5.11). However, as is noticeable from Fig 5.11, the concentration of MgO, as well as the concentration of CaO vary strongly. The variations in MgO and CaO, however, match well with the separation of TF-1 and TF-2. In fact, the former was characterized by a concentration of roughly 10% for both MgO and CaO, while the second presented a concentration of MgO above 15 % and hardly any CaO. The explanation for the discrepancy in MgO concentrations is connected to the differences in talc concentration in the samples, while CaO diversity was already highlighted by the XRD identification of calcite in TF-1, and its absence in TF-2.

When looking at the distribution of signals of the individual samples from BF, it is possible to notice an important degree of variability. Most of the inequality is connected to the concentration of Al_2O_3 , K_2O , CaO, Fe_2O_3 and TiO_2 and can be explained by the variability in amount of clay material (Al_2O_3) and the nature of the inclusions, such as the variability in plagioclase concentration highlighted by the XRD analysis. Notwithstanding the small variations, Fig. 5.12 demonstrates strong comparability among the samples constituting the BF group.

As mentioned in the petrographic description, the RT also group presented some basalt within the matrix, but the wealth of rice husk recorded within the sample favoured a different classification. In relation to the presence of rice husks, it is important to remember that with the elemental analysis it is very hard to identify the presence of rice husks, especially when considering that they are composed of C and Si, both elements that are subjected to acid attack during the sample preparation. By observing Fig. 5.12 it is possible to notice the relative flatness of the graph, except for Al_2O_3 which represents the basic clay composition together with Fe_2O_3 .

The samples of the FF group were the samples characterized by a composition so fine that the identification of the mineralogical composition was clear only after XRD analysis. On the other

hand, from an elemental composition point of view, as shown in Fig. 5.12, the FF samples are characterized by wealth in CaO and K₂O (related to the calcite and the K-feldspars identified in XRD) and by the common Fe₂O₃ and Al₂O₃ representing the basic clay composition. The membership of the samples to the same group is highlighted in Fig. 5.12 by the constant overlapping of samples.

As is already visible in the BF group, the larger the group, the larger the variability in the behaviour of the samples when investigating their elemental composition. Despite the large dimensions of the group, the MLF samples displayed in Fig. 5.12 show quite high degree of homogeneity. The visible variations are related to the different concentration in Fe₂O₃, Al₂O₃ (both related to the clay minerals), K₂O and TiO₂ (related to the relative variability in inclusions identified by XRD).

Last on the list, the SSF group was composed of 3 samples with an elemental composition that, as presented by Fig. 5.12, is extremely homogenous. The group presented a relatively high CaO concentration of nearly 20%, making it the group with the second highest CaO concentrations. The cause of such high levels of CaO is the presence of shell fragments and crystalized limestone grains. The continuous overlapping of the signals in the graph indicates a perfect match for the samples constituting the SSF group.

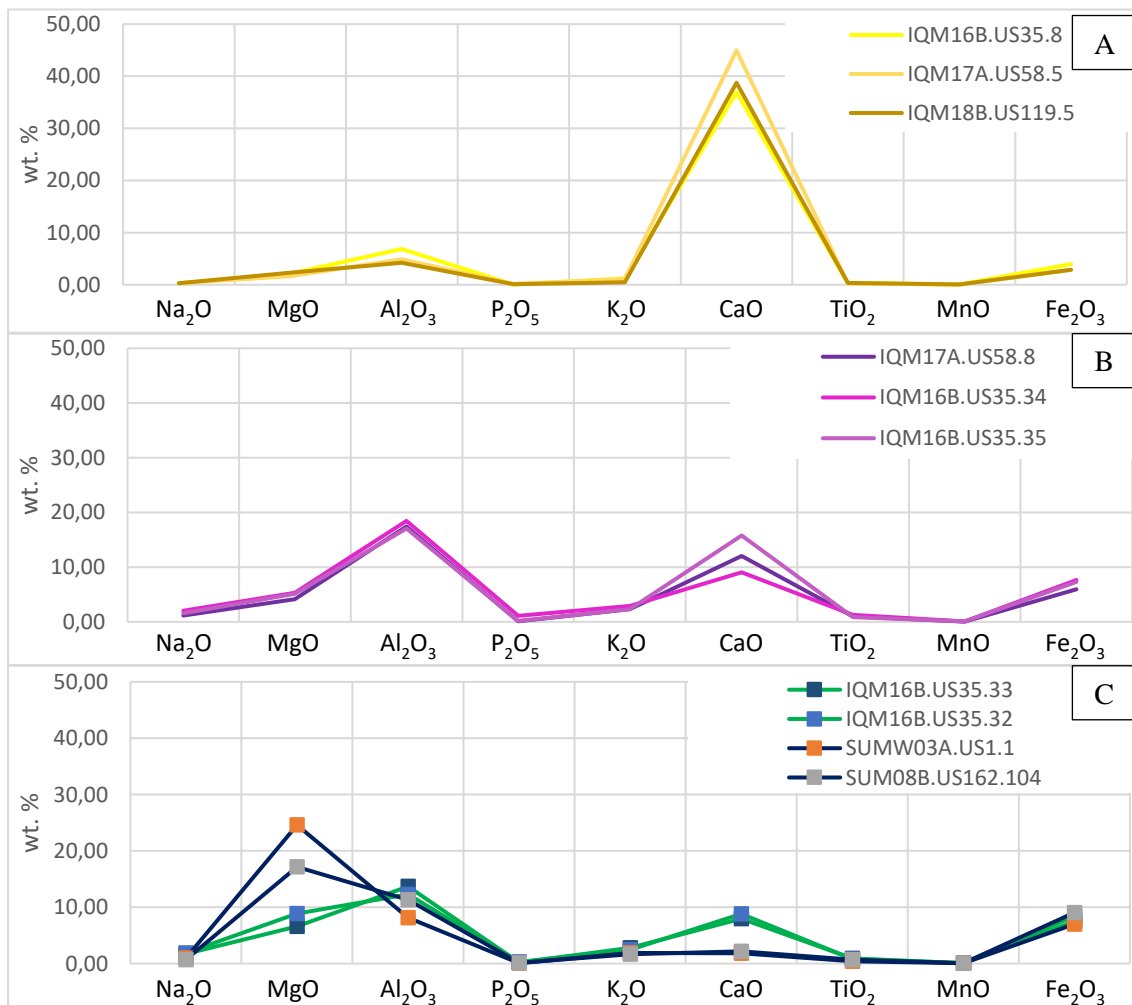


Figure 5.11: Major Elements (wt.%) divided in groups: A) Shell Tempered; B) Shale-rich Fabric; C) Talc-rich Fabric.

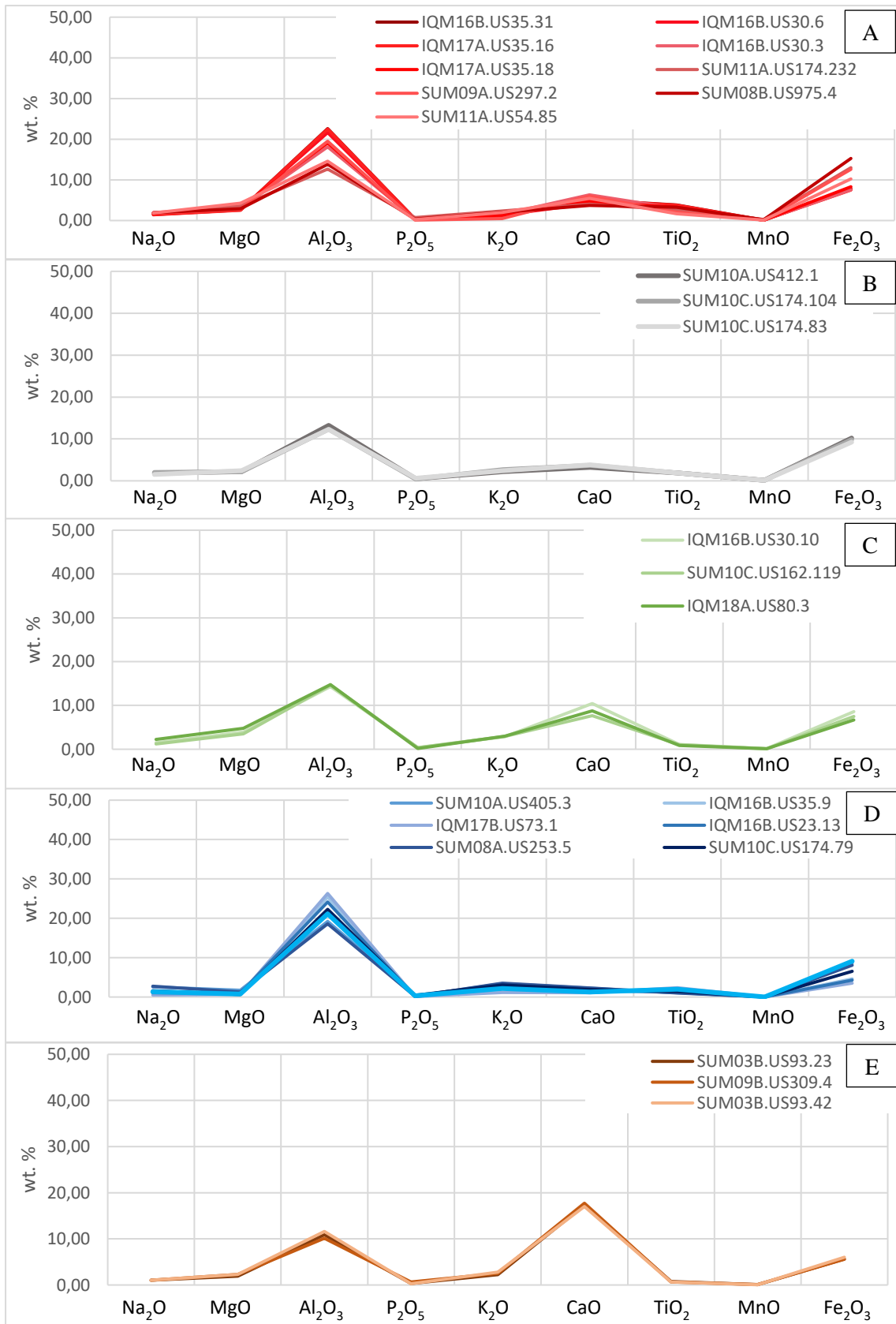


Figure 5.12: Major Element (wt. %) divided in groups: A) Basalt-rich Fabric; B) Rice Tempered; C) Fine Fabric; D) Medium-Large inclusions in fine Fabric; E) Shell and Sand rich Fabric.

Table 5.5: Major elemental composition (wt. %) per sample. SiO₂ is highlighted in yellow because of its indirectly measured values. ST: Shell Tempered; SF: Shale-rich Fabric; TF: Talc-rich Fabric; BF: Basalt-rich Fabric; RT: Rice Tempered; FF: Fine Fabric; MLF: Medium-Large inclusions in fine Fabric; SSF: Shell and Sand rich Fabric.

| Groups | Sample Name | Na ₂ O | MgO | Al ₂ O ₃ | P ₂ O ₅ | K ₂ O | CaO | TiO ₂ | MnO | Fe ₂ O ₃ | SiO ₂ |
|----------------|------------------|-------------------|-------|--------------------------------|-------------------------------|------------------|-------|------------------|-------|--------------------------------|------------------|
| ST | IQM16B.US35.8 | 0,30 | 2,12 | 6,83 | 0,04 | 1,20 | 36,93 | 0,37 | 0,07 | 3,99 | 48,16 |
| | IQM17A.US58.5 | 0,30 | 1,62 | 4,88 | 0,17 | 1,09 | 44,96 | 0,23 | 0,03 | 2,85 | 43,88 |
| | IQM18B.US119.5 | 0,27 | 2,31 | 4,24 | 0,08 | 0,48 | 38,74 | 0,37 | 0,06 | 2,89 | 50,56 |
| SF | IQM17A.US58.8 | 1,14 | 4,14 | 17,43 | 0,12 | 2,34 | 12,06 | 0,97 | 0,05 | 5,93 | 55,82 |
| | IQM16B.US35.34 | 2,05 | 5,33 | 18,45 | 1,08 | 2,93 | 9,04 | 1,27 | 0,07 | 7,67 | 52,10 |
| | IQM16B.US35.35 | 1,58 | 5,11 | 17,06 | 0,14 | 2,30 | 15,81 | 0,89 | 0,08 | 7,31 | 49,72 |
| TF-1 | IQM16B.US35.33 | 1,74 | 6,61 | 13,69 | 0,19 | 2,80 | 7,96 | 0,93 | 0,07 | 7,54 | 58,47 |
| | IQM16B.US35.32 | 1,88 | 8,89 | 12,30 | 0,28 | 2,47 | 8,83 | 0,83 | 0,09 | 8,45 | 55,99 |
| TF-2 | SUMW03A.US1.1 | 1,00 | 24,59 | 8,13 | 0,10 | 1,87 | 1,83 | 0,44 | 0,07 | 6,98 | 54,99 |
| | SUM08B.US162.104 | 0,69 | 17,16 | 11,35 | 0,16 | 1,64 | 2,17 | 0,67 | 0,08 | 9,03 | 57,05 |
| BF | IQM16B.US35.31 | 1,45 | 2,60 | 22,60 | 0,38 | 1,23 | 5,09 | 3,84 | 0,10 | 7,79 | 54,93 |
| | IQM16B.US30.6 | 1,86 | 2,71 | 21,62 | 0,34 | 1,37 | 4,14 | 3,20 | 0,11 | 7,71 | 56,94 |
| | IQM17A.US35.16 | 1,43 | 2,54 | 22,49 | 0,36 | 1,16 | 5,00 | 3,75 | 0,09 | 7,49 | 55,69 |
| | IQM16B.US30.3 | 2,00 | 3,07 | 18,11 | 0,42 | 1,45 | 6,33 | 2,99 | 0,10 | 7,59 | 57,96 |
| | IQM17A.US35.18 | 1,62 | 3,36 | 19,08 | 0,32 | 1,38 | 4,58 | 3,30 | 0,10 | 8,30 | 57,96 |
| | SUM11A.US174.232 | 1,78 | 3,61 | 12,64 | 0,70 | 2,37 | 4,05 | 2,61 | 0,27 | 12,99 | 58,99 |
| | SUM09A.US297.2 | 1,80 | 2,75 | 19,50 | 0,12 | 0,50 | 5,98 | 2,01 | 0,17 | 12,62 | 54,55 |
| | SUM08B.US975.4 | 1,93 | 2,92 | 13,81 | 0,34 | 2,02 | 3,69 | 3,25 | 0,21 | 15,26 | 56,56 |
| SUM11A.US54.85 | 1,86 | 4,29 | 14,59 | 0,26 | 1,99 | 5,45 | 1,63 | 0,13 | 10,21 | 59,58 | |
| RT | SUM10A.US412.1 | 1,80 | 2,21 | 13,24 | 0,48 | 2,19 | 3,21 | 1,88 | 0,13 | 10,21 | 64,64 |
| | SUM10C.US174.104 | 2,01 | 2,21 | 12,34 | 0,43 | 2,69 | 3,72 | 1,88 | 0,15 | 9,86 | 64,71 |
| | SUM10C.US174.83 | 1,54 | 2,46 | 12,28 | 0,64 | 2,43 | 3,84 | 1,90 | 0,13 | 9,26 | 65,52 |
| FF | IQM16B.US30.10 | 1,51 | 3,90 | 14,30 | 0,42 | 2,88 | 10,45 | 1,09 | 0,15 | 8,57 | 56,74 |
| | SUM10C.US162.119 | 1,19 | 3,51 | 14,66 | 0,31 | 2,95 | 7,68 | 1,05 | 0,10 | 7,51 | 61,04 |
| | IQM18A.US80.3 | 2,25 | 4,76 | 14,76 | 0,18 | 2,98 | 8,74 | 0,84 | 0,12 | 6,69 | 58,69 |
| MLF | SUM10A.US405.3 | 2,57 | 1,73 | 19,21 | 0,23 | 3,37 | 2,25 | 1,10 | 0,06 | 8,58 | 60,90 |
| | IQM16B.US35.9 | 0,94 | 0,80 | 25,44 | 0,09 | 1,99 | 1,81 | 1,25 | 0,02 | 4,60 | 63,06 |
| | IQM17B.US73.1 | 0,49 | 0,62 | 26,31 | 0,09 | 1,12 | 1,07 | 2,36 | 0,03 | 3,50 | 64,41 |
| | IQM16B.US23.13 | 1,09 | 0,96 | 24,15 | 0,14 | 2,61 | 1,71 | 1,11 | 0,02 | 4,30 | 63,91 |
| | SUM08A.US253.5 | 2,76 | 1,24 | 18,59 | 0,16 | 3,53 | 2,29 | 1,04 | 0,02 | 8,04 | 62,32 |
| | SUM10C.US174.79 | 1,59 | 0,63 | 22,28 | 0,42 | 3,08 | 1,91 | 1,38 | 0,02 | 6,54 | 62,17 |
| | SUM03A.US133.9 | 1,32 | 0,78 | 21,13 | 0,33 | 2,17 | 1,25 | 1,98 | 0,02 | 9,10 | 61,94 |
| SSF | SUM03B.US93.23 | 1,03 | 1,92 | 10,92 | 0,31 | 2,26 | 17,32 | 0,78 | 0,08 | 5,65 | 59,74 |
| | SUM09B.US309.4 | 1,01 | 2,30 | 10,13 | 0,67 | 2,50 | 17,73 | 0,66 | 0,10 | 5,60 | 59,31 |
| | SUM03B.US93.42 | 1,02 | 2,29 | 11,60 | 0,25 | 2,80 | 17,02 | 0,64 | 0,05 | 6,01 | 58,31 |

Table 5.6: Trace elements composition per sample (ppm). Yellow: Shell Tempered; Purple: Shale-rich Fabric; Blue and green: Talc-rich Fabric; Red: Basalt-rich Fabric; Grey: Rice Tempered; Green: Fine Fabric; Light blue: Medium-Large inclusions in fine Fabric; Brown: Shell and Sand rich Fabric.

| Sample Name | Sc | V | Cr | Co | Ni | Cu | Zn | Ga | Ge | Rb | Sr | Y | Zr | Nb | Cd | Sn | Sb | Cs | Ba |
|------------------|-------|--------|---------|-------|---------|--------|--------|-------|------|--------|---------|-------|--------|-------|------|------|------|------|---------|
| IQM16B.US35.8 | 6,93 | 102,16 | 117,61 | 17,77 | 77,74 | 18,96 | 32,07 | 8,03 | 1,33 | 76,56 | 389,49 | 10,99 | 41,98 | 5,79 | 0,23 | 1,36 | 0,36 | 4,65 | 273,11 |
| IQM17A.US58.5 | 6,93 | 74,29 | 81,70 | 9,73 | 48,54 | 13,02 | 29,05 | 6,03 | 1,12 | 44,12 | 428,56 | 9,73 | 33,28 | 4,26 | 0,48 | 0,84 | 0,23 | 2,17 | 91,63 |
| IQM18B.US119.5 | 5,28 | 45,32 | 43,41 | 5,09 | 20,31 | 6,83 | 34,68 | 6,77 | 1,35 | 17,66 | 588,02 | 10,84 | 43,26 | 6,26 | 0,42 | 0,84 | 0,21 | 0,88 | 128,62 |
| IQM17A.US58.8 | 14,62 | 101,73 | 95,84 | 19,38 | 55,57 | 13,76 | 45,95 | 16,95 | 2,18 | 47,73 | 369,59 | 16,76 | 83,38 | 10,45 | 0,71 | 1,69 | 0,22 | 3,08 | 248,18 |
| IQM16B.US35.34 | 19,89 | 150,11 | 140,63 | 21,72 | 62,27 | 29,12 | 78,64 | 20,57 | 2,87 | 75,97 | 546,40 | 16,51 | 80,25 | 11,62 | 0,43 | 2,75 | 0,23 | 4,36 | 321,68 |
| IQM16B.US35.35 | 14,84 | 96,96 | 93,65 | 25,76 | 72,42 | 31,41 | 66,13 | 18,53 | 2,55 | 57,93 | 287,84 | 24,92 | 118,38 | 10,82 | 0,39 | 2,12 | 0,26 | 2,65 | 306,61 |
| IQM16B.US35.33 | 15,73 | 130,96 | 121,92 | 31,67 | 135,77 | 22,12 | 76,94 | 19,38 | 3,16 | 53,85 | 199,88 | 23,63 | 135,57 | 11,27 | 0,36 | 2,12 | 0,25 | 2,27 | 356,29 |
| IQM16B.US35.32 | 14,13 | 101,90 | 333,03 | 44,94 | 228,10 | 22,28 | 88,56 | 20,14 | 3,51 | 52,01 | 173,51 | 29,78 | 141,53 | 10,50 | 0,37 | 2,27 | 0,26 | 1,92 | 340,65 |
| SUMW03A.US1.1 | 12,65 | 91,76 | 1027,27 | 47,54 | 989,66 | 27,79 | 84,13 | 11,81 | 4,03 | 40,73 | 61,94 | 9,37 | 50,80 | 8,56 | 0,11 | 1,28 | 1,00 | 1,82 | 136,10 |
| SUM08B.US162.104 | 13,04 | 195,98 | 1217,04 | 41,54 | 1017,99 | 33,05 | 110,34 | 14,49 | 3,57 | 55,86 | 1039,72 | 19,54 | 75,96 | 12,60 | 0,19 | 1,92 | 2,39 | 3,99 | 95,14 |
| IQM16B.US35.31 | 82,55 | 257,95 | 551,48 | 20,33 | 67,93 | 88,84 | 73,35 | 32,52 | 5,25 | 21,20 | 412,53 | 22,48 | 292,83 | 25,94 | 0,37 | 3,22 | 0,17 | 0,52 | 372,43 |
| IQM16B.US30.6 | 77,71 | 286,81 | 483,30 | 24,50 | 70,10 | 85,87 | 78,22 | 35,43 | 5,41 | 21,36 | 330,61 | 26,07 | 249,72 | 22,27 | 0,33 | 2,97 | 0,14 | 0,56 | 123,31 |
| IQM17A.US35.16 | 85,69 | 253,54 | 551,40 | 21,16 | 71,02 | 87,97 | 73,21 | 34,32 | 5,44 | 20,99 | 343,17 | 22,91 | 295,41 | 25,62 | 0,38 | 3,27 | 0,15 | 0,52 | 324,14 |
| IQM16B.US30.3 | 75,28 | 260,64 | 426,45 | 26,83 | 74,14 | 92,33 | 79,53 | 35,60 | 5,67 | 18,15 | 265,04 | 25,57 | 240,34 | 22,27 | 0,32 | 2,84 | 0,13 | 0,54 | 129,18 |
| IQM17A.US35.18 | 77,02 | 242,74 | 450,61 | 29,72 | 79,70 | 96,60 | 80,63 | 34,15 | 5,82 | 18,80 | 331,85 | 27,00 | 254,25 | 23,72 | 0,36 | 3,10 | 0,18 | 0,54 | 385,61 |
| SUM11A.US174.232 | 26,12 | 255,32 | 1070,10 | 60,21 | 374,75 | 121,00 | 125,84 | 17,10 | 3,17 | 35,54 | 217,59 | 24,80 | 120,62 | 13,75 | 0,27 | 2,45 | 0,62 | 2,08 | 190,23 |
| SUM09A.US297.2 | 18,01 | 258,65 | 128,04 | 37,71 | 85,15 | 129,47 | 88,79 | 24,29 | 2,92 | 11,64 | 193,36 | 21,17 | 60,24 | 10,97 | 0,13 | 2,28 | 0,23 | 0,72 | 117,18 |
| SUM08B.US975.4 | 29,62 | 364,41 | 599,69 | 53,06 | 130,26 | 134,56 | 128,06 | 20,08 | 3,39 | 30,57 | 243,89 | 23,88 | 122,08 | 14,35 | 0,26 | 1,91 | 0,40 | 0,97 | 265,10 |
| SUM11A.US54.85 | 22,12 | 243,04 | 140,47 | 30,31 | 72,19 | 93,08 | 80,66 | 21,45 | 3,10 | 75,15 | 249,49 | 24,98 | 98,43 | 15,71 | 0,16 | 2,56 | 0,56 | 4,28 | 277,90 |
| SUM10A.US412.1 | 25,09 | 219,06 | 107,17 | 28,32 | 62,56 | 142,23 | 100,69 | 19,60 | 3,44 | 59,66 | 162,68 | 27,28 | 72,69 | 15,74 | 0,27 | 2,84 | 0,52 | 2,84 | 278,51 |
| SUM10C.US174.104 | 26,66 | 200,99 | 113,65 | 35,47 | 71,60 | 122,25 | 98,38 | 20,94 | 4,16 | 65,85 | 260,38 | 27,29 | 120,68 | 16,16 | 0,41 | 3,31 | 0,34 | 2,32 | 305,56 |
| SUM10C.US174.83 | 22,61 | 217,98 | 110,84 | 28,94 | 58,06 | 120,95 | 104,41 | 18,17 | 3,07 | 61,35 | 275,21 | 24,76 | 93,26 | 15,20 | 0,19 | 3,57 | 0,38 | 2,09 | 306,08 |
| IQM16B.US30.10 | 19,15 | 134,80 | 149,88 | 21,51 | 97,04 | 53,47 | 99,01 | 18,71 | 2,85 | 99,88 | 445,95 | 20,59 | 80,14 | 13,21 | 0,25 | 2,81 | 0,50 | 6,83 | 278,26 |
| SUM10C.US162.119 | 16,55 | 154,90 | 158,25 | 22,66 | 113,44 | 79,01 | 103,57 | 20,58 | 3,27 | 118,89 | 226,37 | 23,09 | 61,39 | 16,24 | 0,23 | 3,13 | 0,75 | 9,33 | 285,27 |
| IQM18A.US80.3 | 19,47 | 153,40 | 165,09 | 24,05 | 115,10 | 49,90 | 86,20 | 20,36 | 3,12 | 111,90 | 302,23 | 22,07 | 86,62 | 14,35 | 0,35 | 3,02 | 0,49 | 8,47 | 426,96 |
| SUM10A.US405.3 | 19,14 | 148,72 | 175,26 | 22,19 | 75,92 | 49,83 | 98,02 | 27,55 | 4,56 | 69,96 | 366,09 | 21,97 | 8,82 | 14,97 | 0,17 | 2,50 | 0,45 | 1,78 | 1452,53 |
| IQM16B.US35.9 | 20,79 | 103,94 | 150,40 | 11,72 | 58,13 | 31,75 | 79,00 | 31,03 | 4,10 | 101,18 | 273,15 | 28,23 | 55,40 | 19,95 | 0,15 | 2,23 | 0,20 | 2,05 | 709,30 |
| IQM17B.US73.1 | 19,42 | 88,60 | 196,54 | 12,21 | 75,13 | 25,59 | 74,31 | 33,85 | 4,51 | 68,55 | 113,88 | 21,71 | 86,77 | 39,76 | 0,16 | 4,00 | 0,42 | 4,06 | 429,89 |
| IQM16B.US23.13 | 20,91 | 113,04 | 147,79 | 13,62 | 60,70 | 22,24 | 84,92 | 34,69 | 4,42 | 105,85 | 237,34 | 28,44 | 58,00 | 21,14 | 0,23 | 2,20 | 0,20 | 2,30 | 617,94 |
| SUM08A.US253.5 | 21,16 | 125,37 | 172,21 | 11,94 | 61,21 | 40,80 | 66,04 | 28,65 | 4,69 | 82,57 | 456,31 | 21,81 | 46,39 | 14,37 | 0,13 | 2,26 | 0,24 | 1,57 | 1550,12 |
| SUM10C.US174.79 | 22,01 | 163,49 | 157,65 | 14,70 | 80,37 | 42,48 | 87,30 | 34,66 | 4,61 | 37,77 | 238,95 | 21,96 | 54,25 | 20,01 | 0,14 | 3,20 | 0,27 | 1,47 | 1174,41 |
| SUM03A.US133.9 | 18,01 | 136,18 | 143,13 | 11,02 | 48,46 | 32,58 | 106,88 | 33,60 | 5,72 | 86,80 | 69,35 | 20,32 | 41,89 | 45,28 | 0,12 | 2,44 | 0,48 | 2,17 | 432,15 |
| SUM03B.US93.23 | 14,31 | 111,55 | 134,60 | 14,46 | 56,27 | 27,72 | 88,51 | 14,11 | 2,42 | 76,80 | 1474,40 | 20,16 | 64,46 | 10,28 | 0,57 | 2,20 | 0,49 | 6,29 | 169,13 |
| SUM09B.US309.4 | 14,49 | 112,21 | 193,46 | 16,03 | 76,14 | 32,24 | 72,92 | 13,40 | 2,43 | 81,90 | 324,51 | 22,14 | 30,47 | 10,09 | 0,27 | 2,08 | 0,57 | 6,32 | 205,59 |
| SUM03B.US93.42 | 12,84 | 111,97 | 121,36 | 13,54 | 73,63 | 33,66 | 80,55 | 15,46 | 2,63 | 102,91 | 3201,64 | 15,94 | 16,36 | 10,26 | 0,41 | 2,83 | 0,63 | 9,94 | 222,26 |

Table 5.7: Trace elements composition per sample (ppm). (cont.) Yellow: Shell Tempered; Purple: Shale-rich Fabric; Blue and green: Talc-rich Fabric; Red: Basalt-rich Fabric; Grey: Rice Tempered; Green: Fine Fabric; Light blue: Medium-Large inclusions in fine Fabric; Brown: Shell and Sand rich Fabric.

| Sample Name | La | Ce | Pr | Nd | Sm | Eu | Gd | Tb | Dy | Ho | Er | Tm | Yb | Lu | Hf | Pb | Bi | Th | U |
|------------------|-------|--------|-------|-------|-------|------|------|------|------|------|------|------|------|------|------|--------|------|-------|------|
| IQM16B.US35.8 | 14,73 | 34,80 | 4,02 | 14,58 | 3,75 | 0,65 | 2,60 | 0,39 | 2,22 | 0,43 | 1,09 | 0,17 | 0,95 | 0,15 | 1,25 | 9,40 | 0,15 | 5,10 | 1,38 |
| IQM17A.US58.5 | 11,26 | 26,85 | 2,67 | 10,67 | 2,42 | 0,52 | 1,86 | 0,28 | 1,64 | 0,31 | 0,78 | 0,12 | 0,83 | 0,11 | 1,01 | 12,61 | 0,10 | 4,14 | 1,02 |
| IQM18B.US119.5 | 12,59 | 26,75 | 3,20 | 7,84 | 2,99 | 0,71 | 2,09 | 0,31 | 2,02 | 0,40 | 0,93 | 0,16 | 0,99 | 0,13 | 1,27 | 7,66 | 0,02 | 3,43 | 2,22 |
| IQM17A.US58.8 | 16,85 | 37,07 | 4,60 | 16,77 | 4,40 | 0,92 | 3,31 | 0,54 | 3,42 | 0,69 | 1,74 | 0,29 | 1,68 | 0,25 | 2,49 | 9,68 | 0,05 | 4,20 | 1,44 |
| IQM16B.US35.34 | 22,96 | 51,71 | 6,39 | 23,28 | 6,06 | 1,23 | 4,11 | 0,63 | 3,77 | 0,73 | 1,72 | 0,29 | 1,60 | 0,24 | 2,53 | 11,47 | 0,03 | 4,78 | 1,66 |
| IQM16B.US35.35 | 21,72 | 48,39 | 6,00 | 21,67 | 6,09 | 1,09 | 4,39 | 0,73 | 4,80 | 0,98 | 2,33 | 0,40 | 2,25 | 0,33 | 3,46 | 16,08 | 0,02 | 5,14 | 1,60 |
| IQM16B.US35.33 | 22,15 | 50,22 | 6,22 | 25,52 | 5,23 | 1,18 | 4,48 | 0,69 | 4,33 | 0,86 | 2,25 | 0,36 | 2,48 | 0,36 | 3,55 | 11,78 | 0,14 | 4,93 | 1,73 |
| IQM16B.US35.32 | 25,00 | 56,66 | 7,22 | 30,35 | 6,06 | 1,38 | 5,34 | 0,82 | 5,25 | 1,04 | 2,56 | 0,42 | 2,83 | 0,38 | 3,57 | 8,01 | 0,15 | 5,22 | 1,27 |
| SUMW03A.US1.1 | 11,22 | 28,15 | 2,33 | 8,86 | 1,93 | 0,45 | 1,60 | 0,27 | 1,73 | 0,34 | 0,86 | 0,14 | 0,97 | 0,13 | 1,43 | 11,27 | 0,04 | 4,65 | 1,46 |
| SUM08B.US162.104 | 22,36 | 49,14 | 5,42 | 18,57 | 3,86 | 0,78 | 3,52 | 0,54 | 3,53 | 0,72 | 1,87 | 0,31 | 1,87 | 0,30 | 2,47 | 26,78 | 0,09 | 7,12 | 2,44 |
| IQM16B.US35.31 | 18,04 | 45,78 | 6,30 | 25,44 | 9,04 | 2,38 | 5,43 | 0,96 | 6,36 | 1,16 | 2,59 | 0,45 | 2,60 | 0,35 | 7,45 | 6,81 | 0,04 | 7,98 | 1,60 |
| IQM16B.US30.6 | 18,59 | 54,79 | 7,50 | 30,15 | 10,57 | 2,36 | 6,84 | 1,27 | 8,02 | 1,47 | 3,44 | 0,55 | 3,04 | 0,44 | 6,69 | 6,36 | 0,06 | 7,04 | 1,55 |
| IQM17A.US35.16 | 18,75 | 46,52 | 6,56 | 24,51 | 9,32 | 2,32 | 5,58 | 1,00 | 6,60 | 1,21 | 2,70 | 0,47 | 2,58 | 0,36 | 7,52 | 6,22 | 0,06 | 7,76 | 1,64 |
| IQM16B.US30.3 | 17,11 | 40,51 | 7,18 | 32,88 | 9,23 | 2,55 | 6,89 | 1,18 | 7,44 | 1,34 | 3,14 | 0,49 | 3,33 | 0,44 | 5,80 | 7,44 | 0,09 | 6,27 | 1,45 |
| IQM17A.US35.18 | 20,00 | 53,94 | 8,07 | 36,31 | 9,73 | 2,87 | 7,56 | 1,27 | 8,01 | 1,43 | 3,33 | 0,52 | 3,53 | 0,45 | 6,26 | 8,71 | 0,07 | 6,86 | 1,45 |
| SUM11A.US174.232 | 23,05 | 52,51 | 6,30 | 25,66 | 6,10 | 1,47 | 5,46 | 0,84 | 5,10 | 0,99 | 2,53 | 0,37 | 2,09 | 0,33 | 3,48 | 160,59 | 0,08 | 6,96 | 1,21 |
| SUM09A.US297.2 | 11,61 | 29,56 | 3,78 | 16,75 | 4,59 | 1,38 | 4,19 | 0,69 | 4,36 | 0,87 | 2,26 | 0,33 | 1,87 | 0,29 | 1,80 | 11,29 | 0,03 | 1,74 | 0,58 |
| SUM08B.US975.4 | 16,59 | 42,12 | 4,93 | 18,89 | 5,27 | 1,42 | 4,68 | 0,78 | 5,01 | 0,96 | 2,53 | 0,36 | 2,07 | 0,32 | 4,08 | 19,00 | 0,01 | 3,57 | 0,85 |
| SUM11A.US54.85 | 26,25 | 57,95 | 6,67 | 24,55 | 5,40 | 1,34 | 5,19 | 0,78 | 4,92 | 0,96 | 2,28 | 0,37 | 2,12 | 0,33 | 2,77 | 22,93 | 0,01 | 8,50 | 1,44 |
| SUM10A.US412.1 | 26,56 | 54,39 | 6,73 | 26,37 | 6,24 | 1,41 | 5,32 | 0,86 | 5,25 | 1,03 | 2,76 | 0,39 | 2,20 | 0,34 | 3,16 | 69,71 | 0,05 | 9,42 | 1,42 |
| SUM10C.US174.104 | 28,80 | 61,86 | 7,21 | 24,53 | 5,54 | 1,48 | 5,18 | 0,78 | 4,91 | 0,93 | 2,18 | 0,35 | 2,25 | 0,28 | 2,89 | 38,31 | 0,14 | 8,58 | 1,28 |
| SUM10C.US174.83 | 24,32 | 51,92 | 6,16 | 23,31 | 5,19 | 1,31 | 4,93 | 0,76 | 4,77 | 0,93 | 2,24 | 0,35 | 2,04 | 0,32 | 2,61 | 40,89 | 0,08 | 7,78 | 1,25 |
| IQM16B.US30.10 | 25,58 | 55,32 | 6,29 | 20,26 | 5,59 | 1,30 | 4,10 | 0,63 | 3,94 | 0,78 | 1,86 | 0,31 | 1,77 | 0,25 | 2,32 | 16,35 | 0,11 | 9,58 | 1,63 |
| SUM10C.US162.119 | 29,86 | 64,47 | 7,40 | 24,42 | 5,39 | 1,15 | 4,87 | 0,71 | 4,33 | 0,85 | 2,16 | 0,34 | 1,98 | 0,31 | 2,23 | 70,81 | 0,25 | 11,92 | 1,79 |
| IQM18A.US80.3 | 30,71 | 64,24 | 7,43 | 28,24 | 5,32 | 1,23 | 4,69 | 0,68 | 4,04 | 0,79 | 1,97 | 0,31 | 2,13 | 0,29 | 2,24 | 24,05 | 0,05 | 12,69 | 1,78 |
| SUM10A.US405.3 | 63,08 | 128,33 | 13,54 | 47,56 | 8,77 | 2,05 | 6,78 | 0,87 | 4,72 | 0,87 | 2,29 | 0,31 | 1,81 | 0,28 | 1,53 | 242,39 | 0,03 | 13,91 | 0,96 |
| IQM16B.US35.9 | 47,14 | 107,73 | 11,14 | 39,09 | 9,61 | 1,94 | 6,67 | 0,99 | 6,16 | 1,18 | 2,69 | 0,46 | 2,56 | 0,36 | 1,69 | 36,30 | 0,16 | 14,94 | 2,69 |
| IQM17B.US73.1 | 65,11 | 135,25 | 14,12 | 49,72 | 10,57 | 1,64 | 6,71 | 0,88 | 5,04 | 0,92 | 2,12 | 0,35 | 2,05 | 0,27 | 2,54 | 38,41 | 0,20 | 25,42 | 4,52 |
| IQM16B.US23.13 | 56,72 | 124,69 | 13,20 | 49,75 | 9,14 | 1,91 | 7,53 | 1,03 | 6,03 | 1,14 | 2,77 | 0,43 | 2,91 | 0,40 | 1,59 | 48,41 | 0,28 | 19,18 | 2,77 |
| SUM08A.US253.5 | 63,45 | 128,39 | 13,54 | 50,10 | 7,72 | 2,50 | 6,50 | 0,79 | 4,25 | 0,77 | 1,85 | 0,27 | 1,77 | 0,22 | 1,43 | 58,11 | 0,09 | 13,43 | 1,62 |
| SUM10C.US174.79 | 52,53 | 115,10 | 12,09 | 42,81 | 6,89 | 2,19 | 6,32 | 0,82 | 4,71 | 0,86 | 2,04 | 0,31 | 2,01 | 0,24 | 1,72 | 87,40 | 0,09 | 14,51 | 1,27 |
| SUM03A.US133.9 | 85,42 | 193,67 | 21,42 | 78,09 | 12,63 | 1,32 | 9,90 | 1,10 | 5,27 | 0,91 | 2,15 | 0,33 | 2,01 | 0,31 | 2,01 | 42,88 | 0,17 | 46,13 | 4,95 |
| SUM03B.US93.23 | 24,74 | 50,41 | 6,13 | 22,73 | 5,17 | 0,98 | 4,31 | 0,63 | 3,81 | 0,75 | 2,08 | 0,29 | 1,73 | 0,27 | 2,14 | 15,11 | 0,15 | 10,50 | 1,68 |
| SUM09B.US309.4 | 24,21 | 49,88 | 5,78 | 19,20 | 4,65 | 0,94 | 4,14 | 0,62 | 3,85 | 0,77 | 2,06 | 0,30 | 1,76 | 0,28 | 1,61 | 29,11 | 0,10 | 9,26 | 1,43 |
| SUM03B.US93.42 | 21,82 | 45,99 | 5,42 | 20,46 | 4,14 | 0,77 | 3,40 | 0,55 | 3,13 | 0,60 | 1,65 | 0,25 | 1,47 | 0,23 | 1,80 | 17,29 | 0,13 | 10,52 | 1,90 |

5.3.2 Normalised Rare Earth Elements (REE)

ICP-MS analysis also allows one to look at elements with much lower concentrations, elements that are defined here as trace elements. Among the trace elements, for the purpose of the discussion, the attention is focused here on the Rare Earth Elements (REE), a group of elements that are not main components of the most common minerals, and their presence and variability is strongly related to the geological history of the source of raw material. In order to better compare the REE results, the raw data from the ICP-MS measurements were normalised according to Sun & McDonough (1989).

In the Fig. 5.13 it is possible to visualise the graphic representation of one normalized sample per group.

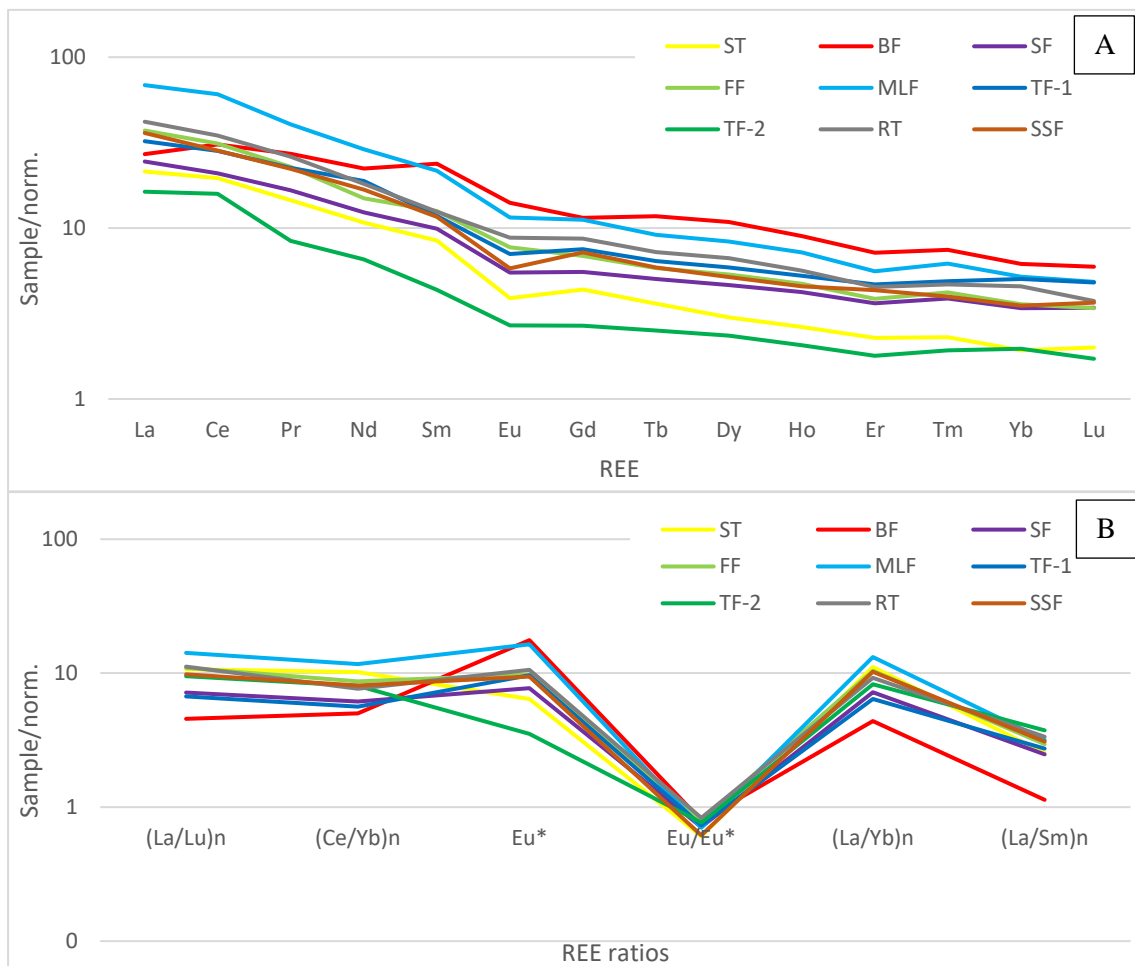


Figure 5.13: REE data normalized to chondrite (McDonough and Sun, 1995). A) REE normalised per group (logarithmic scale); B) Normalised REE ratios per group (logarithmic scale). ST: Shell Tempered; SF: Shale-rich Fabric; TF: Talc-rich Fabric; BF: Basalt-rich Fabric; RT: Rice Tempered; FF: Fine Fabric; MLF: Medium-Large Fabric. The data regarding REE, showed very small variations between groups and even less when observed group by group (Fig. 5.14 to Fig. 5.21). In fact, all groups except for the BF and the MLF groups show important comparability within themselves. The presence of variability among

the REE compositions of the samples constituting the two largest groups is to be expected, but sample SUM08A.US253.5, a member of the MLF group, demonstrates a behaviour that is completely different from the rest of the samples of the same group, and of any other sample as visible in Fig. 5.20 (it is possible that it is an analytical error, but, in absence of certainty, the data related to SUM08A.US253.5 are kept in consideration in this thesis). The variability in the REE data within the BF group is remarkable, probably showing different closely related sources, but there is no case of one sample behaving completely independently from the others. Among the BF samples, SUM09A.US297.2 and SUM08B.US975.4 are the ones manifesting a certain individuality. The behaviour of the TF group, on the other hand, shows distinction between the samples of the TF-1 and TF-2. In particular, the samples from TF-1 show a strongly related REE composition, while the samples from TF-2 behaved differently not only to TF-1, but also among themselves (Fig. 5.16). Sample SUM08B.US162.104 had a REE signal that is comparable to TF-1 samples, while SUMW03A.US1.1 behaved completely differently, with no possible parallels to be drawn with any of the TF samples. In contrast with BF, MLF and TF, the other groups (namely ST, SF, RT, FF and SSF) had no remarkable variability among their components, which maintained a parallelism between the signals, demonstrating direct compatibility among the different members of the groups.

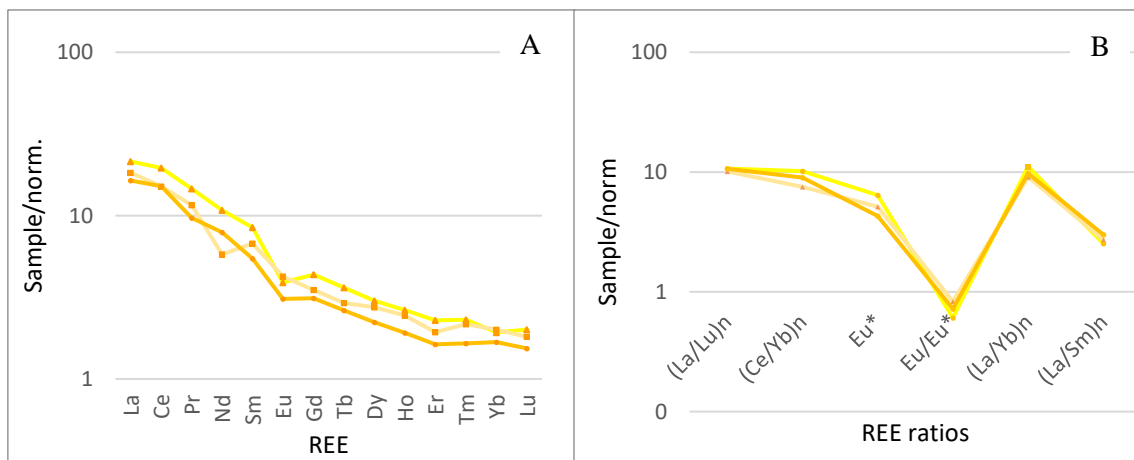


Figure 5.14: REE data normalized to chondrite (McDonough and Sun, 1995). A) Shell Tempered REE Normalized and in logarithmic scale B) Shell Tempered REE ratios in logarithmic scale.

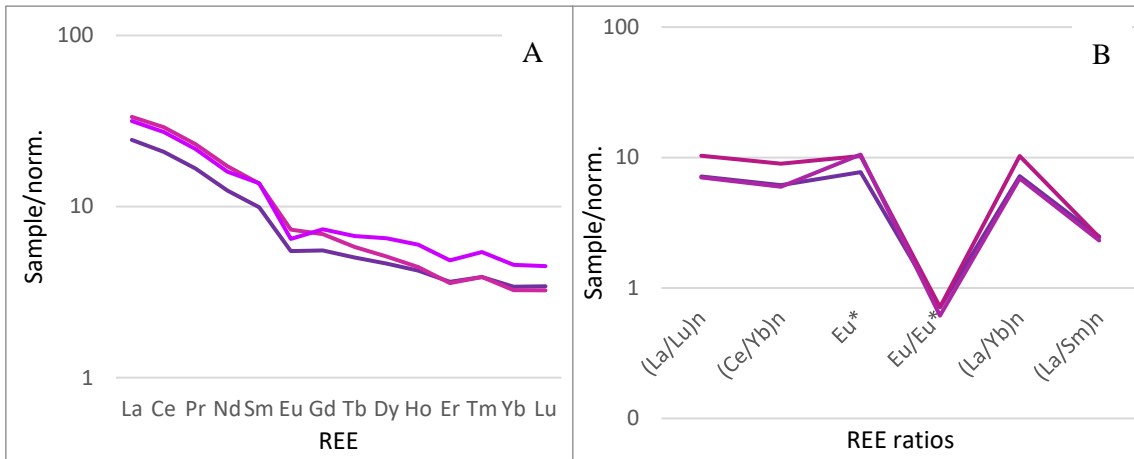


Figure 5.15: REE data normalized to chondrite (McDonough and Sun, 1995). A) Shale- rich Fabric REE Normalized and in logarithmic scale B) Shale-rich Fabric REE ratios in logarithmic scale.

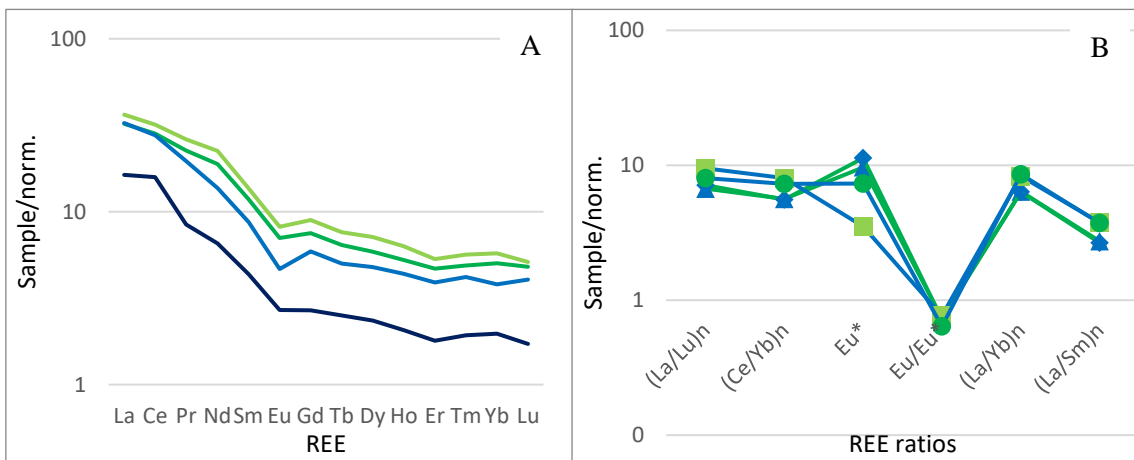


Figure 5.16: REE data normalized to chondrite (McDonough and Sun, 1995). A) Talc-rich Fabric REE Normalized and in logarithmic scale B) Talc-rich Fabric REE ratios in logarithmic scale.

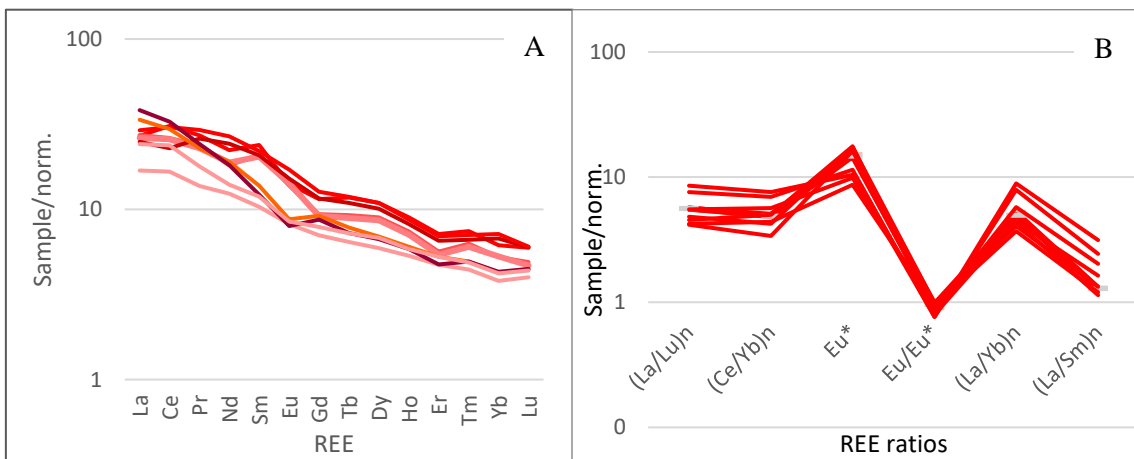


Figure 5.17: REE data normalized to chondrite (McDonough and Sun, 1995). A) Basalt-rich Fabric REE Normalized and in logarithmic scale B) Basalt- rich Fabric REE compared in logarithmic scale.

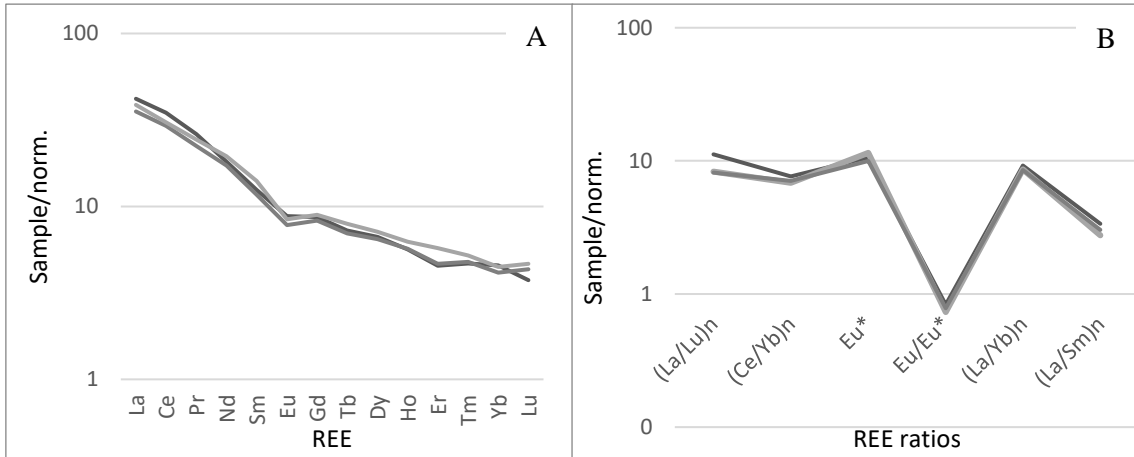


Figure 5.18: REE data normalized to chondrite (McDonough and Sun, 1995). A) Rice Tempered REE Normalized and in logarithmic scale B) Rice Tempered REE ratios in logarithmic scale.

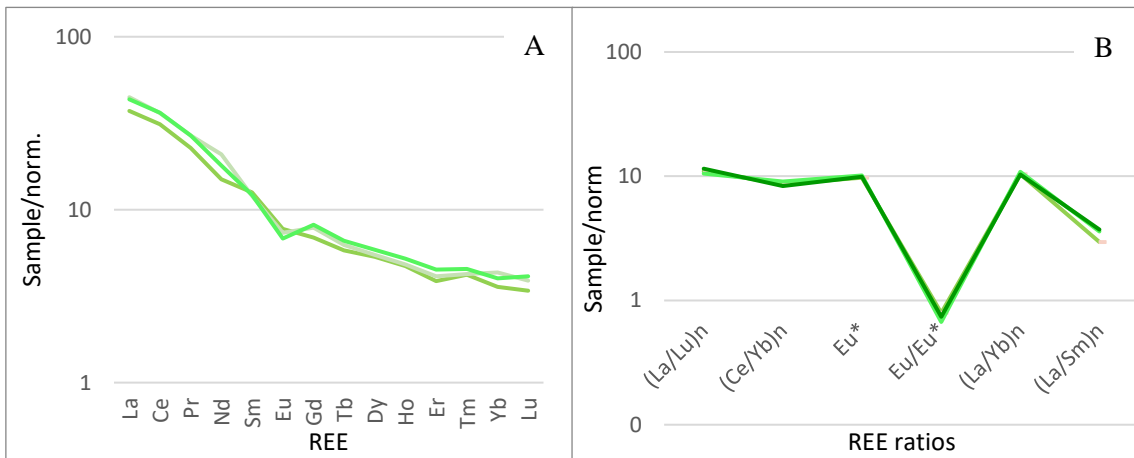


Figure 5.19: REE data normalized to chondrite (McDonough and Sun, 1995). A) Fine Fabric REE Normalized and in logarithmic scale B) Fine Fabric REE ratios in logarithmic scale.

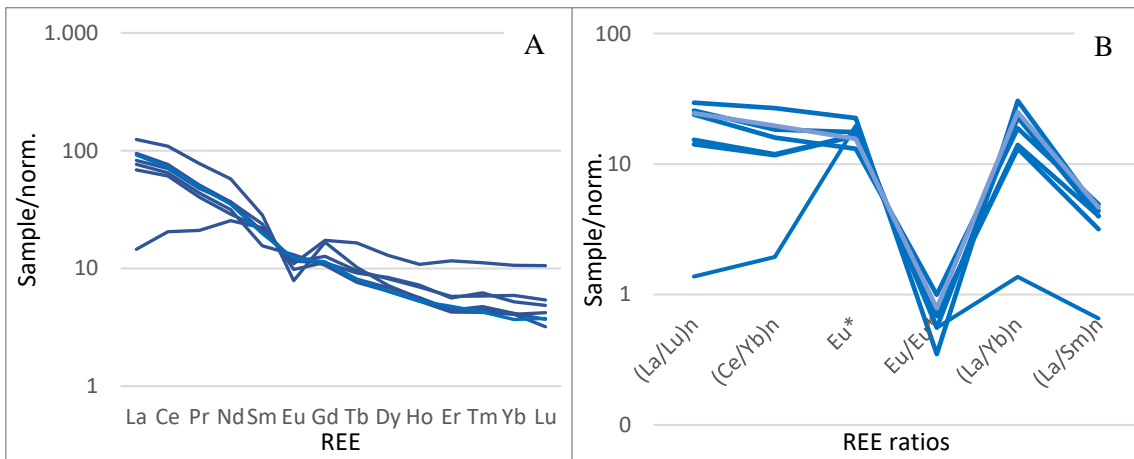


Figure 5.20: REE data normalized to chondrite (McDonough and Sun, 1995). A) Medium-Large inclusions in fine Fabric REE Normalized and in logarithmic scale B) Medium-Large inclusions in fine Fabric REE ratios in logarithmic scale.

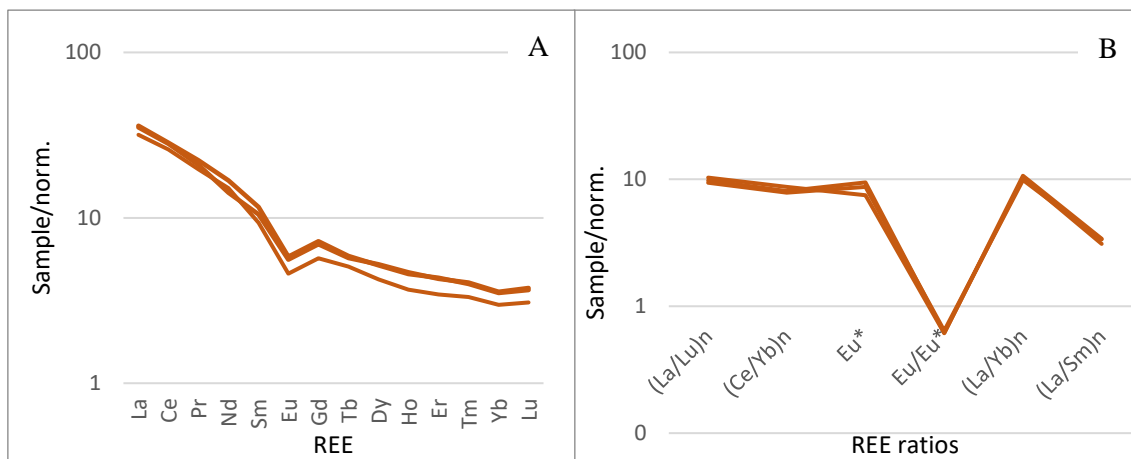


Figure 5.21: REE data normalized to chondrite (McDonough and Sun, 1995). A) Shell and Sand rich Fabric REE Normalized and in logarithmic scale B) Shell and Sand rich Fabric REE ratios in logarithmic scale.

5.3.3 General comparison Local vs Indian

The most important aim of the thesis, presented here, is to answer the question regarding the possibility of distinguishing local and non-local material from an archaeometric point of view. In order to do so, the elemental composition or the ratios of the elemental concentrations of the samples can be used to distinguishing between local and Indian material.

In trying to find the best comparison between elements or ratios, the samples were taken into consideration independently from the grouping, and from the provenance defined archaeologically. The best result from the process was provided by the comparison of the $\text{Al}_2\text{O}_3/\text{SiO}_2$ and MgO/SiO_2 (Fig. 5.22) ratios, and by the comparison of SiO_2 , Al_2O_3 and $\text{CaO}+\text{MgO}$ (Fig. 5.23). The comparison was able to highlight the differences among samples according to the major fabric groups and, when considering the identification of archaeological provenance, also between local and Indian. The definition of the local (blue) and Indian (red) circles is based on the stylistic identification (done prior to the thesis) of Indian and local material provided prior to the analysis. In the case of Fig. 5.23 the separation is not as clear as in Fig. 5.22 as it is highlighted by the correspondence of SSF and TF as well as by the very close relation between FF and TF-1 samples. It is evident, however, that the grouping done based on the fabric of the samples has proved to be considerably efficient in Fig. 5.22, so efficient that even the distinction between the TF-1 and TF-2 is clear. The comparison in both Fig. 5.22 and 5.23 highlights the enrichment in MgO and CaO in the local samples, which is relatable to the shell, talc and amphibole temper grains. Other comparisons between both raw data and ratios, even if less representative, are presented in the appendix 9.4 together with the graphic representation of the trace elements concentration in ppm per group.

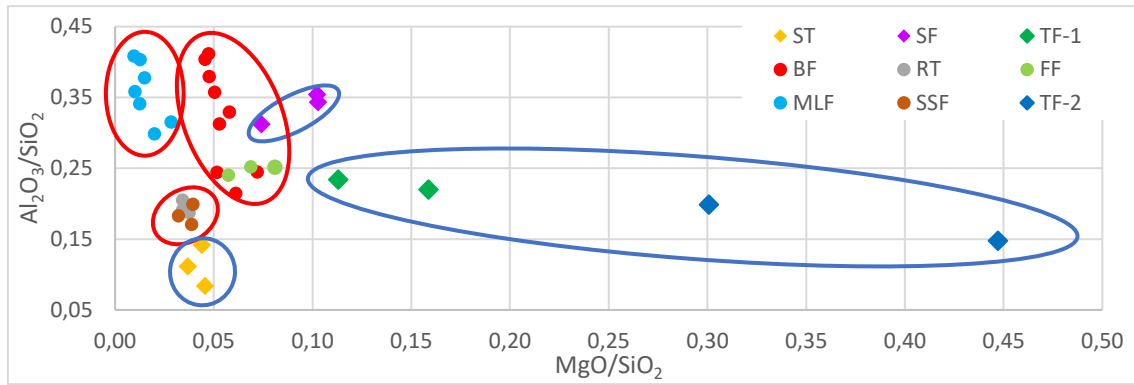


Figure 5.22: Binary plot comparing $\text{Al}_2\text{O}_3/\text{SiO}_2$ and MgO/SiO_2 with local samples in blue circle and Indian samples in red circle stylistically identified. ST: Shell Tempered; SF: Shale-rich Fabric; TF: Talc-rich Fabric; BF: Basalt-rich Fabric; RT: Rice Tempered; FF: Fine Fabric; MLF: Medium-Large inclusions in fine Fabric; SSF: Shell and Sand rich Fabric.

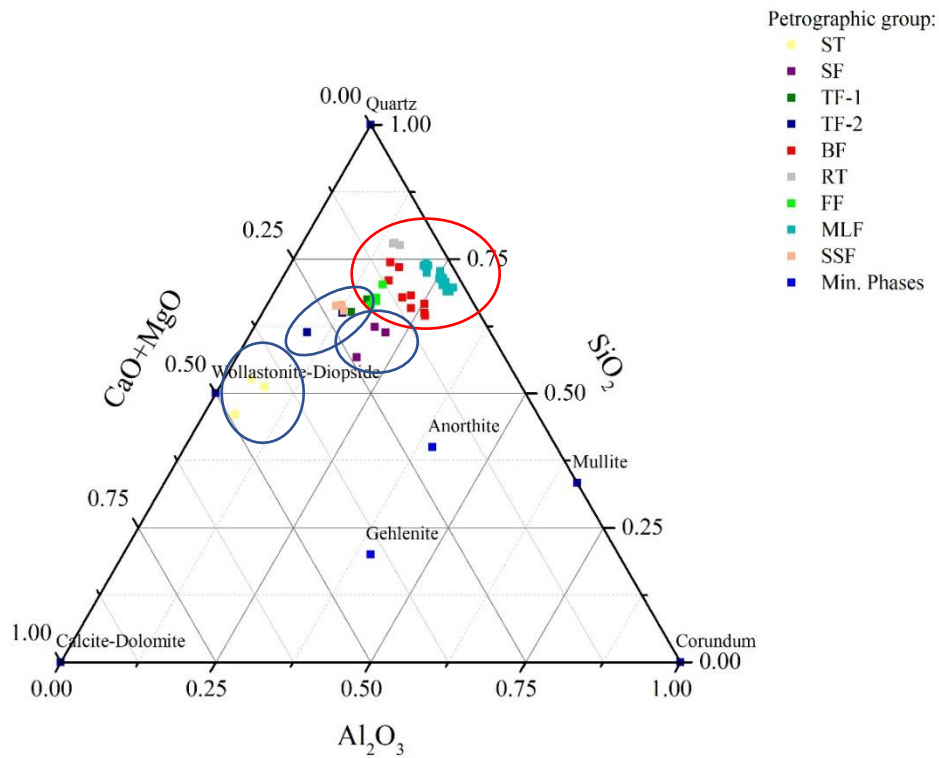


Figure 5.23: Ternary diagram of major oxides in correspondence of Al_2O_3 , SiO_2 and $\text{CaO}+\text{MgO}$ with local in blue circle and Indian in red circle stylistically identified (after Heimann and Maggetti 2019). ST: Shell Tempered; SF: Shale-rich Fabric; TF: Talc-rich Fabric; BF: Basalt-rich Fabric; RT: Rice Tempered; FF: Fine Fabric; MLF: Medium-Large inclusions in fine Fabric; SSF: Shell and Sand rich Fabric.

5.4 Scanning Electron Microscopy – Energy Dispersive X-rays Spectroscopy (SEM-EDS)

The final methodology adopted was the SEM-EDS analysis. The purpose of it is to characterize the composition of matrix and temper of ceramics. In fact, with SEM-EDS it was possible to investigate the chemical composition as well as visualise the structure and the inclusions in the

same thin sections that were already analysed in the polarized microscope. Due to its potential, and the depth of analysis possible with SEM-EDS, the process of data collection is time consuming, which results in the impossibility of analysing all the samples, especially in situations with a tight schedule. In this case study, the selection of the samples to study was done with the aim of investigating at least one member of each group. In addition to those, the samples had results which were problematic in terms of identification and grouping were analysed, with the aim of better understanding and, possibly, grouping them. The presentation of the results, similar to the previous sections, is divided here into groups with the aim of providing a complete understanding of the fabrics characterising the different groups. Matrix composition analysis were obtained with EDS multipoint analysis and presented in table 5.8 and Fig. 5.46. All the data, the recorded images and the graphs, in addition to the one presented in the following sections, are presented in the appendix 9.5.

5.4.1 Shell Tempered (ST)

The representative of the ST group was sample IQM16B.US35.8. The composition of the sample, similar to any other sample from the same group was characterized by the presence of crushed shells. The first approach, namely a visual survey of the sample with SEM-EDS, confirmed what was proposed by the petrographic analysis: most of the inclusions, if not all of them, were crushed shells. Among the non-shell inclusions, some large grains of quartz and or carbonates could be identified, but no other particularities were evident from the visual survey of the sample.

In addition to the visual overview of the sample, SEM-EDS allows one conduct chemical composition and distribution analysis. The chemical composition analysis is, generally, performed in two different ways with two different purposes. The first approach is that of mapping the distribution of the elements within a large area of the sample with the aim of understanding the behaviour of the single element within the sample, hence where it is present and where not. The second approach to the chemical analysis is the semi-quantification of the elements present and constituting the paste of the sample. This approach allows the comparison with other samples.

The elemental mapping (Fig. 5.24), highlighted the very high concentration of Ca in relation to the shells fragments, but the low concentration of it in correspondence to the paste. Differently to Ca, Si mapping highlighted its presence within the matrix, as expectable, but was also included in the composition of some shell fragments. The composition of the paste, avoiding any contamination provoked by shell fragments is presented on table 5.8.

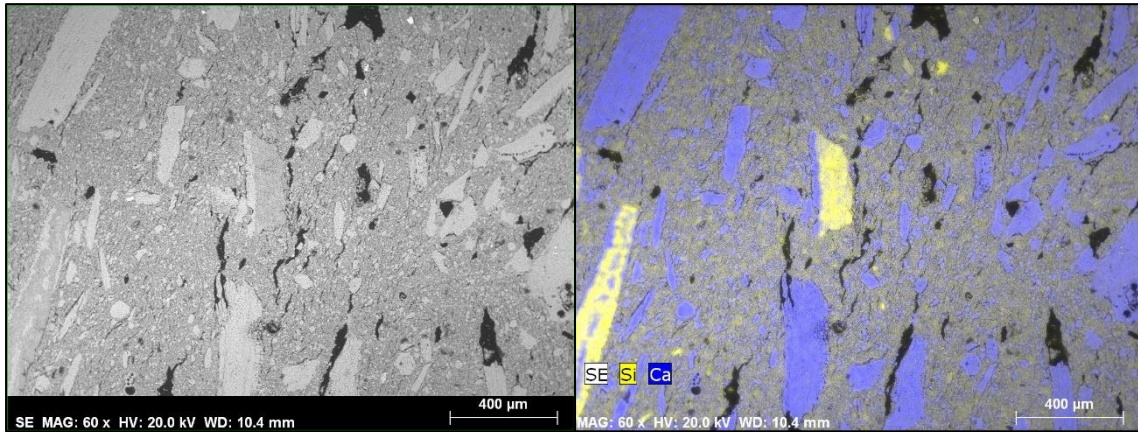


Figure 5.24: BSE image of ST on the left and the elemental distribution mapping with distribution of Si (yellow) and Ca (blue) on the right.

5.4.2 Shale-rich Fabric (SF)

The same analysis conducted in the ST group was also conducted on the SF representative: sample IQM16B.US35.34. The different composition of the fabric and the more complex nature of the inclusions in SF compared to ST was also evident in this analytical approach, as it was before. The initial visual survey of the sample composition highlighted the presence of shell material and bone material (Fig. 5.25), elements that need to be added to the large list of inclusions present in SF. The identification of the bone material is curious, especially considering of the lack of darkening of the bone fragments, (highlighted on a supplementary observation by optical microscopy) darkening that usually is the result of the firing of the ceramic. Identifying the nature of the bone material within the matrix is not possible without the confirmation of the chemical composition (Fig. 5.26). The mapping approach was applied, not only on the general composition analysis (Fig. 5.27), but also in the study of the composition within the shale grains (Fig. 5.28) and it highlighted the clay nature of the matrix (characterized by the presence of Al) of the shale with some microscopic inclusions, possibly identifiable as quartz. The chemical analysis also focused on understanding the matrix composition in order to identify the nature of the clay composing the ceramic. The method was the same as for the paste in ST: quantification of the chemical composition within an area in which there was no contamination from the inclusions. The results of the chemical analysis of the matrix are presented in table. 5.8.

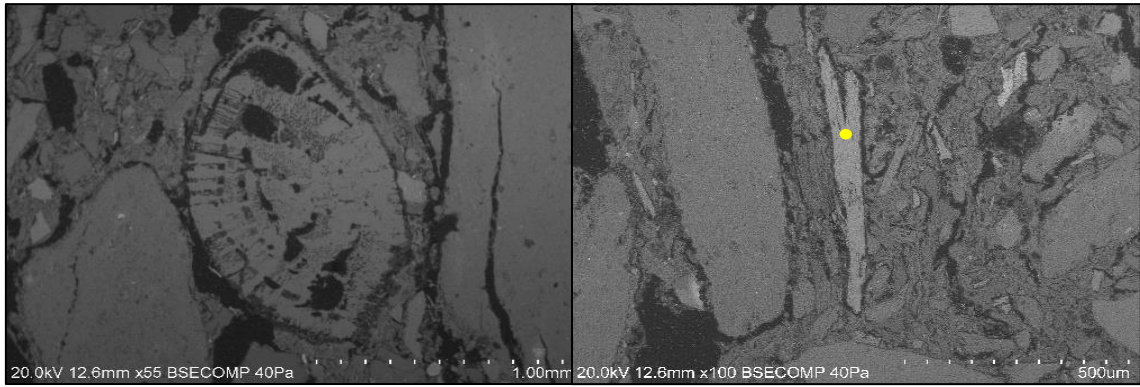


Figure 5.25: BSE images of SF group: On the left a shell fragment and on the right a bone fragment within SF with point of elemental composition analysis.

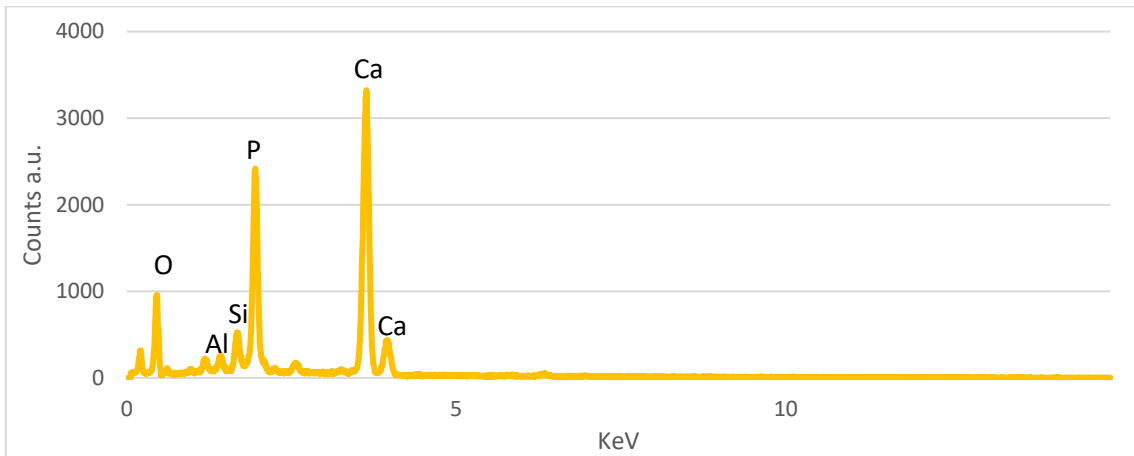


Figure 5.26: Point analysis of bone fragment.

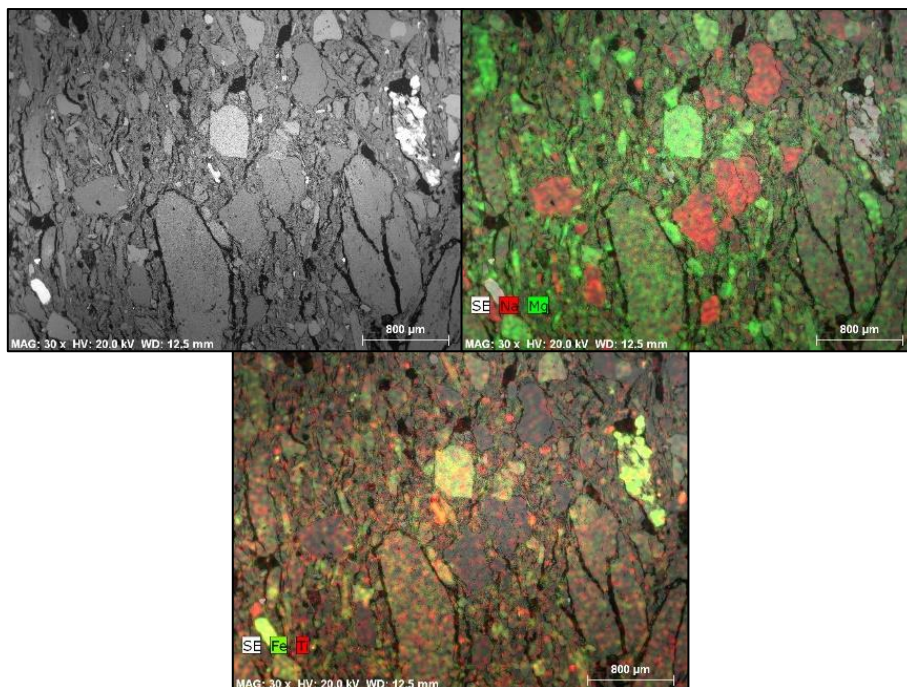


Figure 5.27: BSE image of SF on the top left and the elemental distribution mapping with in the centre the distribution of Fe (green) and Ti (red) and on the top right the distribution of Na (red) and Mg (green).

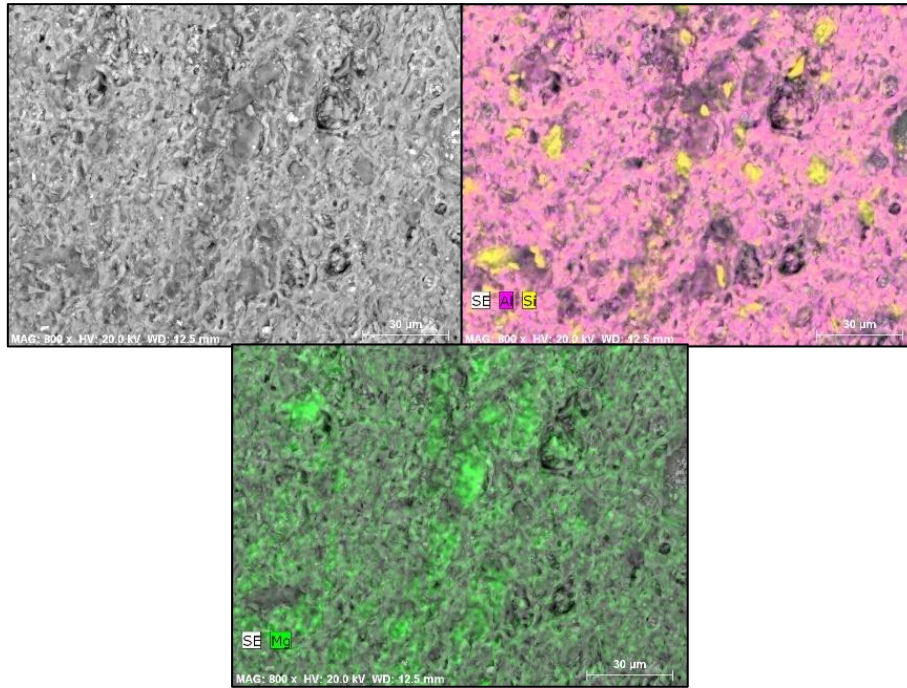


Figure 5.28: BSE image of shale grain in SF on the left and the elemental distribution mapping with in the centre the distribution of Mg (green) and on the right the distribution of Al (pink) and Si (yellow).

5.4.3 Talc-rich Fabric (TF)

Despite the fact that the TF group is composed of two subgroups, only one sample was analysed by means of SEM-EDS. The sample analysed was SUMW03A.US1.1, member of the TF-2 group. The visual survey of the sample highlighted the extremely high concentration of talc grains. Together with the talc grains, however, the sample presented important concentrations of iron oxides. Another particular characteristic underlined from the visual overview was the unclear nature of the clasts present within the matrix of the ceramic Fig. 5.31 which could be interpreted as evidence of bio-colonization (Skadiņš et al. 2019). Coupled with the visual investigation of the composition of the clasts, a map of the elemental composition was also done and applied to the investigation of the general distribution of elements within the fabric Fig. 5.30. The high concentration of talc grains is highlighted by the different distribution of Al and Mg in the picture, with Mg identifying the talc clasts (Fig. 5.29). The bright white grain indicates the presence of oxide. Except for the presence of talc and oxide grains, no extra information was provided by the general mapping. Similar to what was done for SF, a quantification analysis of the elements constituting the TF matrix is presented here. The methodology was the same as before: identification of the elemental composition by means of the analysis of an area as free from the contamination of inclusions as possible. The results are presented in table 5.8.

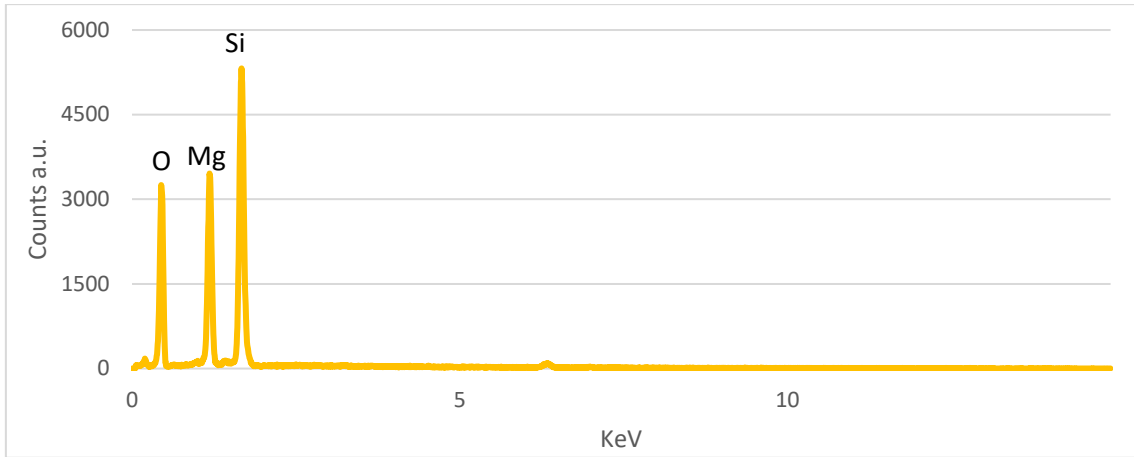


Figure 5.29: Point analysis of talc inclusion.

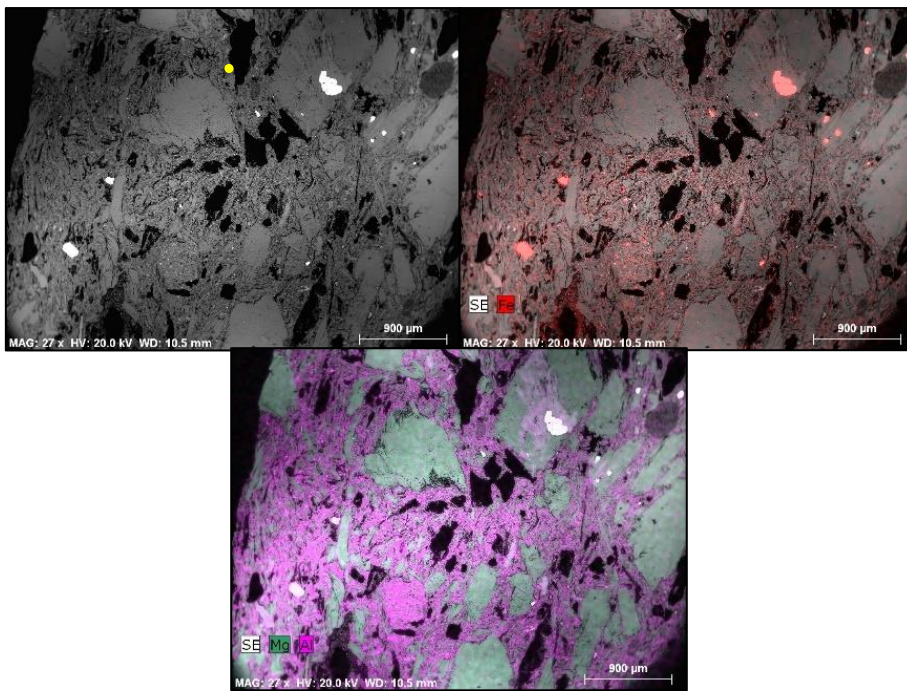


Figure 5.30: BSE image of TF on the top left and the elemental distribution mapping with in the centre the distribution of Mg (green-talc) and Al (pink-paste) and on the top right the distribution of Fe (red-oxide).

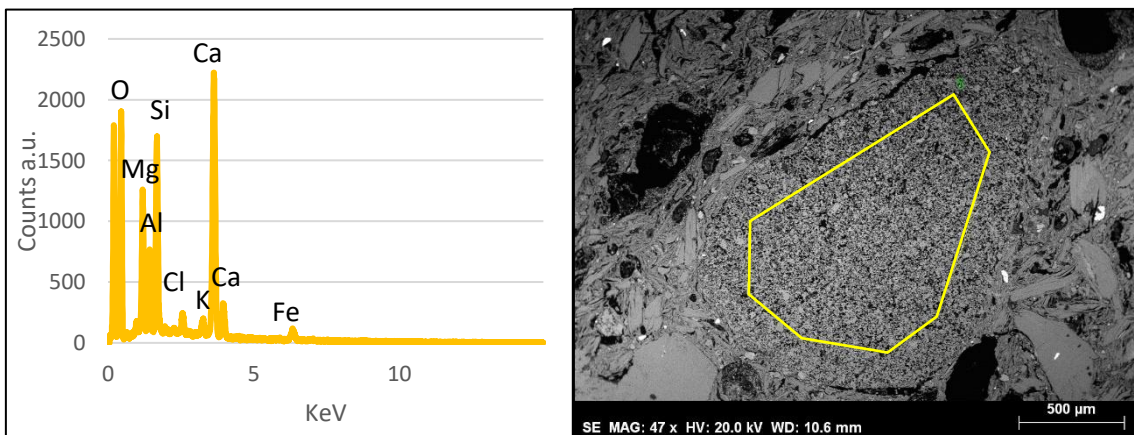


Figure 5.31: On the left the elemental composition and on the right BSE image of the clast.

5.4.4 Basalt-rich Fabric (BF)

Due to the large composition of the BF group, two samples analysed with SEM-EDS are here presented. The samples selected were IQM16B.US30.6 and SUM08B.US975.4. The selection of the first sample was dictated by its representativity of the BF general composition, while sample SUM08B.US975.4 was quite unique and it also included grains that were identified as volcanic glass. Starting with the visual survey of the samples, it was possible to observe the presence of singular rounded basalt grains, rice husks and, in SUM08B.US975.4, of volcanic glass (Fig. 5.32).

Mapping of the elemental distribution aids the visual observation in the identification of the lithic grains and other components. In particular, in addition to the common general mapping of the sample composition (Fig. 5.33), in the case of the two samples presented here, a map of the basalt was compared with the mapping of a partially vitreous igneous grain (Fig. 5.34 and Fig. 5.35). The comparison between the basalt grains and the glass grains showed some similarities, but in the case of the volcanic glass, glass-like needles were the main representative characteristic. Furthermore, the crystalline composition was less clear and not as predominant as it was in the basaltic grain.

In addition to the visual analysis and to the mapping, chemical analysis of areas and points were conducted in different parts of the samples, with the aim of better understanding the paste composition, but also to allow comparison of the inclusions among the samples. The comparison between the pastes is presented in table 5.8 where clear similarities are visible. Last, but not least, a composition analysis of the pyroxenes located within and outside basalt grains was done. The results are presented along with the results of pyroxene analysis from the RT group in Fig. 5.37.

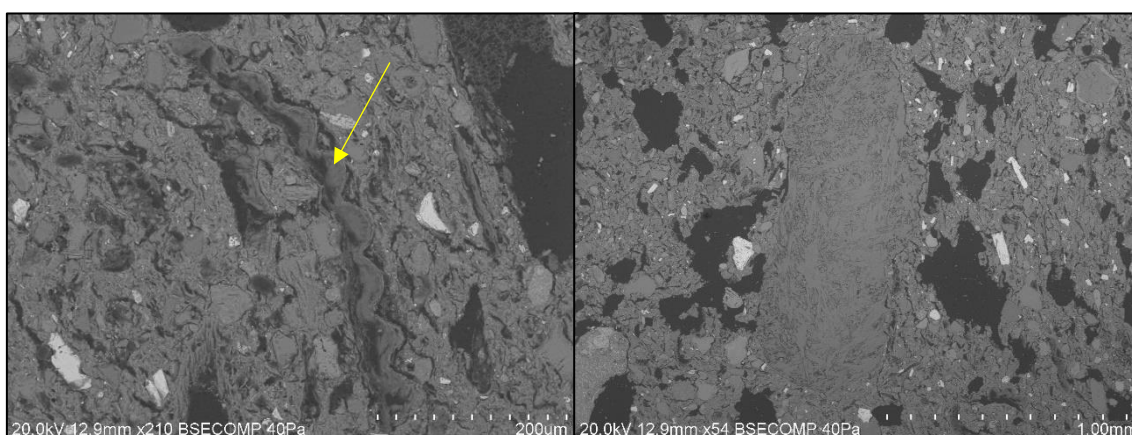


Figure 5.32: BSE images of BF group: On the left a rice husk and on the right an example of volcanic glass grain.

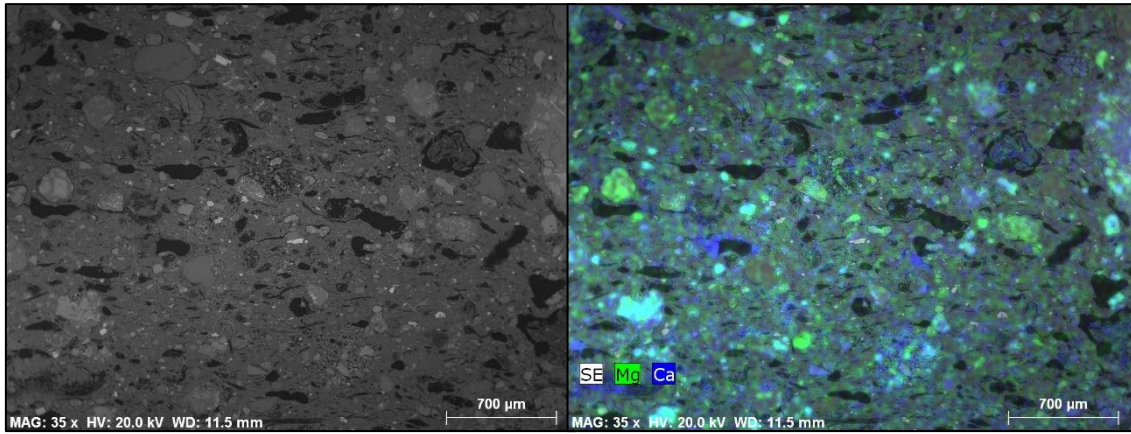


Figure 5.33: BSE image of BF on the left and on the right the elemental distribution mapping with the distribution of Mg (green-pyroxene) and Ca (blue plagioclase and pyroxene).

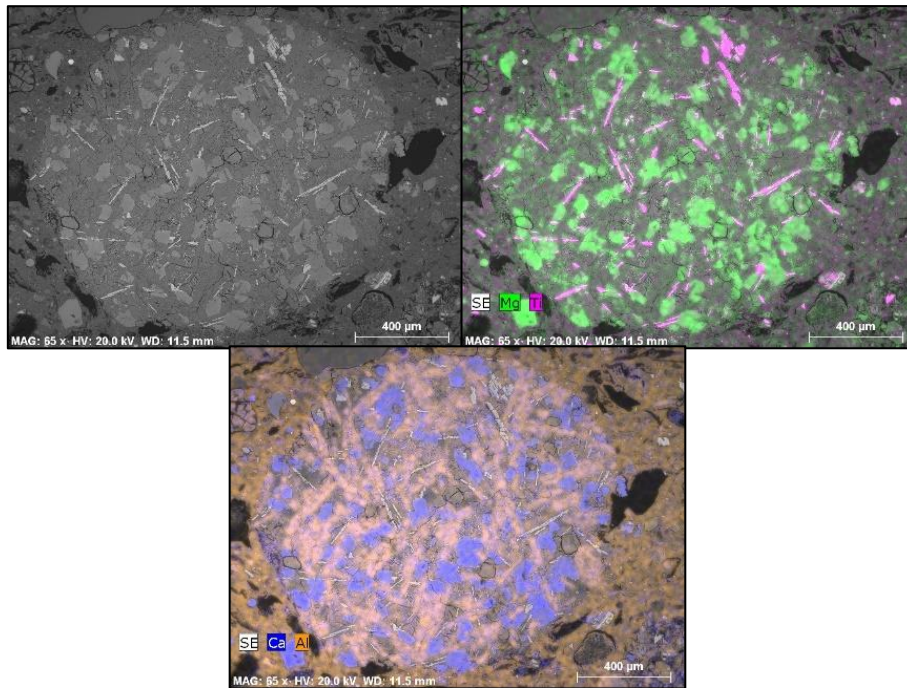


Figure 5.34: BSE image of basalt grain in BF on the top left and the elemental distribution mapping with in the centre the distribution of Ca (blue-pyroxene) and Al (orange-plagioclase and paste) and on the top right the distribution of Mg (green-pyroxene) and Ti (pink-oxide).

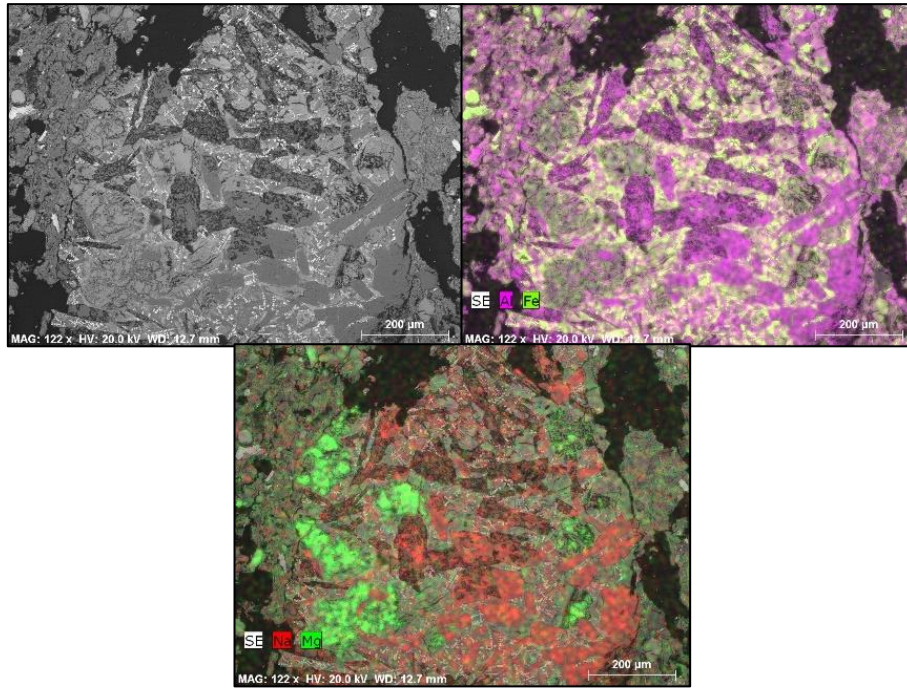


Figure 5.35: BSE image of volcanic glass grain in BF on the top left and the elemental distribution mapping with in the centre the distribution of Mg (green-pyroxene) and Na (red-plagioclase) and on the top right the distribution of Fe (green-pyroxene) and Al (pink-plagioclase and paste).

5.4.5 Rice-rich Fabric (RT)

The sample selected as representative of the RT group was SUM10C.US174.104. As already mentioned, the visual investigation of the samples from RT highlighted the very high concentration of rice husks within the matrix. In the visual survey of the sample by means of SEM-EDS, no particularities were identified in addition to the observation conducted by optical microscopy. The main inclusions were the rice husks which were, mostly, preserved with the internal structures still visible with SEM-EDS (Fig. 5.36). On the other hand, the mapping of the general elemental distribution highlighted the presence of inclusions of very small dimensions. Those inclusions were mainly identifiable as quartz grains and rare plagioclase as visible in Fig. 5.38. As a last step of analysis, the quantification of the elemental composition was then performed, avoiding the contamination of inclusions, on the matrix as well as on pyroxene grains present in the general composition. The possibility of running similar analysis allows the comparison between groups and within the same groups, as already presented. The data related to pyroxene in RT are represented in green Fig. 5.37 and they were remarkably different from the same minerals present within the two BF Samples. On the other hand, the results of the elemental quantifications of the pastes are presented in table 5.8.

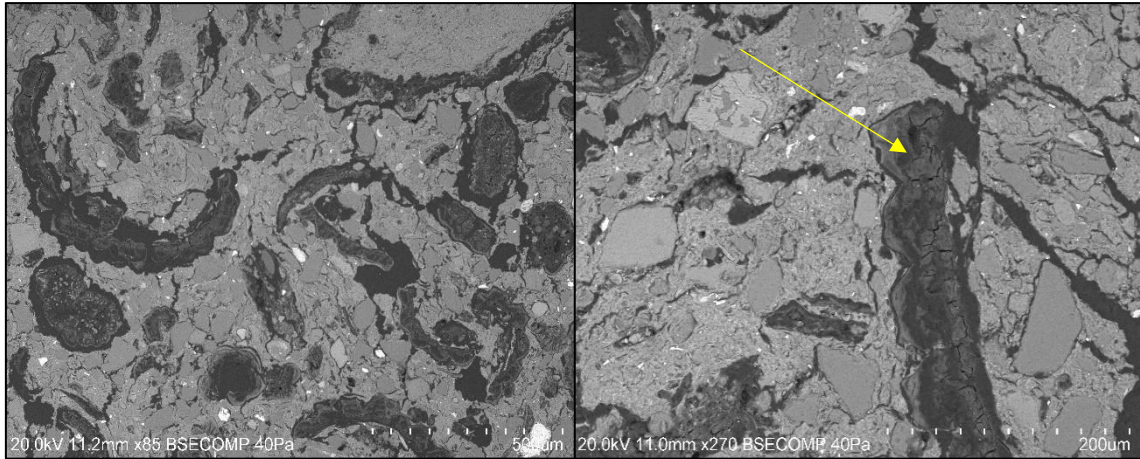


Figure 5.36: BSE images of RT group: On the left a general view and on the right a zoom-in on a rice husk.

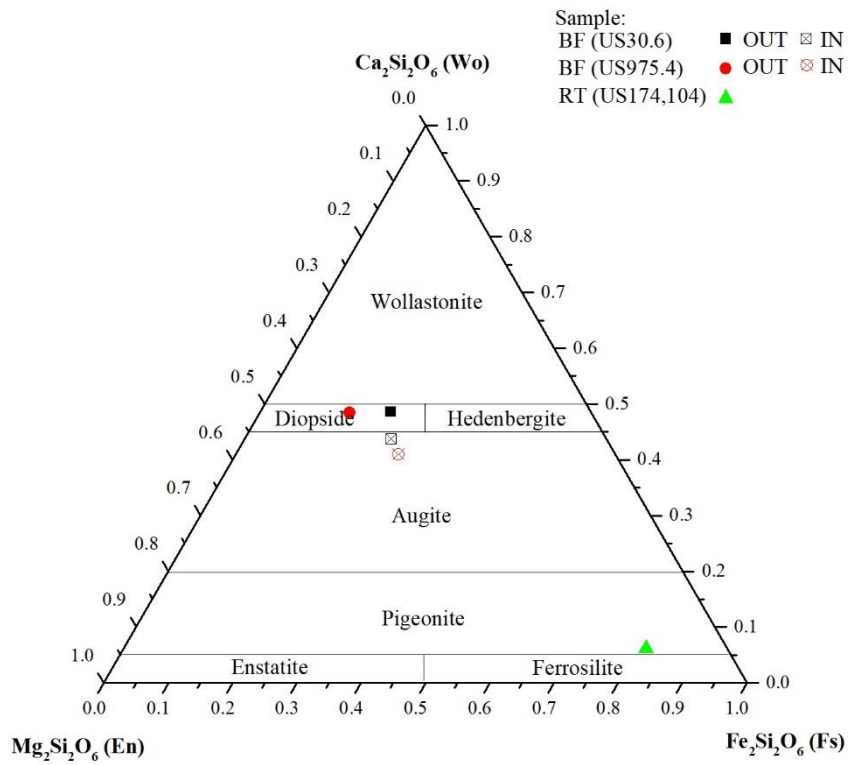


Figure 5.37: Ternary diagram of pyroxenes from BF samples and RT sample. The comparison is also among pyroxene located within basalt grains (crossed empty symbol) and single pyroxene grains (full coloured symbols), both within BF samples (after Heimann and Maggetti 2019).

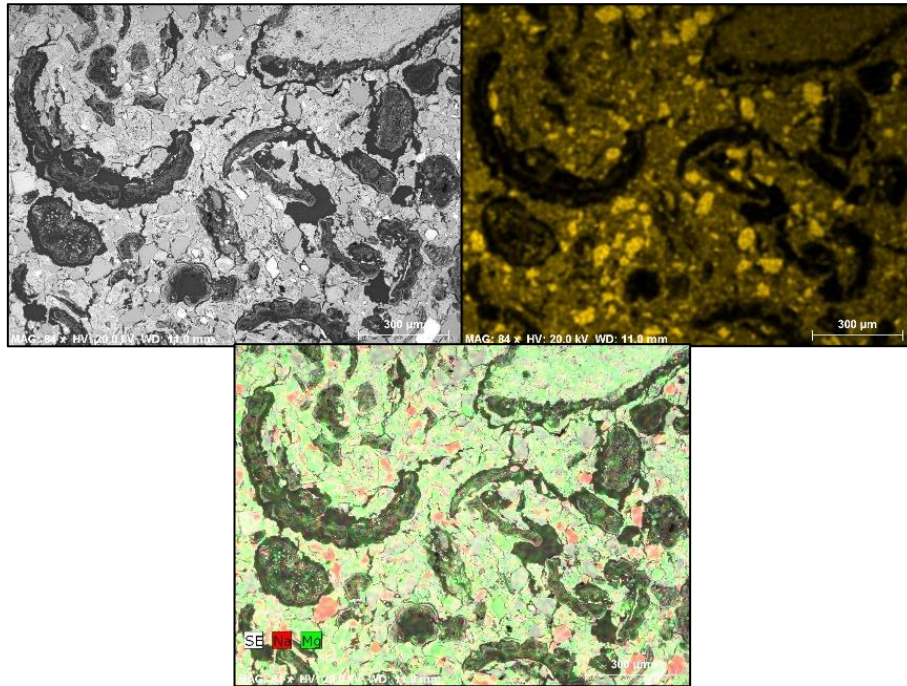


Figure 5.38: BSE image of RT on the top left and the elemental distribution mapping with in the centre the distribution of Mg (green-paste) and Na (red-plagioclase) and on the top right the distribution of Si (yellow-quartz).

5.4.6 Fine Fabric (FF)

The analysis by means of SEM-EDS is of extreme importance for the better understanding of the composition of the FF group. Of this group, two out of three samples were analysed: IQM18A.US80.3 and SUM10C.US162.119. The analysis of the two samples was made necessary due to the particularly high quality of the sample IQM18A.US80.3. The first approach towards the samples was the analysis of the composition by means of a visual survey. The visual approach highlighted the diversity among the two samples grouped together, with the first being of extremely high quality and, even with SEM-EDS, the composition appeared to be uniform (Fig. 5.39). On the other hand, sample SUM10C.US162.119 displayed few examples of rice husks and it also presented some bone fragments (Fig. 5.39). The identification of the bone fragments was possible with the identification of the elemental composition of the fragments by means of point analysis (Fig. 5.40). The results of the mapping, on the other hand, provide interesting differences between the two samples. The mapping of the sample SUM10C.US162.119 not only provided the confirmation of the presence of bone fragments, but it also highlighted the strong difference between the material used for the body of the ceramic and the material used for the slip (Fig. 5.41). On the other hand, sample IQM18A.US80.3 showed extreme uniformity in the general composition (Fig. 5.42). Similar to the other samples from the previous groups, the matrix elemental quantification analysis was done for the two samples presented here. The comparison of the pastes is highlighted in Fig. 5.47.

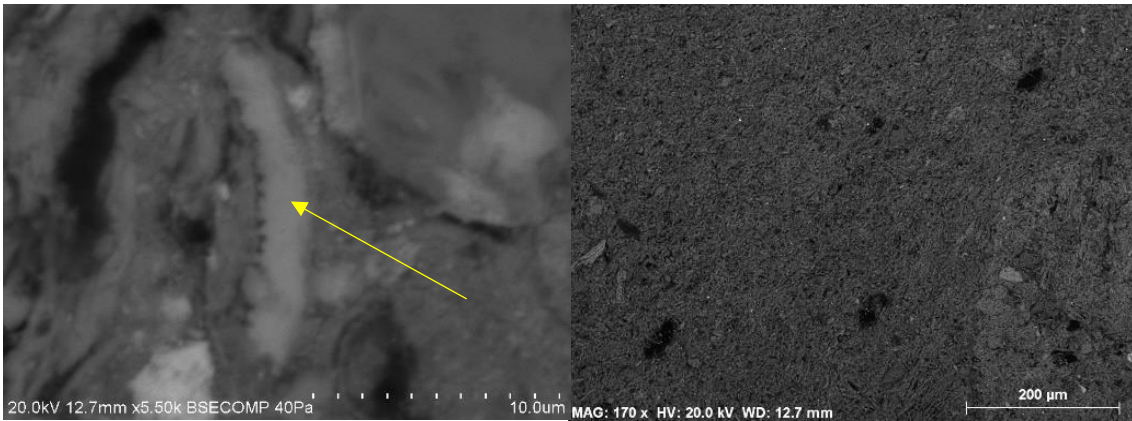


Figure 5.39: BSE images of FF group: On the left a bone fragment and on the right a general view of the US80.3 sample composition.

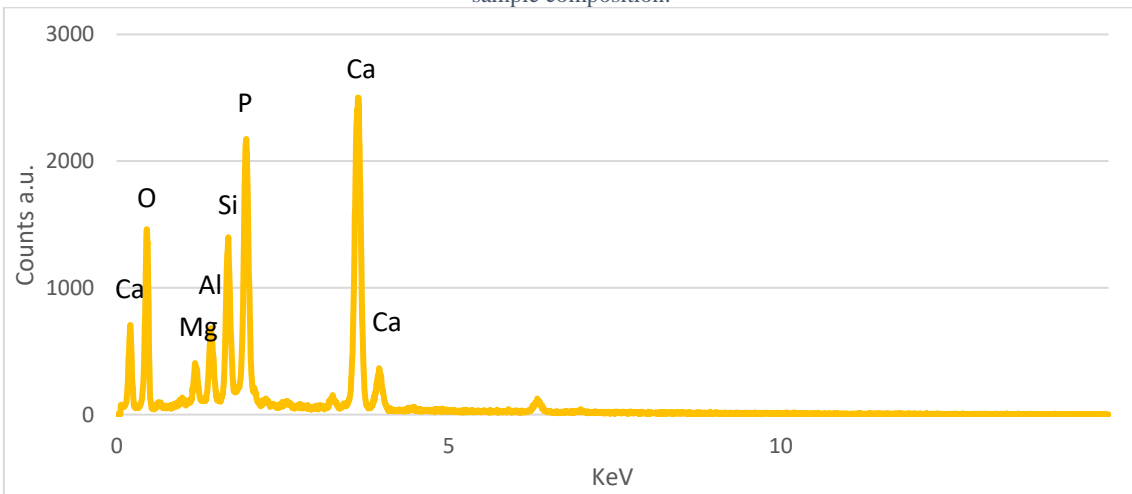


Figure 5.40: Point analysis of bone fragment.

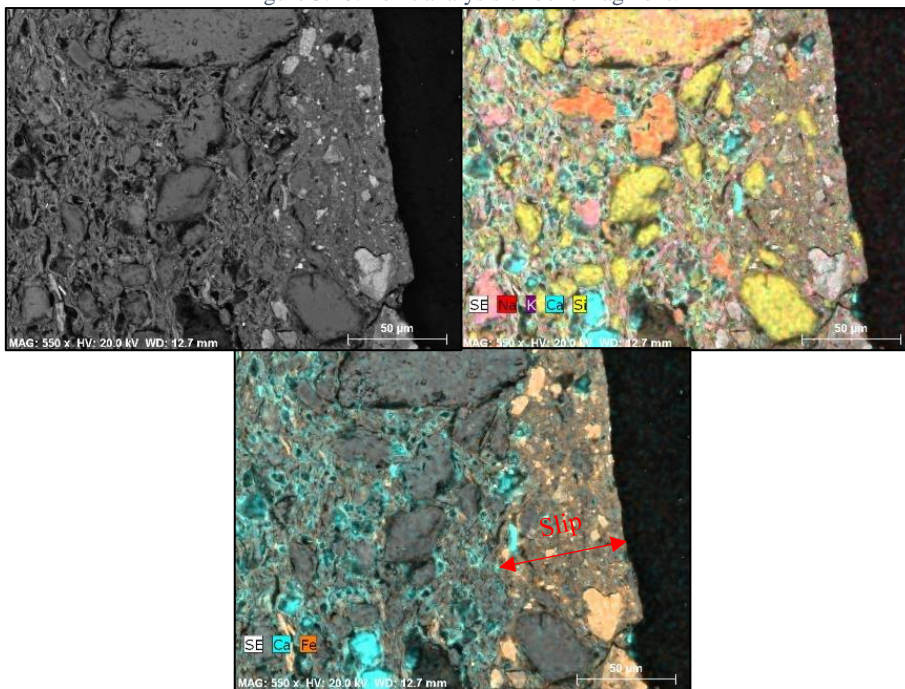


Figure 5.41: BSE image of FF on the top left and the elemental distribution mapping with in the centre the distribution of Ca (blue-pores, bone fragments and plagioclase) and Fe (orange-micas) and on the top right the distribution of Na (red-lithoclast), K (purple), Ca (blue) and Si (yellow-quartz).

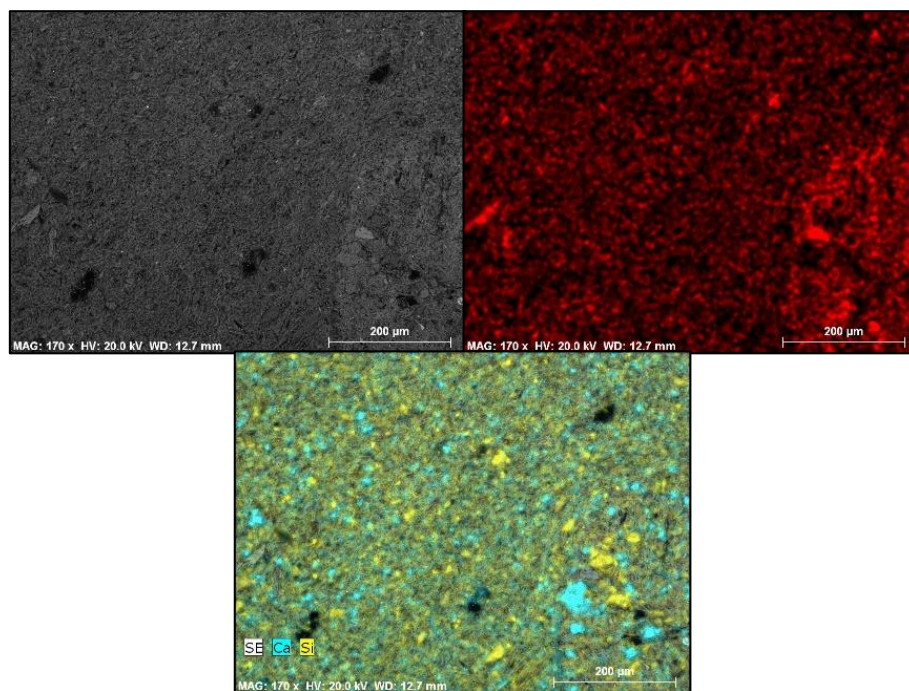


Figure 5.42: BSE image of FF on the top left and the elemental distribution mapping with in the centre the distribution of Ca (blue) and Si (yellow) and on the top right the distribution of Fe (red).

5.4.7 Medium-Large inclusions in fine Fabric (MLF)

Two samples were analysed for the MLF group: IQM16B.US35.9 and SUM08A.US253.5. The selection of the two samples was based on the fact that the first was the most representative of the MLF group while the latter was the sample that manifested the most striking differences, especially from the analysis of the REE data. As was presented in the optical microscopy analysis, the visual survey of the two samples with SEM-EDS also confirmed that the main characteristic is the homogeneity among the large inclusion grains (Fig. 5.43). Both samples, according to petrographic analysis, were characterized by the presence of large quartz and feldspar grains, and this characteristic was also proved correct by the mapping of the elemental distribution (Fig. 5.44 and 5.45). Further analysis and comparisons, between the two samples, were focused on the matrix composition. The results from the quantification of the pastes elemental composition are presented in table 5.8 and, when compared, it is possible to notice some limited differences. However, the differences could be explained by the minor presence of amphiboles within SUM08A.US253.5 manifested by XRD and characterizing a more flat behaviour in ICP-MS results. However, also sample SUM10A.US405.3 is rich in amphiboles and it does not behave similarly to SUM08A.US253.5. Moreover, the differences in the matrix composition may be indicating that the MLF group is possibly composed by different subgroups.



Figure 5.43: BSE images of MLF group: On the left a view of US35.9 and on the right a view of US253.5.

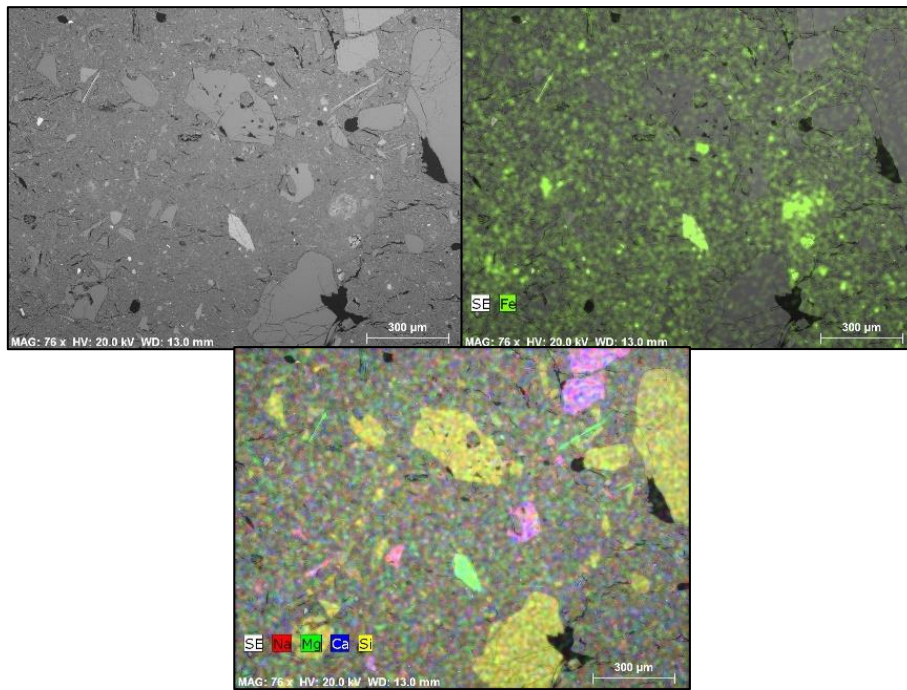


Figure 5.44: BSE image of MLF on the top left and the elemental distribution mapping with in the centre the distribution of Na (red-feldspar), Mg (green-micas), Ca (blue) and Si (yellow-quartz) and on the top right the distribution of Fe (green-micas).

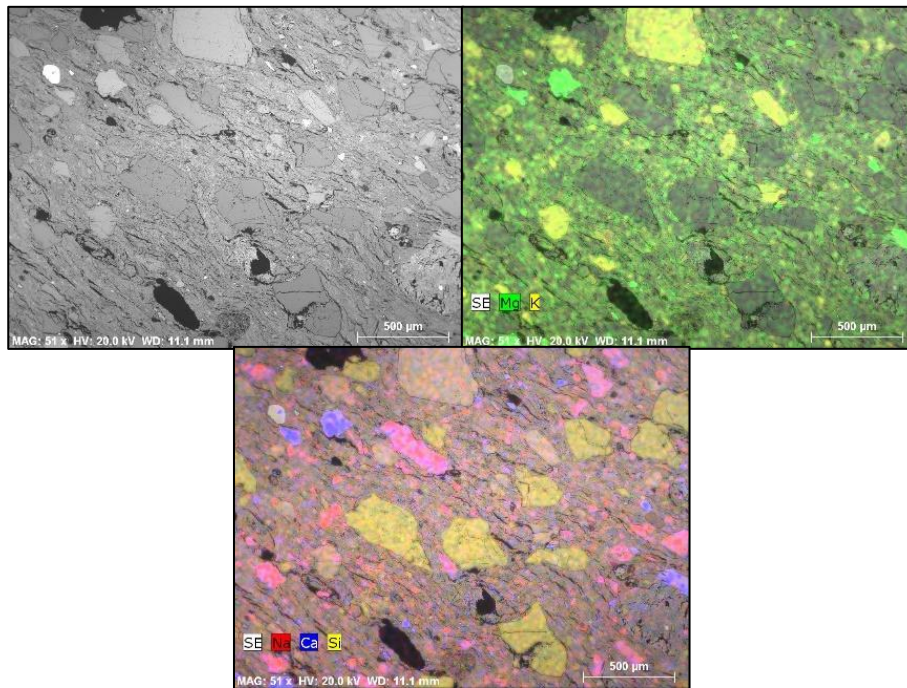


Figure 5.45: BSE image of MLF on the left and the elemental distribution mapping with in the centre the distribution of Na (red- feldspar), Ca (blue-amphiboles) and Si (yellow-quartz) and on the right the distribution of Mg (green-amphiboles) and K (yellow-k-feldspar).

5.4.8 Shell and Sand rich (SSF)

The sample selected as representative of the SSF was SUM03B.US93.42. The selection of only one sample was a consequence of the small size of the group (only 3 samples) and of the remarkable similarities between samples. As the name suggests, the characteristic of the group was the high concentration of shell fragments and sand grains within the matrix. The visual survey of the sample by SEM-EDS confirmed the high concentration of shell fragments, but it also highlighted the presence of some other inclusions. In Fig. 5.46, the attention is focused on the structure that covers the neck, a structure interpreted as a mistake in the production of the neck of the vase. In the structure, as well as in the rest of the sample, the concentration of very rounded shell fragments was remarkably high. In order to be sure of the shell nature of the rounded grains, and in order to investigate the nature of the other inclusions, a mapping of the elemental distribution is presented here (Fig. 5.46). The mapping highlighted the calcitic nature of the shells, and the presence of quartz grains in limited quantity. The last step of analysis, the step of the matrix composition and quantification analysis, is presented in table 5.8.

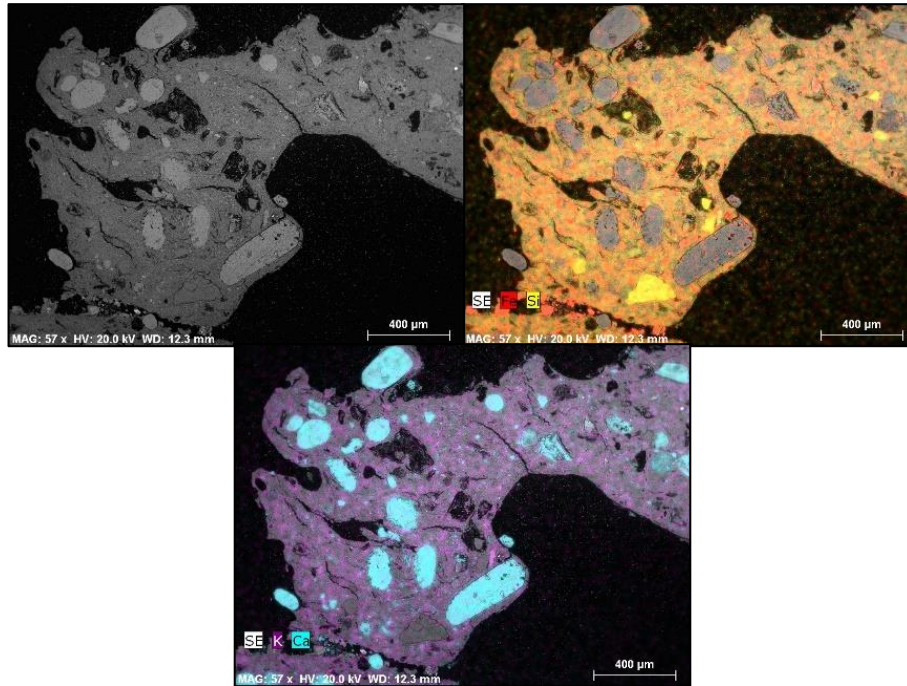


Figure 5.46: BSE image of SFF on the top left and the elemental distribution mapping with in the centre the distribution of K (purple-paste) and Ca (blue-calcitic shell) and on the top right the distribution of Fe (red-oxides) and Si (yellow- quartz).

5.4.9 Paste comparison

The most important component of the ceramic is the paste that is the clay constituting the core structure of the pots. Comparing the pastes allows the comparison of the nature of this raw material without the risk of including the compositional effect of the inclusions intentionally added and naturally different from the bulk composition. Moreover, a further step in the analysis of the relations between groups is represented by the comparison of the pastes quantification analysis. In order to do so, the comparison was done after the translation of the raw elemental data into their major oxides (Tab. 5.8).

Table 5.8: Summary of the major oxides' composition done by EDS of the pastes (wt. %). The colour of the samples identifies the group of membership: Shell Tempered (yellow), Shale-rich Fabric (purple), Talc-rich Fabric (dark blue), Basalt-rich Fabric (red), Rice Tempered (grey), Fine Fabric (green), Medium-Large inclusions in fine Fabric (light blue) and Shell and Sand rich Fabric (brown).

| | Na ₂ O | MgO | Al ₂ O ₃ | SiO ₂ | K ₂ O | CaO | TiO ₂ | FeO |
|------------------|-------------------|------|--------------------------------|------------------|------------------|------|------------------|------|
| IQM16B.US35.8 | 1,1 | 5,0 | 16,5 | 41,8 | 3,1 | 23,0 | 1,0 | 8,6 |
| IQM6B.US35.34 | 2,6 | 7,5 | 22,6 | 46,6 | 3,7 | 7,0 | 1,4 | 8,6 |
| SUMW03A.US1.1 | 2,4 | 18,4 | 15,8 | 49,7 | 3,2 | 0,8 | 1,1 | 8,5 |
| SUM08B.US975.4 | 2,8 | 2,7 | 31,7 | 45,4 | 2,0 | 3,2 | 4,5 | 7,5 |
| IQM16B.US30.6 | 4,8 | 2,1 | 25,5 | 47,6 | 1,6 | 8,1 | 1,6 | 8,7 |
| SUM10C.US174.104 | 2,2 | 4,3 | 21,2 | 48,8 | 3,8 | 3,1 | 1,8 | 14,9 |
| IQM18A.US80.3 | 2,3 | 5,1 | 15,4 | 47,6 | 2,7 | 18,4 | 1,1 | 7,5 |
| SUM10C.US162.119 | 1,9 | 4,9 | 18,5 | 47,3 | 3,9 | 14,0 | 1,2 | 8,3 |
| SUM08A.US253.5 | 2,2 | 2,6 | 24,3 | 53,0 | 4,4 | 1,4 | 1,7 | 10,4 |
| IQM16B.US35.9 | 1,9 | 2,2 | 37,5 | 45,5 | 2,2 | 1,7 | 1,9 | 7,0 |
| SUM03B.US93.42 | 2,4 | 4,2 | 24,2 | 46,2 | 5,2 | 8,0 | 1,3 | 8,4 |

The comparison was done by comparing the position in the graph, but the comparison of the % of CaO within the matrix is also highlighted. In fact, particular attention is given to the CaO % concentration in order to identify if the clay raw material was calcareous or non-calcareous. The definition of calcareous was given to samples with a CaO concentration above 6% (for a bulk composition) of the sample (Naseerutheen et al. 2014). The identification is highlighted with the samples having a calcareous paste being identified in green, while the non-calcareous samples are highlighted in red. On the other hand, Fig. 5.47 presents all the samples together within a graphic representation of the proportions of SiO₂, Al₂O₃ and CaO+MgO wt.% of the different pastes. As it is visible in the ternary diagram (Fig. 5.48), in the case of BF and FF samples, both are located close to each other, but in case of the MLF samples, the two samples are distant, suggesting possible different raw materials. The distinction among the different groups is not strong and clear reflecting the tendency that clays have in being similar. ST and FF represent the exception because characterized by lower Al₂O₃ than the most of the other samples.

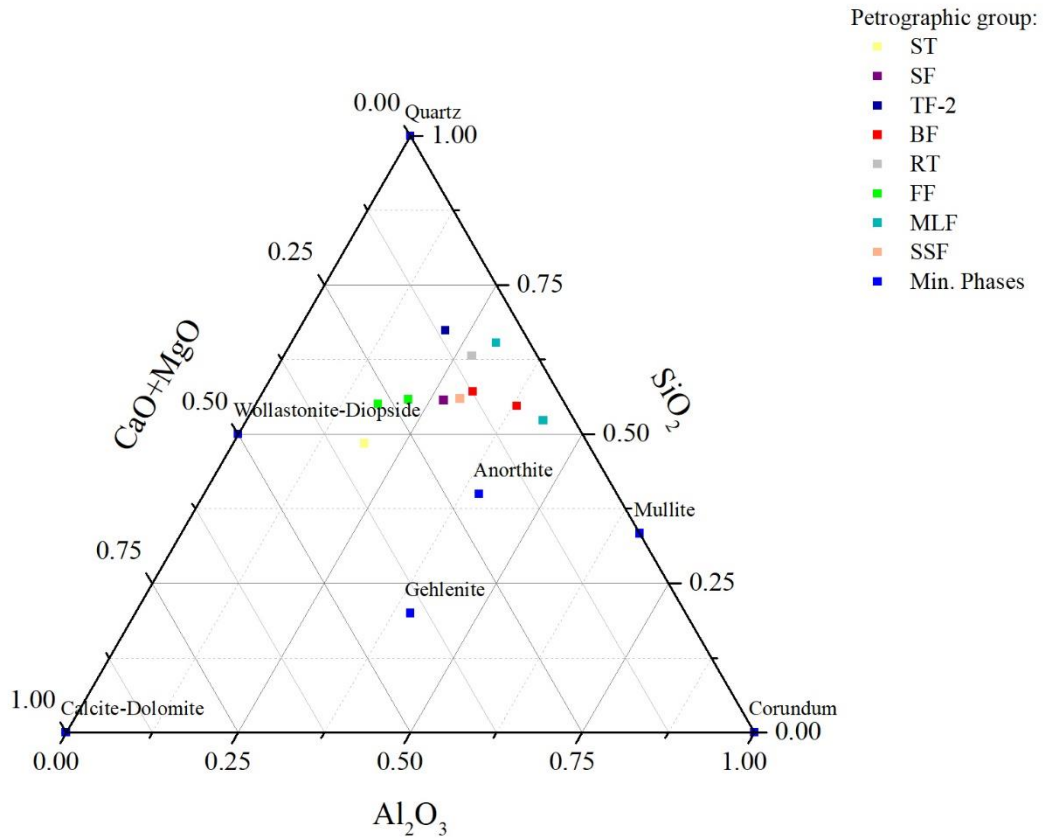


Figure 5.47: Ternary plot representing the comparison of the binders according to CaO+MgO, SiO₂ and Al₂O₃ (wt.%). ST: Shell Tempered; SF: Shale-rich Fabric; TF: Talc-rich Fabric; BF: Basalt-rich Fabric; RT: Rice Tempered; FF: Fine Fabric; MLF: Medium-Large inclusions in fine Fabric; SSF: Shell and Sand rich Fabric.

5.5 Geological data

Of particular importance for the research is the geological information regarding the areas under investigation, in fact information regarding geology is the baseline used to compare the raw materials data. As explained previously, the basic concept of the presentation of this thesis, is the direct comparability between geological formations of the sourcing area, and raw material. It is, with the aim of providing the reader a good base of comparison, that the author presents here the geological description of the regions taken in considerations: India and Southern Arabia.

5.5.1 Arabia

The geology of the southern side of the Arabic peninsula (Fig. 5.48) is characterized by three important geological formations: a sandy desertic region to the north (green), the uplifting of oceanic basement forming the central part of the Southern Arabian region (green area along the coast) and 2 areas presenting metamorphic (purple) and igneous formations (red for the plutonic,

pink for the volcanic), one on the West coast of Yemen, the other on the north-eastern coast of Oman.

Starting from the Western section (Fig. 5.48), a plateau is located along the Red Sea coast of Yemen. The plateau is comparable to the plateau located on the opposite shore of the Red Sea, suggesting that the plateau predates the connection of the Red Sea with the Arabic Sea. The Yemen-Aden plateau is characterized by igneous formations, in particular by

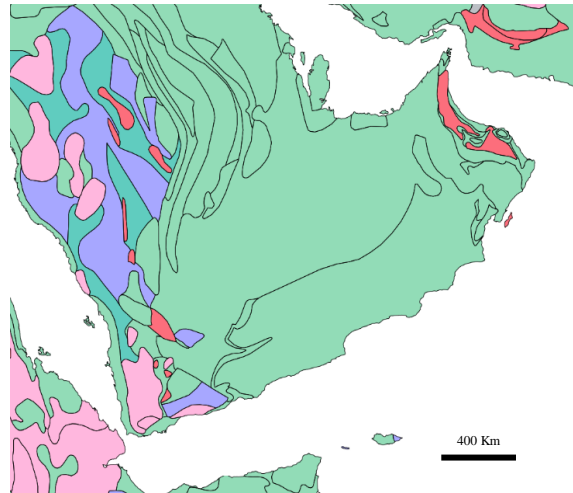


Figure 5.48: Generic view of the geology of Yemen, Oman and south Saudi Arabia (after www.usgs.gov).

volcanic layers. It is bordered to the north by flat sedimentary rocks and to the southern side by regional and contact metamorphic formations. Such metamorphic formations are covered by layers of shale, limestone and sand-stone resulting from the period in which the metamorphic formations were below the sea (Powers et al. 1966).

The coastal area can be identified as the result of a combination of tectonic uplifting with strong oceanic influence. In particular, two regions can be identified: the Hadramwat plateau and the plane of Salalah. The first, within modern day Yemen, is a plateau extending from the Gulf of Aden towards the Dhofar region. It is characterized by formations of limestone and by the presence of some faults crossing it, allowing the draining of seasonal waters by means of wadis (Powers et al. 1966). The plane of Salalah (Fig. 5.49) is, on the other hand, a low plain protected on the north by Jebel Qara mountain range. The mountain range is the result of strong uplifting of the ocean basin and it has a notheastern-southwestern orientation. Its formation separates the low plain of Salalah from the Rub' al Khali desertic basin extending from the Hadramawt plateau all the way to the eastern Oman. The Jebel Qara is formed mainly of limestone affected by karstic phenomena and tufa formations along the wadis cutting through the mountains, sometimes following tectonic fractures, sometimes cutting the mountains by means of their erosion activity (Zerboni et al. 2020). Most of the wadis cutting through the Jebel Qara formation then cross the Salalah plain to get to the Arabic Sea. The plain is mainly fluvial, formed by gravel, smaller fluvial deposit and carbonates. The carbonates are deposited towards the mouth of the wadis, a mouth that is mostly characterized by sandy ridges forming estuaries while, behind the sand ridges, lagoons host mangroves (Zerboni et al. 2020). The general composition of the plain, except for the alluvial deposits derived from the erosion of the Jebel Qara, is characterized by a base of limestone and sedimentary bedrock. Outcrops are present around the plain and they show

presence of marls, limestones, dolomites in few cases, sandstones and breccia limestones (Khalifa 1988).

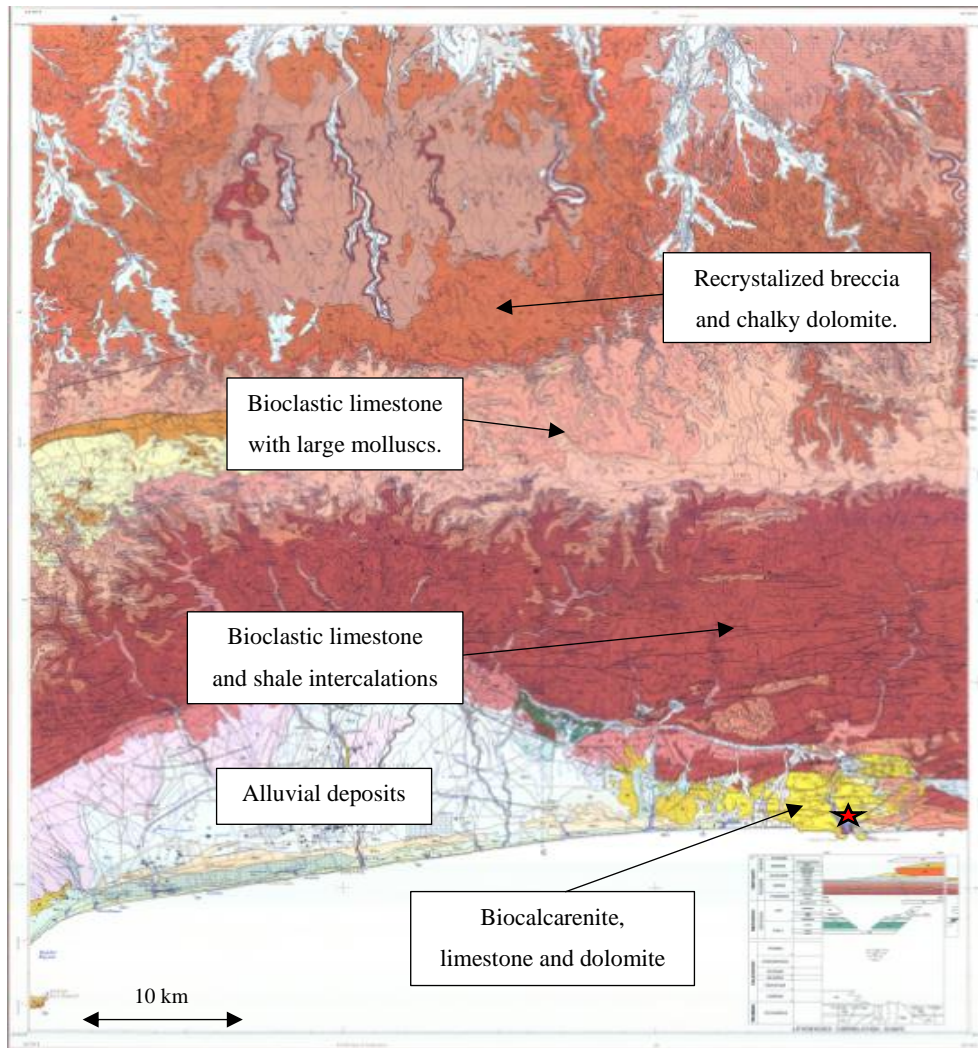


Figure 5.49: Geological close up of the Salalah region with including the sites of Sumhuram and Inqitat indicated by the red star (after M. I. Khaifa, 1988).

As mentioned before, the Jebel Qara range separates the fluvial plane of Salalah in the south and the Rub’al Khali desertic basin on the north. The desertic basin is characterized by a massive deposition of aeolian sands. The amount of sand varies from area to area, with the immediate proximities to the Jebel Qara characterized more by a rocky desert than a sandy desert. The desertic formation covers all the central area of the Arabic peninsula and it pushes itself to the Omani coastline of the Arabic Sea (Powers et al. 1966).

The last feature to be mentioned, when talking about the southern Arabian Peninsula coast are the mountains of Oman. The mountains define the core of the Persian Gulf coastline of Oman. The Omani mountain range is characterized by the presence of igneous and metamorphic formations

(including Semail ophiolite) as well as salt formations from the Palaeozoic era. Despite the presence of igneous and metamorphic formations, the most common geological formations are later marine deposition, both of clastic and chemical nature (Powers et al. 1966). To the southern flank of the Omani mountains, gently formed hills of sedimentary nature border with a large homogenous uplifted plateau, also of sedimentary nature (Powers et al. 1966).

5.5.2 Indian Subcontinent

Due to its large dimensions, the Indian Subcontinent is characterized by an extremely large variability of geological formations. In this thesis, the aim is not that of presenting an accurate description of the geological structures of the Indian Subcontinent, but a general overview of the most characteristic and important features (in relation to the archaeological material analysed) (Fig. 5.50). With that intent in mind, the description of the geological formations of the Indian Subcontinent are here presented separated in 4 main areas: Himalaya (complex system in the north) and the alluvial planes in the north-west (green large area), the Deccan trap in the centre-west of India (pink area), the eastern alluvial plains (green areas on the east coast) and the plutonic and metamorphic southern tip, which includes Sri Lanka (including purple and red areas).

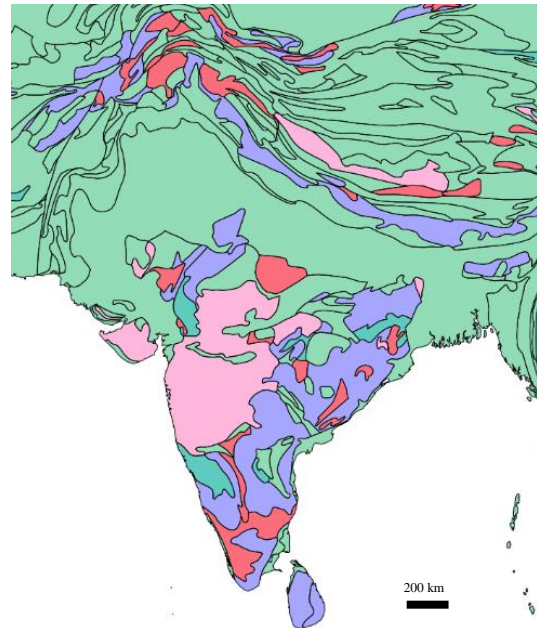


Figure 5.50: Generic geological map of South Asia (after www.usgs.gov).

The region of the Himalayan ridge is characterized by the very imponent structures of the mountains and by the debris eroded by the rivers flowing within the valleys (Fig. 5.50). The Himalayan range is mainly composed of marine deposits that, due to the extension of the geological area, is of a different nature. Among the components of the body of the mountains, we can find important deposits of limestones, sandstones, fossiliferous layers and many other deposits connectable to ancient ocean floors. It is from these mountains that a very well developed and perennial working system of rivers flows towards the northern plain of the Indian subcontinent. The northern plain collects debris transported by the rivers flowing down from the Himalayas as well as from the center of the Indian peninsula. The result is that of a very complex fluvial deposit system with the dimensions of the debris getting smaller, the closer the river gets to the oceans. The general composition, then, of sediments coming from the north of India can be

described as of sedimentary origins, either directly from the bedrock outcrops of the Himalayas or from the fluvial deposits (Wadia, 1919).

The Deccan trap, the formation that covers the most of the attachment of the Indian peninsula to the continental body, is characterized by its volcanic nature (Fig. 5.50). The Deccan trap is characterized by fast-cooling igneous rocks, such as basalt or, even, volcanic glass. Nowadays it consists of a hilly plateau cut by river valleys, but originally it was a large flat surface of cooled lava. The distribution of such a formation includes the small peninsula of Gujarat and all the region including Maharashtra, Madhya Pradesh and parts of the bordering states. The limits of the region are defined by the fluvial plain on the north, west and east, while, in the south, the Deccan trap faces older formations that shape the final part of the Indian peninsula. Along the western side, the Deccan trap is directly in contact with the Arabian sea by means of gently shaped beaches with lagoon formations along the coast, especially in correspondence with the mouths of the rivers draining from the plateau of the Deccan trap actively eroding it (Wadia, 1919).

Moving to the southern tip of the Indian peninsula, it is possible to find contact with extremely old geological formations (Fig. 5.50). In fact, it is believed that the southern part of the peninsula is composed of a landmass which has never been submerged since its formation. The mountain ranges define the skyline of the southern and eastern regions are mostly relicts of ancient mountains and plateaus strongly eroded by winds and water. Nowadays, the fluvial erosion power is much lower as a consequence of most of the rivers reaching the base level. The very core composition of the region is characterised by coarse grained rocks such as granites, as well as by gneisses ranging from granulous to shist-like gneisses. Due to its extremely long-lasting erosion, the region is also characterized by the presence of sedimentary layers, mainly resulting from the erosion of the local bedrock and its deposition by means of the alluvial system (Wadia 1919).

To conclude, the coastline of eastern India is characterized by the fluvial deposits composed of the very old crystalline rocks of the southern peninsula, by the basaltic gravels from the Deccan trap and by the local marine deposits uplifted due to the tendency of the Indian landmass to be uplifted uniformly. It is also important to remember that the flow of the river system covering the Indian Peninsula has the tendency to move towards the Bay of Bengal with very few, short and torrential rivers flowing from the top of the Deccan trap plateau to the Arabian sea and few rivers flowing northwards towards the alluvial plain at the feet of the Himalaya (Wadia 1919).

6. Discussion

The results presented in the previous chapter are taken as the starting point for the discussion of their possible interpretative significance here. The main objective, by following the bottom-up approach, is to be able to answer the leading research questions and, possibly, the sub-questions presented in chapter 1:

The leading research questions guiding the work are:

- *“Are the Indian pottery sherds manifesting a different archaeometric composition from the local pottery sherds?”*
- *“Can we suggest the provenance of the ceramic samples we are analysing?”*

To the previously presented main research questions, three sub-questions are added:

- *“Is it possible to identify specific archaeometric signatures differentiating Indian and local pottery sherds?”*
- *“What is the relation between the archaeometric classification and the stylistic typology?”*
- *“Is it possible to develop a better understanding of the technology used for the production of the artefacts?”*

With the aim of reaching conclusions that answer the questions presented above to the fullest potential possible, the presentation of the discussion is divided into the two sections (one per question) and, more importantly, it is divided into small steps, in order to allow the reader to follow the logic of the discussion. To conclude the discussion chapter, a section dedicated to the implications of results of the discussion in the understanding of the past is included. The discussion starts with the presentation and the discussion of the possibility of distinguishing Indian and local pottery composition.

6.1 Local vs. Indian pottery

The identification of local and Indian pottery, as expressed in the presentation section, has always been based on stylistic descriptions and, to a certain degree, on material analysis. The most-used approach is that of archaeological description, which is focused on details such as colour, general shape, texture, decorations, dimensions and description of the inclusions, from a macroscopical point of view. It is with that approach that the artefacts were given a provenance by the researchers

of the two main projects, namely IMTO and DHOMIAP. A summary of the information provided to the author prior to the analysis is presented in table 6.1.

As is visible, the information provided to the author prior to the analysis were actually quite clear, with only few uncertainties. To help the reader in identifying the groups of artefacts, the samples from the same petrographic grouping are clustered together in cells of the same colour: Shell Tempered (yellow), Shale-rich Fabric (violet), Talc-rich Fabric-1 (dark green), Talc-rich Fabric-2 (blue), Medium-Large inclusions in fine Fabric (light blue), Basalt-rich Fabric (red), Fine Fabric (light green), Rice Tempered (grey) and Shell and Sand rich Fabric (brown). The grouping highlights how the identification of the provenance provided prior to the analysis is constant per group. In fact, all the samples from the same group have the same provenance according to the archaeological description, except for sample IQM16B.US35.31 which is part of the BF group, but is uniquely identified as “local”. Another particular noticeable in the table 6.1 is the uncertainty of the provenance of the samples from TF-2. Both of the samples were tentatively identified as locals, but neither of them was identified as local with as much certainty as the TF-1 samples appear to be. Lastly, sample IQM16B.US35.34 was also unsurely identified as local, but by being grouped with two other local samples from the SF group, the identification can be considered as local. When looking at the local and Indian classification, however, it is remarkable how, despite the fact that the provenances are, technically, only two, the number of different groups are 8 or 9, if the separation between TF-1 and TF-2 is taken in consideration. In particular, the definition of local fits 3 different macro groups, groups that present remarkable difference among each other. If the reader considers the geological description of the area where Inqitat and Sumhuram are located, it can be noted that it is difficult to explain such strong variability in local material, even if we consider an area of collection of some kilometres.

Table 6.1: Table of provenance and fabric type identification prior to the archaeometric analysis. The colouring reflects the grouping resulting from the petrographic analysis: ST (yellow), SF (violet), TF-1 (dark green), TF-2 (blue), MLF (light blue), BF (red), FF (light green), RT (grey), SSF (brown).

| Sample code | Fabric Type | Provenance | Sample code | Fabric Type | Provenance |
|------------------|-------------|------------|------------------|-------------|------------|
| IQM16B.US35.8 | SHTW2 | Local | IQM16B.US30.6 | CRW | Indian |
| IQM18B.US119.5 | SHTW2 | Local | IQM16B.US30.3 | CRW | Indian |
| IQM17A.US58.5 | ? | Local | IQM17A.US35.16 | CRW | Indian |
| IQM17A.US58.8 | STW | local | IQM16B.US35.31 | CRW | Local |
| IQM16B.US35.34 | STW | Local (?) | IQM17A.US35.18 | CRW | Indian |
| IQM16B.US35.35 | STW | Local | SUM08B.US975.4 | ? | Indian |
| IQM16B.US35.33 | STW | local | SUM11A.US174.232 | CRW | Indian |
| IQM16B.US35.32 | STW | Local | SUM09A.US297.2 | GTW | Indian |
| SUMW03A.US1.1 | STW | Local (?) | SUM11A.US54.85 | FRSW | Indian |
| SUM08B.US162.104 | STW | Local (?) | SUM10C.US162.119 | CRW | Indian |
| IQM16B.US35.9 | CRW1 | Indian | IQM16B.US30.10 | RSW | Indian |

| | | |
|-----------------|------|--------|
| IQM17B.US73.1 | RSW | Indian |
| IQM16B.US23.13 | PDW | Indian |
| SUM08A.US253.5 | CRW1 | Indian |
| SUM10C.US174.79 | CRW1 | Indian |
| SUM03A.US133.9 | CRW1 | Indian |
| SUM10A.US405.3 | CRW1 | Indian |

| | | |
|------------------|-----|--------|
| IQM18A.US80.3 | BSW | Indian |
| SUM10C.US174.104 | VTW | Indian |
| SUM10A.US412.1 | VTW | Indian |
| SUM10C. US174.83 | CRW | Indian |
| SUM03B.US93.23 | CRW | Indian |
| SUM09B. US309.4 | CRW | Indian |
| SUM03B.US93.42 | CRW | Indian |

Another particular to be noticed in table 6.1 is the comparison between the fabric typology provided prior to the analysis and the differentiation by group resulting from the archaeometric analysis. The discrepancy is highlighted mainly in correspondence of the CRW and the STW classifications that actually include material from very different archaeometric groups, possibly indicating the use of different materials and techniques for the production of the same ceramic type. To verify the efficiency of the division in local and Indian, the elemental composition is the fundamental next step in the discussion. As already mentioned in the previous part, the elemental composition of the groups is quite homogeneous within the groups and quite different between them. The most striking piece of information presented among the results, however, is represented by the graph Fig. 6.1 already presented in chapter 4. Within the graph, it is possible to recognise the usual groups identified with the usual colours, but, more importantly, it is possible to observe how the groups are quite well separated from each other. By adding the circles in correspondence to the material identified as “local” (blue) and “Indian” (red), clear patterns are identifiable, with the red circles focused on samples with high concentrations of Al_2O_3 and low MgO concentrations. On the other hand, the “local” groups are distinct from each other, with groups SF and TF-1 containing the same level of Al_2O_3 as most of the Indian material, but with a generally higher concentration of MgO. The most striking behaviours are those presented by the ST and TF-2 groups. ST shows much lower Al_2O_3 concentrations than any other group and MgO concentrations in line with the average Indian compositions, but with a clear distinction in CaO composition. TF-2, on the other hand, shows a very unique high concentration in MgO. In the same graph, but without the sample of TF-2 (Fig. 6.2), the separation between the groups is even more demarcated. With the identification of the separation among the different local groups, it is difficult to define what is really local and what is to be considered “culturally-local”, on the other hand, the identification of Indian material is clearer, at least from an Al_2O_3 and MgO point of view. Important note to be underlined here is the incapability of trace elements in distinguish different groups, as already observed by Tsoupra (2017).

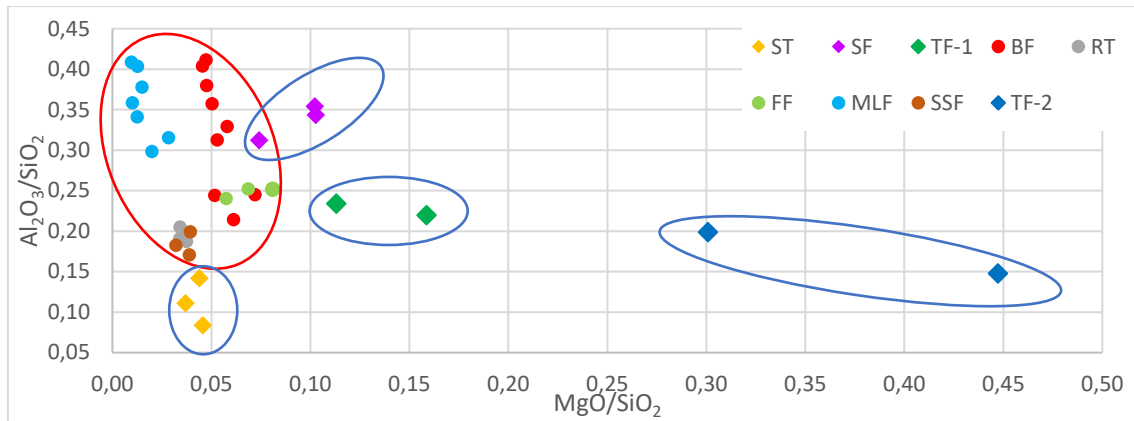


Figure 6.1: Binary plot comparing $\text{Al}_2\text{O}_3/\text{SiO}_2$ and MgO/SiO_2 with local identified in blue circle, non-local in red circle and TF-2 in black. ST: Shell Tempered; SF: Shale-rich Fabric; TF: Talc-rich Fabric; BF: Basalt-rich Fabric; RT: Rice Tempered; FF: Fine Fabric; MLF: Medium-Large inclusions in fine Fabric; SSF: Shell and Sand rich Fabric.

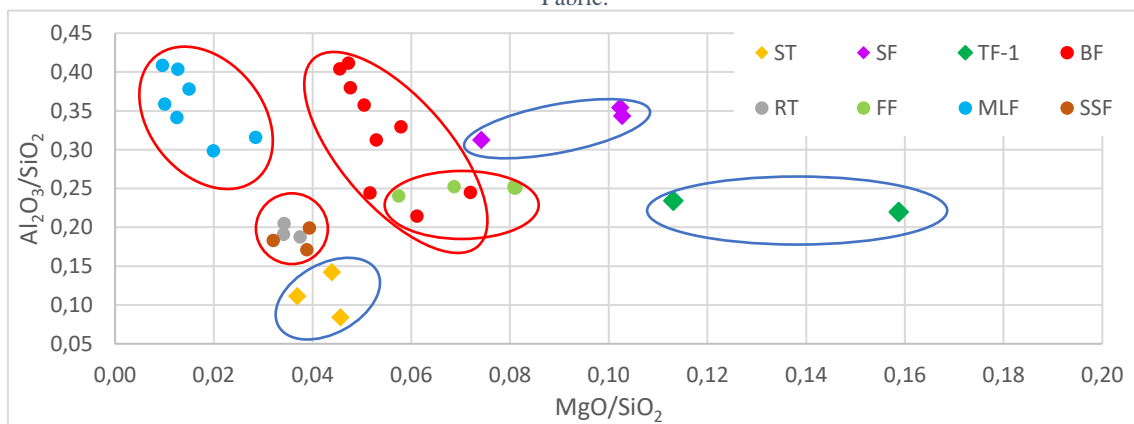


Figure 6.2: Binary plot comparing $\text{Al}_2\text{O}_3/\text{SiO}_2$ and MgO/SiO_2 for all samples excluding TF-2. ST: Shell Tempered; SF: Shale-rich Fabric; TF: Talc-rich Fabric; BF: Basalt-rich Fabric; RT: Rice Tempered; FF: Fine Fabric; MLF: Medium-Large inclusions in fine Fabric; SSF: Shell and Sand rich Fabric.

In addition to the elemental analysis from ICP-MS, it is possible to consider also the SEM-EDS elemental analysis, especially the comparison of the pastes. However, when considering the separation of the “local” and Indian material by means of the results from SEM-EDS, the understanding becomes problematic. The graph presented in the previous chapter, representing the elemental composition of the pastes, show how the signal from the ST and FF are closely related to each other. At the same time, the signals from SF and SSF are close to each other and relatively close to most of the Indian groups’ signals (Fig. 5.46). The explanation that can be given is that, in theory, the pastes, hence clay material, tend to have very similar composition and that, in the case of ST and FF, the clay used appears to share important similarities when analysed free from the inclusions. Similarly, SF and SSF show comparable raw material composition, which in both cases is an unprepared clay. An additional observation is related to the strong difference that is visible between the two MLF samples, difference that could be indication of a different raw material source, indication that the MLF group is probably including materials from a very wide geographic area. Notwithstanding the possible explanation for the similar behaviour

of the pastes from different groups, the separation between “local” and Indian can be considered certain. Moreover, the definition of the “local” raw material remains unclear, probably as a consequence of the fact that some of the materials from the two sites is not “local” by geological definition, but “local” by cultural definition. The meaning of the distinction is connected to the presentation of the historical background done in the introduction: Sumharam, being founded by the Hadramawt and intensely connected to the motherland, probably presents a very high concentration of “local” material that actually originally came from the modern day Yemen territory (Buffa 2019). It is for this reason that it is better to define local as from Dhofar and distinguish it from the ceramic from Yemen.

Table 6.2: Summary of most important characteristics of ceramics by region. ST: Shell Tempered; SF: Shale-rich Fabric; TF: Talc-rich Fabric; BF: Basalt-rich Fabric; RT: Rice Tempered; FF: Fine Fabric; MLF: Medium-Large inclusions in fine Fabric; SSF: Shell and Sand rich Fabric.

| REGION | GROUPS | MAIN CHARACTERISTICS |
|---------|---|--|
| DHOFAR | • ST | <ul style="list-style-type: none"> • Shell fragments as main (nearly only) temper • Lower Al₂O₃ and MgO concentration compared to others |
| YEMEN | <ul style="list-style-type: none"> • SF • TF | <ul style="list-style-type: none"> • Shale grains • Talc grains |
| INDIA | <ul style="list-style-type: none"> • BF • RT • FF • MLF | <ul style="list-style-type: none"> • Presence of Basalt grains • Rice husks used as temper • Lower MgO concentration compared to Arabian material • High attention in raw material preparation |
| UNKNOWN | • SSF | <ul style="list-style-type: none"> • Sand grains • Rounded shell fragments |

6.2 Provenance

Distinguishing the local and Indian material, as shown, can be done. However, according to the definition of “local” proposed by Arnold E. (1981), only the ceramics of the group ST from the Dhofar region can be defined as local, while the ceramics from Yemen are to be considered non-local. At the same time, defining something as Indian is already a big step forward, but being able to restrict the area of provenance would be more useful for the understanding of the past. It is for these reasons that, in this section, the aim is to present arguments in favour of more geographically-specific possible provenances of the different groups of samples identified by the analysis. The identification of the provenance is done by means of comparison, either between the raw materials and geological formations, or by means of archaeological material comparison. The first approach is the most direct one for geological provenance. It is based on the comparison of the archaeological raw material with the geological composition, a comparison based on the nature of the inclusions and on the composition of the matrix. The second method is based on the comparison between the results of the analysis previously presented with the results of analysis

published regarding other materials of known provenance. In this way, the comparison is not directly with the geological source, but it is with material that is identified as originating from that geological source. Of course, the assumption at the bases of the second method is that the material used as junction between the geological source and the samples in this thesis is of certain origins, but unfortunately it is not always the case. In both cases presented above, the interpretation is based on a series of indicators, particularities that can be identified in both the samples analysed and the source of comparison. In the absence of such characteristics, particularities that can be of unique understanding, the comparison of small traces, and the cross-referencing of data can help in limiting the area of provenance. With the purpose of making the discussion clearer for the reader, at the beginning of every discussion point, a summary of the most indicative data is given.

6.2.1 Shell Tempered provenance

The main characteristic presented regarding the ST group is the presence of crushed shells as temper. The shell fragments are extremely angular and they show no sorting by dimensions. The vessels, at least two out of three from this group, present decorative motives such as incisions and dots. The colouring of the fabrics is not homogeneous within the group and sample IQM17A.US58.5 was characterized by higher variability of inclusion material than the others. As presented

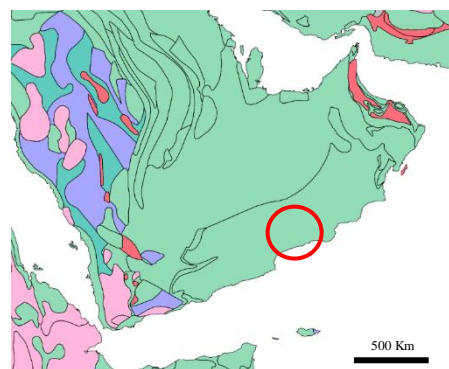


Figure 6.3: ST possible provenance (after www.usgs.gov).

previously, the ST group shows quite a unique behaviour within the distribution graph (Fig. 6.3) with low Al_2O_3 and MgO concentrations. The lack of Al and Mg is substituted by the very high concentration in CaO manifested, reflecting the very rich composition of calcitic shell fragments, but also by the matrix elemental analysis. In fact, the behaviour presented in the paste composition graph is quite unique, with a very high CaO concentration. The only samples that can be comparable to this behaviour are the samples from the FF group. As is understandable from the overview of the main characteristics, the ST group lacks specific geological features that can help to identify a possible geographical location of provenance. It is for this reason that the provenance analysis was conducted by comparison with the descriptions of other materials published. In particular, in the case of the ST samples, a comparable description is provided by A. Avanzini in “Along the Aroma and Spice routes” (Alessandra Avanzini 2011) where she describes the Dhofar pottery tradition as producing reddish to buff coloured fabrics, rich in crushed shells as temper, calcareous microfossils and with quartz, micas and feldspars. Similar indications regarding shell

tempered ceramics are provided by A. Reddy (Reddy 2015). In both cases, the indications of the presence of local production of intentionally-crashed shell fragments used as temper for pottery are clear arguments in favour of a Dhofar provenance of the ST samples (Fig. 6.3).

6.2.2 Shale-rich Fabric group

The major characteristic of the SF group is the presence of nicely rounded shale grains as described in the previous chapter. The presence of shale grains is coupled with a very wide variety of inclusions, variety that argues in favour of a low level of preparation of the raw material prior to the production of the ceramic. In fact, among the inclusions present in the matrix, it is possible to find shale grains, bone fragments, shells, but also plagioclases and amphiboles of remarkable dimensions together with other crystals. The chemical analysis conducted by ICP-MS and presented in the distribution graph shown above demonstrated an Al_2O_3 concentration comparable to that of samples rich in igneous inclusions (such as basalt) but with a higher concentration of MgO, concentrations comparable to that of the TF-1 group. TF-1 also manifests the presence of shale along with the presence of grains of talc. Unfortunately, up to the moment in which this thesis was written, no comparable material analysis has been found to allow any kind of chemical or geological comparison. In addition to that, the limited number of samples constituting the group (only 3) does not allow for a large enough database of information to be used to pinpoint a specific area of sourcing. It is, however, possible to notice the similarity between SF and TF-1 due to the comparable presence of shale and of other inclusions except for talc. The comparability with TF-1 is of stronger consideration than the comparability of SF with SSF as presented by the matrix composition analysis.

6.2.3 Talc-rich Fabric group

The TF group, divided into TF-1 and TF-2, is characterized by the presence of talc. Talc is just one of the many inclusions constituting the TF-1 subgroup, but it becomes the main temper of the clearly prepared fabric characterizing TF-2. The difference between the two groups, then, is the level of preparation of the raw material prior to the pottery production, but it is possible to assume that both groups came from the same geographical region. The presence of talc as inclusion is not common among the samples analysed and can be used as a tracing characteristic for the provenance of the samples. The nature of talc is very specific: metamorphic mineral formed from

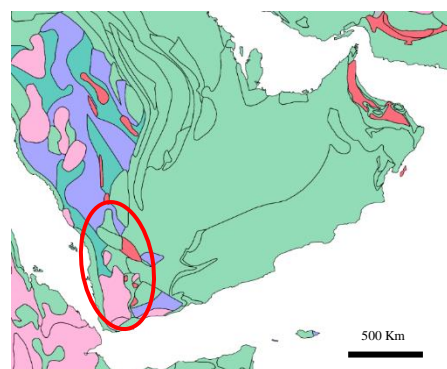


Figure 6.4: TF and SF possible provenance (after www.usgs.gov).

ultramafic (hence very rich in MgO and relatively poor in SiO₂) parental rocks. Among the classes of ceramic types presented by A. Pavan in “A Cosmopolitan City on the Arabian Coast: “The imported and local pottery from Khor Rori. Khor Rori Report 3”, steatite tempered group is identified as characteristic of Arabic production (Pavan 2017). However, the geological structure of the Salalah plain, as explained, is that of alluvial deposits derived from the erosion of the Jebel Qana range which is composed mainly of limestones and tufa. Talc rich geological formations, from the Arabic peninsula, can be found along the Omani mountains as well as along the Yemen mountain ranges. According to A. Pavan, the provenance of talc rich ceramics is considered to be of South Arabian (hence Yemen) and not from the Oman area (Fig. 6.4). The argument in favour of that identification is the intense cultural connections that Sumhuram had with the South Arabian kingdoms. However, from a practical point of view, both Sumhuram and Inqitat are located equally-distant from the two geological sources of talc identified in the Southern end of the Arabic Peninsula. With the objective of leaving no doubt regarding the provenance of the TF samples, the author compared the elemental composition signals of the TF samples with Iron Age stone ware from the sites of Muweilah and Jebel Buhais in the United Arab Emirates. The comparison was based on the data published by P. Magee *et al.* (Magee et al. 2005), in particular on the comparison of the trace elements signals. Even if the samples presented by P. Magee *et al.* are classified as stoneware, the comparison of rare earth elements with ceramic samples can be considered as a starting point, but not as definitive proof. In fact, if the ceramic is of the same source region, it is safe to assume that the signal of the trace elements, even if possibly of different concentrations, should be comparable. The comparison, as done previously, was based on the overlapping of graphs, as visible in the graph below (Fig. 6.5) where the TF group is represented in green (TF-1) and blue (TF-2) while the signals of the stoneware from the UAE are in the different shades of yellow. The comparison clearly shows two different trends for the general

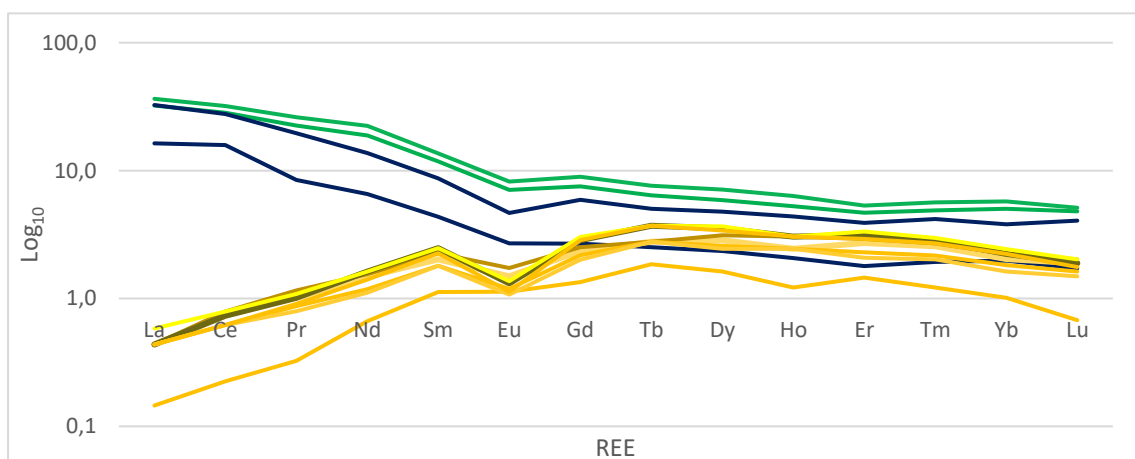


Figure 6.5: Comparison between TF samples (blue and green) and stoneware samples from UAE in yellow (Magee et al. 2005).

trace elements behaviour, trends that are of dubious compatibility.

The same analysis could not be done with samples from the South Arabian region due to lack of comparable data, but the exclusion of the Persian Gulf as possible region of origin and, considering the strong cultural connections that the site of Sumhuram had with the South Arabian kingdoms (Pavan and Pallecchi 2009), argues in favour of a South Arabian origin of the TF group, hence of “culturally local” origins. Moreover, as previously mentioned, the shale grains present within the SF group are comparable with TF-1 shale grains, which are compatible with the sedimentary layers formed on top of the metamorphic formation of South Arabia. Considering the shale comparability and the fact that, except for the talc phases, SF and TF-1 share similar mineralogical components, it is then possible to tentatively connect SF with South Arabia as well (Fig. 6.4).

6.2.4 Basalt-rich Fabric group

The BF group is characterized by the presence of basalt grains among other inclusions. The basalt grains are, from a technological point of view, not a remarkable component of the matrix, but from a provenance analysis point of view, they define a specific geological context (Fig. 6.6). The presence of basalt grains, even if more or less rounded and/or more or less common within the matrix, still showing the relation between the sample raw material and a volcanic region. Basalt is a type of volcanic rock characterized by fast cooling, hence characterized by the small dimensions of the crystals within it. Among the samples included in the BF group, one sample (namely SUM08B.US975.4), as described in the SEM-EDS section, included not only basalt, but also volcanic glass. Volcanic glass is the result of extremely fast cooling lava, fast enough to not give time to the elements to organise in a crystalline structure. The presence of a sample including volcanic glass is an example of the large variety of compositions that the BF group includes. The same variability is noticeable within the data regarding the elemental composition of the samples, both from the ICP-MS and from the SEM_EDS analysis. Similar behaviour is manifested by mineralogical content resulting from the XRD analysis. However, when comparing the composition of the pyroxenes constituting the samples analysed in SEM-EDS, it was possible to notice a perfect match. The variability in elemental composition, but the constant presence of basalt and the direct comparability of pyroxenes can be indicators of a very large, basalt-rich area, large enough to allow differences in composition of the raw material, but still part of the same geological formation explaining the constant composition of the pyroxenes. An area large enough

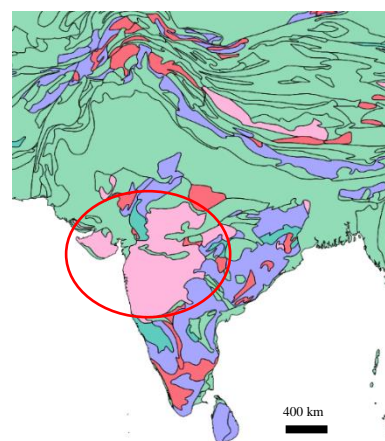


Figure 6.6: Possible provenance BF group (after www.usgs.gov).

to combine the previously mentioned characteristics can be identified in the Deccan Trap area in India (Fig. 6.6). In fact, as presented by N. Rani *et al.* (2015), the Deccan trap region in India is mainly characterized by basalt, but it manifests the presence of volcanic glass formations, allowing the samples including basalt and volcanic glass to be grouped together and identified as originally coming from western Indian. Furthermore, the basalt and glass grains in the BF group are very rounded, characteristic that can be suggesting the production area to be close to the coastal area.

6.2.5 Rice Tempered group

As mentioned in the description of the group, RT is characterized mainly from the presence of rice husks, but it also includes small grains of basalt. It is due to the presence of the basalt grains that RT can be considered a peculiar subgroup of the larger BF group. The direct relation between RT and BF is also proven by the presence of few examples of rice husk inclusions in some of the BF members. Despite the similarities, RT and BF samples are distinguishable due to the incomparable amount of rice husks and basalt grains, a difference that is probably related to different technology. In addition to the unrelatable technology of the two groups, a

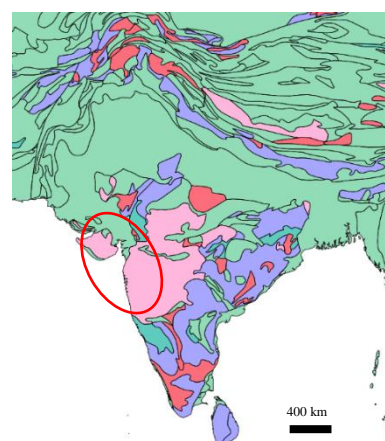


Figure 6.7: Possible provenance RT group (after www.usgs.gov).

a differentiation of the materials is also provided by the discrepancy between the RT and BF pyroxenes signals, as proposed by the SEM-EDS data presented in chapter. 4. In fact, while the BF samples present a perfect match regarding the composition of the pyroxenes, when compared between RT and BF, the composition of the same type of mineral highlights some differences, enough to suggest possible different areas of origin. The similarities and the contemporaneous differences between RT and BF possibly argue for a different area of provenance within the same big region, a region that has been defined as that of the Deccan trap in central and western India. The definition of the Deccan trap as the correct region to look at, for the provenance of the RT sample is also proved by R. Tomber *et al.* (Tomber, Cartwright, and Gupta 2011). In the paper, samples rich in rice husks from the sites of Kuda, Dhatva, Kamrej, Baroda, Nagara and Berenike were analysed. Unfortunately, the samples were not analysed to an elemental composition level, but the SEM analysis of the rice husks and the petrographic descriptions are directly comparable with that of the RT group from this thesis. The argument presented by R. Tomber *et al.* suggests that the production of pottery with rice husks as temper can be considered a tradition of the centre-north Indian region, especially of the Gujarat region, a region that is included in the area of the

Deccan trap geological formation (Fig. 6.7). The argument fits perfectly with the definition of the RT group as related to the BF group, also from the Deccan trap, but the differences between the RT and the BF groups are, possibly, related to different provenance (which would exclude BF as from the Gujarat region). Moreover, the use of rice husk as temper in RT and the lack of it in BF, indicate different technological traditions and, if RT is to be considered typically home-made (Tomber, Cartwright, and Gupta 2011), then it is possible to suggest a more “industrialized” production of BF, an argument that could explain the relatively standardized macro characteristics manifested by the BF group (Fig. 6.6).

6.2.6 Fine Fabric group

The FF group, characterized by its very fine fabric presents no particular characteristics that can be related to a specific geological formation as the BF or the TF group could. The presence of inclusions was limited and difficult to identify, but an important characteristic could be identified in sample IQM18A.US80.3. In fact, among the few inclusions present within the fabric, one relatively big grain of crystallised carbonate was recognisable. Carbonate that, in addition to the relatively high concentration of CaO highlighted by the ICP-MS analysis, can be interpreted as indicative of the sedimentary nature of the raw material used for the ceramic production. In addition to the raw material characteristics, another important aspect to be considered is the technological level demonstrated in producing the samples composing the FF group. In fact, as demonstrated by sample SUM10C.US162.119, the surface of the sample was carefully prepared by the addition of a slip that shows different characteristics to that of the material constituting the ceramic itself. In addition, sample IQM18A.US80.3, except for the carbonated grain and few other inclusions, presented an extremely well-refined clay material. Similar levels of preparation of the clay and of the surface have no parallel to be found in South Arabia, but similar material to sample IQM18A.US80.3 is identifiable among the Northern India material culture, according to E. Odelli *et al.* (Odelli et al. 2020). In fact, E. Odelli *et al.* present a series of samples excavated in the region of Tamil Nadu, from the sites of Alagankulam and Keeladi, and, notwithstanding the fact that the majority of the samples are of local production, among the artefacts, examples of the very high quality Northern black pottery and Northern red pottery are found. By comparing the petrographic analysis of the samples presented by E. Odelli

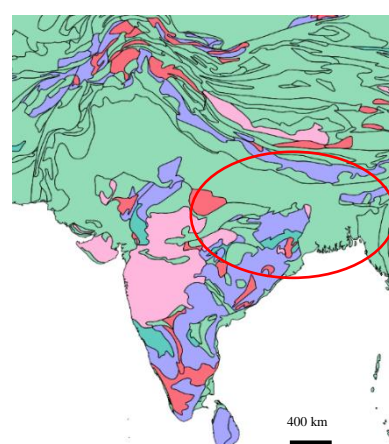


Figure 6.8: Possible provenance FF group (after www.usgs.gov).

Odelli *et al.* present a series of samples excavated in the region of Tamil Nadu, from the sites of Alagankulam and Keeladi, and, notwithstanding the fact that the majority of the samples are of local production, among the artefacts, examples of the very high quality Northern black pottery and Northern red pottery are found. By comparing the petrographic analysis of the samples presented by E. Odelli

et al. with that of the samples included here in the FF group, it is possible to suggest that they are part of the same tradition (Fig. 6.8).

Particular attention is to be given to the sample SUM11A.US54.85 which is part of the BF group, but is also relatable to FF. In fact, it shows extremely well refined raw material and careful surface preparation, but it presented a grain of basalt included in the matrix and an elemental composition signature that is directly comparable to the BF group. The explanations for the unique behaviour of sample SUM11A.US54.85, according to the author, are two. The first explanation is that it is an example of cultural and technological diffusion involving potters from the area of the Deccan trap learning and reproducing the quality of pottery produced somewhere else in Northern India. The second possible explanation is that it is an example of the same pottery culture and technology being widely present in North India, including the area of the Deccan trap. Despite the impossibility of identifying which of the two options is the most representative of reality, the evident similarities between SUM11A.US54.85 and the FF group as well as between the FF group and the imported samples presented by E. Odelli *et al.* (Odelli et al. 2020) are sufficient to suggest an Northern Indian origin for the FF group. Furthermore, if we consider the arguments presented by E. Odelli, it is possible to tentatively limit the origins of the FF group samples to the North-eastern fluvial plains of India towards the Bengal Bay (Fig. 6.8).

6.2.7 Medium-Large inclusions in fine Fabric group

The MLF group is characterized by the presence of medium-large crystals (principally quartz, but also feldspars and carbonates) with preserved faces. The behaviour of the members of the groups was quite unique compared to other groups, because of the presence of homogeneously large inclusions in a matrix characterized by a quite well-levigated paste. The samples presented no specific indications for geological formations, but the presence of such large angular grains of nicely crystalized quartz and feldspars can be considering as excluding raw material of sedimentary origins and the Deccan trap area. The same angular and faced crystals can be related to the granitic nature of the metamorphic region of south India. When looking at the distribution graph, the samples from the MLF group are clearly isolated from all the rest of the groups with a very low presence of MgO and high concentration of Al₂O₃. The clear isolation from the rest of the samples suggests a source of raw material for the members of the group that cannot be found close to the previously described groups.

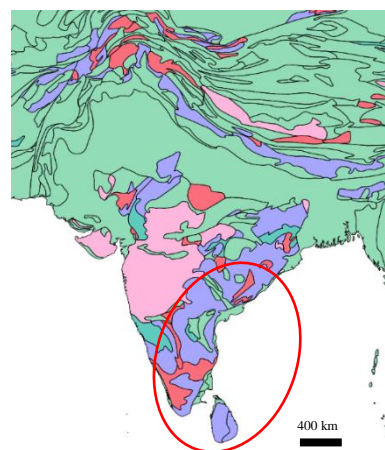


Figure 6.9: Possible provenance MLF group (after www.usgs.gov).

The MLF group is characterized by the hard red walls and by the fact that most of the samples can be identified as “handi” pots, quite commonly identified as originally coming from south of India (Fig. 6.9). In favour of this interpretation, once again, the paper from E. Odelli *et al.* (2020) provided a starting point for comparison of the artefacts. The data provided by E. Odelli, in fact, are comparable stylistically, petrographically and mineralogically with some of the samples included in the MLF group. The comparability between some samples and some of the material published by E. Odelli indicates that the south of India can be considered as a first possible source of comparison. In order to do so, comparisons between the MLF group with data related to samples from the Tamil Nadu region were done as well as with data from Sri Lanka. In particular, the comparison was done on data that were collected from archaeological publications as well as from geological analysis of the elemental composition of the sediments. The result of the comparison with published data produced a picture that is not clear, meaning that there was no uniformity in the results, as visible in the following graphs (Fig. 6.10). In fact, the comparison was positive with samples from the excavations in the Arikamedu, Chandraketugarh and Tamluk sites (graph C) but that, according to S. K. Das *et al.* (2017), are all from the Tamil Nadu region. At the same time, the comparison presented in the graph B was based on the data published by Naseerutheen, A. *et al.* (2014), related to samples collected from Vallore Dist in Tamil Nadu, but the samples are not all from the same age. Graph A, in conclusion, compares MLF samples with data published by Hettiarachchi, P. *et al.* (2010) regarding modern clay sources from Sri Lanka. The signal was directly comparable with only two samples from MLF. To conclude, the comparisons showed that the samples from MLF are comparable, even if not always perfectly, with different data sets from south India and Sri Lanka (the island shares the same geological structure as that of the Indian peninsula: metamorphic rocks). The meaning is that, even if it was not possible to pinpoint a site for the origin of MLF or any of its members, it is possible to suggest a southern Indian origin for the members of the MLF group, probably with different production centres involved, and with different locations for the sourcing of raw material. Of particular interest is the peculiar behaviour of sample SUM08A.US253.5, as demonstrated in the REE graphs in chapter 4, and it shows a signal that is strongly compatible with that of clay sources from the island of Sri Lanka, even if the same sample was also comparable with the results of the other two publications.

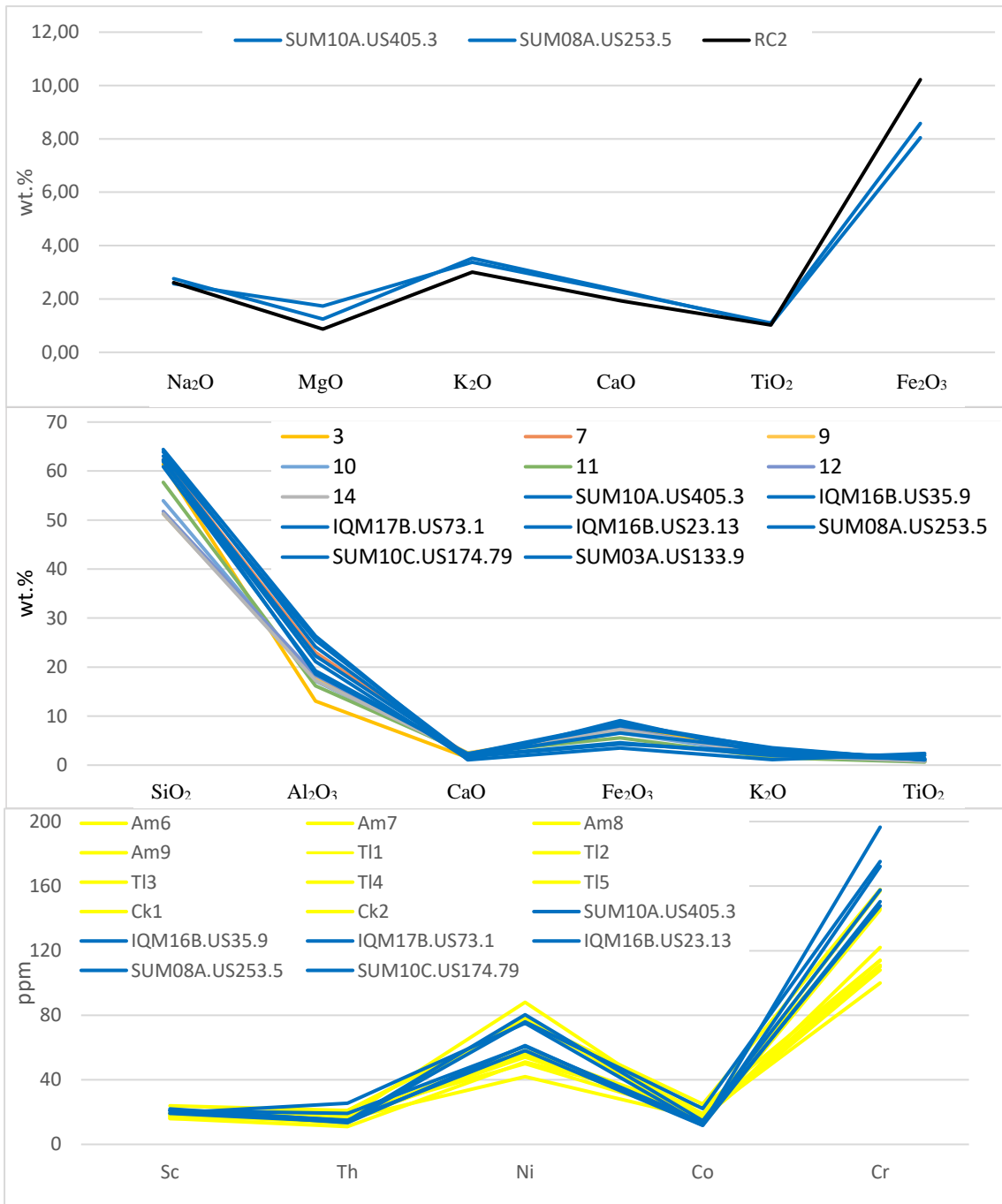


Figure 6.10: Graphic comparison of the samples from MLF (blue) with different dataset: A) sedimentary composition in Sri Lanka (Hettiarachchi, Motha, and Pitawala 2010); B) sample oxide composition from Vellore (Naseerutheen et al. 2014); C) sample trace element composition from Arikamedu, Chandraketugarh and Tamluk (Das et al. 2017).

6.2.8 Shell and Sand rich Fabric group

The SSF group is the most problematic one to deal with. Identified as of Indian origins from the style of the samples, it also behaved exactly like the RT samples in the distribution graph presented above. However, when looking at the signal of the matrix composition analysis conducted by means of SEM-EDS, the signal presented by the SSF sample was perfectly comparable with that of the SF sample.

In the description of the sample, it is clear that there is no specific geological component that can be identified as the samples are characterized by nicely rounded shell fragments recrystallized limestones, sedimentary grains and quartz. The reason why the samples constituting the SSF group were not grouped with the ST samples was because, in SSF, the shell fragments were very rounded, and they are not the only inclusion present. What separates the two fabrics is the very nature of the pottery itself. ST is clearly composed mainly of crushed shells that were added to the clay intentionally, while SSF is characterized by the presence of shells as part of the raw material itself. In addition to the composition characteristics, the elemental analysis also showed differences, not only between SSF and ST (with SSF clearly showing a lower CaO concentration) but also between SSF and any other group.

Despite the clear distinctive characteristics of the group, the localisation of the origins is not clear, up to the date of the thesis writing. In fact, no comparison from a geological and or archaeological point of view is available. The indications that can be taken to argue in favour of the Indian origin of the samples are two: the similar location that the SSF samples occupy in the distribution graph compared to RT, and the stylistic comparison with the Indian material culture. On the other hand, in favour of the local identification of the sample, are the facts that, as with SSF, ST was also composed of shell fragments and was considered local, and that SSF paste composition was a perfect match with the SF paste signal. In addition to the arguments provided by the results of the analysis, another point in favour of a local origin for the SSF is found in A. Reddy's work "Sourcing Indian ceramics in Arabia: actual imports and local imitation" (Reddy 2015) where the author indicates how Dhofar pottery production is characterized by shell tempered ceramics and how no Indian parallel can be found. In the publication, the suggested idea is that, in the Dhofar region, possible imitation of Indian imported ceramics was produced with the local technique of shell inclusions. Unfortunately, except for the similar description of the fabric and of the reddish-brown colouring of the artefacts, no argument was provided, neither from the publication nor by the raw material analysis, in favour of the "local" origin. However, it is important to mention, that, if the SSF is an example of locally-produced copies of foreign ceramic, it would not be the

only example. In fact, among the artefacts retrieved in Sumhuram, archaeologists found fragments of what turned out to be local copies of Roman amphorae (Pavan and Pallecchi 2009)

6.2.9 General distribution

The previous arguments introduced the identification of the probable geographical provenance of most of the groups presented in chapter 4. The identification of the provenance, not only helps to limit the dimensions of the geographical regions included as possible origins, but also helps in arguing in favour or against the Arabic and Indian provenance identification (Fig. 6.11).

Starting with the Arabic and Indian definition, it is shown here that the distinctions made stylistically, prior to the analysis, and made by the identification of the groups in the distribution graph, presented multiple times by now, can generally be considered to be correct. Interesting insight provided by the provenance analysis is connect to the definition of “local”. According to the provenance analysis presented previously, the three groups considered as “local” are the ST, SF and TF groups. Of those 3 groups, only ST, by comparison with archaeological material, can be related to the Dhofar region. On the other hand, TF can be considered as of South Arabian origins, both because of the remarkable tradition of talc tempered ceramics produced in South Arabia and because of the possibility of excluding the Gulf region as a possible source of the raw material. Lastly, SF is here argued in favour of a South Arabian origin as well. The argument is connected to the comparable shale inclusions between TF-1 and SF and to the fact that, in the distribution graph, the SF group is located closer to TF-1 than to the ST group. It is clear, then, that among the 10 identified “local” samples, only 3 are actually considerable as from the Dhofar region, while the other 7, namely SF and TF, can be considered as “culturally local” but of South Arabian provenance.

Regarding the definition of Indian artefacts, the geographical inclusion of such a definition is of remarkable importance, but it is no help in defining specific trade networks. With the aim of reaching a better understanding of the network developed in the Arabian Sea, the identification of the provenance of specific artefacts inhabitants a key role. In this thesis the results of the survey related to the provenance of the material were already presented and it is evident that, within 25 samples of Indian origin, according to the indication prior to this analysis, 22 are from the greater Indian subcontinent and 3 are of dubious provenance. Of the 22 of certain Indian provenance, 9 of the BF group and 3 of the RT group can be identified as having a centre-west Indian origin, with particular attention towards the area of Gujarat, Maharashtra and Madhya Pradesh. In addition to those 12 samples, the 7 samples from MLF group can be connected to the southern region of India and, possibly, to the Sri Lankan island. Last, but not least, the 3 samples included

in the FF group are of a less-defined area, but indicatively, they should be connected to the alluvial plains of the North-West Indian, especially towards the West Bengal region. In conclusion, with the insights provided by the survey analysis run on the 25 samples of Indian provenance, it is possible to notice a very diverse provenance distribution. The meaning of that, within the understanding of such a complex network system as the Arabic Sea trade network, is the topic of the following paragraph.

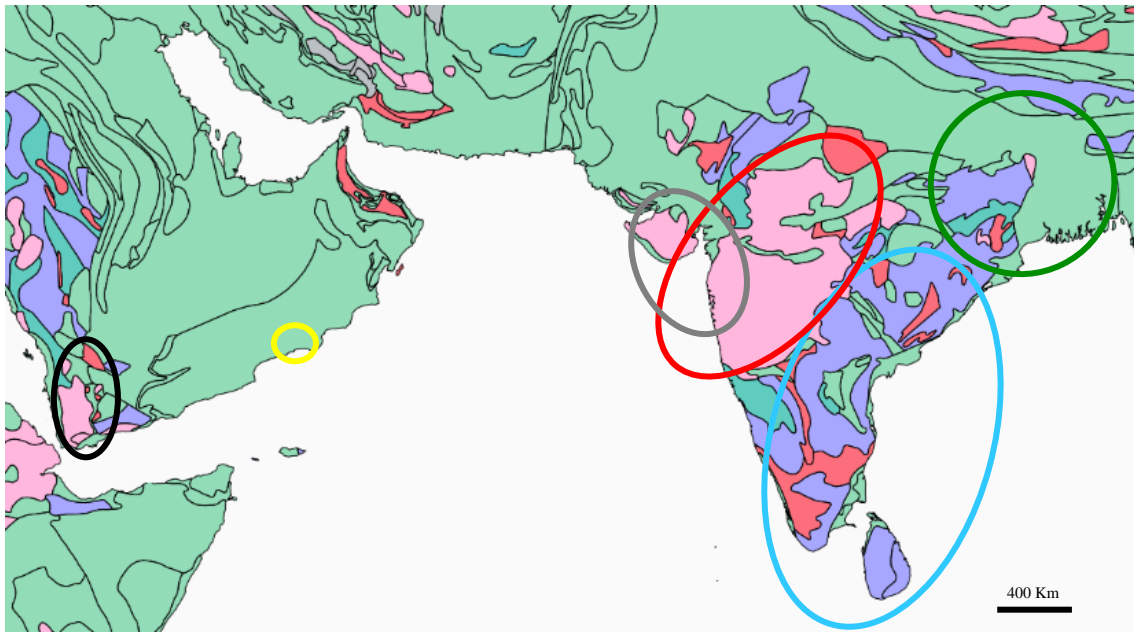


Figure 6.11: General map of South Arabian and Indian geology (after www.usgs.gov) with provenance of the different groups highlighted by means of circles of different colours: Shell Tempered (yellow), Shale-rich Fabric and Talc-rich Fabric (black), Basalt-rich Fabric (red), Rice Tempered (grey), Fine Fabric (green), Medium-Large inclusions in fine Fabric (blue).

6.2.10 Technological characteristics

In the process of analysing the samples, important data related to the technology adopted in the production of ceramics was recorded. The first type of data (Tab. 6.3) is connected to the presence of specific minerals that can be used in the understanding of the temperature reached in the firing process of the ceramics. The data are recorded in table 6.3 and the minerals are divided according to the temperature that is roughly needed for them to form. In particular, minerals identified with the colour green start to develop from 950°C, minerals highlighted in yellow require a temperature above 1000°C and the minerals in red, a temperature above 1100 °C (El Ouahabi et al. 2015). table 6.3 is divided according to the calcareous and non-calcareous group identified by means of the paste composition analysis and the samples included are only those samples that, according to XRD analysis, presented some of the minerals here considered. Plotting the samples in this way helps to indicate the possible temperature of firing that were reached by the samples during

their production process. In particular, samples from SF (purple), ST (yellow) and SSF (brown) groups manifest minerals that, if resulting from the firing process, indicate a firing temperature of more than 950 °C, which would be compatible with the LOI results, but the presence of shell fragments in ST and SSF, together with the lack of darkening of the bone fragments in SF, are to be considered as probable indication low firing temperature. When observing the behaviour of FF samples, especially in sample SUM10C.US162.119, the presence of the minerals indicating a firing temperature above 1100 °C was noticeable. Considering the firing temperature exceeding 1100 °C, however, can be misleading. In fact, considering the presence of bone fragments in SUM10C.US162.119 and the LOI results for the group, it is more probable that the firing temperature was much lower than the mineralogical analysis would suggest.

Lastly, in the non-calcareous group, only samples from the MLF group manifest the presence of firing-related minerals. However, K-feldspars are present in MLF already as temper material, making their consideration for firing temperature analysis unsuitable.

Table 6.3: Division of calcareous and non-calcareous ceramics according to table 5.9 and presence of specific minerals in relation to cooking temperature (El Ouahabi et al. 2015).

| Samples | | D | G | H | C | M |
|----------------|------------------|-----|---|---|---|---|
| Calcareous | IQM16B.US35.8 | X | - | - | - | - |
| | IQM6B.US35.34 | X | - | - | - | - |
| | IQM18A.US80.3 | X | - | X | - | X |
| | SUM10C.US162.119 | X | X | X | X | X |
| | SUM03B.US93.42 | X | X | - | - | x |
| | S | K-f | M | C | | |
| Non-calcareous | SUM08A.US253.5 | - | X | - | - | |
| | IQM16B.US35.9 | - | X | - | - | |

X = present; D= diopside; G = gehlenite; H = hematite; C = cristobalite; M = mullite; K-f = K-feldspars; S= spinel

6.3: Implications from a general point of view

In the following section of the discussion chapter, the attention is moved from the samples themselves, to the implications of the results of the analysis in the general picture of the international trade system involving the Dhofar region, but also the implications that the results have in the understanding of the two sites considered here.

6.3.1 *Sumhuram vs. Inqitat*

When looking at the samples from a distinctive Sumhuram-Inqitat point of view and their identification, it is noticeable that most of the local and the “culturally-local” samples were found in Inqitat. In fact, all the samples from ST, SF and TF-1 are of Inqitat provenance, only the samples from TF-2 are found in the Sumhuram sample group. The first note that has to be

mentioned is that, among the Inqitat samples there is a much higher amount of Arabic material than from the sample group taken from the site of Sumhuram. The selection of the samples, then, cannot be considered as representative of the actual distribution of Indian and Arabic material within the sites. However, the perfect distinction between Sumhuram and Inqitat, related to the TF subgroups is of particular interest, but, unfortunately, the distinction between groups of only two samples is not statistically meaningful. What is particularly interesting to underline, is the fact that South Arabian artefacts were included in the materials retrieved within Inqitat in correspondence with local artefacts. Such coexistence emphasises the existence of a regular interaction between the village and the city, at least from a material exchange point of view. In judging the type of interactions, the only information available from the set of samples analysed in this thesis is that the South Arabian ceramics present in Inqitat are of a generally low quality, possibly connected with the transportation and storage of goods, but no evidence of high quality South Arabian goods can be identified in Inqitat. The lack of high-quality ceramics, probably, is connected to the semi-nomadic nature of the Inqitat population, characteristic that would explain the limited use of high-quality ceramic by being too heavy and fragile to be transported and the reuse of storage ceramic for long time and different purposes *in situ*. Notwithstanding the differences in the amount of Arabic and Indian material, the distribution of Indian samples within the sites does not seem to be related to which site the samples came from. In fact, especially in the two major Indian groups, BF and MLF, the representation of samples from both sites is equal and, even in the FF group it is possible to have samples from both centres. The only two exceptions are provided by the SSF and the RT groups, both represented only by samples from Sumhuram. If the reader, however, considers the very small group sizes of SSF and RT, it is understandable that the exclusion of Inqitat samples from the two groups cannot be considered as representative data, but only as an indication for further investigations related to the stratigraphy and to the use of such ceramics. In fact, it is possible that the dating of SSF and RT groups is later to the destruction and abandonment of Inqitat.

The presence of Indian material equally-distributed between the two sites can be taken to argue in favour of an equal involvement of the sites in international trade, at least until the abandonment of HAS1. The uniformity in the distribution of Indian material between Inqitat and Sumhuram shows that both sites had access to Indian goods equally, but it does not explain the way in which Indian material was reaching Inqitat. The position of both sites is on top of a hill or a promontory, a position that exclude the incorporation of the harbour structures within either settlement. Notwithstanding the similar location and the equal distance that the two sites have from the wadi where the traded goods were most probably arriving, it is worth considering the probable role of

Sumhuram as the centre of redistribution of imported goods, as it was the centre of collection of goods to be exported.

Regarding the classification of the wares included in the set of samples analysed here, it is possible to notice how some of the samples defined as of the same ware type, are actually from two different groups. An example is provided by the samples SUM11A.US174.232, identified as CRW and part of the BF group, and by the sample SUM03B.US93.23 classified as CRW as well, but part of the SSF group. Other similar examples are available, such as sample SUM10C.US174.83 being of the RT group and still identifiable as CRW. The discrepancy between the ware typology and the grouping presented in this thesis can be explained by the different approach used. The typological definition of the ware type was based on the archaeological description, while the grouping presented in this thesis was only based on the raw material composition. The existence of differences is not a sign of errors in the typological classification or on the raw material-based grouping. In fact, the discrepancy was probably highlights the distribution of stylistic standards in India that are not bound to the raw material sources as suggested by A. Reddy (Reddy 2015). In addition to that factor, it is important to consider the fact that most of the ceramic artefacts are small sherds. Of the large amounts of sherds collected, only a part is diagnostic, hence identifiable with relative certainty, while the majority of the sherds are just body sherds, difficult to identify as part of specific groups.

6.3.2 Trade network

The definition of a network, as presented in chapter 2, includes the presence of close connection among a group of cultures, people and entities (Hodos 2016). According to the data recorded and the discussion points presented above, it is safe to suggest that the term “network” can be adopted when defining the phenomena taking place in the Indian Ocean between the 2nd century BC and the 5th century AD. Moreover, the first and, probably, the most important factor to be considered is that the presence of Indian material in Sumhuram predates the intervention of the Roman Empire in the trade network developed in the Arabian Sea. In fact, the site of Sumhuram was founded at the end of the 3rd/beginning of the 2nd century BC and the first occupation layers already present Indian material being excavated *in situ* (Buffa 2019). The presence of Indian material in Sumhuram predating the Roman Empire directly entering in the trade network via Egypt underlines one fact that is of extreme importance: the trade network connecting the different shores of the Arabian Sea was already existent prior to the Romans (Pavan and Schenk 2012). Another important aspect to be considered, is the fact that, since the beginning of the existence of Sumhuram, Indian material has been present at the site, a fact that underlines the role of the site, not only as a production and collection point for the Hadramawt kingdom, but also as

a redistribution and trading centre. Considering the previous points, then, it is interesting to analyse the description of the site of Sumhuram proposed by the unknown author of the PME. As already mentioned in the introduction section of this thesis, the description provided by the PME of the site of Sumhuram is that of a “limen”, hence not a trading point, but a collection centre for redistribution of the frankincense (Alessandra Avanzini 2011). The definition of the site as “limen” implies a limitation of the trade taking place at the site, trading that, at the time of the PME being written, was already well-developed and of an important scale in connection to India. The discrepancy between the Latin source and the reality of the Indian presence suggests that the definition provided by E. H. Seland of the PME as a guiding book for the sailors whose interests are centred in the Roman Egypt (Seland 2008) can be considered as insightful. With such a west-centred point of view, the routes described by the PME were those most suitable for the traders whose starting point and final destination was Egypt, but they are not necessarily the best routes for the traders initialising their travels and ending them in the east. In particular, according to E. H. Seland, it is probable that the travellers who were aiming to sail back to the west coasts of the Indian subcontinent had to wait for the right moment to set sail, and that they were probably waiting in *Moscha limen* (Seland 2008). The existence of two “points of view “of the trade and two systems of connection that preferred one or the other site for trading, i.e. Romans not considering Sumhuram as important for trading, while artefacts show very intense Indian trading at the site, could be considered as indicative of the presence of a very complex network composed of two separate systems of trading, but functioning as a single network. It is, however, impossible to enter in a similar topic with the data presented in this thesis. Further analysis of material from Sumhuram together with further analysis of Indian and other non-Arabian material is needed to be able to identify the dimensions and the core routes that formed the network that connected the shores of the Indian Ocean.

Furthermore, according to the PME, the areas of Indian most involved in the trade were the northern and the south western coasts. Among the sites that the PME mentions as major trading centres, it is possible to identify the site of Barygaza (PME 41-49), a port located in the Gujarat region, and the site of Muziris (PME 53-54), located on the coast of the modern day Kerala state. Interestingly, the two major groups identified from the samples presented in this work are the BF and MLF groups, respectively from the area of Barygaza and from the area of Muziris. According to the arguments presented above, the BF group, composed of 9 samples, and the RT group, identifiable as a subgroup of the BF and composed of 3 samples, are suggested to be from the area including the modern day states of Gujarat, Maharashtra and Madhya Pradesh. Contemporaneously, the MLF group, representing 7 samples, has been argued in favour of a southern Indian provenance. Unfortunately, in the case of the MLF, there is no direct parallel or

geological characteristic that can assure the provenance with certainty. Notwithstanding the difficulty in designating clear areas of provenance, the possibility of having the two most represented regions of Indian corresponding to the regions from where the PME identifies the two major trading centres is actually very telling of the importance that the trade network had for the economy of those two areas of India. In particular, considering that the PME describes an economic mechanism that was already developed before the presence of the Roman Empire, it is possible to hypothesise that the areas of Gujarat and of the South of India were this strongly involved in the trades since before the interests of the Roman Empire. From that hypothesis, it would be possible to suggest that either the trade network in the Arabic Sea was stronger than the interest of the single political entity involved in the trade or that the impact of the Roman interests was not as strong as previously suggested. A similar apolitical hypothesis has also been proposed by M. van Aerde (van Aerde and Zampierin 2020) when analysing the similarities and differences between two harbours, namely Berenike and Arikamedu, involved in the trade. Similar to the Indian and Roman-Egyptian sites, Sumhuram was also founded purely for economic reasons in a land that was not directly exploited by the founders and in a favourable location for ships to travel to (van Aerde and Zampierin 2020). Despite the important steps forward done in this discussion, the topic of the degree of independence that the trade network had from the power and desire of the single political entity, needs further analysis. In particular, more attention should be given to understanding the reasons why the network died in the late 4th century AD as the abandonment of Sumhuram would suggest.

In addition to the BF, RT and MLF groups, and excluding the unclear provenance of the group SSF, the analysis also identified the group FF as of Indian origin. The presence of FF samples within Sumhuram is of importance in relation to two points: the origins of FF can be placed in the fluvial planes of North-East India and it represents a group of samples that had no transportation purpose. Starting from the first discussion point, as argued before, the FF samples are considered to be of North Indian production, with the possibility that they could be identified as coming from the Bengal region. The inclusion of this region in the map of the provenance of material found in Sumhuram and Inqitat is of particular interest. When talking of provenance of Indian material found in the West side of the Arabian sea, most of the materials are identified as coming from the area of Gujarat or from the South of India, and the possibility of including the eastern side of the subcontinent is commonly discarded. It has to be underlined, however, that among the BF samples, one sample (SUM11A.US54.85) shares all the main stylistic characteristics as the FF samples do, but it has a typically BF raw material signal. The similarities shared between SUM11A.US54.85 and the FF group can be explained by the spreading of the style and the knowledge to produce similar ceramics or by the moving of potters with that same knowledge.

Despite which explanation is a better fit for the reality, it is clear that the connectivity between the BF production area and the FF area is strong and, considering the geographical location of BF and FF origins, an inland route could be suggested for the movement of the FF samples before being transported all the way to Sumhuram. Another possible route followed, is that through the south of India. In this case the explanation is connected with the interconnection between the southern and north-eastern Indian coast. It is, in fact, possible to identify similar material to that constituting FF in the Tamil Nadu region. The presence of similar artefacts in that area of India is explained as result of the trade interactions taking place along the Indian coast (Odelli et al. 2020). If pottery from the north of India was available in the south of India, in sites like Arikamedu and Alagankulam, then it is possible to hypothesize that the same pottery was also able to travel, along with South Indian artefacts, to the Arabian coast where it was found. In order to develop a proper understanding of the movements of the FF group and the pathways followed, it is necessary to have a more in-depth analysis related to the distribution of ceramics of the same type and analysis of the material composition of those mentioned. On the other hand, there is no need for further analysis to understand that the quality of such artefacts suggests different purposes other than transportation of goods, for the members of the FF group. The classification of the sample from the site of Sumhuram is that of a bowl for table use. Even if the other two samples from Inqitat have not yet been classified, it is safe to assume that they had similar table-related uses. However, it is hard to suggest that similar artefacts were the main object of trade, not only from a merely economical and practical point of view, but also because of the small number of similar artefacts retrieved, too few to be material of importance. If FF samples were not trade objects, nor containers for the transportation of goods, then it is possible to suggest that they were part of the personal objects of the travellers. A similar observation is presented by S. Lischi (Lischi 2015) who notes the relatively high concentration of utilitarian pots within the Sumhuram site. That observations, together with other observation like the presence of unique artefacts, such as the Indian statuettes or Indian coins can, according to her, suggest a permanence, at least temporarily, of Indian people at the site of Sumhuram (Lischi 2015). At the same time, similar considerations can also be driven from the analysis of the RT group. The samples are all very coarse and thick walled. The explanation for that and for the addition of rice husks in the matrix is probably correlated to the low quality of the raw clay material (Tomber, Cartwright, and Gupta 2011). Further interpretations presented by R. Tomber *et al.* suggest that, considering the low quality and the large variability in forms and composition, RT samples can be interpreted as being home-made pottery, probably for the personal use of the producers (Tomber, Cartwright, and Gupta 2011). The interpretation proposed in relation to RT samples is that people from the coastal region of Gujarat were making pots for their own use and that they were part of the goods that sailors would bring with themselves (Tomber, Cartwright, and Gupta 2011). The presence of RT samples

in Sumhuram, together with table wares of high quality, the slow substitution of South Arabian talc-rich cooking pots in favour of Indian (or Indian-like) cooking pots from the 1st century BC (Pavan 2017) and the presence of unique Indian artefact can be considered as an important indication of the possible long term permanence of Indian people at the site of Sumhuram. Despite the fact that the evidence is not indicative of absolute certainty, by combining artefacts such as the bronze statuettes and the presence of personal items, as suggested by the RT group, it is possible to hypothesise the existence of an Indian community present within the site of Sumhuram, whether constantly or seasonally is not yet clear.

To summarise the discussion regarding the practical outcomes of the results in this thesis, it has been proved that groups such as BF, RT and MLF are of Indian origins, with the first two from the north-west and the third from the south of India. Similarly, the samples composing group FF are also of clear Indian origin, their provenance, however, is tentatively located in the North-East of India, but it is not as certain as it is for the BF, RT and MLF groups. Moreover, it is also argued here that the definition of “local” can be divided into “local”, meaning produced in Dhofar, which is the case of the ST group, and those produced in Yemen, like the TF group and, possibly, the SF group. Regarding the comparison of the data with the identification of local and Indian, done prior to this analysis, there was a clear misinterpretation of provenance in only one case with sample IQM16B.US35.31 being originally identified as local, but, after the analysis, resulting as part of the BF group, hence originally from India. On the other hand, it was not possible to identify the provenance of the samples composing the SSF group with clarity, it is not even possible to suggest with certainty if they can be identified as Indian, as suggested from a stylistic point of view, or local, as suggested from the presence of shells within the matrix. The results also prove the existence of a strong trading network involving the majority of the Indian subcontinent and most of the South Arabian coast. Being a survey of only a limited amount of samples, this thesis cannot infer with absolute certainty any of the characteristics of the network, but, as presented above, it is possible to suppose, as main connections, the one involving West India, South India and Dhofar, representing the core of the long-distance trade network, from which a variety of shorter connections of redistribution of goods departed. However, it is important to remember that the material is all coming from two sites and that there has been a selection of the material before the analysis, a selection that excluded material from other geographical areas that were not India or South Arabia. So, the data presented here are valid as proof of the existence of a long-distance trading network between India and the sites of Sumhuram and Inqitat, but they are not enough for further characterization and understanding of the network.

7. Summary and Conclusion

In this chapter, the author presents the conclusions that result from the presentation of the data and from the discussion of the same. This chapter firstly aims to provide a clear answer to the two research questions that were the guidelines of the discussion, but it also reassumes the topics of wider understanding consequently discussed. In addition, the summary also presents the questions and doubts that can become future research question for projects.

7.2 Summary

The main research question guiding the analysis presented in this thesis was: “*Are the Indian pottery sherds manifesting a different archaeometric composition from the local pottery sherds?*”. As faced in the discussion, the distinction between Indian and local resulted more complex than expected, due to the presence of material not only from the Dhofar, but also from the Yemen area. However, it has been demonstrated that it is possible to define few characteristics that can be considered as guidelines, but not rules, in the distinction among ceramics from Dhofar, Yemen and India. The characteristics identified, already presented in table 6.2, are the presence of shell fragments as temper in a Al_2O_3 and MgO poor ceramic from Dhofar, the presence of shale and talc grains as temper of the ceramics from Yemen and the presence of basalt grains and rice husks as temper in a highly prepared and MgO poor Indian ceramics. In conclusion, the effort of answering the previously mentioned research question highlighted that archaeometry provides important insights into the provenance of the artefacts, but, as suggested by E.H. Seland (2014), it is fundamental to expand the database.

Secondly, the thesis aimed to prove that, with the proper set of analysis and the proper set of data comparison, the identification of different areas of provenance of the Indian material is possible. In relation to that aim, the discussion chapter already demonstrated that it was feasible to identify different groups of samples, to propose probable areas of provenance and that the methodology can even help the improvement of the interpretation and understanding of the trade network that was established in the Indian Ocean. Unfortunately, in most cases, the areas highlighted remain large, but the distinction of the groups and of the provenance has proved possible. The analysis, in fact, provided an answer to the provenance question for most of the samples, a response based on the direct comparison of data. However, the lack of a large and well-structured database, in the case of the SSF group, comported the impossibility of providing a certain answer. Despite the remaining question of the SSF, the other identified groups provided important indications for

their provenance. ST, with its extremely high concentration of shell fragments, is identified as originally from Dhofar. The presence of shale grains in SF comparable to that of TF-1 and the presence of talc temper in TF-1 and TF-2 identified Yemen as the most probable production area. BF and RT, both presenting basalt grains, are identified as originally from the centre-west India. In particular, the use of rice husk as main temper in RT is directly comparable with material produced in the coastal area of the Gujarat region in India. Moreover, MLF group is characterized by relatively high firing temperature and by the presence of large crystal grains, relating to the metamorphic formations and ceramic productions of south Indian and Sri Lanka. Lastly, the high level of clay preparation and the high level of CaO in the paste composition are indications of a north-western Indian origin for the FF group, possibly relating to the Bengal region.

In relation to the definition of the groups, the trace elements were not able to provide important insights in the distinction among the different groups. It is possible, however, that the geographic area taken into consideration was too large for trace elements to be of help. Further researches related to the importance of trace elements can be done in relation to a micro-regional investigation in connection to the specific analysis of each group and its provenance region identified above. Micro-regional analysis is of extreme importance also for the further understanding of ceramic provenance and for the identification of possible subgroups. Another major step to be done towards the understanding of the origins of different materials is the study of geological samples and the comparison of them with the data collected in this and other archaeometric analysis of archaeological ceramics. An example of such approach was proposed in this thesis, in relation to the analysis of the MLF origins, and it highlights the importance of expanding the geological and geochemical database. Further provenance analysis can also be done in relation to the isotopic signals of Pb and Sr, which would provide an extra source of data possibly providing further insights into the sample subdivision into groups and, possibly, contributing in the identification of more restricted geographical areas of origin of the samples analysed.

In addition to the conclusions provided above, it is also possible to mention a few other topics that have no conclusive answer, but that were discussed in the previous chapter and that can become important future research topics. One of such topics is the type of relation that connected the site of Sumhuram and the site of Inqitat. The equal representation of both sites within the major Indian groups of samples (namely BF and MLF), together with the presence of South Arabian ceramics in Inqitat, is taken here as indicative of a freedom of movement of goods between the two sites. Freedom of movement that can either be extended to the people, or it can be a sign of very good and intense economic and trading connection between the two sites. It is

not possible, with the data presented here, to determine if the presence of foreign goods in a location also included the presence of foreign people, but future analysis focused on “local” materials, i.e. material of the ST group for example, from the city of Sumhuram could provide better insight on the type of relationship present between the sites. Moreover, another similar unanswered puzzle is the way in which the Indian goods reached the site of Inqitat and the site of Sumhuram. In fact, the presence of the Indian ceramics equally in both sites can be indicative both of a harbour infrastructure freely accessible from both sites, and/or the possibility of Sumhuram functioning as middleman. Unfortunately, harbour facilities are yet to be found and excavated, hence the problem cannot be solved until the facilities are actually found.

Further studies are also needed to compare the structure and the life of the sites involved in the trade. Material analysis of transportable goods is of extreme importance for the understanding of the trading network, but the structural analysis and comparison between sites can be of importance for the understanding of the economic impact that the trading network had in the single site as well as in understanding if and how a general knowledge in harbour structures can be identified within the Arabic sea environment. In fact, similarities were found between the site of Arikamedu and Berenike in previous projects (van Aerde and Zampierin 2020), but most of those similarities can also be found in Sumhuram, which was founded before the intervention of the Roman Empire in trade. Comparison is also needed to identify the reason why Sumhuram is classified as a collection point and not trading harbour in the PME. In fact, as mentioned before, Sumhuram predates the Roman participation in the trade, and it was involved in the trade with an important amount of imported Indian material since the foundation. Moreover, similar to many other important sites involved in the trade, Sumhuram is also subject of the doubt of a possible Indian community present within the city. The location of the city, however suggests that the seasonal stopping of Indian traders at the site is highly probable favouring the possibility of a permanent community located in the city. It is difficult to suggest the presence of a foreign community by analysing the site alone, but comparison with other ports that have the same possible phenomenon allows one to identify possible indications in favour or against such interpretation. To better understand the differences between the PME and the actual importance of certain ports as well as to identify possible general phenomena characterizing the world of the Arabic Sea trade network, it is necessary for a general database of information, data and questions to be developed and shared among the researchers involved in complex reality that is the Indian Ocean trade network. The same database would be also the most promising way to develop a clear mapping of the material origins. In fact, the uncertainty of defining the specific geographical origins of all the BF and MLF samples was discussed before together with the lack of clarity for the provenance of the SSF samples. In addition to that, the FF group also presented the unresolved question of the

direction within which it reached the Arabic Shores. In all of the cases presented above, the database previously suggested for the site comparison, would also be the base of comparison for the stylistic and material analysis of objects becoming the most direct and efficient way for researchers to be able to localise the sourcing, the production and the pathways of distribution of the material studied. In other words, due to the large geographical area involved, the very large and different cultural diversity included in the network, and because of the important amount of variables to be considered and questions still to be answered, it is not yet possible to define to which degree the Indian Ocean trade network can be considered as an example of a globalization phenomenon, but it is clear that a larger and better-shared database can be the leading tool to reach a better interpretation.

7.2 Conclusion

To conclude, this thesis has proved that it was possible to identify materials from India, Dhofar and Yemen by means of archaeometric analysis. The thesis also proved that, by means of the analysis of the raw material by fusing archaeometric techniques, it was possible to restrict the geographical areas identifiable as the origin of the Indian ceramics. In particular, the BF and RT groups are identified as from the centre-west India, MLF from south India and/or Sri Lanka and FF from the north-east of India. Lastly, this research not only has provided answers, but it has also created some new questions to be answered in future research, such as the mechanism of distribution of goods from the harbour to Sumhuram and Inqitat, how the FF group travelled within the Indian region to then be transported all the way to the Arabic coast, and the general question to what degree it is possible to take the Indian Ocean trade network as example of “globalization”.

8. References

A

- ~ Van Aerde, M.E.J.J. 2019. “The Archaeology of Continuation in East Africa: The Pre-Islamic Ports of Adulis, Berenike, and Myos Hormos.” : 1–24.
- ~ van Aerde, Marike, and Daniele Zampierin. 2020. “A LOT OF PEPPER AND A LITTLE GARUM : AN ARCHAEOLOGICAL COMPARISON OF THE ROMAN PRESENCE AT BERENIKE AND ARIKAMEDU.” *Ancient West & East* 19: 145–66.
- ~ Albaroot, M., A. Ahmad, N. Al-Areeq, and M. Sultan. 2016. “Tectonostratigraphy of Yemen And Geological Evolution: A New Prospective.” *International Journal of New Technology and Research* 2(2): 19–33.
- ~ Arnold, E. 1981. “A Model for the Identification of Non-Local Ceramic Distribution: A View from the Present.” In *Production and Distribution: A Ceramic Viewpoint*, Oxford: B.A.R., 31– 44.
- ~ Ast, Rodney, and Roger Shaler Bagnall. 2015. “The Receivers of Berenike. New Inscriptions from the 2015 Season.” *Chiron Mitteilungen der Kommission für alte Geschichte und Epigraphik des Deutschen Archaeologischen Instituts* 45: 171–185.
- ~ Autiero, Serena. 2019. “Foreign Iconographic Elements in South Arabian Art: The Indian Contribution.” In *Stories of Globalisation: The Red Sea and the Persian Gulf from Late Prehistory to Early Modernity*, , 408–45.
- ~ Avanzini, A., and R. Orazi. 2001. “The Construction Phases of Khor Rori’s Monumental Gate.” *Arabian Archaeology and Epigraphy* 12(2): 249–59.
- ~ Avanzini, Alessandra. 2007. Roma: “L’Erma” di Bretschneider *A Port in Arabia Between Rome and the Indian Ocean (3rd C. BC-5th C. AD)*. *Khor Rori Report 2*.
- ~ Avanzini, Alessndra. 2011. *Along the Aroma and Spice Routes. The Harbour of Sumhuram, Its Territory and the Trade between the Mediterranean, Arabia and India*.

B

- ~ Beltrame, Massimo et al. 2019. “Islamic and Post Islamic Ceramics from the Town of Santarém (Portugal): The Continuity of Ceramic Technology in a Transforming Society.” *Journal of Archaeological Science: Reports* 23(July 2018): 910–28. <https://doi.org/10.1016/j.jasrep.2018.11.029>.
- ~ Buffa, Vittoria. 2019. Roma: “L’Erma” di Bretschneider *Sumhuram The Becoming of the Town Khor Rori Report 4*.

C

- ~ Casson, Lionel. 1914. *The Periplus Maris Erythraei Text with Introduction, Translation, and Commentary*. Princeton: Princeton University Press.
- ~ Cobb, Matthew. 2015. “The Chronology of Roman Trade in the Indian Ocean from Augustus to Early Third Century CE.” *Journal of the economic and social history of the Orient* 58: 362–418.

D

- ~ D’Ancona, Mirella Levi. 1950. “An Indian Statuette from Pompeii.” *Artibus Asiae* 13(3): 166–80.
- ~ Das, Supriyo Kumar et al. 2017. “Provenance Study of Ancient Potteries from West Bengal and Tamil Nadu: Application of Major Element Oxides and Trace Element Geochemistry.” *Man and Environment XLII* (2): 11–20.

E

- ~ Eiggins, S. M. et al. 1997. “A Simple Method for the Precise Determination of ≥ 40 Trace Elements in Geological Samples by ICPMS Using Enriched Isotope Internal Standardisation.” *Chemical Geology* 134(4): 311–26.

F

- ~ Finlay, A.J. et al. 2012. “Trace Element Fingerprinting of Ceramic Building Material from Carpow and York Roman Fortresses Manufactured by the VI Legion.” *Journal of Archaeological Science* 39(7): 2385–91.
- ~ Ford, L. A., A. M. Pollard, R. A.E. Coningham, and B. Stern. 2005. “A Geochemical Investigation of the Origin of Rouletted and Other Related South Asian Fine Wares.” *Antiquity* 79(306): 909–20.
- ~ Froh, J. 2004. “Archaeological Ceramics Studied by Scanning Electron Microscopy.” *Hyperfine Interactions* 154(1–4): 159–76.

H

- ~ Hart, George. 1999. *The Poem of Ancient Tamil*. New Delhi: Oxford University Press.
- ~ Heimann, Robert B., and Marino Maggetti. 2019. “The Struggle between Thermodynamics and Kinetics: Phase Evolution of Ancient and Historical Ceramics.” *European Mineralogical Union Notes in Mineralogy* 20: 233–81.
- ~ Hettiarachchi, P., J. T.S. Motha, and H. M.T.G.A. Pitawala. 2010. “Identification of an Appropriate Body Composition for Red Clay Products (Identificação de Uma Composição Adequada Para Produtos de Argila Vermelha).” *Ceramica* 56(339): 285–90.

- ~ Hodos, Tamar. 2017. The Routledge Handbook of Archaeology and Globalization *The Routledge Handbook of Archaeology and Globalization*. ed. Tamar Hodos.

K

- ~ Khalifa, Mohed Ishag. 1988. *Geological Map of Salalah*. Sultanate of Oman, Ministry of Petroleum and Minerals, Directorate General of Minerals.

L

- ~ Lee-Thorp, J. A. 2008. "On Isotopes and Old Bones." *Archaeometry* 50(6): 925–50.
- ~ Lischi, Silvia. 2015. "Traces of Indian Community in the City of Sumhuram, Oman: Investiigation of Materials Found during Excavations." In *Invisible Cultures*, , 227–40.
- ~ ———. 2016a. "Dal Paleolitico Al Periodo Islamico: La Storia Del Dhofar Attraverso Lo Studio Archeologico Dell'Inqitat." In *Sognatori. 40 Anni Di Ricerche Archaeologiche Italiane in Oman*, ISMEO, 149–51.
- ~ ———. 2016b. *Inqitat Archaeological Mission First Season of the Italian Mission to Oman (IMTO) in the Site of Inqitat- Khor Rori Archaeological Site, Dhofar, Sultanate of Oman. 15 September 2016- 7 December 2016*.
- ~ ———. 2017. *Inqitat Archaeological Mission Nqitat Archaeological Mission Second and Third Season of the Italian Mission to Oman (IMTO) in Season of the Italian Mission to Oman (IMTO) in the Site of Inqitat - Khor Rori Archaeological Site, Dhofar, Sultanate Khor Rori .*
- ~ ———. 2018. *Inqitat Archaeological Mission Nqitat Archaeological Mission Fourth and Fifth Season of the Italian Mission to Oman (IMTO) in Season of the Italian Mission to Oman (IMTO) in the Site of Inqitat - Khor Rori Archaeological Site, Dhofar, Sultanate of Oman 28*.
- ~ ———. 2019a. *Inqitat Archaeological Mission Nqitat Archaeological Mission Sixth and Seven Season s of the Archaeological Mission Archaeological Mission in the Site of Inqitat - Khor Rori Archaeological Site, Dhofar, Sultanate of Khor Rori Archaeological Site, Dhofar, .*
- ~ ———. 2019b. "Risultati Preliminari Delle Ricerche Archaeologiche Presso l'Insedimento HAS1 Di Inqitat, Dhofar (2016-2019)." *Egitto e Vicino Oriente* 42: 119–33.
- ~ ———. 2019c. "The Inqitat Archaeological Project." (*IASA*) *News and Research by Country* (24): 19–20.
- ~ ———. 2020. "Indian Ocean Trade Connections: Characterization and Commercial Routes of Torpedo Jars." *Heritage Science* 8: 1–14. <https://doi.org/10.1186/s40494-020-00425-9>.
- ~ ———. *La Ceramica Locale in Dhofar (Oman Meridionale): Tipi , Tecniche Produttive e Circolazione Dall ' Età Del Ferro Al Periodo Islamico*.
- ~ Lischi, Silvia, Alexia Pavan, and Agnese Fusaro. 2020. "Preliminary Investigations on the

Local Pottery in Dhofar (Southern Oman) from the Iron Age to the Islamic Period.” *International Association for the Study of Arabia (IASA) News and Research by Country* (25): 15–17.

~ Liu, Xinru. 2010. *The Silk Road in World History*. New York: Oxford University Press.

M

~ Magee, Peter. 2010. “Revisiting Indian Rouletted Ware and the Impact of Indian Ocean Trade in Early Historic South Asia.” *Antiquity* 84(326): 1043–54.

~ Magee, Peter, Don Barber, Marta Sobur, and Sabah Jasim. 2005. “Sourcing Iron Age Softstone Artefacts in Southeastern Arabia: Results from a Programme of Analysis Using Inductively Coupled Plasma-Mass Spectrometry/Optical Emission Spectrometry (ICP-MS/OES).” *Arabian Archaeology and Epigraphy* 16(2): 129–43.

~ Maiuri, A. 1939. “Statuetta Eburnea Di Arte Indiani a Pompei.” *Bolettino d’Arte*: 111–15.

~ Makarona, C, K Nys, and P Claeys. 2012. “Sr Isotope Analysis for the Provenance Study of Ancient Ceramics : An Integrated Approach.” In *Proceeding of the 39th International Symposium for Archaeometry, Leuven, ,* 1–8.

~ Mattern, Frank et al. 2018. “Coastal Dynamics of Uplifted and Emerged Late Pleistocene Near-Shore Coral Patch Reefs at Fins (Eastern Coastal Oman, Gulf of Oman).” *Journal of African Earth Sciences* 138: 192–200. <https://doi.org/10.1016/j.jafrearsci.2017.11.018>.

~ McDonough, W. F., and S. Sun. 1995. “Composition of the Earth.” *Chemical Geology* 120: 223–53.

~ McCrindle, J. W. 1879. *The Commerce and Navigation of the Erythraean Sea: Being a Translation of the Periplus Maris Erythraei by an Anonymous Writer, and of Arrian’s Account of the Voyage of Nearchos. With Introductions, Commentary, Notes, and Index*. Amsterdam: Philo Press.

~ Mirulla, Fabio. 2011. Bari *LA FOTOGRAFIA ARCHEOLOGICA DIGITALE - Dallo Scatto All’elaborazione*. Edipuglia srl.

N

~ Naseerutheen, A., A. Chandrasekaran, A. Rajalakshmi, and R. Ravisankar. 2014. “Elemental Analysis of Ancient Potteries of Vellore Dist, Tamil Nadu, India by ED-XRF Technique with Statistical Approach.” *Beni-Suef University Journal of Basic and Applied Sciences* 3(1): 45–51. <http://dx.doi.org/10.1016/j.bjbas.2014.02.006>.

~ Newton, Lynne S., and Juris Zarins. 2010. “Preliminary Results of the Dhofar Archaeological Survey.” In *Proceedings of the Seminar for Arabian Studies, ,* 247–66.

O

- ~ Odelli, E. et al. 2020. “Pottery Production and Trades in Tamil Nadu Region: New Insights from Alagankulam and Keeladi Excavation Sites.” *Heritage Science* 8(1): 1–13. <https://doi.org/10.1186/s40494-020-00402-2>.
- ~ Ottley, C. J., D. G. Pearson, and G. J. Irvine. 2003. “A Routine Method for the Dissolution of Geological Samples for the Analysis of REE and Trace Elements via ICP-MS.” In *The Proceedings of the 5th International M. Beltrame et Al. Journal of Archaeological Science: Reports 23 (2019) 910–928 927 Conference on Plasma Source Mass Spectrometry Held at the University of Durham on 8–13 September 2002*, eds. H.D. Grenville and S. Tunner. Cambridge: The Royal Society of Chemistry, 221–30.
- ~ El Ouahabi, M., L. Daoudi, F. Hatert, and N. Fagel. 2015. “Modified Mineral Phases during Clay Ceramic Firing.” *Clays and Clay Minerals* 63(5): 404–13.

P

- ~ Pavan, Alexia. 2015. “Trade and Commercial Routes along the Indian Ocean from the Early Centuries BC to the Beginning of Christian Era. New Lights from the Indian Pottery Discovered at Sumhuran (Sultanate of Oman).” In *South Arabia and Its Neighbors: Phenomena of Intercultural Contacts*, , 121–133.
- ~ ———. 2016. “Relations between Southern Arabia and India: Recent Discoveries from Sumhuram (Sultanate of Oman).” *Journal of Indian* 12: 129–35.
- ~ ———. 2017. 12 Roma: “L’Erma” di Bretschneider *A Cosmopolitan City on the Arabian Coast: The Imported and Local Pottery from Khor Rori. Khor Rori Report 3*.
- ~ Pavan, Alexia, and Pasquino Pallecchi. 2009. “Considerazioni Su Alcuni Frammenti Di Anfore Con Impasto a Base Di Talco Rinvenute Nell’Antico Porto Di Sumhuram (Oman).” *Egitto e Vicino Oriente* 32: 221–30.
- ~ Pavan, Alexia, and Heidrun Schenk. 2012. “Crossing the Indian Ocean before the Periplus: A Comparison of Pottery Assemblages at the Sites of Sumhuram (Oman) and Tissamaharama (Sri Lanka).” *Arabian Archaeology and epigraphy* 23: 191–202.
- ~ Pollard, Mark, Catherine Batt, Ben Stern, and Suzanne M.M. Young. 2007. New York *Analytical Chemistry in Archaeology*. Cambridge University Press.
- ~ Pollastro, Richard M, Amy S Karshbaum, and Roland J Viger. 1998. *MAPS SHOWING GEOLOGY, OIL AND GAS FIELDS AND GEOLOGIC PROVINCES OF THE ARABIAN PENINSULA*.
- ~ Potts, D.T. 2010. “The Arabian Peninsula, 600 BCE to 600 CE.” In *Coinage of the Caravan Kingdoms: Studies in Ancient Arabian Monetization*, The American Numismatic Society

New York, 27–64.

- ~ Powers, R W, L.F. Ramirez, C.D. Redmond, and E.L. Jr Elberg. 1966. “Geology of the Arabian Peninsula Sedimentary Geology of Saudi Arabia.” *U.S. Geological Survey Professional Paper 560-D*: 154.

Q

- ~ Quinn, Patrick S. 2009. *INTERPRETING SILENT ARTEFACTS Petrographic Approaches to Archaeological Ceramics*. Oxford: Archaeopress.

R

- ~ Rani, Nishi, J. P. Shrivastava, and R. K. Bajpai. 2015. “Natural Glass from Deccan Volcanic Province: An Analogue for Radioactive Waste Form.” *International Journal of Earth Sciences* 104(8): 2163–77.
- ~ Reddy, Anjana. 2015. “Sourcing Indian Ceramics in Arabia: Actual Imports and Local Imitations.” In *Proceedings of the Seminar for Arabian Studies*, eds. Alessandra Avanzini et al. Archaeopress Oxford, 253–72.
- ~ Renson, V. et al. 2014. “Coupling Lead Isotope Analysis and Petrography to Characterize Fabrics of Storage and Trade Containers from Hala Sultan Tekke (Cyprus).” *Archaeometry* 56(2): 261–78.
- ~ De Romanis, Federico. 2006. *Cassia Cinnamomo Ossidiana Uomini e Merci Tra Oceano Indiano e Mediterraneo*. Roma: L’ERMA di BRETSCHIEDER.
- ~ De Romanis, Federico, and Andre Tchernia. 1997. *Crossings. Early Mediterranean Contacts with India*. eds. Federico De Romanis and Andre Tchernia. New Delhi: Manohar Publishers & Distributors.

S

- ~ Seetha, Duraisamy, and Gothandapani Velraj. 2016. “Characterization and Chemometric Analysis of Ancient Pot Shards Trenched from Arpakkam, Tamil Nadu, India.” *Journal of Applied Research and Technology* 14(5): 345–53. <http://dx.doi.org/10.1016/j.jart.2016.08.002>.
- ~ Seland, Eivind Heldaas. 2008. “The Indian Ships at Moscha and the Indo-Arabian Trading Circuit.” In *Proceedings of the Seminar for Arabian Studies*, Archaeopress Oxford, 283–88.
- ~ ———. 2009. “Shipwreck, Maroons and Monsters: The Hazards of Ancient Red Sea Navigation.” In *Connected Hinterlands: Proceedings of Red Sea Project IV: Held at the University of Southampton September 2008*, , 179–85.
- ~ ———. 2014. “Archaeology of Trade in the Western Indian Ocean, 300 BC–AD 700.” *Journal of Archaeological Research* 22(4): 367–402.

- ~ Sharmin, Dilruba, and Fumio Okada. 2012. "Surface Coating Technique of Northern Black Polished Ware by the Microscopic Analysis." *Ancient Asia* 3: 49–65.
- ~ Sidebotham, Steven E. 2011. *Berenike and the Ancient Maritime Spice Route*. Berkeley: University of California Press.
- ~ ———. 2017. "Rethinking Classical Indo-Roman Trade. Political Economy of Eastern Mediterranean Exchange Relations, by Rajan Gurukkal." *South Asia: Journal of South Asian Studies* 40(2): 426–28.
- ~ Sir. Wheeler, Mortimer. 1971. *Rome Beyond the Imperial Frontiers*. Westport, Connecticut (USA): Greenwood Press, Publishers.
- ~ Skadiņš, Ingus et al. 2019. "Adhesion and Colonisation of Microorganisms on Porous TiO₂ and TiO₂-Silver Biomaterials." *Proceedings of the Latvian Academy of Sciences, Section B: Natural, Exact, and Applied Sciences* 73(4): 325–31.
- ~ Snyder, R. (1992). The Use of Reference Intensity Ratios in X-Ray Quantitative Analysis. *Powder Diffraction*, 7(4), 186-193. doi:10.1017/S0885715600018686
- ~ Speidel, Michael A. 2015. "Wars, Trade and Treaties: New, Revised, and Neglected Sources for the Political, Diplomatic, and Military Aspects of Imperial Rome's Relations with the Red Sea Basin and India, from Augustus to Diocletian." In *Imperial Rome, Indian Ocean Regions and Muziris: New Perspectives On Maritime Trade*, ed. K.S. Mathew. Manohar Books, 83–128.
- ~ Subramanian, Thirumanilaiyur Sitapati Ramana. 2012. "Potsherd with Tamil-Brahmi Script Found in Oman." *The Hindu*: 1–2.
- ~ Sun, Shen Su, and William F. McDonough. 1989. "Chemical and Isotopic Systematics of Oceanic Basalts: Implications for Mantle Composition and Processes." *Geological Society Special Publication* 42(1): 313–45.

T

- ~ Tite, M.S., I.C. Freestone, N.D. Meeks, and M. Bimson. 1982. "The Use of Scanning Electron Microscopy in the Technological Examination of Ancient Ceramic." *Archaeological ceramics*.
- ~ Tite, M S. 1991. "The Impact of Electron Microscopy on Ceramic Studies." *The British Academy* 77(February 1991): 111–31. <https://www.thebritishacademy.ac.uk/sites/default/files/77p111.pdf>.
- ~ Tomber, Roberta, Lucy Blue, and Shinu Abraham. 2009. "Migration, Trade and Peoples Part 1: INDIAN OCEAN COMMERCE AND THE ARCHAEOLOGY OF WESTERN INDIA." In *Issues in Indian Ocean Commerce and the Archaeology of Western India*, London: The British Association for South Asian Studies, 1–57.

- ~ Tomber, Roberta, Caroline Cartwright, and Sunil Gupta. 2011. "Rice Temper: Technological Solutions and Source Identification in the Indian Ocean." *Journal of Archaeological Science* 38(2): 360–66.
- ~ Tsoupra, Anna. 2017. "Multi-Analytical Material Characterization of the 14th-18th Century Kongo Kingdom Pottery."

V

- ~ Velde, Bruce, and Isabelle C. Druc. 1999. *Archaeological Ceramic Materials Origin and Utilization*. 1st ed. eds. Gunther A Wagner and Bernd Herrmann. Heidelberg: Springer.

W

- ~ Wadia, Darashaw Noshawan. 1919. London *Geology of India for Students*. London: Macmillan and Co.
- ~ Wandrey, Craig J., and Ben E. Law. 1998. *MAPS SHOWING GEOLOGY, OIL AND GAS FIELDS AND GEOLOGIC PROVINCES OF SOUTH ASIA*.

Z

- ~ Zerboni, Andrea et al. 2020. "Geomorphology of the Jebel Qara and Coastal Plain of Salalah (Dhofar, Southern Sultanate of Oman)." *Journal of Maps* 16(2): 187–98.

9. Appendixes

9.1 sample recording

In the following appendix, the pictures of the samples prior to any sample preparation are presented. The samples are separated between samples from Inqitat and samples from Sumhuram. Among the Sumhuram samples, some samples that are not subject of the analysis are presented. Those samples were not selected because of their limited dimensions. In addition to the archaeological pictures, some samples were recorded in 3D, and here an example is presented.

Inqitat (HAS1)

SUM16B.US35.8 (ST) external, internal and lateral views:



IQM17A.US58.5 (ST) external, internal and lateral views



IQM18B.US119.5 (ST) external, internal and lateral views:



IQM17A.US58.8 (SF) external, internal and lateral views:



IQM16B.US35.34 (SF) external, internal and lateral views:



IQM16B.US35.33 (TF-1) external, internal and lateral views:



IQM16B.US35.31 (BF) external, internal and lateral views:



IQM17A.US35.16 (BF) external, internal and lateral views:



IQM16B.US35.35 (SF) external, internal and lateral views:



IQM16B.US35.32 (TF-1) external, internal and lateral views:



IQM16B.US30.6 (BF) external, internal views and lateral views:



IQM16B.US30.3 (BF): external, internal and lateral views:



IQM17A.US35.18 (BF) external, internal and lateral views:



IQM18A.US80.3 (FF) external, internal and lateral views:



IQM17B.US73.1 (MLF) external, internal and lateral views:



IQM16B.US30.10 (FF) external, internal and lateral views:



IQM16B.US35.9 (MLF) external, internal and lateral views:



IQM16B.US23.13 (MLF) external, internal and lateral views:



Sumhuram

SUMW03A.US1.1 (TF-2) external, internal and lateral views:



SUM08B.US162.104 (TF-2) external, internal and lateral views:



SUM11A.US174.232 (BF) external, internal and lateral views:



SUM08B.US975.4 (BF) external, internal and lateral views:



SUM10A.US412.1 (RT) external, internal and lateral views:



SUM10C.US174.83 (RT) external, internal and lateral views:



SUM09A.US297.2 (BF) external, internal and lateral views:



SUM11A.US58.85 (BF) external, internal and lateral views:



SUM10C.US174.104 (RT) external, internal and lateral views:



SUM10C.US162.119 (FF) external, internal and lateral views:



SUM10A.US405.3 (MLF) external, internal and lateral views:



SUM10C.US174.79 (MLF) external, internal and lateral view:



SUM03B.US93.23 (SSF) external, internal and lateral views:



SUM09B.US309.4 (SSF) external, internal and two lateral views:



SUM08.US253.5 (MLF) external, internal and lateral views:



SUM03A.US133.9 (MLF) external, internal and lateral views:



SUM03B.US93.42 (SSF) external, internal and lateral views:



9.2 Polarized optical microscopy observations

In this appendix, it is possible to find the results of the polarized optical microscopy observations. The presentation of the data is divided according to the grouping (colour coded) and according to site of excavation.

The presentation of the description tables is according to the following order:

1. SUMW03A.US1.1 (TF-2)
2. SUM08B.US162.104 (TF-2)
3. SUM11A.US174.232 (BF)
4. SUM09A.US297.2 (BF)
5. SUM08B.US975.4 (BF)
6. SUM11A.US54.85 (BF)
7. SUM08A.US253.5 (MLF)
8. SUM10C.US174.79 (MLF)
9. SUM03A.US133.9 (MLF)
10. SUM10A.US405.3 (MLF)
11. SUM10C.US174.104 (RT)
12. SUM10A.US412.1 (RT)
13. SUM10C.US174.83 (RT)
14. SUM03B.US93.23 (SSF)
15. SUM09B.US309.4 (SSF)
16. SUM03.US93.42 (SSF)
17. SUM10C.US162.119 (FF)
18. IQM16B.US35.33 (TF-1)
19. IQM16B.US35.32 (TF-1)
20. IQM16B.US35.31 (BF)
21. IQM16B.US30.6 (BF)
22. IQM16B.US30.3 (BF)
23. IQM17A.US35.16 (BF)
24. IQM17A.US35.18 (BF)
25. IQM16B.US23.13 (MLF)
26. IQM16B.US35.9 (MLF)
27. IQM17B.US73.1 (MLF)
28. IQM16B.US30.10 (FF)
29. IQM18A.US80.3 (FF)
30. IQM18B.US119.5 (ST)
31. IQM16B.US35.8 (ST)
32. IQM17A.US58.5 (ST)
33. IQM17A.US58.8 (SF)
34. IQM16B.US35.35 (SF)
35. IQM16B.US35.34 (SF)

| Sample | Site | Provenance | Temper- matrix ratio | Temper sorting | Temper grain size | Temper Roundness | Surface Treatment | Inclusions | | |
|-------------------|------|------------|-------------------------|-------------------|----------------------------------|---------------------|----------------------|-----------------------|--------------------------|--------------------|
| | | | | | | | | Mineral | Rock inclusions | Others |
| SUMW03A.US1.1 | SUM | Local | 40% | Poorly | Small to large | Unrounded | - | Talc, Q, C, O, | Sedimentary (c) | - |
| SUM08B.US162.104 | SUM | Local | 50% | Poorly | Small to large | Unrounded | - | Talc, Q, C, O, M | Sedimentary (c) | - |
| SUM11A.US174.232 | SUM | Indian | 20% | Moderately | Small to medium | Rounded | Slip | Q, C, O, Py | Basalt | Rice husks |
| SUM09A.US297.2 | SUM | Indian | 50 % | Poorly | Small to large | Unrounded | - | Q, C, Py, Ol, M | Basalt | - |
| SUM08B.US975.4 | SUM | Indian | 30% | Very Poorly | Very small to extremely large | Subangular | - | Q, C, O, Py, Ol, | Basalt/Volcanic glass | Rice husks |
| SUM11A.US54.85* | SUM | Indian | 50% | Well | Small | Rounded | Slip | Q, O, C, Py | Basalt | - |
| SUM08A.US253.5 | SUM | Indian | 50% | Moderately | Small to medium | Sub angular | Slip | Q, F, Py, O, B, Am | - | - |
| SUM10C.US174.79 | SUM | Indian | 30% | Poorly | Small to large | Poorly rounded | Slip | Q, C, O, | Sedimentary (d) | - |
| SUM03A.US133.9* | SUM | Indian | 40% | Moderately | Small to medium | Poorly rounded | - | Q, O, Py, M | Sedimentary (d) | - |
| SUM10A.US405.3 | SUM | Indian | 50 % | Moderately | Small to medium | Poorly rounded | Slip | Q, F, M, O | Sedimentary (d) | - |
| SUM10C.US174.104 | SUM | Indian | 30% | Well | Very small to small | Poorly rounded | - | Q, O | Basalt | Rice husks |
| SUM10A.US412.1 | SUM | Indian | 50% | Well | Small | Rounded | - | Q, O, M | Basalt | Rice husks |
| SUM10C. US174.83 | SUM | Indian | 40% | Well | Very small to small | Rounded | - | Q, C, O, Py | Basalt | Rice husks |
| SUM03B.US93.23 | SUM | Indian | 30% | Moderately | Small to medium | Poorly rounded | Slip | Q, O, C, Py | Sedimentary (c) | Shell fragments |
| SUM09B. US309.4 | SUM | Indian | 30% | Moderately | Small to medium | Poorly rounded | - | Q, Py, O, C | - | Shell fragments |
| SUM03B.US93.42 | SUM | Indian | 40% | Well | Very small to small | Poorly rounded | - | Q, O, C | Sedimentary (c) | Shell fragments |
| SUM10C.US162.119* | SUM | Indian | 40% | Well | Small | Well-rounded | Slip | Q, C, O, Py, Am | - | Rice husks |

SUM= Sumhuram, Q= quartz, C= carbonate, O= opaques, Py= pyroxene, M= micas, B= biotite, F= feldspars, Am= amphiboles, Ol= Olivine, (c)= chemogenic, (d)= detritic

| Sample | Site | Provenance | Temper-matrix ratio | Temper sorting | Temper grain size | Temper Roundness | Surface Treatment | Inclusions | | |
|----------------|------|------------|---------------------|----------------|--------------------------|--------------------------------|-------------------|-------------------|-----------------|-----------------|
| | | | | | | | | Mineral | Rock inclusions | Others |
| IQM16B.US35.33 | IQM | Local | 30% | Poorly | Small to large | Rounded and Angular | - | Talc, Q, C, O, Am | Shale | - |
| IQM16B.US35.32 | IQM | Local | 50% | Poorly | Small to large | Rounded and Angular | - | Talc, C, O, | Shale | - |
| IQM16B.US35.31 | IQM | Local | 30% | Poorly | Very small to medium | Poorly | Slip | Q, Pl, C, O | Basalt | Rice husks |
| IQM16B.US30.6 | IQM | Indian | 30% | Moderately | Small to medium | Rounded and Angular | Slip | Q, C, Py, Ol, O | Basalt | Rice husks |
| IQM16B.US30.3 | IQM | Indian | 30% | Poorly | Very small to medium | Poorly rounded | - | Q, O, Py, Pl | Basalt | - |
| IQM17A.US35.16 | IQM | Indian | 20% | Moderately | Small to medium | Poorly rounded | - | Q, O | Basalt | - |
| IQM17A.US35.18 | IQM | Indian | 30% | Very poorly | Very small to very large | Poorly | - | Q, Pl, O, | Basalt | Rice husks |
| IQM16B.US23.13 | IQM | Indian | 30% | Moderately | Very small to medium | Subangular | - | Q, Pl, O, | - | - |
| IQM16B.US35.9 | IQM | Indian | 30% | Moderately | Small to medium | Subangular | Slip | Q, Pl, C, Mu, O | - | - |
| IQM17B.US73.1 | IQM | Indian | 20% | Poorly | Very small to medium | Rounded and Angular | Slip | Q, O, M, C | Sedimentary (d) | - |
| IQM16B.US30.10 | IQM | Indian | 20% | Moderately | Small to medium | Poorly rounded | Slip | Q, C, Mu, O | Sedimentary (c) | Shell fragments |
| IQM18A.US80.3 | IQM | Indian | 20% | Well | Small | Angular | Slip | Q, C, | Sedimentary (c) | Shell fragments |
| IQM18B.US119.5 | IQM | Local | 40% | Poorly | Very small to large | Rounded and Angular | - | Q | Limestone | Shell fragments |
| IQM16B.US35.8 | IQM | Local | 40% | Moderately | Very small to medium | Angular | - | Q, Am, O | - | Shell fragments |
| IQM17A.US58.5 | IQM | Local | 50% | Poorly | Very small to large | Unrounded | - | Q | - | Shell fragments |
| IQM17A.US58.8 | IQM | Local | 30% | Very Poorly | Very small to very large | Poorly rounded to well-rounded | - | Q, O, M, | Shale | Shell fragments |
| IQM16B.US35.35 | IQM | Local | 40% | Poorly | Very small to large | Poorly rounded to well-rounded | - | Q, C, Am, Py, O | Shale | - |
| IQM16B.US35.34 | IQM | Local | 50% | Very poorly | Very small to very large | Subangular to well-rounded | - | Q, Am, C, O, M | Shale | Shell fragments |

IQM=Inqitat, Q= quartz, C= carbonate, O= opaques, Py= pyroxene, M= micas, Mu= muscovite, Am= amphiboles, Ol= Olivine, Pl= plagioclase, (c)= chemogenic

9.3 X-ray Diffraction

The following appendix presents the results of XRD analysis conducted on each sample. The results are presented in a general table colour coded according to groups and followed by the presentation of each sample's diffractogram.

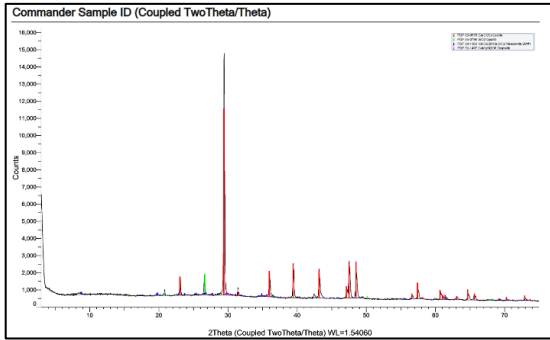
The order of presentation of the result for each sample follows the same as the one followed in the Petrographic appendix.

| | |
|----------------------------|--------------------------|
| 1.IQM18B.US35.8 (ST) | 19.SUM11A.US54.85 (BF) |
| 2.IQM17A.US58.5 (ST) | 20.SUM10C.US174.83 (RT) |
| 3.IQM18B.US119.5 (ST) | 21.SUM10A.US412.1 (RT) |
| 4.IQM17A.US58.8 (SF) | 22.SUM10C.US174.104 (RT) |
| 5.IQM16B.US35.34 (SF) | 23.IQM18A.US80.3 (FF) |
| 6.IQM16B.US35.35 (SF) | 24.SUM10C.US162.119 (FF) |
| 7.IQM16B.US35.33 (TF-1) | 25.IQM16B.US30.10 (FF) |
| 8.IQM16B.US35.32 (TF-1) | 26.IQM16B.US23.13 (MLF) |
| 9.SUMW03A.US1.1 (TF-2) | 27.SUM10A.US405.3 (MLF) |
| 10.SUM08B.US162.104 (TF-2) | 28.SUM03A.US133.9 (MLF) |
| 11.IQM16B.US30.6 (BF) | 29.IQM16B.US35.9 (MLF) |
| 12.IQM17B.US35.16 (BF) | 30.IQM17B.US73.1 (MLF) |
| 13.IQM16B.US30.3 (BF) | 31.SUM08A.US253.5 (MLF) |
| 14.IQM17A.US35.18 (BF) | 32.SUM10C.US174.79 (MLF) |
| 15.IQM16B.US35.31 (BF) | 33.SUM03B.US93.23 (SSF) |
| 16.SUM11A.US174.232 (BF) | 34.SUM09B.US309.4 (SSF) |
| 17.SUM09A.US297.2 (BF) | 35.SUM03.US93.42 (SSF) |
| 18.SUM08B.US975.4 (BF) | |

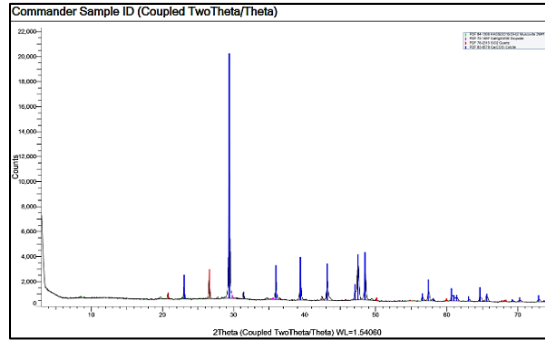
| Sample Name | Q | C | Do | Pl | K-F | H | M | Ol | Py | Am | An | Ta | Gy | Ze | Ch | Sp | Cr | Di | Mu | Ge | Wo | Ka | Go | Si | Rh |
|--------------------|------|------|----|-----|-----|---|----|----|----|-----|----|------|----|----|----|----|----|----|----|----|----|----|----|----|----|
| IQM16B.US35.8 | x | xxxx | - | - | - | - | xx | - | - | - | - | - | - | - | - | - | - | x | - | - | - | - | - | - | - |
| IQM17A.US58.5 | xx | xxxx | - | - | - | - | x | - | - | - | - | - | - | - | - | - | - | x | - | - | - | - | - | - | - |
| IQM18B.US119.5 | xxx | xxx | - | - | - | - | x | - | - | - | - | - | - | - | - | - | - | x | + | - | - | - | - | - | - |
| IQM17A.US58.8 | xx | xxx | - | x | - | - | x | - | - | xx | - | - | - | - | xx | - | + | - | x | - | - | - | - | - | - |
| IQM16B.US35.34 | xx | x | - | xx | - | - | xx | - | - | xx | - | - | - | - | - | - | - | x | - | - | - | - | - | - | - |
| IQM16B.US35.35 | xx | x | - | xx | - | x | - | - | - | xxx | - | - | - | - | - | - | - | x | - | x | - | - | - | - | - |
| IQM16B.US35.33 | xx | x | - | x | - | - | - | - | - | xx | - | xxx | - | - | xx | - | - | x | - | - | - | - | - | - | - |
| IQM16B.US35.32 | x | x | - | x | - | - | - | - | - | xx | - | xxx | - | x | - | - | - | + | - | - | - | x | - | - | - |
| SUMW03A.US1.1 | x | + | - | - | - | - | x | - | - | - | - | xxxx | - | + | x | - | - | - | - | - | - | - | - | - | - |
| SUM08B.US162.104 | + | + | - | - | - | + | + | - | - | - | - | xxxx | + | - | + | - | - | - | - | - | - | - | - | - | - |
| IQM16B.US35.31 | xx | x | x | xxx | - | + | x | - | - | - | x | - | - | - | - | - | - | x | - | - | - | - | - | - | - |
| IQM16B.US30.6 | xx | - | x | xx | - | x | - | - | - | x | x | - | x | - | - | - | - | x | - | - | - | - | - | - | - |
| IQM17A.US35.16 | xxx | x | - | xx | - | x | - | - | - | - | x | - | - | - | - | - | - | x | x | - | - | - | - | - | - |
| IQM16B.US30.3 | xx | - | x | xx | - | x | xx | - | x | - | x | - | xx | - | - | - | - | x | - | - | - | - | - | - | - |
| IQM17A.US35.18 | xx | x | - | xxx | - | x | - | - | xx | - | x | - | - | - | - | - | - | - | - | - | - | - | - | - | - |
| SUM11A.US174.232 | xxx | x | - | xx | - | x | xx | - | - | - | + | - | - | - | - | - | - | x | - | - | - | - | - | - | - |
| SUM09A.US297.2 (*) | xx | x | - | xxx | - | x | x | - | x | - | - | - | + | - | - | - | + | - | - | - | - | - | - | - | x |
| SUM08B.US975.4 | xx | + | - | xx | x | x | xx | x | - | - | - | - | - | - | - | x | - | x | - | + | - | - | - | - | - |
| SUM11A.US54.85 | xxx | x | - | xx | - | x | x | - | x | - | - | - | - | - | - | - | + | x | - | - | - | - | - | - | - |
| SUM10A.US412.1 | xxx | + | - | xx | - | - | x | - | x | - | - | - | - | - | - | - | - | - | - | - | x | - | - | - | - |
| SUM10C.US174.104 | xxx | + | - | xx | xx | - | xx | x | x | - | - | - | - | - | - | - | - | - | - | - | - | - | - | - | - |
| SUM10C.US174.83 | xxx | + | - | xx | x | x | x | - | - | - | - | - | - | - | - | - | - | x | x | - | - | - | - | - | - |
| IQM16B.US30.10 | xxx | x | - | xx | - | + | xx | - | - | - | - | - | xx | - | - | - | - | x | x | + | - | - | - | - | - |
| SUM10C.US162.119 | xxx | x | - | xx | xx | + | xx | - | - | - | - | - | - | - | - | - | + | x | x | x | - | - | - | - | - |
| IQM18A.US80.3 | xxx | x | - | x | x | + | xx | - | - | - | - | - | - | - | - | - | - | x | x | - | - | - | - | - | - |
| SUM10A.US405.3 | xx | - | - | xx | xx | - | x | - | - | xx | - | - | - | - | - | - | - | - | - | - | - | - | - | - | - |
| IQM16B.US35.9 | xxx | - | x | x | xx | - | xx | - | - | - | + | - | - | - | - | - | - | x | - | - | x | - | x | x | - |
| IQM17B.US73.1 | xxxx | + | - | x | xx | - | - | - | - | - | x | - | - | - | - | - | - | - | x | - | - | - | x | - | - |
| IQM16B.US23.13 | xxx | + | - | xx | xx | - | - | - | x | - | - | - | - | - | - | - | - | x | - | - | - | - | - | - | - |
| SUM08A.US253.5 | xx | + | - | xx | xx | - | x | - | - | x | - | - | - | - | - | - | - | - | - | - | - | - | - | - | - |
| SUM10C.US174.79 | xxx | - | - | x | xx | - | xx | - | x | - | - | - | - | - | - | - | - | - | x | - | - | - | - | - | - |
| SUM03A.US133.9 | xxx | - | - | - | xx | + | x | - | - | - | - | - | - | - | - | - | - | - | x | - | - | - | - | - | - |
| SUM03B.US93.23 | xxx | xx | - | x | x | - | xx | - | - | - | - | - | - | - | - | - | - | - | x | + | x | - | - | - | - |
| SUM09B.US309.4 | xx | xxx | - | x | x | + | x | - | x | - | - | - | + | - | - | - | - | x | x | x | - | - | - | - | - |
| SUM03B.US93.42 | xx | xx | - | x | x | - | xx | - | - | - | - | - | - | - | - | - | - | - | x | x | x | - | - | - | - |

xxxx = between 70% and 100 %; xxx = between 40% and 70%; xx = between 10% and 40%; x = less than 10%; + = present; - = absent; (*) = rhodonite present

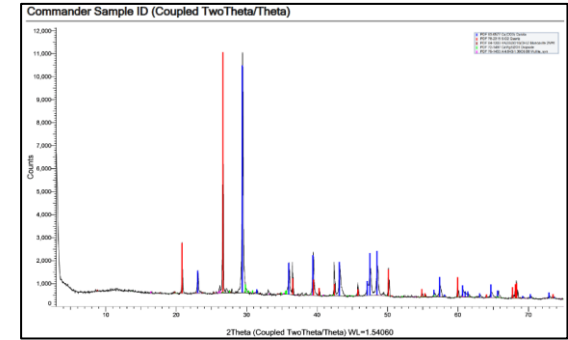
Q= Quartz; C= Calcite; Do= Dolomite; Pl= Plagioclase; K-F= K-feldspars; H= Hematite; M= Micas; Ol= Olivine; Py= Pyroxene; Am= Amphiboles; Ta= Talc; Gy= Gypsum; Ze= Zeolite; Ch= Chlorite; Sp= Spinel; Cr= Cristobalite; Di= Diopside; Mu= Mullite; Ge= Gehlenite; Wo= Wollastonite; Ka= Kaolinite; Go= Goethite; Si= Sillimanite; Rh= Rhodonite



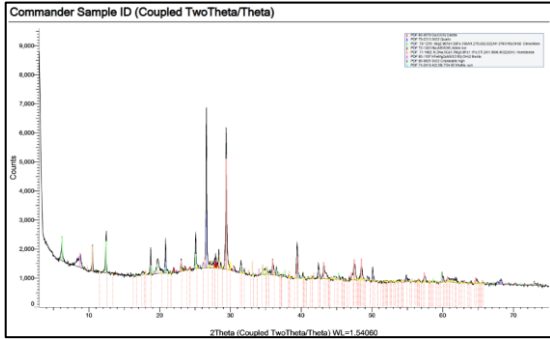
IQM16B.US35.8 (ST)



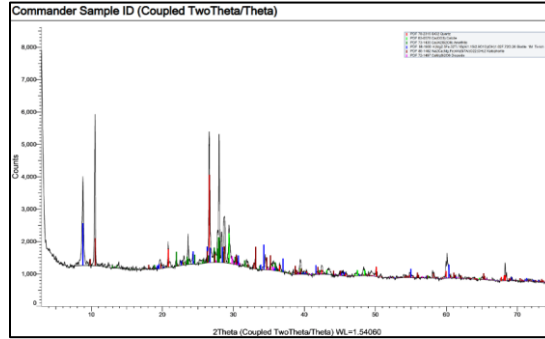
IQM16B.58.5 (ST):



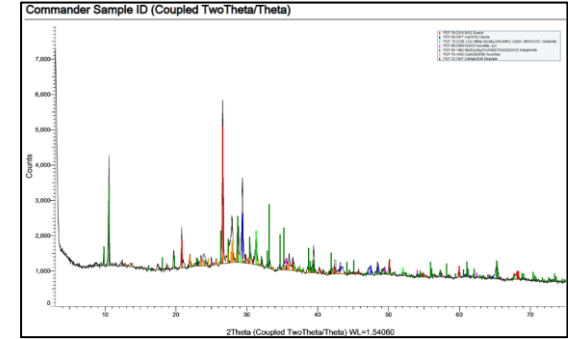
IQM18B.US119.5 (ST)



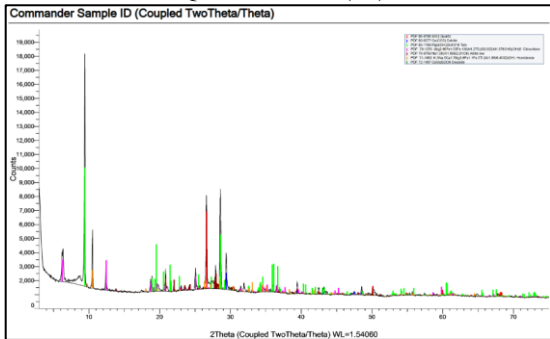
IQM16B.US58.8 (SF)



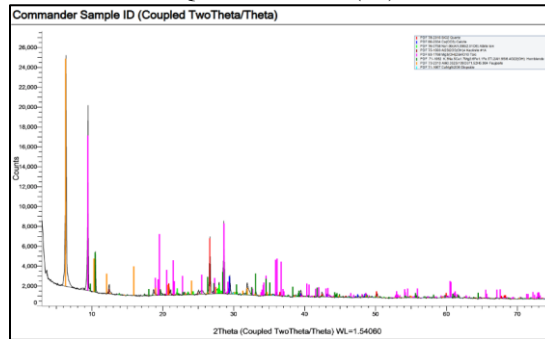
IQM16B.US35.34 (SF)



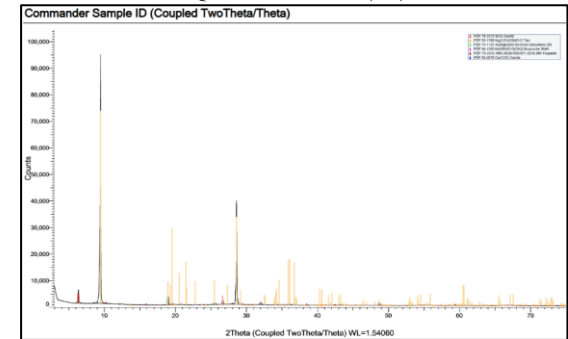
IQM16B.US35.35 (SF)



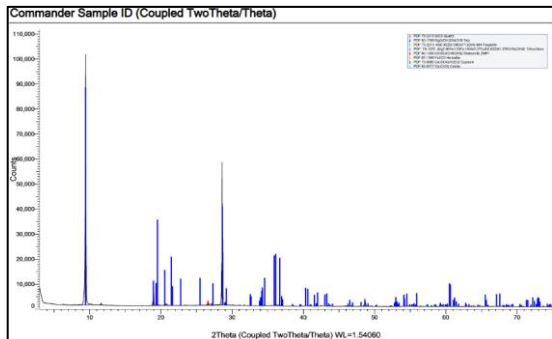
IQM16B.US35.33 (TF-1)



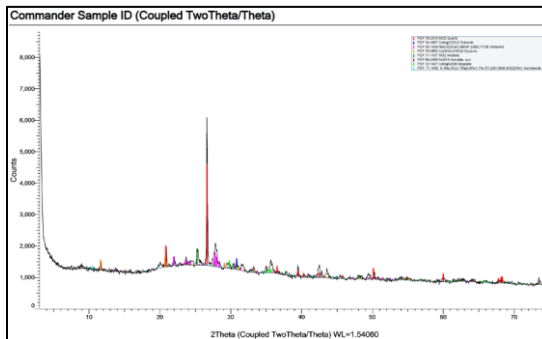
IQM16B.US35.32 (TF-1)



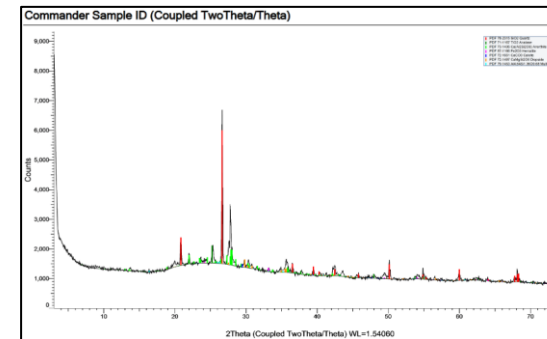
SUMW03A.US1.1 (TF-2)



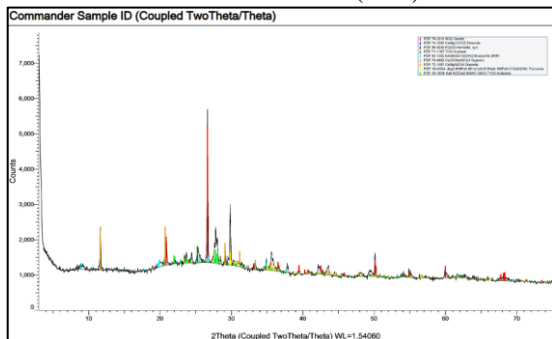
SUM08B.US162.104 (TF-2)



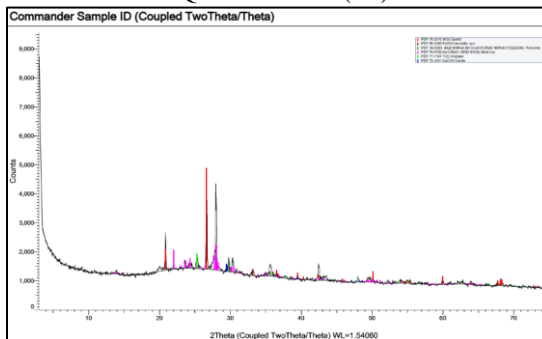
IQM16B.US30.6 (BF)



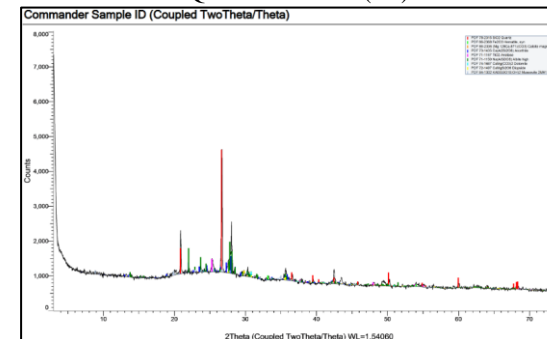
IQM17B.US35.16 (BF)



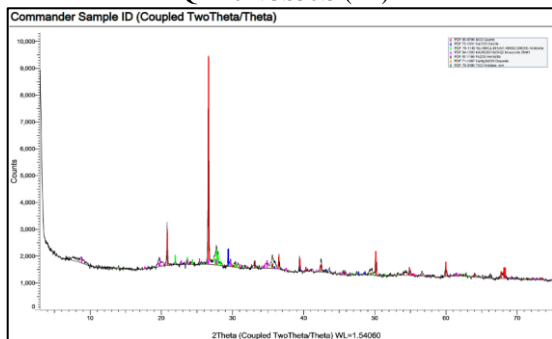
IQM16B.US30.3 (BF)



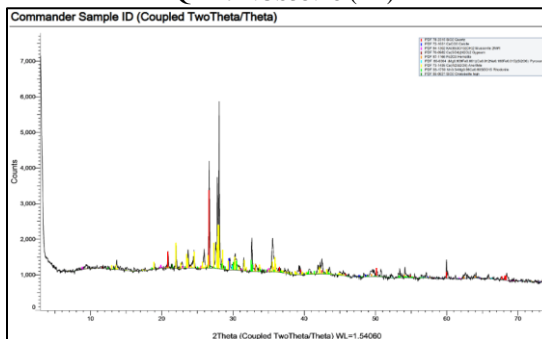
IQM17B.US35.18 (BF)



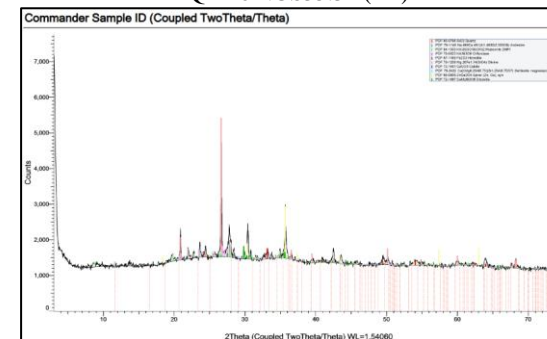
IQM16B.US35.31 (BF)



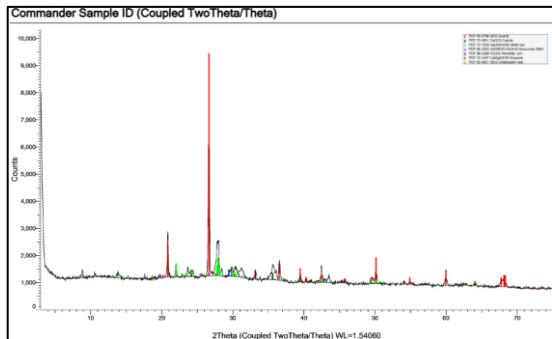
SUM11A.US174.232 (BF)



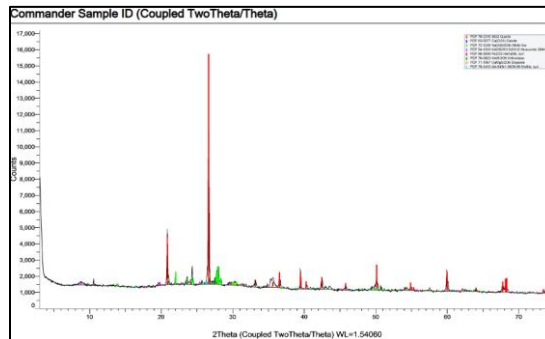
SUM09A.US297.2 (BF)



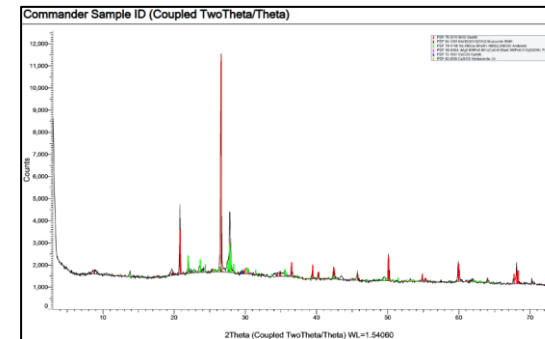
SUM08B.US975.4 (BF)



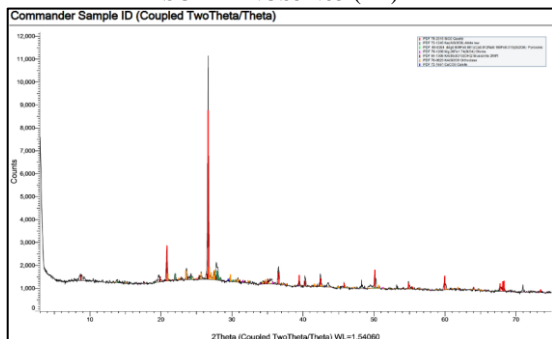
SUM11A.US54.85 (BF)



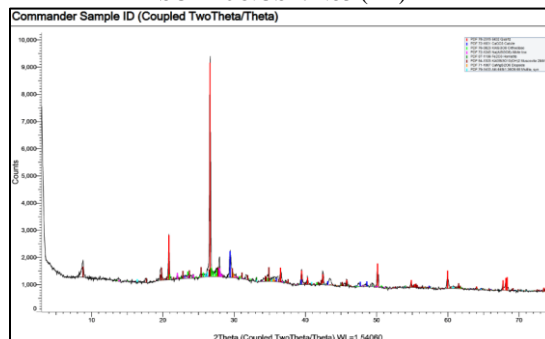
SUM10C.US174.83 (RT)



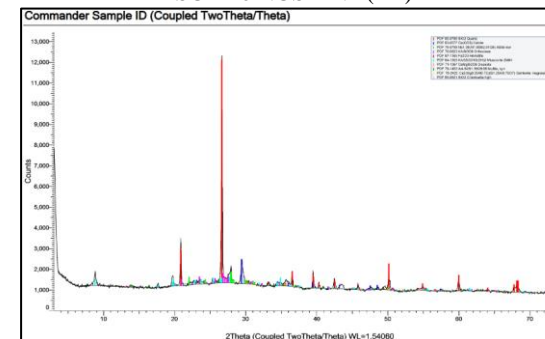
SUM10A.US412.1 (RT)



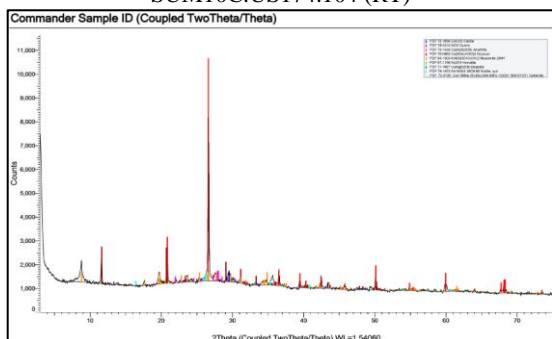
SUM10C.US174.104 (RT)



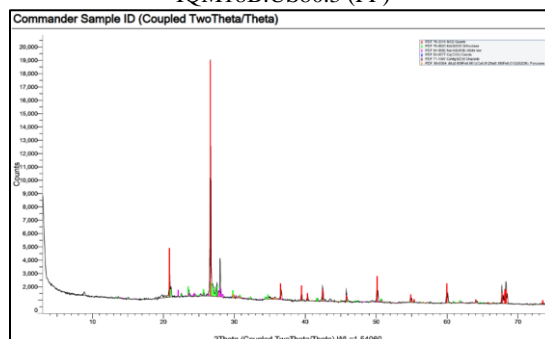
IQM18B.US80.3 (FF)



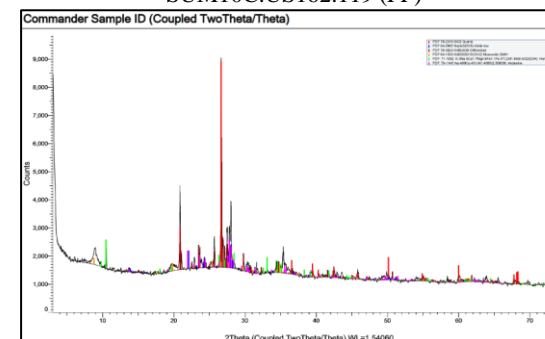
SUM10C.US162.119 (FF)



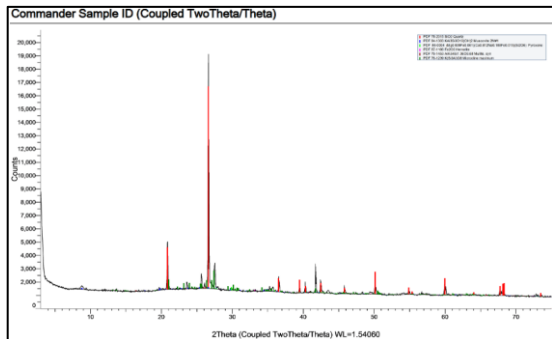
IQM16B.US30.10 (FF)



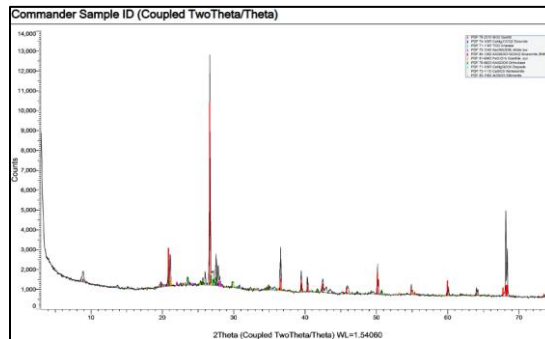
IQM16B.US23.13 (MLF)



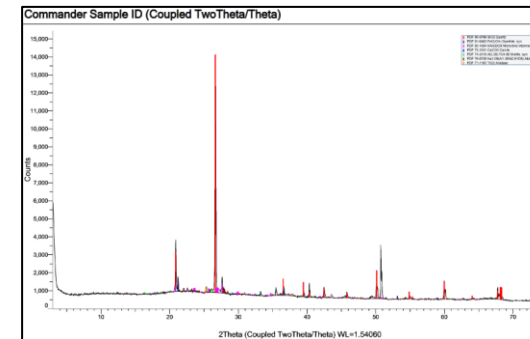
SUM10C.US405.3 (MLF)



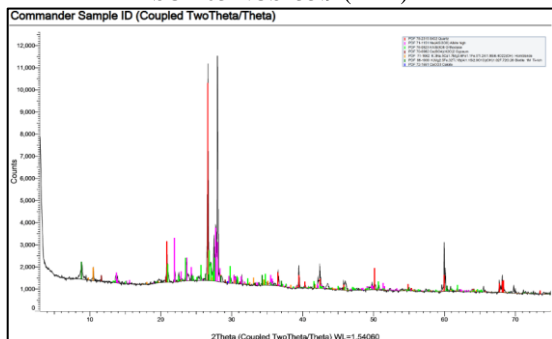
SUM03A.US133.9 (MLF)



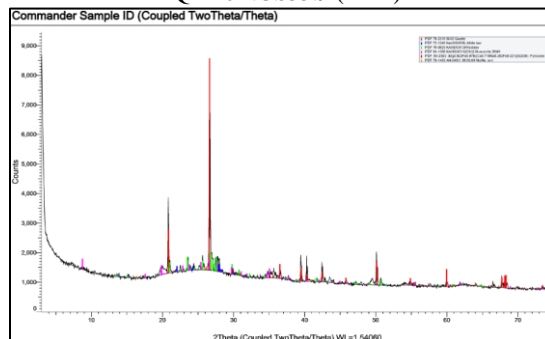
IQM16B.US35.9 (MLF)



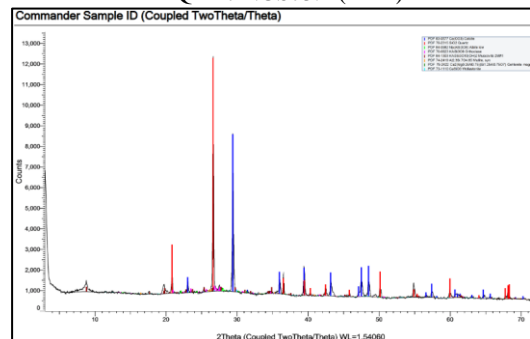
IQM17B.US73.1 (MLF)



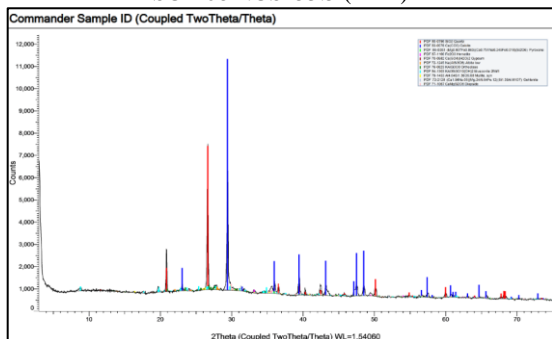
SUM08A.US253.5 (MLF)



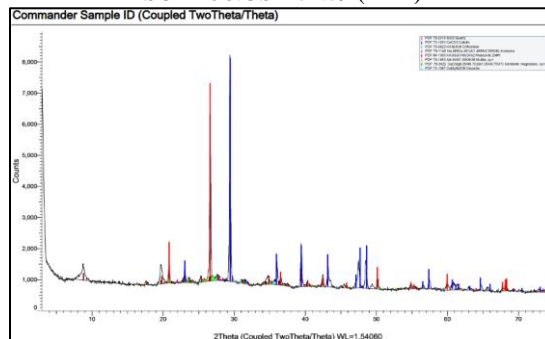
SUM10C.US2174.79 (MLF)



SUM03B.US93.23 (SSF)



SUM09B.US309.4 (SSF)

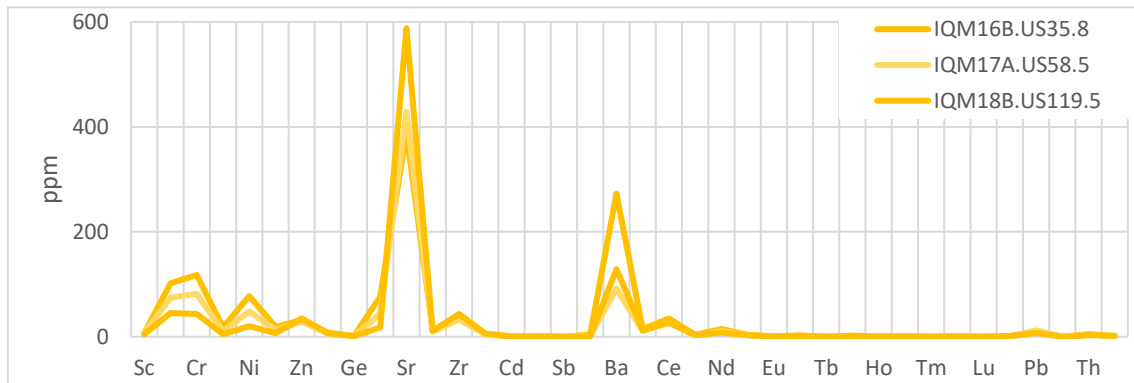


SUM03B.US93.42 (SSF)

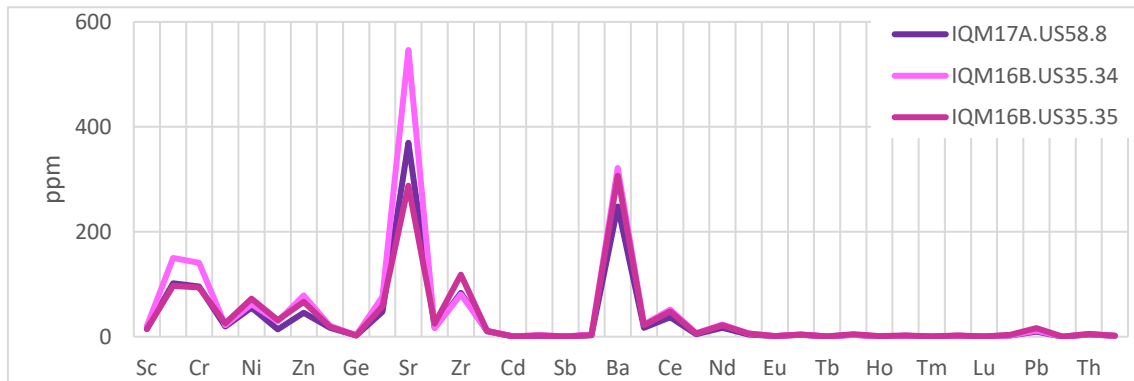
9.4 ICP-MS results and graphic representations

In the following appendix the author presents the results of the ICP-MS analysis, in particular the graphic representation of the trace elements (in ppm) of the different groups and the most representative distribution graphs related to the provenance analysis.

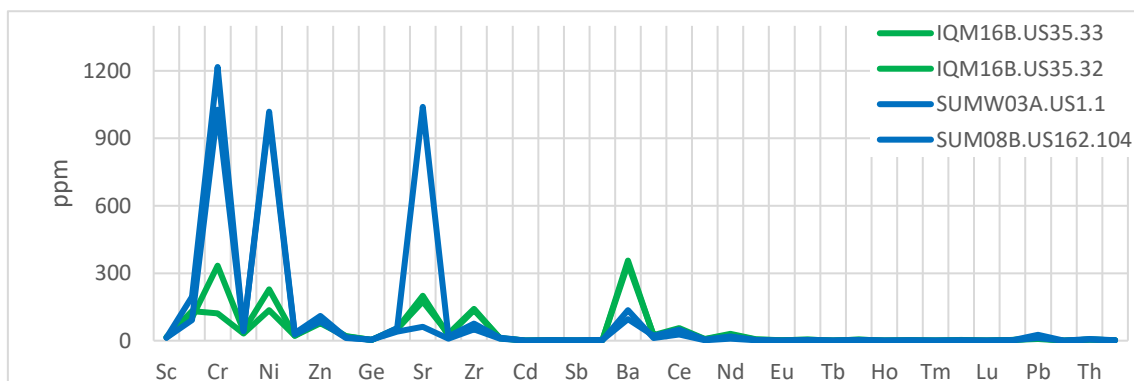
1. ST group



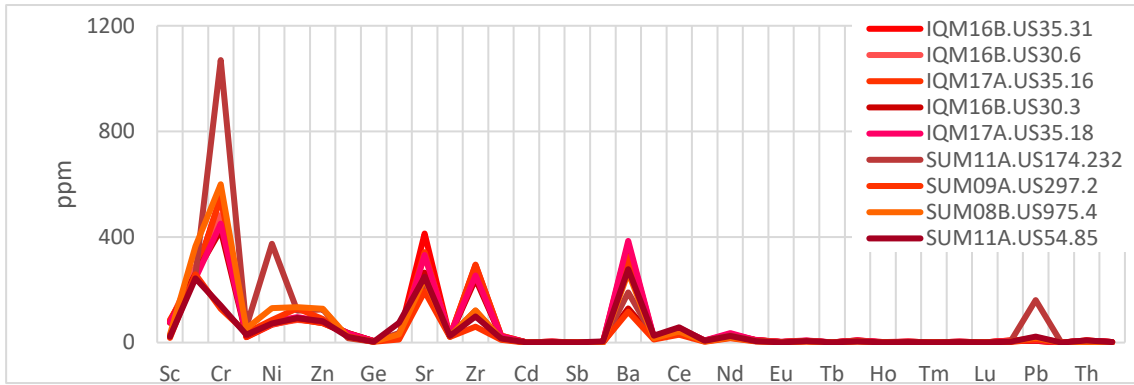
2. SF group



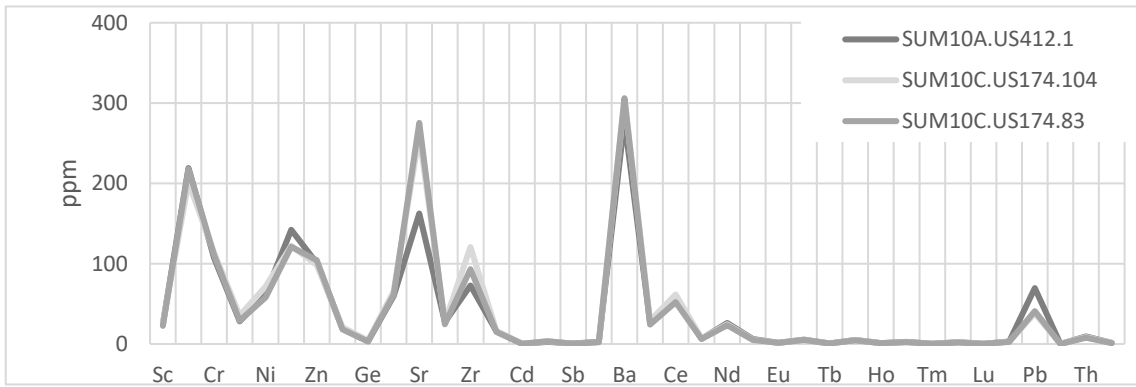
3. TF group



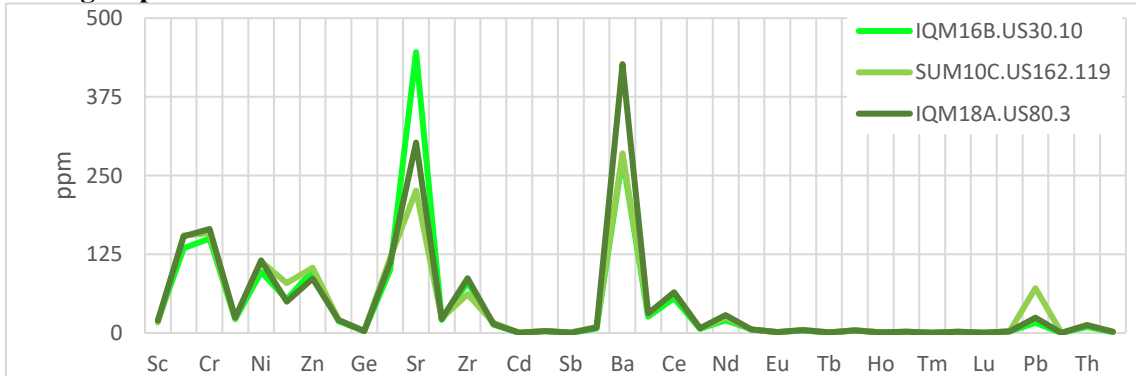
4. BF group



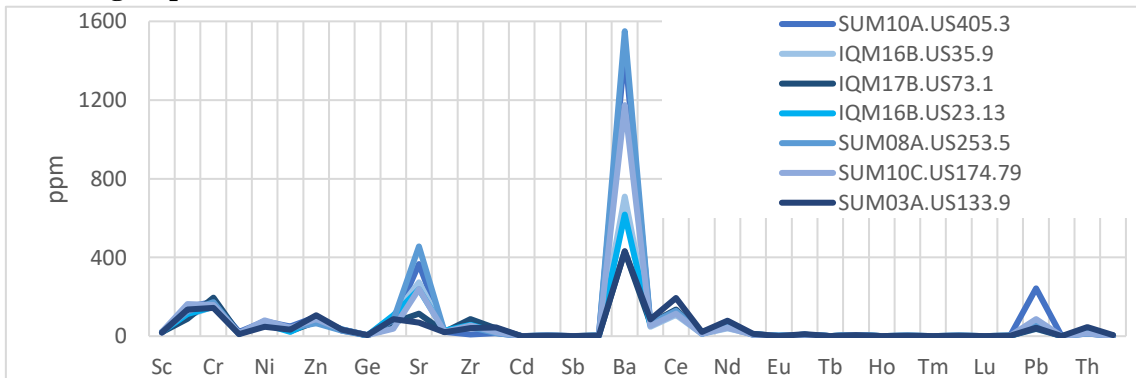
5. RT group



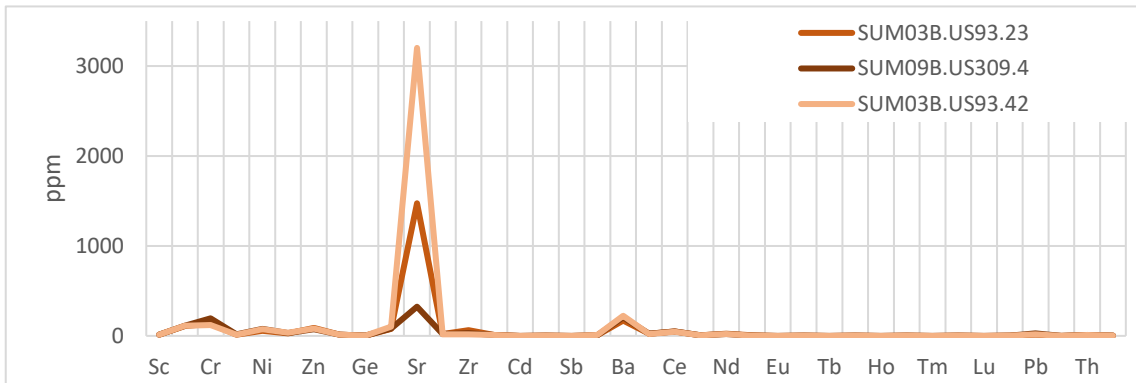
6. FF group



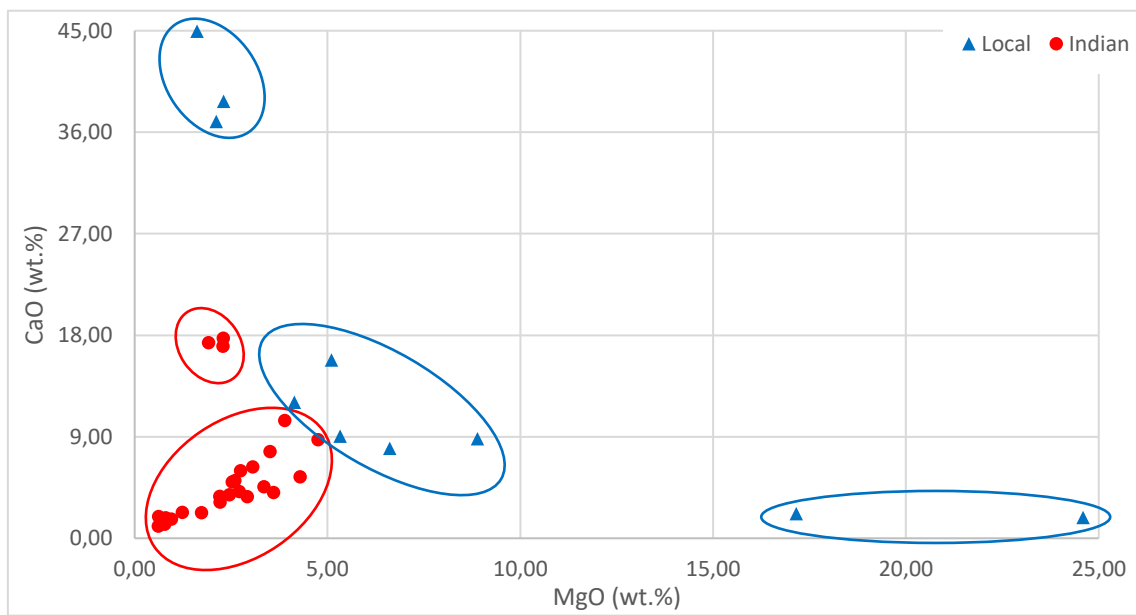
7. MFL group



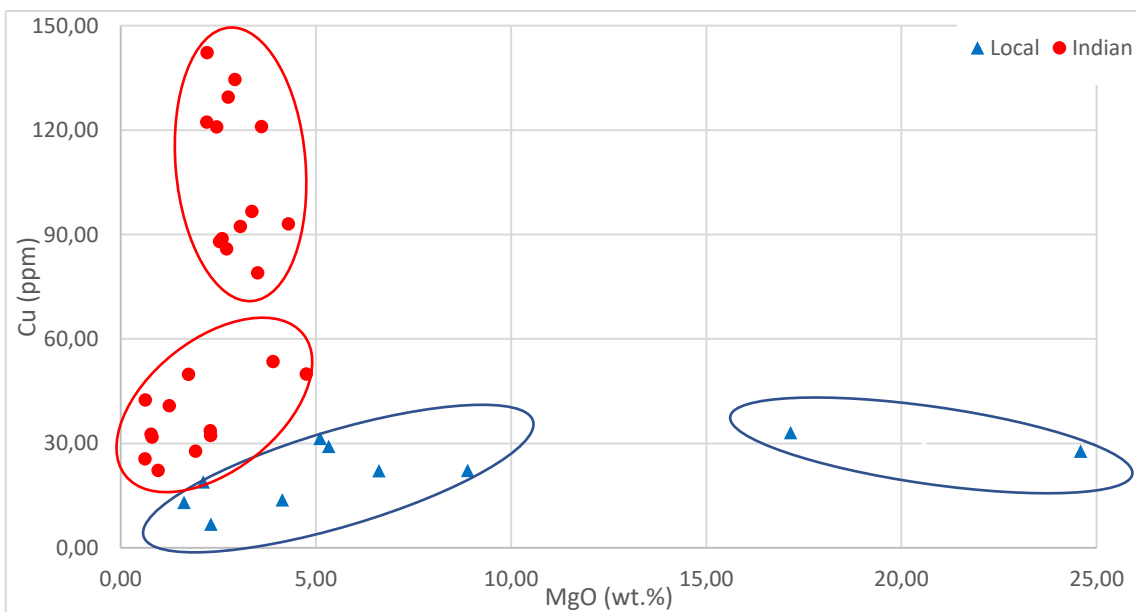
8. SSF group



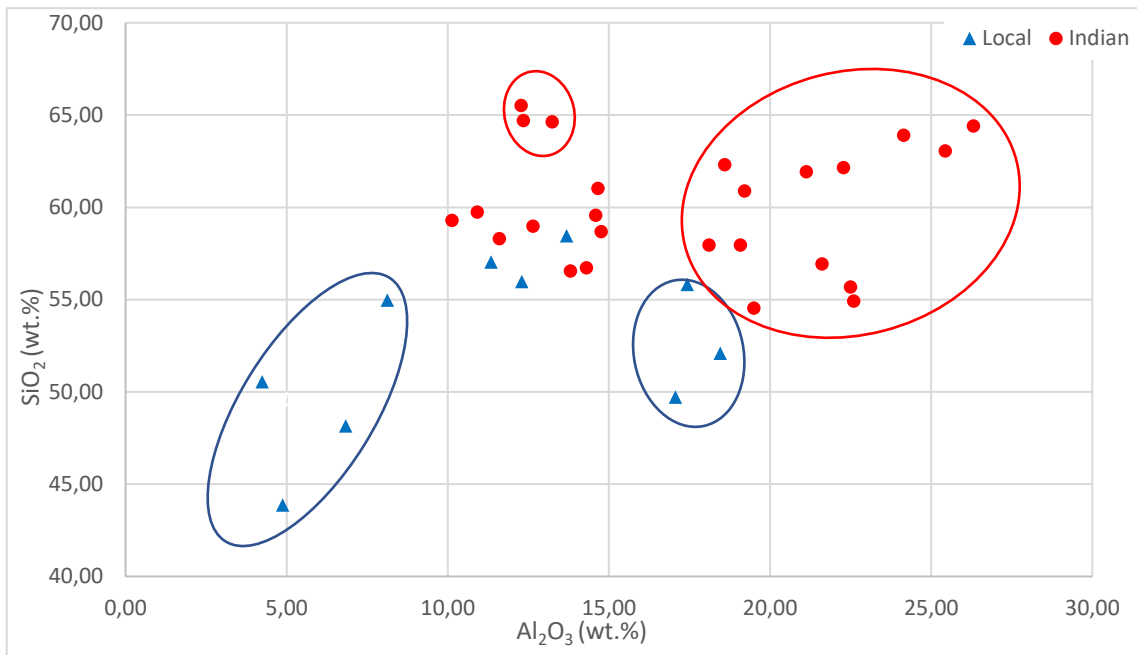
9. CaO vs MgO



10. Cu vs MgO



11. SiO₂ vs Al₂O₃



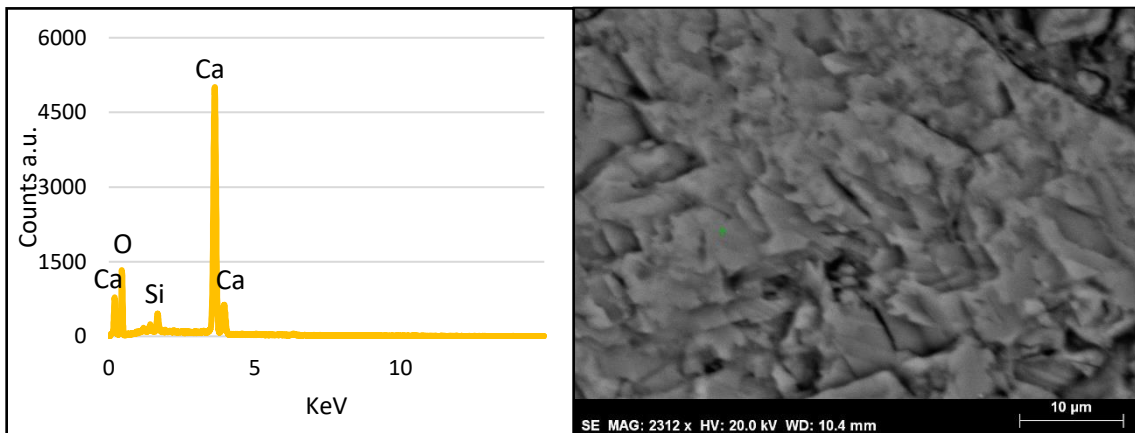
9.5 SEM-EDS data

In the following appendix, the author presents the data and the observation resulted from the SEM-EDS analysis of the samples and not reported along the main text. The presentation of the data is sample based.

SAMPLE: IQM16B.US35.8 (ST)

Shell fragment composition analysis and BSE image of the location:

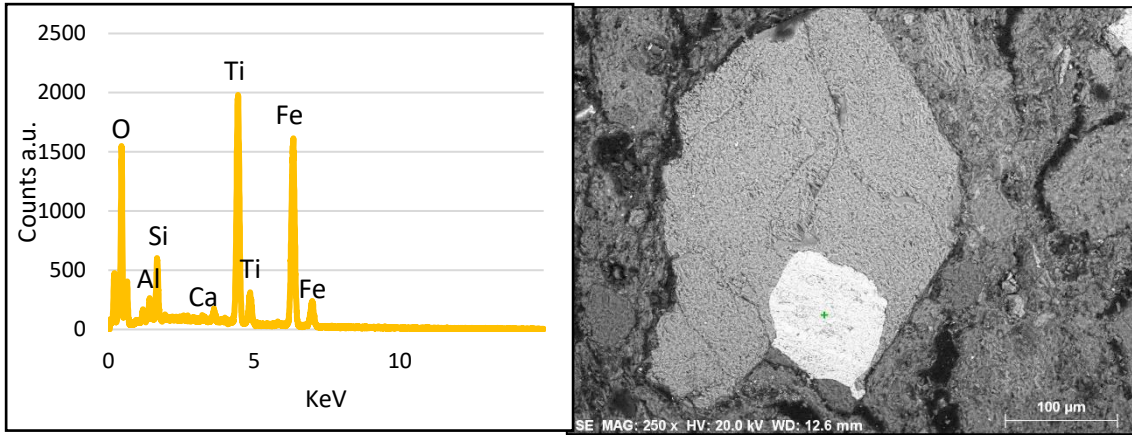
| Element | AN | series | [wt.%] | [norm. wt.%] | [norm. at.%] | Error in wt.% (1 Sigma) |
|-----------|----|----------|----------|--------------|--------------|-------------------------|
| Carbon | 6 | K-series | 7,446404 | 7,277167 | 12,78422 | 1,971849 |
| Oxygen | 8 | K-series | 49,0903 | 47,97461 | 63,27012 | 6,499255 |
| Magnesium | 12 | K-series | 0,302234 | 0,295365 | 0,256422 | 0,047265 |
| Aluminium | 13 | K-series | 0,460575 | 0,450107 | 0,351998 | 0,052301 |
| Silicon | 14 | K-series | 1,203602 | 1,176247 | 0,883705 | 0,080967 |
| Potassium | 19 | K-series | 0,43621 | 0,426296 | 0,230062 | 0,043001 |
| Calcium | 20 | K-series | 42,70108 | 41,7306 | 21,97048 | 1,276496 |
| Iron | 26 | K-series | 0,685187 | 0,669615 | 0,252997 | 0,056472 |
| | | Sum: | 102,3256 | 100 | 100 | |



SAMPLE: IQM16B.US35.34 (SF)

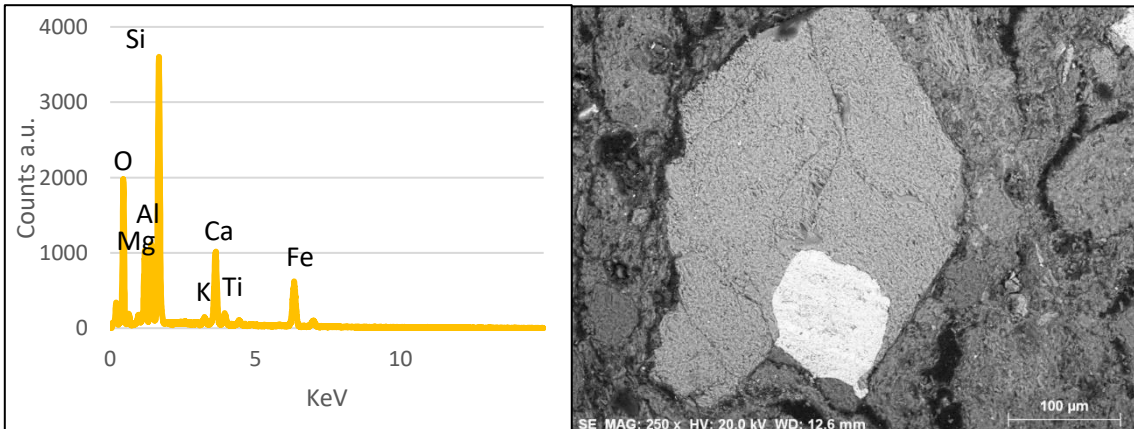
Point analysis oxide and BSE image of the location:

| Element | AN | series | [wt.%] | [norm. wt.%] | [norm. at. %] | Error in wt.% (1 Sigma) |
|-----------|----|----------|----------|--------------|---------------|-------------------------|
| Oxygen | 8 | K-series | 35,79512 | 33,83976 | 60,88061 | 23,16565 |
| Sodium | 11 | K-series | 0,73693 | 0,696674 | 0,872269 | 0,088546 |
| Magnesium | 12 | K-series | 0,914464 | 0,864511 | 1,023835 | 0,086414 |
| Aluminium | 13 | K-series | 1,253381 | 1,184914 | 1,264082 | 0,094053 |
| Silicon | 14 | K-series | 2,548822 | 2,409589 | 2,469541 | 0,14046 |
| Potassium | 19 | K-series | 0,208818 | 0,197411 | 0,145334 | 0,035971 |
| Calcium | 20 | K-series | 0,515247 | 0,487101 | 0,349839 | 0,045958 |
| Titanium | 22 | K-series | 23,42007 | 22,14072 | 13,31045 | 0,682479 |
| Manganese | 25 | K-series | 0,733133 | 0,693084 | 0,363135 | 0,078222 |
| Iron | 26 | K-series | 39,6523 | 37,48624 | 19,3209 | 1,094156 |
| | | Sum: | 105,7783 | 100 | 100 | |



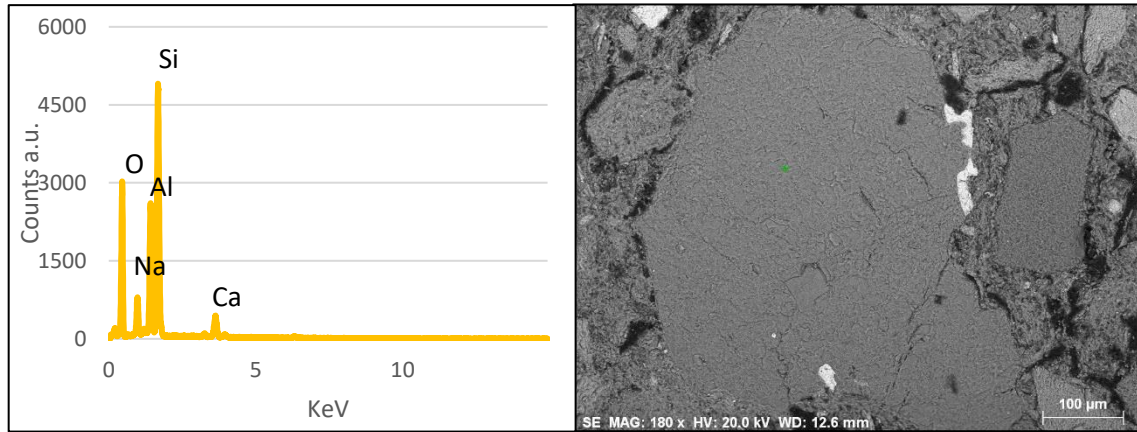
Point analysis hornblende and BSE image of the location:

| Element | AN | series | [wt.%] | [norm. wt.%] | [norm. at.%] | Error in wt.% (1 Sigma) |
|-----------|----|----------|----------|--------------|--------------|-------------------------|
| Oxygen | 8 | K-series | 43,74176 | 43,77516 | 61,52949 | 22,43835 |
| Sodium | 11 | K-series | 1,838995 | 1,840399 | 1,800266 | 0,158155 |
| Magnesium | 12 | K-series | 6,501967 | 6,506931 | 6,020601 | 0,391392 |
| Aluminium | 13 | K-series | 6,54641 | 6,551408 | 5,460434 | 0,346621 |
| Silicon | 14 | K-series | 17,69009 | 17,7036 | 14,17551 | 0,785062 |
| Potassium | 19 | K-series | 0,690894 | 0,691421 | 0,397689 | 0,05252 |
| Calcium | 20 | K-series | 8,365883 | 8,372269 | 4,697821 | 0,277961 |
| Titanium | 22 | K-series | 0,82999 | 0,830623 | 0,39013 | 0,057976 |
| Iron | 26 | K-series | 13,71772 | 13,72819 | 5,52806 | 0,407464 |
| | | Sum: | 99,92371 | 100 | 100 | |



Point analysis feldspar grain and BSE image of the location:

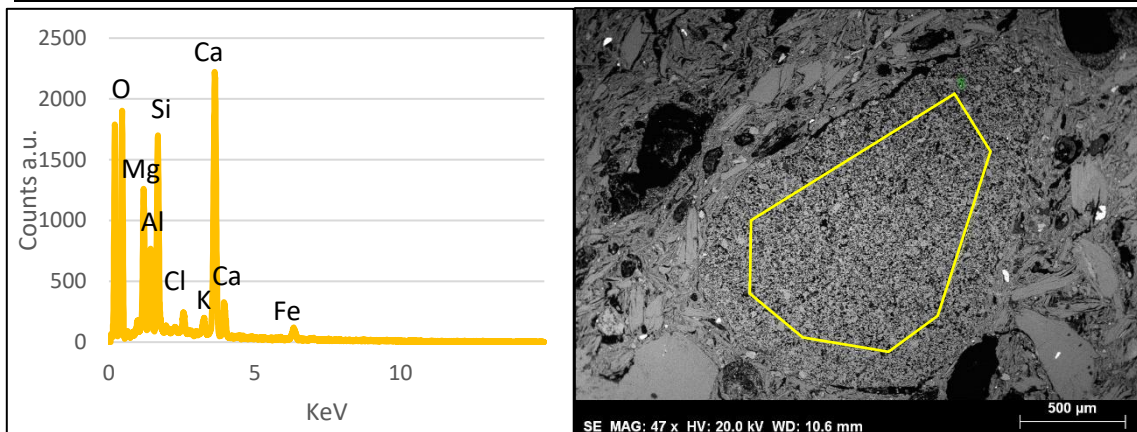
| Element | AN | series | [wt.%] | [norm. wt.%] | [norm. at.%] | Error in wt.% (1 Sigma) |
|-----------|----|----------|----------|--------------|--------------|-------------------------|
| Oxygen | 8 | K-series | 48,14878 | 48,36284 | 62,24579 | 5,874113 |
| Sodium | 11 | K-series | 6,278568 | 6,306481 | 5,648776 | 0,442038 |
| Magnesium | 12 | K-series | 0,75278 | 0,756127 | 0,640621 | 0,074251 |
| Aluminium | 13 | K-series | 14,54985 | 14,61453 | 11,15373 | 0,726838 |
| Silicon | 14 | K-series | 22,71543 | 22,81642 | 16,72889 | 0,99866 |
| Potassium | 19 | K-series | 0,377936 | 0,379617 | 0,199935 | 0,043456 |
| Calcium | 20 | K-series | 6,095208 | 6,122306 | 3,145653 | 0,213681 |
| Iron | 26 | K-series | 0,638837 | 0,641677 | 0,236602 | 0,057033 |
| | | Sum: | 99,55739 | 100 | 100 | |



SAMPLE: SUMW03A.US1.1 (TF)

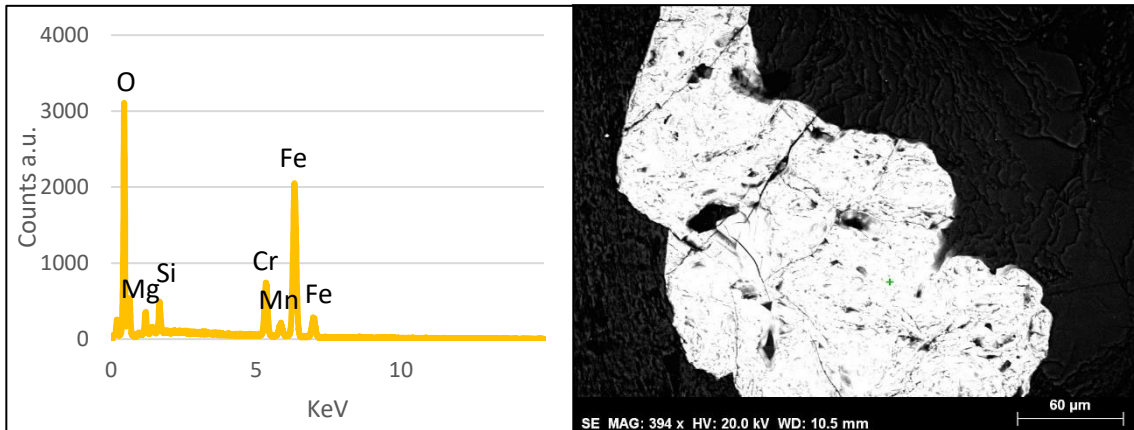
Multipoint analysis of clast grain elemental composition and BSE image of the location:

| Element | AN | series | [wt.%] | [norm. wt.%] | [norm. at.%] | Error in wt.% (1 Sigma) |
|------------|----|----------|----------|--------------|--------------|-------------------------|
| Oxygen | 8 | K-series | 40,57964 | 50,48256 | 67,58552 | 5,177606 |
| Sodium | 11 | K-series | 1,074573 | 1,336808 | 1,245519 | 0,105127 |
| Magnesium | 12 | K-series | 6,427144 | 7,995603 | 7,046469 | 0,384784 |
| Aluminium | 13 | K-series | 3,487236 | 4,33825 | 3,444005 | 0,198654 |
| Silicon | 14 | K-series | 6,269776 | 7,799832 | 5,948659 | 0,297386 |
| Phosphorus | 15 | K-series | 0,221101 | 0,275058 | 0,190215 | 0,03808 |
| Sulphur | 16 | K-series | 0,18209 | 0,226527 | 0,151318 | 0,035547 |
| Chlorine | 17 | K-series | 0,890829 | 1,108224 | 0,669567 | 0,060399 |
| Potassium | 19 | K-series | 0,887902 | 1,104583 | 0,605141 | 0,057649 |
| Calcium | 20 | K-series | 18,09678 | 22,51306 | 12,03219 | 0,560206 |
| Iron | 26 | K-series | 2,266403 | 2,819489 | 1,0814 | 0,101874 |
| | | Sum: | 80,38348 | 100 | 100 | |



Point analysis of Iron oxide grain and BSE image of the location:

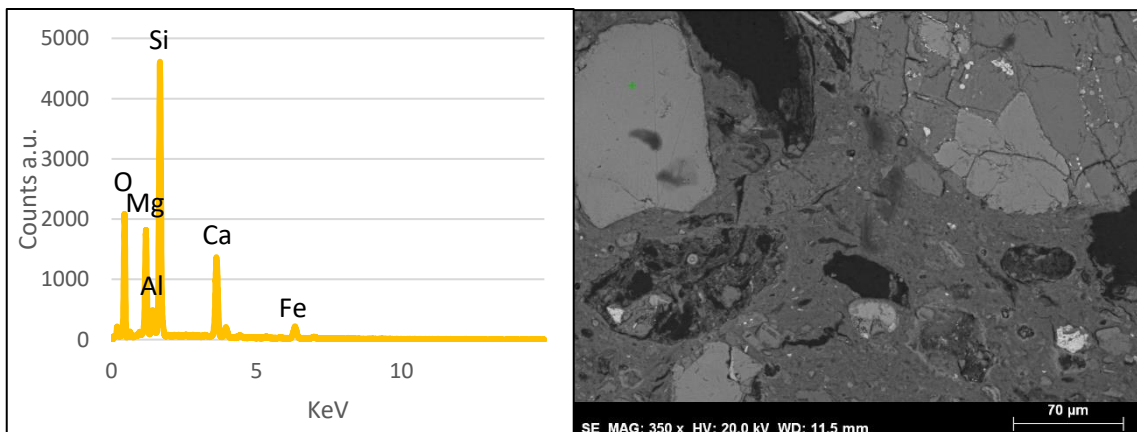
| Element | AN | series | [wt.%] | [norm. wt.%] | [norm. at.%] | Error in wt.% (1 Sigma) |
|-----------|----|----------|----------|--------------|--------------|-------------------------|
| Oxygen | 8 | K-series | 27,9518 | 28,63266 | 55,47396 | 3,730524 |
| Sodium | 11 | K-series | 0,91918 | 0,94157 | 1,269547 | 0,102453 |
| Magnesium | 12 | K-series | 2,9355 | 3,007004 | 3,835037 | 0,199941 |
| Aluminium | 13 | K-series | 0,69832 | 0,71533 | 0,821808 | 0,067416 |
| Silicon | 14 | K-series | 2,038647 | 2,088305 | 2,304852 | 0,119117 |
| Chromium | 24 | K-series | 9,798341 | 10,03701 | 5,983643 | 0,304573 |
| Manganese | 25 | K-series | 1,874115 | 1,919766 | 1,083195 | 0,131866 |
| Iron | 26 | K-series | 51,40617 | 52,65835 | 29,22796 | 1,405211 |
| | | Sum: | 97,62208 | 100 | 100 | |



IQM16B.US30.6 (BF)

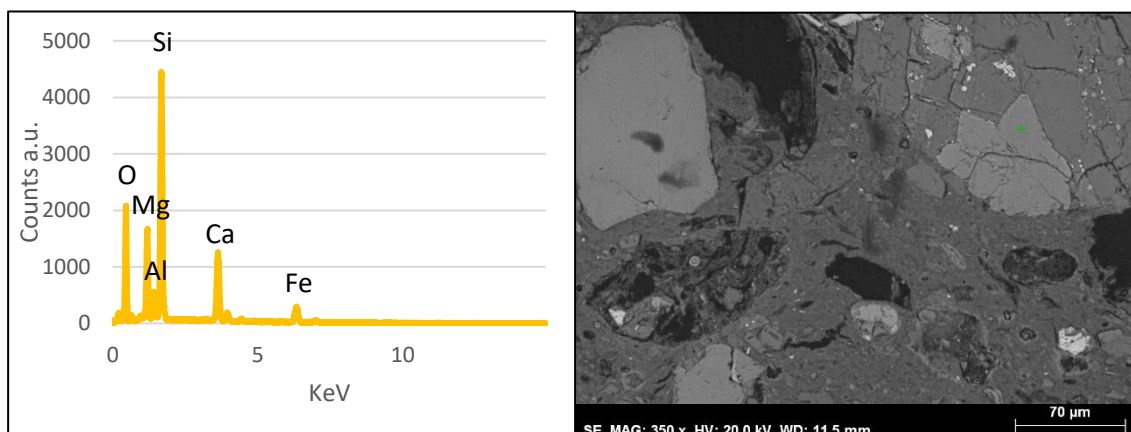
Point analysis in pyroxene grain and BSE image of the location:

| Element | AN | series | [wt.%] | [norm. wt.%] | [norm. at.%] | Error in wt.% (1 Sigma) |
|-----------|----|----------|----------|--------------|--------------|-------------------------|
| Oxygen | 8 | K-series | 38,39002 | 43,40697 | 60,36477 | 34,03582 |
| Magnesium | 12 | K-series | 8,370671 | 9,464579 | 8,6643 | 0,490358 |
| Aluminium | 13 | K-series | 2,164267 | 2,447101 | 2,017962 | 0,135618 |
| Silicon | 14 | K-series | 19,67354 | 22,24454 | 17,62257 | 0,868495 |
| Calcium | 20 | K-series | 13,08038 | 14,78977 | 8,210756 | 0,415949 |
| Titanium | 22 | K-series | 0,712833 | 0,805989 | 0,374544 | 0,055521 |
| Chromium | 24 | K-series | 0,586787 | 0,66347 | 0,283909 | 0,051915 |
| Iron | 26 | K-series | 5,463584 | 6,177584 | 2,461198 | 0,19034 |
| | | Sum: | 88,44208 | 100 | 100 | |



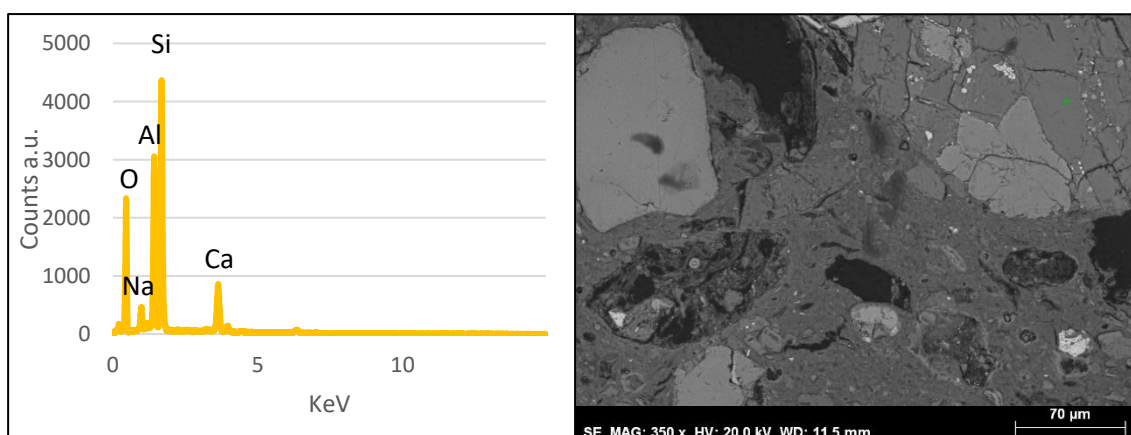
Point analysis in pyroxene in basalt grain and BSE image of the location:

| Element | AN | series | [wt.%] | [norm. wt.%] | [norm. at.%] | Error in wt.% (1 Sigma) |
|-----------|----|----------|----------|--------------|--------------|-------------------------|
| Oxygen | 8 | K-series | 41,58972 | 43,79256 | 60,39126 | 22,68283 |
| Sodium | 11 | K-series | 1,058077 | 1,114119 | 1,069238 | 0,105017 |
| Magnesium | 12 | K-series | 9,551913 | 10,05784 | 9,130331 | 0,5566 |
| Aluminium | 13 | K-series | 2,983316 | 3,14133 | 2,568764 | 0,175702 |
| Silicon | 14 | K-series | 19,90439 | 20,95865 | 16,46488 | 0,878474 |
| Calcium | 20 | K-series | 12,48734 | 13,14874 | 7,238617 | 0,398814 |
| Titanium | 22 | K-series | 0,874971 | 0,921315 | 0,424552 | 0,060325 |
| Iron | 26 | K-series | 6,520106 | 6,86545 | 2,712356 | 0,216863 |
| | | Sum: | 94,96984 | 100 | 100 | |



Point analysis in plagioclase in basalt grain and BSE image of the location:

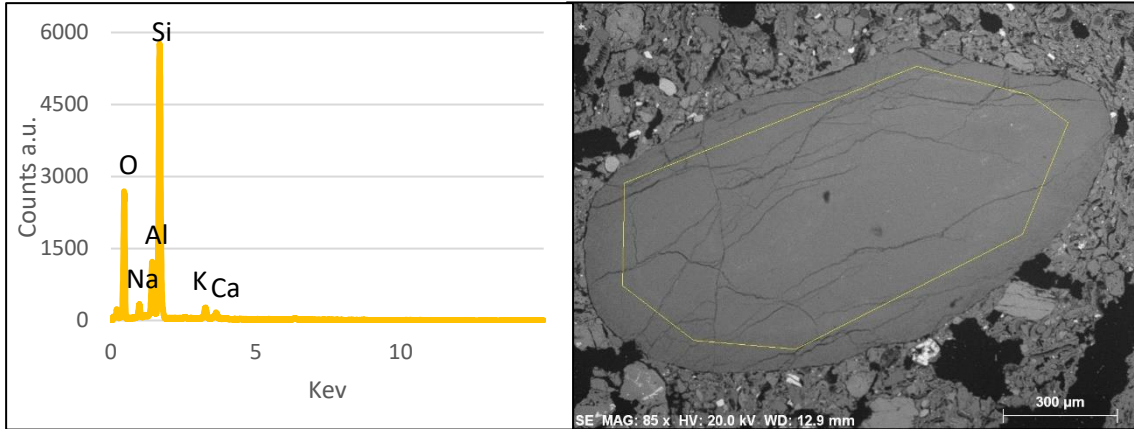
| Element | AN | series | [wt.%] | [norm. wt.%] | [norm. at.%] | Error in wt.% (1 Sigma) |
|-----------|----|----------|----------|--------------|--------------|-------------------------|
| Oxygen | 8 | K-series | 45,12898 | 45,93026 | 60,76857 | 5,605437 |
| Sodium | 11 | K-series | 3,811831 | 3,879511 | 3,572121 | 0,283518 |
| Magnesium | 12 | K-series | 0,992198 | 1,009814 | 0,879488 | 0,08764 |
| Aluminium | 13 | K-series | 15,85133 | 16,13278 | 12,65687 | 0,788885 |
| Silicon | 14 | K-series | 21,45531 | 21,83626 | 16,45811 | 0,945159 |
| Potassium | 19 | K-series | 0,490286 | 0,498991 | 0,270159 | 0,046732 |
| Calcium | 20 | K-series | 8,790629 | 8,946709 | 4,725427 | 0,291627 |
| Iron | 26 | K-series | 1,734881 | 1,765684 | 0,669263 | 0,089072 |
| | | Sum: | 98,25545 | 100 | 100 | |



SUM08B.US975.4 (BF)

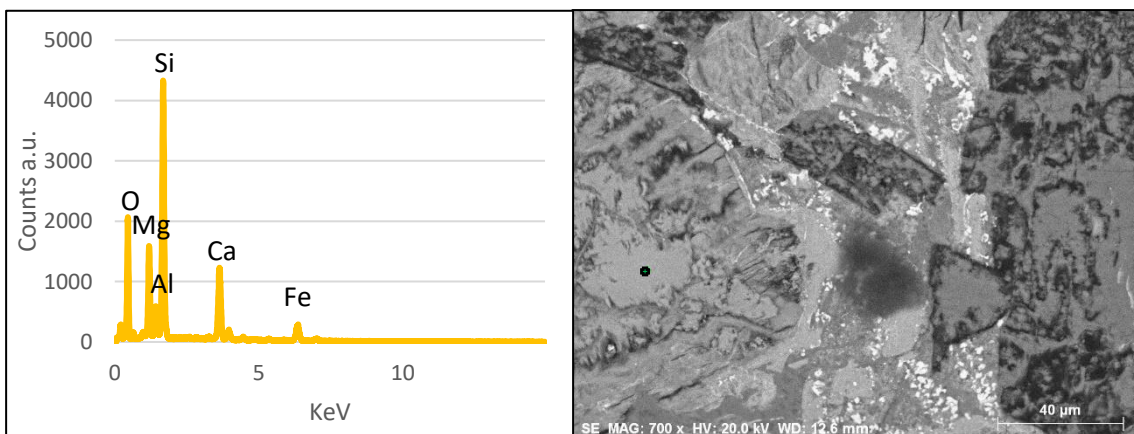
Multipoint analysis volcanic glass grain and BSE image of the location:

| Element | AN | series | [wt.%] | [norm. wt.%] | [norm. at.%] | Error in wt.% (1 Sigma) |
|-----------|----|----------|----------|--------------|--------------|-------------------------|
| Oxygen | 8 | K-series | 38,8272 | 52,07905 | 66,33356 | 4,763892 |
| Sodium | 11 | K-series | 1,588923 | 2,131228 | 1,889162 | 0,137025 |
| Aluminium | 13 | K-series | 4,913862 | 6,590978 | 4,978026 | 0,265645 |
| Silicon | 14 | K-series | 24,2105 | 32,47362 | 23,56256 | 1,061342 |
| Potassium | 19 | K-series | 2,455561 | 3,293651 | 1,716697 | 0,109407 |
| Calcium | 20 | K-series | 1,390856 | 1,86556 | 0,948587 | 0,076285 |
| Iron | 26 | K-series | 1,167459 | 1,565916 | 0,571403 | 0,075047 |
| | | Sum: | 74,55436 | 100 | 100 | |



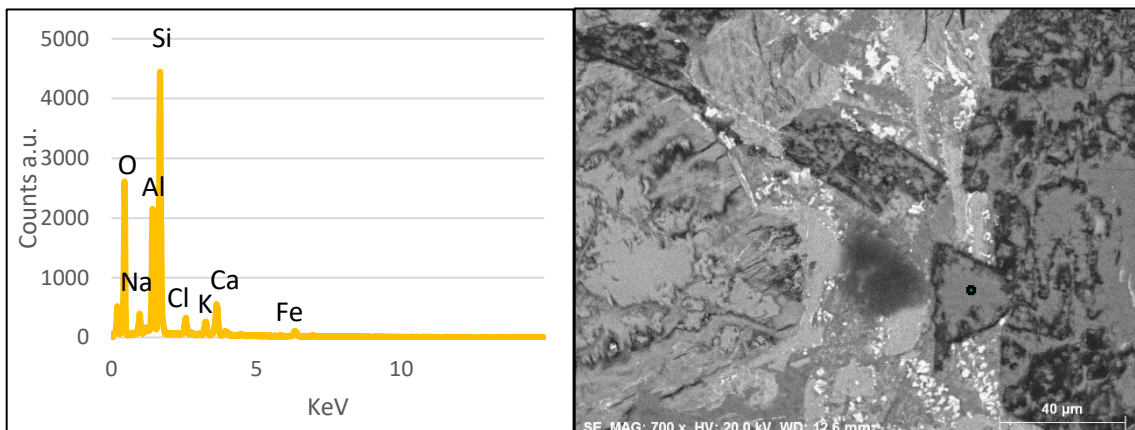
Point analysis pyroxene in basalt grain and BSE image of the location:

| Element | AN | series | [wt.%] | [norm. wt.%] | [norm. at.%] | Error in wt.% (1 Sigma) |
|-----------|----|----------|----------|--------------|--------------|-------------------------|
| Oxygen | 8 | K-series | 40,44549 | 43,74132 | 60,31412 | 22,14368 |
| Sodium | 11 | K-series | 1,22805 | 1,328121 | 1,274483 | 0,116188 |
| Magnesium | 12 | K-series | 9,379199 | 10,14349 | 9,207096 | 0,547124 |
| Aluminium | 13 | K-series | 3,162452 | 3,420154 | 2,796467 | 0,184241 |
| Silicon | 14 | K-series | 19,19879 | 20,76327 | 16,30964 | 0,848437 |
| Calcium | 20 | K-series | 11,40505 | 12,33442 | 6,789592 | 0,366673 |
| Titanium | 22 | K-series | 0,590975 | 0,639133 | 0,294488 | 0,050891 |
| Iron | 26 | K-series | 7,055174 | 7,630087 | 3,014119 | 0,232177 |
| | | Sum: | 92,46518 | 100 | 100 | |



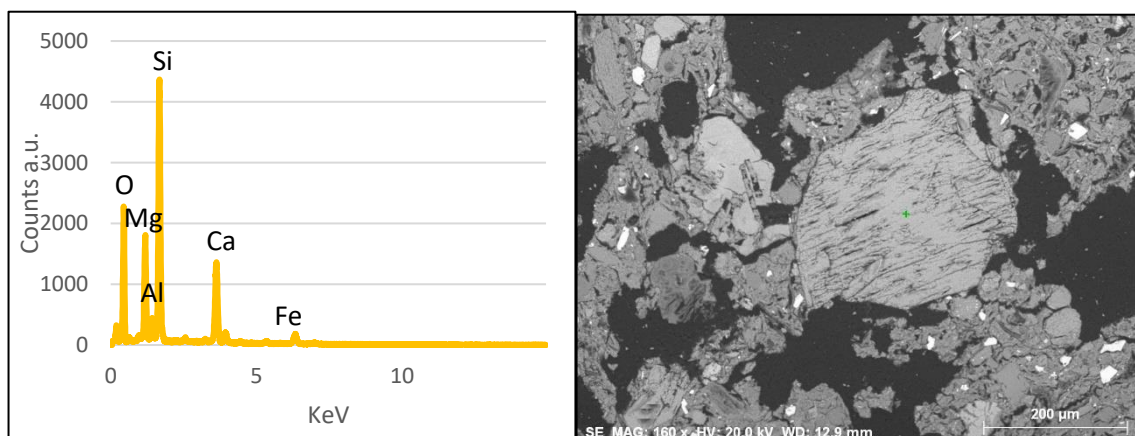
Point analysis feldspar in basalt grain and BSE image of the location:

| Element | AN | series | [wt.%] | [norm. wt.%] | [norm. at.%] | Error in wt.% (1 Sigma) |
|-----------|----|----------|----------|--------------|--------------|-------------------------|
| Oxygen | 8 | K-series | 41,29615 | 49,09765 | 64,15426 | 20,64058 |
| Sodium | 11 | K-series | 2,996566 | 3,562666 | 3,239731 | 0,230031 |
| Magnesium | 12 | K-series | 0,682211 | 0,811091 | 0,697658 | 0,069662 |
| Aluminium | 13 | K-series | 10,22072 | 12,15158 | 9,415305 | 0,519648 |
| Silicon | 14 | K-series | 18,90646 | 22,47819 | 16,73199 | 0,835709 |
| Potassium | 19 | K-series | 1,715782 | 2,03992 | 1,090746 | 0,084852 |
| Calcium | 20 | K-series | 5,367962 | 6,382055 | 3,32907 | 0,191521 |
| Titanium | 22 | K-series | 0,536199 | 0,637495 | 0,27835 | 0,049982 |
| Iron | 26 | K-series | 2,388191 | 2,839359 | 1,062891 | 0,106666 |
| | | Sum: | 84,11024 | 100 | 100 | |



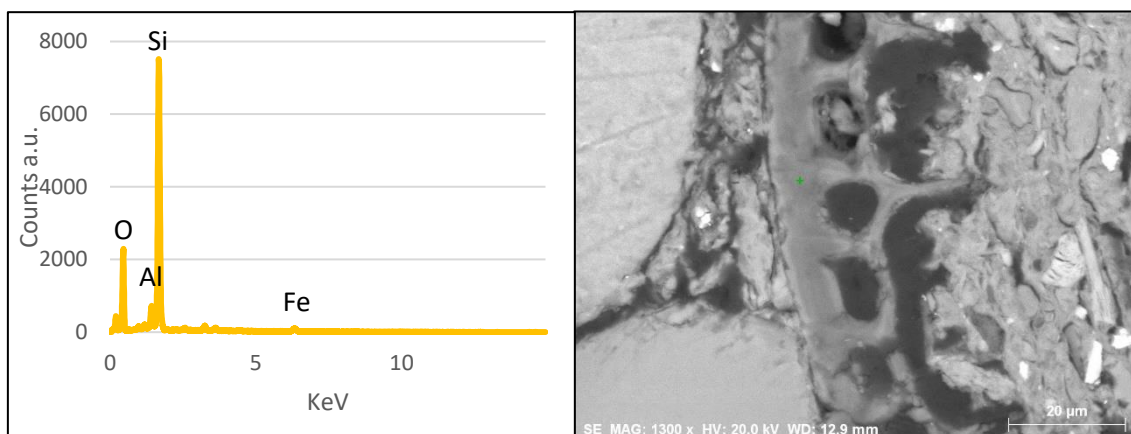
Point analysis pyroxene and BSE image of the location:

| Element | AN | series | [wt.%] | [norm. wt.%] | [norm. at.%] | Error in wt.% (1 Sigma) |
|-----------|----|----------|----------|--------------|--------------|-------------------------|
| Oxygen | 8 | K-series | 44,47459 | 45,48782 | 61,68122 | 38,15637 |
| Sodium | 11 | K-series | 1,339413 | 1,369928 | 1,29278 | 0,123578 |
| Magnesium | 12 | K-series | 10,66409 | 10,90704 | 9,735828 | 0,61743 |
| Aluminium | 13 | K-series | 2,330897 | 2,384001 | 1,916908 | 0,144612 |
| Silicon | 14 | K-series | 19,33882 | 19,7794 | 15,27891 | 0,854479 |
| Potassium | 19 | K-series | 0,542296 | 0,554651 | 0,307768 | 0,048336 |
| Calcium | 20 | K-series | 13,73864 | 14,05164 | 7,60646 | 0,435623 |
| Titanium | 22 | K-series | 0,467094 | 0,477736 | 0,216469 | 0,047755 |
| Chromium | 24 | K-series | 0,884507 | 0,904658 | 0,377464 | 0,061535 |
| Iron | 26 | K-series | 3,992172 | 4,083123 | 1,586186 | 0,149924 |
| | | Sum: | 97,77252 | 100 | 100 | |



Point analysis singular Silicon structure and BSE image of the location:

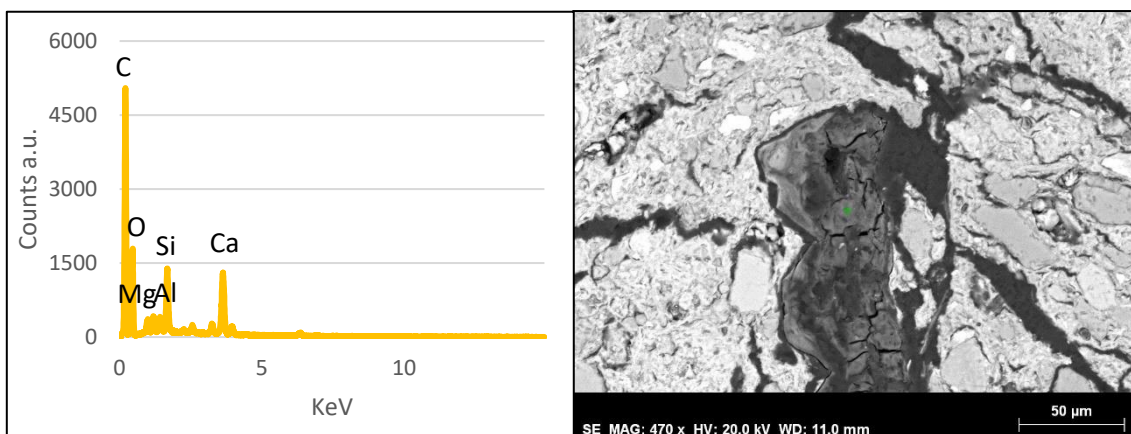
| Element | AN | series | [wt.%] | [norm. wt.%] | [norm. at.%] | Error in wt.% (1 Sigma) |
|-----------|----|----------|----------|--------------|--------------|-------------------------|
| Oxygen | 8 | K-series | 32,10062 | 45,5272 | 60,49093 | 17,1034 |
| Sodium | 11 | K-series | 0,905366 | 1,284049 | 1,187326 | 0,093608 |
| Magnesium | 12 | K-series | 0,747971 | 1,060821 | 0,927832 | 0,073087 |
| Aluminium | 13 | K-series | 3,107409 | 4,407132 | 3,47226 | 0,180022 |
| Silicon | 14 | K-series | 28,6491 | 40,63203 | 30,75455 | 1,24964 |
| Potassium | 19 | K-series | 1,126128 | 1,597149 | 0,868381 | 0,067156 |
| Calcium | 20 | K-series | 0,699249 | 0,991721 | 0,526025 | 0,053722 |
| Titanium | 22 | K-series | 0,666022 | 0,944596 | 0,419387 | 0,055021 |
| Iron | 26 | K-series | 2,506793 | 3,555298 | 1,353316 | 0,110727 |
| | | Sum: | 70,50866 | 100 | 100 | |



SUM10C.US174.104 (RT)

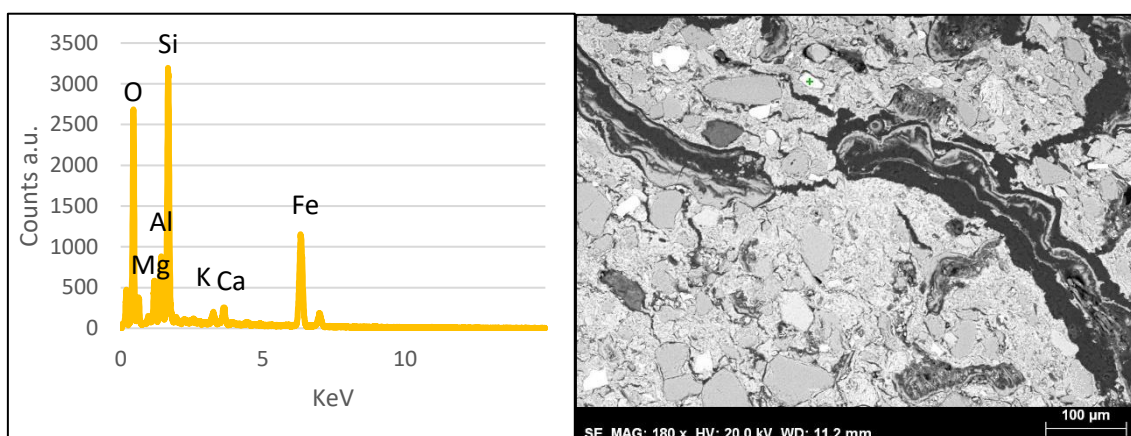
Point elemental analysis of rice husk and BSE image of the location:

| Element | AN | series | [wt.%] | [norm. wt.%] | [norm. at.%] | Error in wt.% (1 Sigma) |
|-----------|----|----------|----------|--------------|--------------|-------------------------|
| Carbon | 6 | K-series | 42,54135 | 45,34804 | 57,163 | 7,518282 |
| Oxygen | 8 | K-series | 34,38555 | 36,65415 | 34,68608 | 4,417889 |
| Sodium | 11 | K-series | 1,456216 | 1,55229 | 1,02229 | 0,12623 |
| Magnesium | 12 | K-series | 1,113067 | 1,186502 | 0,739109 | 0,090943 |
| Aluminium | 13 | K-series | 0,907566 | 0,967443 | 0,542868 | 0,072423 |
| Silicon | 14 | K-series | 2,989111 | 3,18632 | 1,717682 | 0,15551 |
| Sulphur | 16 | K-series | 0,20598 | 0,21957 | 0,103673 | 0,035414 |
| Chlorine | 17 | K-series | 0,512092 | 0,545878 | 0,233121 | 0,045819 |
| Potassium | 19 | K-series | 0,967719 | 1,031564 | 0,399461 | 0,058756 |
| Calcium | 20 | K-series | 7,64447 | 8,148818 | 3,078395 | 0,2536 |
| Iron | 26 | K-series | 1,087663 | 1,159422 | 0,314324 | 0,064961 |
| | | Sum: | 93,81078 | 100 | 100 | |



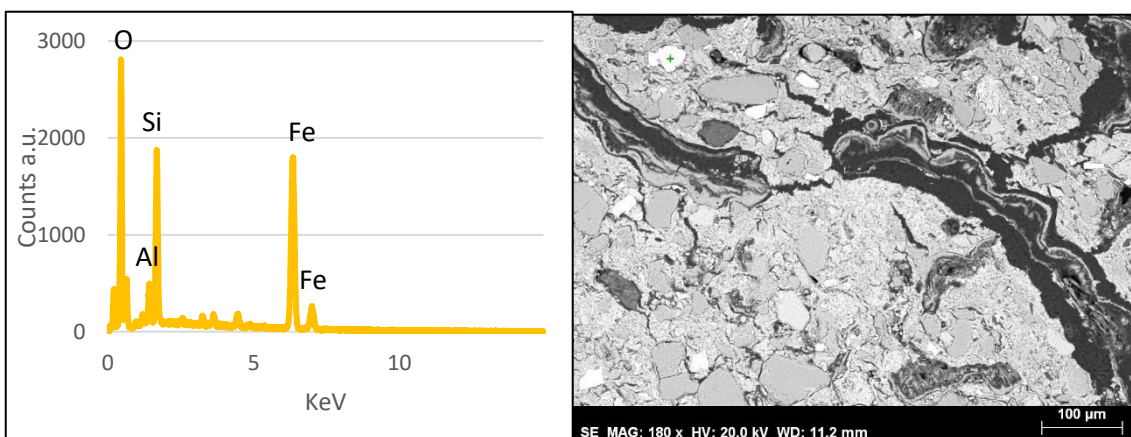
Point elemental analysis pyroxene and BSE image of the location:

| Element | AN | Series | unn. C [wt.%] | norm. C [wt.%] | Atom. C [at.%] | Error (1 Sigma) [wt.%] |
|---------|----|----------|---------------|----------------|----------------|------------------------|
| O | 8 | K-series | 34.01 | 39.61 | 60.18 | 16.87 |
| Na | 11 | K-series | 1.09 | 1.27 | 1.34 | 0.11 |
| Mg | 12 | K-series | 3.80 | 4.42 | 4.42 | 0.24 |
| Al | 13 | K-series | 4.46 | 5.20 | 4.68 | 0.25 |
| Si | 14 | K-series | 14.29 | 16.65 | 14.41 | 0.64 |
| K | 19 | K-series | 1.06 | 1.24 | 0.77 | 0.06 |
| Ca | 20 | K-series | 1.87 | 2.17 | 1.32 | 0.09 |
| Ti | 22 | K-series | 0.78 | 0.91 | 0.46 | 0.06 |
| Fe | 26 | K-series | 24.50 | 28.53 | 12.42 | 0.69 |
| | | Total: | 85.87 | 100.00 | 100.00 | |



Point elemental analysis olivine and BSE image of the location:

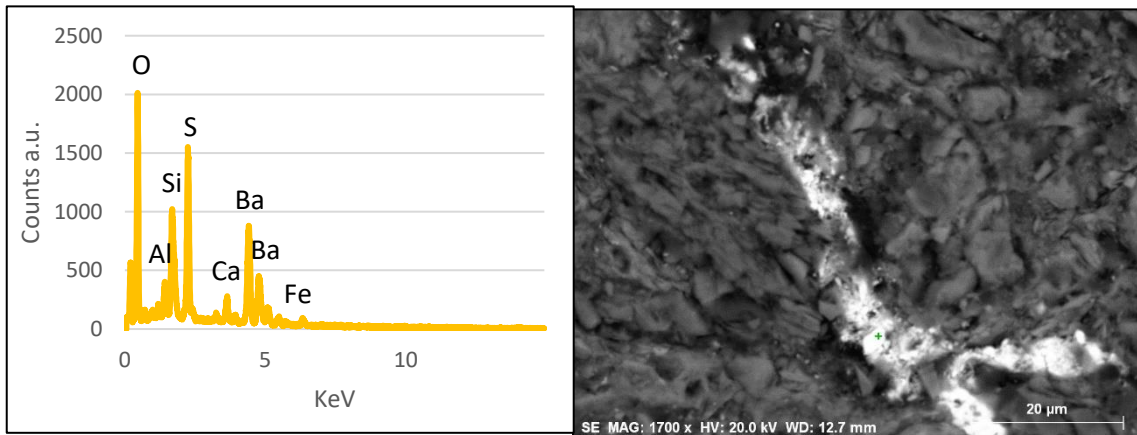
| Element | AN | series | [wt.%] | [norm. wt.%] | [norm. at.%] | Error in wt.% (1 Sigma) |
|-----------|----|----------|----------|--------------|--------------|-------------------------|
| Oxygen | 8 | K-series | 32,40788 | 36,37969 | 61,42111 | 15,86008 |
| Sodium | 11 | K-series | 0,901843 | 1,012371 | 1,189508 | 0,098456 |
| Magnesium | 12 | K-series | 0,944057 | 1,059758 | 1,177805 | 0,087055 |
| Aluminium | 13 | K-series | 2,69223 | 3,022181 | 3,025632 | 0,162452 |
| Silicon | 14 | K-series | 8,250197 | 9,261317 | 8,907441 | 0,382759 |
| Potassium | 19 | K-series | 0,567296 | 0,636822 | 0,43997 | 0,048259 |
| Calcium | 20 | K-series | 0,736607 | 0,826883 | 0,557315 | 0,053494 |
| Titanium | 22 | K-series | 1,77762 | 1,995479 | 1,125785 | 0,084477 |
| Iron | 26 | K-series | 40,80461 | 45,8055 | 22,15543 | 1,121776 |
| | | Sum: | 89,08234 | 100 | 100 | |



IQM18A.US80.3 (FF)

Point analysis Ba-rich vein and BSE image of the location:

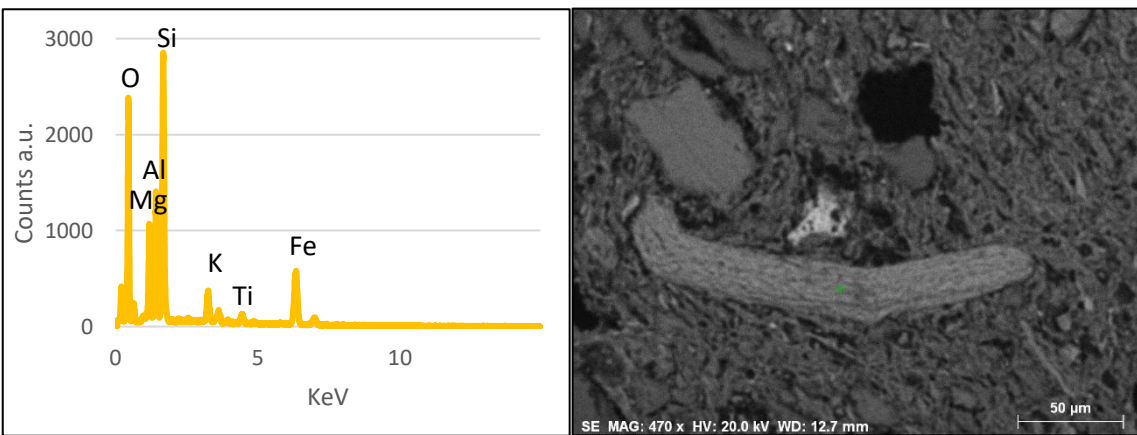
| Element | AN | series | [wt.%] | [norm. wt.%] | [norm. at.%] | Error in wt.% (1 Sigma) |
|-----------|----|----------|----------|--------------|--------------|-------------------------|
| Oxygen | 8 | K-series | 28,39938 | 34,04511 | 64,10525 | 3,597099 |
| Sodium | 11 | K-series | 0,897592 | 1,076031 | 1,410044 | 0,265863 |
| Magnesium | 12 | K-series | 0,934724 | 1,120545 | 1,388916 | 0,085999 |
| Aluminium | 13 | K-series | 1,813401 | 2,173901 | 2,427256 | 0,120079 |
| Silicon | 14 | K-series | 6,308561 | 7,562689 | 8,112163 | 0,299935 |
| Sulphur | 16 | K-series | 9,289553 | 11,1363 | 10,46257 | 0,364951 |
| Potassium | 19 | K-series | 0,643641 | 0,771595 | 0,594531 | 0,052431 |
| Calcium | 20 | K-series | 2,188325 | 2,623359 | 1,971943 | 0,099711 |
| Iron | 26 | K-series | 2,252535 | 2,700334 | 1,456667 | 0,10648 |
| Barium | 56 | L-series | 30,6892 | 36,79015 | 8,070654 | 0,883093 |
| | | Sum: | 83,41691 | 100 | 100 | |



SUM10C.US162.119 (FF)

Point analysis mica inclusion and BSE image of the location:

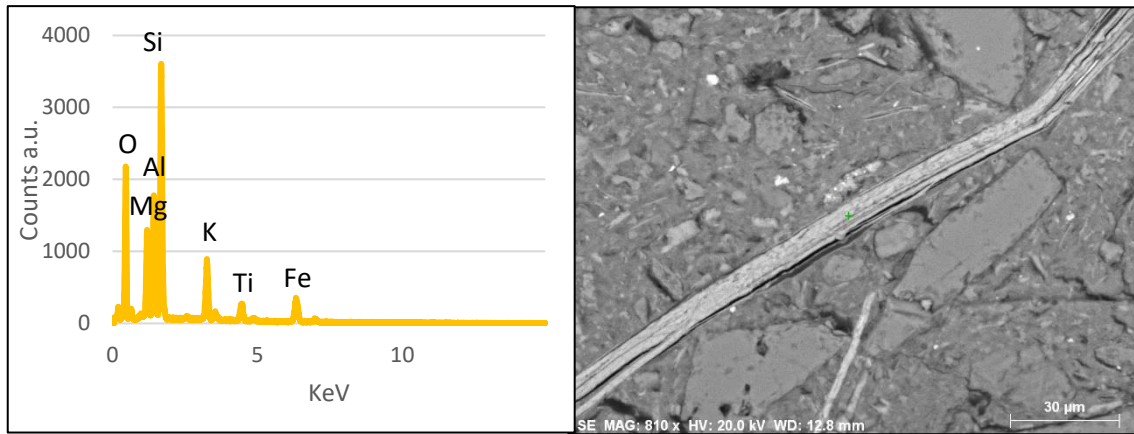
| Element | AN | series | [wt.%] | [norm. wt.%] | [norm. at.%] | Error in wt.% (1 Sigma) |
|-----------|----|----------|----------|--------------|--------------|-------------------------|
| Oxygen | 8 | K-series | 35,93356 | 41,88304 | 59,61171 | 18,96375 |
| Sodium | 11 | K-series | 0,938561 | 1,093958 | 1,083585 | 0,098316 |
| Magnesium | 12 | K-series | 6,933901 | 8,08194 | 7,572112 | 0,414613 |
| Aluminium | 13 | K-series | 8,215514 | 9,575748 | 8,081705 | 0,426137 |
| Silicon | 14 | K-series | 14,39796 | 16,78182 | 13,60673 | 0,645087 |
| Potassium | 19 | K-series | 2,394963 | 2,791494 | 1,625833 | 0,105298 |
| Calcium | 20 | K-series | 1,146942 | 1,33684 | 0,759575 | 0,067148 |
| Titanium | 22 | K-series | 1,689393 | 1,969104 | 0,936508 | 0,084116 |
| Iron | 26 | K-series | 14,14421 | 16,48606 | 6,72224 | 0,418652 |
| | | Sum: | 85,79501 | 100 | 100 | |



IQM16B.US35.9 (MLF)

Point analysis on mica inclusion and BSE image of the location:

| Element | AN | series | [wt.%] | [norm. wt.%] | [norm. at.%] | Error in wt.% (1 Sigma) |
|-----------|----|----------|----------|--------------|--------------|-------------------------|
| Oxygen | 8 | K-series | 39,01555 | 42,55186 | 59,35147 | 20,85387 |
| Sodium | 11 | K-series | 1,033687 | 1,127379 | 1,094339 | 0,103267 |
| Magnesium | 12 | K-series | 7,431477 | 8,105055 | 7,441782 | 0,440581 |
| Aluminium | 13 | K-series | 9,346768 | 10,19395 | 8,431254 | 0,479166 |
| Silicon | 14 | K-series | 16,29164 | 17,76829 | 14,11822 | 0,72506 |
| Chlorine | 17 | K-series | 0,326612 | 0,356216 | 0,224223 | 0,041793 |
| Potassium | 19 | K-series | 6,045667 | 6,593638 | 3,76343 | 0,215578 |
| Titanium | 22 | K-series | 3,575211 | 3,899263 | 1,817377 | 0,136181 |
| Iron | 26 | K-series | 8,622796 | 9,404353 | 3,757904 | 0,273607 |
| | | Sum: | 91,68941 | 100 | 100 | |



SUM03B.US93.42 (SSF)

Strontiumsulfate Point analysis and BSE image of the location:

| Element | AN | series | [wt.%] | [norm. wt.%] | [norm. at.%] | Error in wt.% (1 Sigma) |
|-----------|----|----------|----------|--------------|--------------|-------------------------|
| Carbon | 6 | K-series | 2,657252 | 2,290058 | 5,368461 | 3,593268 |
| Oxygen | 8 | K-series | 44,00815 | 37,92685 | 66,74606 | 5,807459 |
| Magnesium | 12 | K-series | 0,638098 | 0,549922 | 0,637071 | 0,06821 |
| Aluminium | 13 | K-series | 1,37084 | 1,181409 | 1,232867 | 0,100511 |
| Sulphur | 16 | K-series | 13,57762 | 11,70139 | 10,27484 | 0,520904 |
| Potassium | 19 | K-series | 0,608014 | 0,523995 | 0,377357 | 0,052327 |
| Calcium | 20 | K-series | 1,90266 | 1,63974 | 1,151997 | 0,092295 |
| Iron | 26 | K-series | 1,157478 | 0,997531 | 0,502932 | 0,072494 |
| Strontium | 38 | L-series | 48,41395 | 41,72383 | 13,40799 | 2,029395 |
| Barium | 56 | L-series | 1,700217 | 1,465271 | 0,300424 | 0,089625 |
| | | Sum: | 116,0343 | 100 | 100 | |

